A Spectral Representation Solution for Electromagnetic Scattering from Complex Structures

Robert James Fleming

A thesis submitted to the Faculty of Engineering, University of the Witwatersrand, Johannesburg, in fulfilment of the requirements for the degree of Doctor of Philosophy.

Johannesburg, January 2010

Declaration

I declare that this thesis is my own, unaided work, except where otherwise acknowledged. It is being submitted for the degree of Doctor of Philosophy in the University of the Witwatersrand, Johannesburg. It has not been submitted before for any degree or examination in any other university.

Signed this 30th day of January 2010

Robert James Fleming.

Preface

This Doctoral thesis documents an investigation into the motivating theory, limitations and integration into SuperNEC of a technique for the analytical, continuous, wideband description of the response of a complex conducting body to an electromagnetic excitation.

The breadth of materials drawn on to reach the conclusions in this thesis are covered in 200+ references from the mathematics, physics and engineering literature, necessitating a balanced presentation of background, theory, implementation and results. This thesis is not a collection of papers, but a stand-alone treatment that the author believes to be a valuable contribution to the field.

Chronologically, the work began with analysis and implementation of Model-Based Parameter Estimation (MBPE) with a goal of evaluating this technique for simulation of various electromagnetic responses over a wide frequency band. The numerical results and implementation of the software with SuperNEC were completed and published in technical reports and a dissertation. These documents have been peer-reviewed or formally examined.

- "A Transfer Function Estimation Method Integrated into SuperNEC for the Approximation of the Wideband Electromagnetic Response of Complex Structures", MSc Dissertation, University of Witwatersrand, Successfully examined and sealed for conversion to PhD, 2003.
- "Model Based Parameter Estimation applied to SuperNEC", Technical Report, University of Witwatersrand Electromagnetics Laboratory, 1996.

While the integration of these techniques into a commercial standard C++ software package was necessary to validate the results, the software engineering effort was not included in this thesis.

The theoretical work followed, in large part to explain both exceptional and anomalous results discovered in the early part of the research. The scope of the effort spanned over 60 years of keystone theories developed in the literature, and resulted in work that is both relevant and expanding in interest in the recent literature. The author believes that the contents

of this thesis will result in several publications, both theoretical and numerical in nature. The following papers are published or in the peer-review process with leading international journals in this field.

- "A Common Theoretical Basis for Preconditioned Field Integral Equations and the Singularity Expansion Method", *Progress in Electromagnetic Research M*, Volume 5, pages 111-136, 2008.
- "Singular Function Expansions to Precondition Electric Field integral Equations", *Progress in Electromagnetic Research*, Submitted 2009.
- "A Calderon Preconditioner and SEM Equivalence Relation applied to Wideband Frequency-Domain EFIE Solutions", *IEEE Transactions on Antennas and Propagation*, Submitted 2008.
- "Transfer Function Estimation: A Wideband Estimation Tool for Complex Structures", *Applied Computational Electromagnetic Society Journal*, to be submitted, 2009.

The substance of the published theoretical and numerical work is predominantly interspersed through chapters 4 to 8.

Abstract

Significant effort has been directed towards improving computational efficiency in calculating radiated or scattered fields from a complex structure over a broad frequency band. The formulation and solution of boundary integral equation methods in commercial and scientific software has seen considerable attention; methods presented in the literature are often abstract, "curve-fits" or lacking a sound foundation in the underlying physics of the problem. Anomalous results are often characterized incorrectly, or require user expertise for analysis, a clear disadvantage in a computer-aided design tool.

This dissertation documents an investigation into the motivating theory, limitations and integration into SuperNEC of a technique for the analytical, continuous, wideband description of the response of a complex conducting body to an electromagnetic excitation. The method, referred to by the author as Transfer Function Estimation (TFE) has its foundations in the Singularity Expansion Method (SEM). For scattering and radiation from a perfect electric conductor, the Electric-Field Integral Equation (EFIE) and Magnetic-Field Integral Equation (MFIE) formulations in their Stratton-Chu form are used. Solution by spectral representation methods including the Singular Value Decomposition (SVD), the Singular Value Expansion (SVE), the Singular Function Method (SFM), Singularity Expansion Method (SEM), the Eigenmode Expansion Method (EEM) and Model-Based Parameter Estimation (MBPE) are evaluated for applicability to the perfect electric conductor. The relationships between them and applicability to the scattering problem are reviewed. A common theoretical basis is derived.

The EFIE and MFIE are known to have challenges due to ill-posedness and uniqueness considerations. Known preconditioners present possible solutions. The Modified EFIE (MEFIE) and Modified Combined Integral Equation (MCFIE) preconditioner is shown to be consistent with the fundamental derivations of the SEM. Prony's method applied to the SEM pole-residue approximation enables a flexible implementation of a reduced-order method to be defined, for integration into SuperNEC.

The computational expense inherent to the calculation of the impedance matrix in SuperNEC is substantially reduced by a physically-motivated approximation based on the TFE method.

Using an adaptive approach and relative error measures, SuperNEC iteratively calculates the best continuous-function approximation to the response of a conducting body over a frequency band of interest. The responses of structures with different degrees of resonant behaviour were evaluated: these included an attack helicopter, a log-periodic dipole array and a simple dipole. Remarkable agreement was achieved.

To my Parents, Dave and Patricia Fleming

Who encouraged me to be the best that I could be
... and to reach for the stars!!

To the Maughans ,the Harrisons, the Youngs and the Flemings - what a family.
To my little one, Caitlin Grace -

Acknowledgements

Dr Ragini Saxena for her constant enthusiasm, probing questions and support.
Professor Robert de Mello Koch for inspiring me in his search for G'.

Contents

List of Figures

List of Tables

List of Symbols

c_k	k-th complex Fourier Coefficient	10
i	Imaginary number $= \sqrt{-1}$	10
k	Complex wavenumber $= 2\pi/\lambda$	10
T_0	Fundamental period with corresponding angular frequency ω_0	10
$H(s)$	Transfer function of complex frequency s, the laplace transformed impulse response $h(t)$	12
$L\left(\nabla, \frac{\partial}{\partial t}\right)$	Linear operator L, a function of spatial operator ∇ and temporal gradient operator $\frac{\partial}{\partial t}$	14
$\mathbf{\Psi}(\mathbf{r}), \mathbf{\Phi}(\mathbf{r})$	Column vector of complex electromagnetic field vectors	14
$\mathbf{1}$	Identity operator	14
$\mu(\mathbf{r})$	Permeability of the medium at $\mathbf{r}$. Excluding $\mathbf{r}$ implies constant permeability for medium	14
$\mathbf{F}(\mathbf{r})$	Vector function of $\mathbf{r}$	14
Υ	Transverse component operator of linear operator L	14
Λ	Longitudinal component operator of linear operator L	14
$G(\rho, \rho', t, t', z, z')$	Green's function corresponding to impulse excitation at ρ', t', z'	15
$\mathbf{E}_{t\alpha}, \mathbf{H}_{t\alpha}$	α-th tangential electric and magnetic field mode components	16
$E_{z\alpha}, H_{z\alpha}$	α-th longitudinal electric and magnetic field mode components	16
$\mathbf{e}(\boldsymbol{\rho})$, $\mathbf{h}(\boldsymbol{\rho})$	Transverse electric field and magnetic field eigenvectors	16
$\delta(\mathbf{r} - \mathbf{r}')$	Dirac delta function at $\mathbf{r} = \mathbf{r}'$	19
$\mathbf{R}_\beta(\mathbf{r}, s)$, $\mathbf{L}_\beta(\mathbf{r}, s)$	Complex frequency-dependent eigenmode functions, for eigenmode index β	28

$\lambda_\beta(s)$	Complex frequency dependent eigenvalue with index β	28
$\mathbf{R}^N$	$N-$dimensional space of real numbers	29
$\Gamma(\mathbf{r}, \mathbf{r}'; s_\alpha)$	Impedance dyadic operator as a function of source and position vectors, evaluated at frequency s_α	31
$\mathbf{M}_\alpha(\mathbf{r})$	α-th Singularity Expansion Method natural mode vector	31
$\mathbf{C}_\alpha(\mathbf{r})$	α-th Singularity Expansion Method coupling mode vector	31
$\langle\cdot,\cdot\rangle, (\cdot,\cdot)$	Inner product	31
$\mathbf{I}(\mathbf{r}, s)$	Spatial current distribution with complex frequency dependency	31
$\eta_\alpha(s)$	α-th mode frequency-dependent coupling coefficient	31
S_{inf}	Surface S extending to infinity	36
$\varrho(\mathbf{r})$	Charge density at point $\mathbf{r}$	36
$\phi(\mathbf{r})$	Scalar potential function of position $\mathbf{r}$	36
V_{inf}	Volume V extending to infinity	36
$\epsilon(\mathbf{r})$	Permittivity of the medium at $\mathbf{r}$. With $(\mathbf{r})$ excluded, ϵ is constant for the medium	36
$\mathbf{r}, \mathbf{r}'$	Field/observation coordinates and source point coordinates in space	37
$\hat{\mathbf{n}}(\mathbf{r})$	Unit normal vector at $\mathbf{r}$	37
R	Distance scalar from source point $\mathbf{r}'$ to field point $\mathbf{r}$	38
∇'	Gradient symbolic vector denoting derivative with respect to source coordinates	38
$\hat{a}$	Arbitrarily-directed unit vector	44
$G(\mathbf{r}, \mathbf{r}')$	Free Space Green's function	44
$\mathbf{E}_\pm(\mathbf{r})$	Hybrid symbol for incident (-) and scattered(+) field from a surface, at point $\mathbf{r}$	46
$\mathbf{E}^{inc}(\mathbf{r})$	Electric Field incident on a surface at $\mathbf{r}$	46
$\mathbf{E}^S(\mathbf{r})$	Electric field scattered from a surface at $\mathbf{r}$	46
$\overline{\mathbf{G}}(\mathbf{r}, \mathbf{r}')$	Dyadic Green's function, with source at $\mathbf{r}'$, observed at $\mathbf{r}$	47
$\overline{\mathbf{I}}$	Unit dyad	47

$\overline{G}_{ee}$	Conventional electric field Green's dyadic	48
H^n	n-dimensional Hilbert Space	53
$\|\cdot\|$	Norm	53
(S_i, d_i)	A metric space defined as the set S_i with distance function d_i	54
$C^k(\Omega)$	The space of k-times differentiable continuous functions on domain Ω	55
$\subset$	$X \subset Y$ denotes that X is a proper subset of Y	55
$L^2(\Omega)$	The space of Lebesgue-square integrable functions on Ω	55
D^α	Generalized weak derivative of order α of some function, e.g. $D^1 f$ is first derivative	56
$W^{s,p}(\Omega)$	Sobolev Space of order s, defined on Ω containing functions that are $p-$integrable	56
$\mathcal{D}(T)$	Denotes the domain of operator T	59
$\mathcal{R}(T)$	Denotes the range of operator T	59
$\mathcal{N}(T)$	Null space of operator T	60
T^*	Adjoint of operator T	65
T_s, T_h	T_s, T_h are smoothing and hypersingular components of operator T found by Helmholtz decomposition	69
I	Identity operator	70
$k(\mathbf{x}, \mathbf{y})$	Integral kernel function of position vectors $\mathbf{x}$ and $\mathbf{y}$ corresponding to operator K	81
$D_\lambda(s, t)$	Modified first Fredholm minor of kernel $K(s, t)$ derived from infinite series approximation of kernel matrix	82
$D \equiv D(\mathbf{r}, \mathbf{r}'; s)$	Modified first Fredholm minor for MMFIE and MEFIE	84
$P(\mathbf{r}, \mathbf{r}'; s)$	Preconditioning operator for MEFIE and MMFIE	87
$\Phi^m_\alpha(s)$	MMFIE coupling coefficients of class 2 for $s = s_\alpha$	87
$\Phi^e_\alpha(s)$	MEFIE coupling coefficients of class 2 for $s = s_\alpha$	87
$\Psi^{e,m}_\alpha(s_\alpha)$	EFIE and MFIE class 1 coupling coeffients, calculated at $s = s_\alpha$	87
$R_b(H)$	Riesz basis of Hilbert space H with brackets	92

$K^{\dagger}(\mathbf{r}, \mathbf{r}')$	Adjoint kernel to integral kernel K(**r**,**r**')	96
μ_i	Singular value used in singular function expansions	96
Ω	Defines a region of space, has boundary $\partial\Omega$ or S, as required, with unit of volume $d\Omega = dxdydz$	105
$L^p(\Omega)^3$	The set of all Lebesgue-square integrable functions (integrable to the $p-$th power in 3-dimensional space	106
$\|\mathbf{f}\|^2_{\text{curl},\Omega}$, $\|\mathbf{f}\|^2_{\text{div},\Omega}$	Norm in L^2 defined by usual norm with additional curl- and div-norms on f	106
Z_{mn}	System impedance matrix calculated at $s = s_\alpha$ for a source and observation points m and n	112
$\delta(\lambda)$	Modified Fredholm determinant in terms of continuous eigenvalue λ, used in Fredholm Determinant Theory	180
$H_\lambda(s,t)$	Resolvent funtion corresponding to integral kernel $K(s,t)$	180
$\Delta_\lambda(s,t)$	Modified first Fredholm minor of kernel $K(s,t)$	180

Chapter 1

Introduction

1.1 Statement of the Problem

The Goal of this Theoretical and Computational Work:
To develop mathematically justifiable motivating theory, limitations and integration into SuperNEC of a technique for the analytical, continuous, wideband description of the response of an arbitrarily complex conducting body to an electromagnetic excitation. Existing spectral expansions and select parametric models will be critically reviewed as part of the development of this technique, leading to a broad theoretical basis for the solution of our problem. A substantive theory linking spectral expansion methods and integral equation techniques will be explored.

Summary Statement of the Problem:
The computational expense required to calculate some electromagnetic response by a complex structure to an excitation over a wide frequency range is prohibitive. Techniques for approximation of such "system responses" have a mathematically weak basis, though have demonstrated utility in providing reduced-order models that can drastically reduce this computational expense.

1.1.1 Prohibitive Computational Expense

Radiation and scattering from homogeneous bodies embedded in some medium is defined by Maxwell's partial differential equations, that in the general form can be written as inhomogeneous vector and scalar wave equations. It is well known [2, p.22] that these equations can be solved by separation of variables, integral equation (Green's function) techniques and by variational methods. A class of integral equation techniques, known as Surface Integral Equations (SIEs), which exist in an electric field form (EFIE) and a magnetic field form (MFIE), are well known and have been the substance of considerable theoretical and numerical work over the last three decades. The unknown in these integral equations, the surface current distribution, can be solved using a technique known as the Method of Moments, which projects the infinite dimensional integral operator into a finite-dimensional space, suitable for numerical computation [3].

This discretization enables an N-dimensional square matrix formulation, known as the *Impedance* matrix to be defined. The dimension of the matrix is a function of the electrical size of the body and the frequency of interest. Solution of the standard $Ax = b$ linear, matrix equation gives the surface current distribution at N points on the exterior of the scattering body, satisfying the boundary conditions at those points.

The Numerical Electromagnetics Code (NEC2) [4] and its successor, SuperNEC [5] are recognized computer codes used in such analysis for the calculation of the electromagnetic response of an arbitrary structure, modeled with wire segments in free space or over a ground plane. These frequency domain codes use a Method of Moments (MoM), numerical solution of an electric field integral equation for the induced currents on the structure [6]. The formulation and solution of the system impedance matrix in SuperNEC is of $\mathcal{O}(N^2 + N^3)$, typical for a direct solution to a dense matrix equation. For typical structures, having large N, the computational effort is significant, and simulation run-time excessive for the user of a design software package.

The problem is exacerbated when the electromagnetic response is required over a large frequency band. A wideband response of some structure is found by solving for the induced currents over the entire structure at a number of discrete frequencies. The characteristics of the response at intermediate frequencies are typically obtained through linear or parabolic interpolation. Sample placement is often arbitrary or chosen to satisfy aesthetic criteria, resulting in more samples being used to describe a response than stipulated by information theory constraints. The application itself may require many samples over a range of interest. As an example, airborne VHF radio equipment operating in international airspace are channel-spaced 8.33 kHz apart, providing $>$ 2250 available channels between 118 and 137 MHz. The design engineer needs a detailed characterization of all performance parameters of

the aircraft antenna system for these radios over this range, a requirement which may require major simulation time, depending on the resolution sought.

Any anomalous features prevalent to some structure, for example narrow resonances in the input impedance (as a function of frequency), are often missed as a consequence of undersampling the band of interest. The computational expense inherent in finding the response of a system over a spectrum of frequencies is dependent on both the number of samples required to obtain a meaningful interpolation and the expense of calculating the response at one frequency. It follows that for M frequency samples, the formulation and solution over that frequency range would be $\mathcal{O}[M \times (N^2 + N^3)]$, thus imposing a serious computational penalty on excessive sample use. An accurate method of describing the response with as fine a resolution as possible, yet still minimizing the number of frequencies at which the matrix needs to be solved, represents first prize.

1.1.2 Weak Theoretical (or Common) Basis for Reduced-Order Models

A migration in the philosophy of approximation of a system response from a purely mathematical curve-fit to a physically-motivated reduced-order model presents a viable solution to our problem. Miller [7] has presented a formulation, known as Model-Based Parameter Estimation (MBPE) where approximation of electromagnetic *observables*, such as induced current, or input impedance, is made in the generic spectral and waveform domains. Rational function models can be constructed in the time and frequency domain for typical problems, introducing typical linear systems concepts of poles and zeros to electromagnetic analysis. It follows that summations of damped sinusoids could be used to approximate the response of some observable. These methods were generalized and published in great number with a plethora of applications. This author, in earlier work [8], used these techniques with some success, showing that certain electromagnetic phenomena could be modeled with such an approximation.

The abstraction of the MBPE model has completely detached the technique from any rigorous mathematical basis. The challenge is that unpredictable behavior, inherent in the model, based on its mathematical heritage/origins is always present.

The earlier statement, "summations of damped sinusoids" is in fact the point of departure into an array of theories, which are in fact linked, though not demonstrated or proven as such, in the literature. Since we know that "separation of variables" approaches do provide solutions to select problems, it begs the question of how modes, such as cavity modes from waveguide theory are related to MBPE. A "separation of variables" technique, also referred to as a Fourier Series or eigenfunction expansion technique, could also support a "summation of damped sinusoids". Is there a common theory? We go on to consider natural frequencies

and natural modes, related to the theory of the Singularity Expansion Method (SEM) [9]. Again, what is the relation? We therefore need to assess the theoretical basis and relationships between spectral expansion methods in their application to the computational efficient solution of our scattering problem.

Finally, we question the relationship between integral equation methods, such as the EFIE used for the SuperNEC numerical model, and the spectral expansion methods. We use operator theory and functional analysis to provide the theoretical framework for this effort.

1.2 Context of the Problem

Consider the following aviation application: International Aviation Authorities have a mandated requirement for aircraft communications, navigation and surveillance for air traffic management (CNS/ATM).

This requirement for Air Traffic Management results in complex suites of avionics hardware that are integrated onto aircraft with complex antenna systems. EMI/EMC and radiation performance are critical to safe qualification of aircraft for use in international airspace. An integral part of the aircraft system design is the placement of antennas for radios, Instrument Landing Systems (ILS), Terrain/Collision-Avoidance Warning Systems (T/CAWS), Global Positioning Systems (GPS) and VHF Omnidirectional Range (VOR) equipment, to name but a few. Each of these systems operates within a specific frequency band, though together occupy frequencies from 100 MHz up into the low GHz range - much of this document is focused on the frequency dependent nature of antenna systems.

These requirements are decomposed into key design requirements or parameters such as radiation patterns, input impedance of antennas, VSWR, coupling, gain and directivity for different bank angles, pitch attitudes and yaw angles. For each antenna, the frequency dependence of these parameters is integral to the design of electronic interface equipment.

Abstracting this design requirement; the design engineer typically mounts radiating or scattering elements on some structure. The radiation and scattering problems are to be considered interchangeable for the analysis in this document. Meaningful "information" is typically phase-, frequency- or amplitude-modulated onto the carrier/resonant frequency of the radiating element. The design parameters of interest, such as radiation patterns and input impedances are *electromagnetic observables*.

1.3 Thesis Outline

This document is divided into 9 chapters; broadly, chapters 2 through 5 address the theoretical development and findings of the research, while chapters 6 through 9 consider application and final conclusions. Three appendices provide additional identities, definitions, derivations and results. Chapter 1 consists of a statement of the problem, and an outline of its significance, noting that this work contains both a theoretical and numerical component.

Chapter 2 presents introductory technical material, introducing the concepts of spectral representation methods through well-understood concepts of Fourier series and modal analysis. A review of the literature follows wherein the abstract Model-Based Parameter Estimation (MBPE) method and its treatment as a generalized Transfer Function Estimation (TFE) method is discussed. Brief overviews of the theory and application of the Eigenmode Expansion Method (EEM) and the Singularity Expansion Method (SEM) follow. A critical analysis, specifically addressing the mathematical foundations and their suitability for application to our radiation and scattering problem is performed.

In chapter 3, we derive the relevant integral equation formulations applicable to scattering and radiation problems for perfectly conducting complex structures. Maxwell's partial differential equations are solved using Green's function methods, leading to electric and magnetic field integral equations. Green's methods and theory are progressively evolved from the scalar through to the dyadic case, proving integral equation representations, such as the electric field (EFIE) and magnetic field integral equations (MFIE), to be useful for solution of the radiation and scattering problem.

Chapter 4 draws together a diverse range of topics in integral theory and functional analysis with a cohesive operator framework treatment. The integral equation formulations from chapter 3 are cast into functional spaces; their characteristics are defined from a functional analysis perspective. In this chapter we focus on analyzing mathematical structure of spaces and operators, including algebraic and topological aspects, in preparation for its application in later chapters. The ill-posedness and non-uniqueness characteristics of the solutions of the integral equations are reviewed, with a survey of regularization methods.

The application of spectral expansions to the electric and magnetic field integral equations for the radiation and scattering problem is presented in chapter 5. Through spectral theory techniques, we establish common theoretical bases, linking together existing methods, such as SEM, with new techniques, such as the "preconditioned" integral equations. Different solution paths are presented, and spectral expansion methods linked; including SEM, EEM, SFM and SVD. Determinant and Fredholm theory is inextricably tied to these common bases.

Chapter 6 examines the application of a specific spectral expansion method to the frequency-domain code SuperNEC; not all expansion methods reviewed in earlier chapters are suitable for this application. The SuperNEC-specific EFIE is used, derived from those in chapter 3. Sobolev space methods are reviewed for the exact and reduced kernel, with determinations made as to applicability for integration into software. The link between SEM, resolvent expansions and MBPE is explored.

The practical aspects of the application of a complex frequency domain parameter estimation technique to the scattering problem are presented in chapter 7. Implementation details of a reduced-order, spectral expansion method suitable for integration into SuperNEC are addressed, including iterative solution methods, formulation of the Method of Moment (MoM) matrix solution and frequency sample placement, to name a few. At completion of chapter 7, simulation parameters and details are defined enabling the 2 and $N + 1$-dimensional TFE method to be used within SuperNEC. Chapter 8 presents the integration details of the TFE module into SuperNEC, the wire-grid structures used for the simulation and the results obtained for two test cases. The iterative sampling strategy is demonstrated in action, followed by an analysis of the computational effort incurred.

The conclusions of the research, contributions to the field and future direction are the subject of chapter 9.

Chapter 2

Select "Physically-Motivated" Parametric Models and Expansion Methods

Physicists and engineers are well-versed in Fourier series analysis, modes propagating in waveguides and concepts of eigenvalues and their application. An intuitive, heuristic approach, based on these principles is provided in this chapter, as a foundation for the thesis.

In section 2.1, we develop an approach to substantiate the value of a physically-motivated model, rather than a "purely mathematical curve-fit". Basis functions are used for approximation of functions, signals and system responses, such that a physically-motivated approximation can be given in terms of an eigenfunction (spectral) expansion. In section 2.2, we segue into the application to electromagnetics of an eigen-representation of Maxwell's equations. The rectangular cavity eigenvalue problem, the scalar representation derived from the vector equations, is considered in section 2.3. Review of traditional eigenvalue theory for the bounded domain problem is extended to the semi-bounded and unbounded problems, within the construct of the specific operator framework. This provides a generalization to open regions and improper eigenfunctions.

In section 2.4, we evaluate prior work on reduced-order models and expansion methods. The first technique, and the most abstracted, is Model-Based Parameter Estimation (MBPE), a reduced-order parametric method, used in both spectral and waveform domains. Relevant applications in the literature are presented, with pertinent questions raised. The concept of the generalized Transfer Function Estimation (TFE) method is briefly reviewed, both in prior application by this author, and in separate publication in the literature; numerical issues are raised for later discussion. The Eigenmode Expansion Method (EEM) is reviewed as a logical formalization of the rectangular cavity methods discussed in section 2.1. The Singularity

Expansion Method (SEM) is introduced - again, our linear superposition of damped sinusoid basis functions is evolved into an applied technique. A brief literature review on the theory and application is provided.

2.1 A Heuristic Approach to System Response Approximation

A physically-motivated approximation of the response of a structure requires using a priori information as to the nature of the structure, be it measured data or theoretical behaviour. This known information, being characteristic of the system, enables a mathematical model to be chosen which maps directly to this information. This section outlines a heuristic approach to substantiate the value of a physically-motivated model, rather than a "purely mathematical curve-fit".

Consider the following approximation problem: *Using a number of discrete samples of an unknown signal, find an optimum analytical description of that signal.* The problem described above has been under scrutiny in physical applications for centuries. It may be viewed from the perspective of approximation theory or system identification. Interpolation or extrapolation of a number of discrete samples is a fundamental approach to this problem in *approximation theory.* Rigorous derivations yield optimum sample placement criteria for various techniques, including polynomial and spline interpolation. The limitation of an approximation theory approach is that it is not dependent on the physical problem itself. A method which models the physics of the underlying problem has greater scope for accurate approximation. This methodology is typically considered to be a *system identification* approach. This is the approach of choice, and accordingly, applied in this text.

2.1.1 The Periodic Signal

Consider a signal which is known to consist of a number of basis functions: the argument will initially deal with the periodic signal and later a generalization to an arbitrary aperiodic signal.

A linear combination of modes to represent some physical quantity was first presented by Euler who examined the harmonically related sinusoidal modes of a vibrating string terminated at both ends. He noted that the configuration of the string at some point in time was a linear combination of these modes, and extended this to the configuration at any subsequent time. The coefficients at two separate times were simply related.

Joseph Fourier found series of harmonically related sinusoids useful in describing the temperature distribution throughout some body [10]. These observations were later extended to

general periodic signals in the form of the Fourier series representation, which expressed a periodic signal as a linear combination of complex sinusoidal basis functions. Fourier claimed that *any* periodic signal, $x(t)$, could be represented with a series,

$$x(t) = \sum_{k=-\infty}^{+\infty} c_k e^{ikw_0 t} \tag{2.1.1}$$

with period $T_0 = \frac{2\pi}{\omega_0}$ and complex Fourier coefficient

$$c_k = \frac{1}{T_0} \int_{-T_0/2}^{T_0/2} x(t) e^{-ikw_0 t} dt \tag{2.1.2}$$

In practice, a periodic signal can be described by a truncated Fourier series, where $-N \leq k \leq N$. The complex Fourier coefficient, c_k, corresponding to a *harmonic* $k\omega_0$, is thus determined by an inner product of $x(t)$ and the complex sinusoid of that harmonic. This coefficient, c_k, is interpreted as the weight of harmonic $k\omega_0$ in the representation of $x(t)$. Given discrete samples of some signal, known only to be periodic, an analytical description of that signal can be found by a Fourier series approximation, assuming there are sufficient samples to account for all the unknowns. The unknowns in the Fourier series approximation (2.1.1) are the complex coefficients and the fundamental period.

Knowing the underlying physical basis of the signal samples in consideration, it is plausible how an approximation based on a series expansion, searching for the unknown coefficients, if you will, would be more accurate than a spline, or least-squares fit to the same samples. The choice and reason for using a Fourier series expansion as our "model" for this introduction will be clear in the next section.

2.1.2 The Aperiodic Signal

The progression of the discussion from the periodic to the *aperiodic* case can be made by noting that a periodic signal denoted $x_p(t)$ can be described by an infinite summation of a *form function*, $x_f(t)$, which is defined from $-T_0/2$ to $T_0/2$,

$$x_p(t) = \sum_{m=-\infty}^{\infty} x_f(t - mT_0) \tag{2.1.3}$$

where T_0 is the fundamental period. Conversely, we may interpret the form function as the periodic signal, "windowed" over 1 period.

The aperiodic signal may be viewed as a periodic signal with an extremely large period, T_0, such that the periodic signal is equal to the form factor signal, $x_p(t) = x_f(t)$. In this case,

the Fourier series coefficient can be represented by

$$c_k = \frac{1}{T_0}\int_{-\infty}^{+\infty} x(t)e^{-ik\omega_o t}dt \tag{2.1.4}$$

Oppenheim [10] recognizes the envelope of $c_k T_0$ as the *Fourier transform* of $x(t)$, such that

$$X(\omega) = \int_{-\infty}^{+\infty} x(t)e^{-i\omega t}dt \tag{2.1.5}$$

The Fourier series coefficients, c_k are thus found by evaluating the envelope at the discrete harmonic, $k\omega_0$,

$$c_k = \frac{1}{T_0}X(kw_0) \tag{2.1.6}$$

and correspond to the frequency content of that harmonic. In the limit as $T_0 \to \infty$, $\omega_0 \to 0$, such that the Fourier transform of $x(t)$ is equal to the envelope given by (2.1.5). By substituting the envelope into the "area" summation of (2.1.1), the summation tends to an integral describing the inverse Fourier transform,

$$x(t) = \frac{1}{2\pi}\int_{-\infty}^{+\infty} X(\omega)e^{i\omega t}d\omega \tag{2.1.7}$$

For aperiodic signals, the approximation problem is more complicated than the periodic signal, as a continuous function in the frequency domain is required to describe the time domain signal.

For a general problem which does not exhibit periodicity, it is therefore still possible to accurately represent some signal with a sum of basis functions which are not necessarily sinusoidal. According to Kreyszig [11], this representation, known as an *eigenfunction expansion* is a generalized Fourier series in which the basis functions are an orthogonal set of eigenfunctions. Sufficient samples of the signal are required to account for the harmonically unrelated (complex) frequency eigenfunctions and the complex coefficients [1].

The restrictions discussed above are motivated by *a priori* information. The suitability of assuming a solution of a particular form is obtained through observation of the characteristics of the system which modulates these input signals to particular outputs. This "physically-motivated" approximation, in terms of an eigenfunction expansion, for example, has a more sound basis than a pure mathematical curve-fit. It is the approach of choice to be used as the basis for reducing the overall computational effort in reaching our wideband response; relating this "physical" motivation to Maxwell's equation is the subject of section 2.2.

[1] The term non-harmonic is frequently used

2.1.3 System Response Perspective

In this section, we review the eigenfunction expansion and an interpretation from a circuits, systems perspective - as either an impulse response or transfer function, as appropriate. It can be shown for a linear, time-invariant (LTI) system that the response to a complex exponential is the same complex exponential, with a change in amplitude [10].

$$e^{st} \rightarrow H(s)e^{st}$$

where in general, $H(s)$ is a function of the complex variable s. This is a well understood concept in linear circuit analysis and synthesis, where some circuit has an excitation and produces a response characteristic of its circuit components. The frequency response of a circuit would be an appropriate frame of reference for the discussions to follow. For some $s = s_\alpha$, $e^{s_\alpha t}$ is the eigenfunction and $H(s_\alpha)$, the eigenvalue. To show this is the case, consider $x(t) = e^{s_\alpha t}$, therefore

$$\begin{aligned} y(t) &= x(t) * h(t) && (2.1.8)\\ &= \int_{-\infty}^{\infty} h(\tau)x(t-\tau)d\tau && (2.1.9)\\ &= \int_{-\infty}^{\infty} e^{s_\alpha t}e^{-s_\alpha \tau}h(\tau)d\tau && (2.1.10)\\ &= e^{s_\alpha t}H(s_\alpha) && (2.1.11) \end{aligned}$$

where $*$ is the convolution operator and $H(s)$ is the Laplace Transform of $h(t)$ given by

$$H(s) = \int_{-\infty}^{\infty} h(\tau)e^{-s\tau}d\tau \qquad (2.1.12)$$

$H(s_\alpha)$ is clearly the response $H(s)$ evaluated at $s = s_\alpha$. From a circuit theory standpoint, $h(t)$ would be the *impulse response* of the system and its transform, $H(s)$, the *transfer function*. For a general linear combination;

$$\sum_k a_k e^{s_k t} \rightarrow \sum_k a_k H(s_k)e^{s_k t} \qquad (2.1.13)$$

Since the system is LTI, the eigenfunctions are complex exponentials and the eigenvalues, complex coefficients. The number of significant harmonic components is typically not known a priori, that is, complex coefficients of those harmonics may all be similar in magnitude. This implies that we may not be able to eliminate harmonics based on coefficient magnitude; this is also applicable to discussions of singular values and eigenvalues (c.f. sections 2.4.3 and 2.4.4). For a linear system, which does not exhibit time-invariance, $H(s)$ is no longer simply a complex coefficient; it will typically contain some time-variance.

Where the samples used for the signal reconstruction are taken from the response of a system to an impulse input, the eigenfunction expansion can be viewed as an *Impulse Response Estimation (IRE)* technique. Clearly, for a general input, which in a discrete system is given by an impulse convolved with some signal, the system response is given by the convolution of the impulse response with the input signal. The complex frequency domain equivalent of impulse response estimation is *Transfer Function Estimation (TFE).*

2.2 Maxwell's Equations - An Eigen Representation

The heuristic prescription of section 2.1 espouses an approach to a physically-motivated approximation of a desired signal or system response, as opposed to a mathematical curve-fit. In keeping with our desires for tieing in the underlying physics of a problem, it follows that we need to more accurately define the problem, as well as advance our conceptual discussions to the specifics of electromagnetics, the subject at hand. Thus far, we have referred to the radiation and scattering problem; this is a logical starting point. It will be followed by a modal-type analysis, as presented earlier for the "general signals".

Maxwell's equations, in practical engineering problems have 3 key areas of application [12, p.1292]:

- Radiation - requires determining the originating sources of the fields.
- Propagation - requires obtaining the fields distant from a known source.
- Scattering - determining the perturbing effects of medium inhomogeneity.

We focus on the radiation and scattering problems in this text, and use them interchangeably; for example, the helicopter numerical models in chapters 7 and 8 are used as scattering targets for incident electromagnetic waves, or as a radiation study, where antennas radiate from the structure.

Miller, in a review of electromagnetic applications, classified various problem types [12, p.1292]

- Solution domain - characterized by time or frequency.
- Solution space - configuration or wavenumber.
- Dimensionality - 1, 2 or 3 dimensions.
- Electrical properties of medium and boundary - dielectric, lossy, perfect conductor, anisotropic, inhomogeneous, nonlinear.

- Boundary geometry - linear, curved, segmented, compound, arbitrary.

The bulk of the work in this text is applied to frequency solution domains, 3 spatial dimensions, perfect electric conductors in isotropic, homogeneous spaces. Boundary geometries are typically piece-wise linear, with thin-wire segmented structures used to construct arbitrarily complex composite bodies.

As mentioned in section 1.2, the application of interest represents a set of requirements; they are decomposed into key design parameters such as radiation patterns, input impedance of antennas, VSWR, coupling, gain and directivity for different bank angles, pitch attitudes and yaw angles. The design parameters of interest, such as radiation patterns and input impedances are *electromagnetic observables*. This catch-all phrase refers to all observables created by driving a radiating or scattering element mounted on some structure.

A general linear field in a homogeneous, stationary medium is described by a linear operator $L\left(\nabla, \frac{\partial}{\partial t}\right)$; L is a function of a spatial and a temporal gradient operator. Maxwell's equations in this source-excited medium can be written in operator form as

$$L\mathbf{\Psi}(\mathbf{r}) = -\mathbf{\Phi}(\mathbf{r}) \tag{2.2.1}$$

For time-harmonic excitation, where the $e^{-i\omega t}$ dependence is omitted,

$$L = -i\begin{bmatrix} \omega\epsilon & -i\nabla\times\mathbf{1} \\ i\nabla\times\mathbf{1} & \omega\mu \end{bmatrix} \quad \mathbf{\Psi} \rightarrow \begin{bmatrix} \mathbf{E}(\mathbf{r}) \\ \mathbf{H}(\mathbf{r}) \end{bmatrix} \quad \mathbf{\Phi} \rightarrow \begin{bmatrix} \mathbf{J}(\mathbf{r}) \\ \mathbf{M}(\mathbf{r}) \end{bmatrix} \tag{2.2.2}$$

where $\mathbf{\Psi}$ and $\mathbf{\Phi}$ are wave and excitation vectors, respectively. For the case of guided waves propagating along the z-axis, symmetry is exhibited along z. Since,

$$\nabla = \mathbf{x_0}\frac{\partial}{\partial x} + \mathbf{y_0}\frac{\partial}{\partial y} + \mathbf{z_0}\frac{\partial}{\partial z}$$

where $\mathbf{x_0}$, $\mathbf{y_0}$, $\mathbf{z_0}$ are unit vectors in the x-, y- and z-directions respectively, a transverse gradient operator can be given by

$$\nabla_t = \nabla - \mathbf{z_0}\frac{\partial}{\partial z} \tag{2.2.3}$$

Operator L can be decomposed into a transverse and longitudinal combination

$$L = -i\left(\Upsilon - \frac{\Lambda}{i}\frac{\partial}{\partial z}\right) \tag{2.2.4}$$

where

$$\Upsilon \rightarrow \begin{bmatrix} \omega\epsilon & -i\nabla_t\times\mathbf{1} \\ i\nabla_t\times\mathbf{1} & \omega\mu \end{bmatrix} \qquad \Lambda \rightarrow \begin{bmatrix} 0 & -\mathbf{z_0}\times\mathbf{1} \\ \mathbf{z_0}\times\mathbf{1} & 0 \end{bmatrix} \tag{2.2.5}$$

Characteristic field vectors are non-trivial solutions of the source-free field equation

$$L\mathbf{\Psi}_\alpha(\mathbf{r}) = 0 \tag{2.2.6}$$

These vectors, known as *modes* or *mode functions* are the basis functions for the construction of the field response, and are excited as a function of the source's characteristics. The modes characterizing the guided wave, with uniform propagation in the z-direction, are of the form

$$\mathbf{\Psi}_\alpha(\mathbf{r}) = \mathbf{\Psi}_\alpha(\boldsymbol{\rho})e^{i\kappa_\alpha z} \tag{2.2.7}$$

where $\mathbf{r} = \boldsymbol{\rho} + \mathbf{z_0}z$ ($\mathbf{z_0}$ is the unit vector in the z-direction, as defined earlier). The corresponding *eigenproblem* is found by substituting (2.2.4) and (2.2.7) into (2.2.6),

$$\Upsilon\left(\nabla_t, \frac{\partial}{\partial t}\right)\mathbf{\Psi}_\alpha(\boldsymbol{\rho}, t) = \kappa_\alpha \Gamma \mathbf{\Psi}_\alpha(\boldsymbol{\rho}, t) \tag{2.2.8}$$

defining eigenfunctions $\mathbf{\Psi}_\alpha(\boldsymbol{\rho}, t)$ and eigenvalues κ_α.

Using the longitudinal and transverse operator representations, the defining equation for the Green's function of a general linear field is

$$-i\left[\Upsilon(\nabla_t, \frac{\partial}{\partial t}) - \frac{\Gamma}{i}\frac{\partial}{\partial z}\right] G(\rho, \rho', t, t', z, z') = \delta(\rho - \rho')\delta(t - t')\delta(z - z') \tag{2.2.9}$$

In terms of (2.2.1), the Green's function is the wave vector corresponding to an impulse excitation occurring at location ρ', z' and time $t = t'$.

2.3 The Rectangular Cavity Eigenvalue Problem

This section presents a guided wave description of the fields confined within a rectangular cavity bounding a homogeneous, stationary medium. Building on the concepts of the eigenproblem with transverse mode functions, the specific solutions to the scalar equations in a cavity are found, in both one- and two-dimensions. Scalarization is applied using separation of variables, a well-known technique for analysis of transverse wave propagation. Concepts of completeness and generalizations for the open cavity are considered in sections 2.3.3 and 2.3.4.

2.3.1 The Scalar Eigenvalue Formulation

The guided wave description enables the overall field to be represented as a superposition of modes of the form $\mathbf{\Psi}_\alpha(\boldsymbol{\rho})\exp(i\kappa_\alpha z)$ [13]. The exponential term accounts for the propagation time-lag along the longitudinal direction. The variable z denotes the guiding axis, along

which propagation of the wave occurs, and κ_α the eigenvalue or wave number of the mode. Note that the $\exp(-i\omega t)$ time-harmonic dependence is implied in these derivations, and that it differs from those defined in Felsen *et al* [13]. The field eigenvector, $\mathbf{\Psi}_\alpha$, depends only on time, t and the $\boldsymbol{\rho}$ co-ordinate, transverse to z. The analysis of the rectangular waveguide can be considerably simplified by a technique known as *scalarization* [13], whereby the vector eigenvalue problem is reduced to a scalar eigenvalue problem. For a cross-section with homogeneous constitutive parameters, scalar eigenfunctions can be introduced which solve a scalar eigenvalue problem. The eigenfields are thus represented by a complete orthonormal set of "guided" eigenfunctions. Further simplification is possible for separable geometries: a 2-dimensional eigenvalue problem can be reduced to 2 1-dimensional problems.

The above representation of total fields in the waveguide is in terms of transverse eigenfunctions $\mathbf{E}_{t\alpha}$ and $\mathbf{H}_{t\alpha}$ and longitudinal components $E_{z\alpha}$ and $H_{z\alpha}$. The transverse nature of the field implies that the z components are derivable from the transverse components. The following decomposition was used

$$\mathbf{E}_\alpha(\mathbf{r}) = \mathbf{E}_{t\alpha} + E_{z\alpha}\mathbf{z_0} \tag{2.3.1}$$

$$\mathbf{H}_\alpha(\mathbf{r}) = \mathbf{H}_{t\alpha} + H_{z\alpha}\mathbf{z_0} \tag{2.3.2}$$

recalling that $\mathbf{z_0}$ is the unit vector in the longitudinal direction, i.e. the direction perpendicular to the travelling guided wave.

The eigenvalue problem has been specified in terms of eigenvectors, $\mathbf{\Psi}_\alpha$ (c.f. equation (2.2.8)), which represent electric and magnetic fields. A more detailed description in terms of eigenvectors, $\mathbf{e}(\boldsymbol{\rho})$ for the electric field and $\mathbf{h}(\boldsymbol{\rho})$ for the magnetic field, is used in this section. Furthermore, the complete eigenvector set for the homogeneous rectangular cavity comprises both TM and TE modes. The electric and magnetic fields in the transverse plane are described by an eigenfunction expansion,

$$\mathbf{E}_t(\boldsymbol{\rho}) = \sum_\alpha V_\alpha^e(z)\mathbf{e}_\alpha^e(\boldsymbol{\rho}) + \sum_\alpha V_\alpha^h(z)\mathbf{e}_\alpha^h(\boldsymbol{\rho}) \tag{2.3.3}$$

$$\mathbf{H}_t(\boldsymbol{\rho}) = \sum_\alpha I_\alpha^e(z)\mathbf{h}_\alpha^e(\boldsymbol{\rho}) + \sum_\alpha I_\alpha^h(z)\mathbf{h}_\alpha^h(\boldsymbol{\rho}) \tag{2.3.4}$$

The superscript, e, denotes that the modal coefficients and eigenfunctions describe the E (TM) modes, while the h refers to the H (TE) modes. It is obvious from this expansion that the TM and TE modes each contain both $\mathbf{e}(\boldsymbol{\rho})$ and $\mathbf{h}(\boldsymbol{\rho})$ mode functions. The exact form of these transverse vector eigenfunctions depends on the geometry and has been defined in Appendix B.2.2 in detail.

The transverse field equations particular to guided waves within a rectangular cavity have been derived for the general, source-excited representation in Appendix B.2.1. In general,

as seen in the transverse field equations, the total field comprises both a longitudinal and transverse component. A particular simplification into E- and H-modes with respect to the z direction (the so-called transverse magnetic (TM) and transverse electric (TE) modes), admits no longitudinal component of magnetic or electric field, respectively,

For the E-modes (TM), the longitudinal component $H_{z\alpha} = 0$, such that the transverse eigenmodes are described by:

$$\nabla_t \nabla_t \cdot \mathbf{e}^e_\alpha(\boldsymbol{\rho}) = -(k^2 - \kappa^2_\alpha)\mathbf{e}^e_\alpha(\boldsymbol{\rho}) \tag{2.3.5}$$

$$\nabla_t \nabla_t \cdot \mathbf{h}^e_\alpha(\boldsymbol{\rho}) = 0 \tag{2.3.6}$$

where $k^2 = \omega^2\mu\epsilon$ and κ_α is the eigenvalue (mode wave number).

For the H-modes (TE), the longitudinal component $E_{z\alpha} = 0$, giving

$$\nabla_t \nabla_t \cdot \mathbf{h}^h_\alpha(\boldsymbol{\rho}) = -(k^2 - \kappa'^2_\alpha)\mathbf{h}^h_\alpha(\boldsymbol{\rho}) \tag{2.3.7}$$

$$\nabla_t \nabla_t \cdot \mathbf{e}^h_\alpha(\boldsymbol{\rho}) = 0 \tag{2.3.8}$$

Noting that any transverse vector can be decomposed into a solenoidal (has no divergence) and irrotational (it has no curl) component, the vector eigenvalue problem can be reduced to a scalar eigenvalue problem. The derivation is given in Appendix B.2.2. The eigenvalue problems for the eigenfunctions, Ψ_α and Φ_α, corresponding to magnetic and electric fields, respectively, are

$$\nabla^2_t \Psi_\alpha + k'^2_{ti}\Psi_\alpha = 0 \qquad \text{in} \quad S \tag{2.3.9}$$

$$\nabla^2_t \Phi_\alpha + k^2_{ti}\Phi_\alpha = 0 \qquad \text{in} \quad S \tag{2.3.10}$$

where $k'^2_{t\alpha} = (k^2 - \kappa'^2_\alpha)$ and $k^2_{t\alpha} = (k^2 - \kappa^2_\alpha)$. The vector eigenvalue problems of (2.3.5) and (2.3.7) have thus been reduced to scalar eigenvalue problems in (2.3.9) and (2.3.10) by scalarization.

2.3.2 Eigenfunctions for the Rectangular Cavity

Consider a cavity which is rectangular in cross-section, extending from $x = 0$ to $x = a$ and $y = 0$ to $y = b$. The scalar eigenvalue equation for the TM modes is,

$$\nabla^2_t \Phi_\alpha + k^2_{t\alpha}\Phi_\alpha = 0 \qquad \text{in} \quad S \tag{2.3.11}$$

Φ_α are mode functions, with boundary conditions $\Phi_\alpha = 0$ on S, if $k_{t\alpha} \neq 0$ and $\partial\Phi_\alpha/\partial s = 0$ on S if $k_{t\alpha} = 0$ [13] and

$$\nabla_t^2 = \frac{\partial^2}{\partial x^2} + \frac{\partial^2}{\partial y^2} \tag{2.3.12}$$

If we assume a solution which is separable, then $\Phi_\alpha(\boldsymbol{\rho}) = \Phi_p(x)\Phi_q(y)$ with boundary condition $\Phi_\alpha(\boldsymbol{\rho}) = 0$ on S. In (2.3.11),

$$\frac{\partial^2}{\partial x^2}\left[\Phi_p(x)\Phi_q(y)\right] + \frac{\partial^2}{\partial y^2}\left[\Phi_p(x)\Phi_q(y)\right] + k_{t\alpha}^2\left[\Phi_p(x)\Phi_q(y)\right] = 0 \tag{2.3.13}$$

Noting the x and y dependencies and dividing through by $\Phi_p(x)\Phi_q(y)$ gives

$$\frac{1}{\Phi_p(x)}\frac{d^2\Phi_p(x)}{dx^2} = -k_{t\alpha}^2 - \frac{1}{\Phi_q(y)}\frac{d^2\Phi_q(y)}{dy^2} \tag{2.3.14}$$

Setting the left hand side equal to k_p^2 gives

$$\left(\frac{d^2}{dx^2} + k_p^2\right)\Phi_p(x) = 0 \tag{2.3.15}$$

Similarly, it can be shown that

$$\left(\frac{d^2}{dy^2} + k_q^2\right)\Phi_q(y) = 0 \tag{2.3.16}$$

where the constants are related by $k_{t\alpha}^2 = k_p^2 + k_q^2$. From the boundary condition, $\Phi_\alpha(\boldsymbol{\rho}) = 0$, it follows that

$$\Phi_p(0) = \Phi_p(a) = 0 \tag{2.3.17}$$

$$\Phi_q(0) = \Phi_q(b) = 0 \tag{2.3.18}$$

The solutions are readily found to be

$$\Phi_p(x) = \sqrt{\frac{2}{a}}\sin(k_p x) \quad \text{for} \quad k_p = \frac{p\pi}{a}, \quad p = 1, 2, 3, \ldots \tag{2.3.19}$$

$$\Phi_q(y) = \sqrt{\frac{2}{b}}\sin(k_q y) \quad \text{for} \quad k_q = \frac{q\pi}{b}, \quad q = 1, 2, 3, \ldots \tag{2.3.20}$$

where the constants have been chosen to normalize the mode sets to unity, i.e.

$$\int_0^a \Phi_p^2(x)dx = \int_0^b \Phi_q^2(y)dy = 1 \tag{2.3.21}$$

The general completeness relation [14] , gives

$$\frac{\delta(\mathbf{r}-\mathbf{r}')}{w(\mathbf{r}')} = \sum_i e_i(\mathbf{r}) e_i^*(\mathbf{r}') \qquad \text{for} \quad \mathbf{r}_1 < \mathbf{r}, \mathbf{r}' < \mathbf{r}_2 \tag{2.3.22}$$

thus relating the dirac-delta function to the eigenfunctions, $e_i(\mathbf{r})$ of the operator L with specified boundary conditions. The general weighting function, $w(\mathbf{r}')$ is determined from the inner-product definition used in the completeness relation. The one-dimensional equivalent of this equation will be used in this section. For the mode functions (eigenfunctions) presented in this discussion, $w(x') = 1$, the eigenfunctions defined by the Φ_p and Φ_q, the operator L, in this case, the transverse Laplacian and the boundary conditions in (2.3.17) and (2.3.18)

$$\delta(x-x') = \sum_p \Phi_p(x)\Phi_p(x') \tag{2.3.23}$$

$$= \frac{2}{a}\sum_{p=1}^{\infty} \sin\frac{p\pi x}{a}\sin\frac{p\pi x'}{a} \qquad \text{for} \quad 0 < x, x' < a \tag{2.3.24}$$

Similarly,

$$\delta(y-y') = \sum_q \Phi_q(y)\Phi_q(y') \tag{2.3.25}$$

$$= \frac{2}{b}\sum_{q=1}^{\infty} \sin\frac{q\pi y}{b}\sin\frac{q\pi y'}{b} \qquad \text{for} \quad 0 < y, y' < b \tag{2.3.26}$$

Therefore, the two-dimensional delta function $\delta(\boldsymbol{\rho}-\boldsymbol{\rho}') = \delta(x-x')\delta(y-y')$ can be expressed in terms of the two-dimensional eigenfunctions,

$$\delta(\boldsymbol{\rho}-\boldsymbol{\rho}') = \sum_\alpha \Phi_\alpha(\boldsymbol{\rho})\Phi_\alpha(\boldsymbol{\rho}') \quad \text{for} \quad 0 < x, x' < a, \quad 0 < y, y' < b \tag{2.3.27}$$

$$= \frac{4}{ab}\sum_{p=1}^{\infty}\sum_{q=1}^{\infty} \sin\frac{p\pi x}{a}\sin\frac{q\pi y}{b}\sin\frac{p\pi x'}{a}\sin\frac{q\pi y'}{b} \tag{2.3.28}$$

Again observing the completeness relation, the 2-dimensional mode function is

$$\Phi_{p,q}(x,y) = \frac{2}{\sqrt{ab}}\sin\frac{p\pi x}{a}\sin\frac{q\pi y}{b} \qquad \text{for} \quad p,q = 1,2,3,\ldots \tag{2.3.29}$$

The transverse wavenumber is

$$k_{t\alpha}^2 = \left(\frac{p\pi}{a}\right)^2 + \left(\frac{q\pi}{b}\right)^2 \tag{2.3.30}$$

A permissible function $F(\boldsymbol{\rho})$ in this rectangular domain is now represented as

$$F(\boldsymbol{\rho}) = \int\int_S F(\boldsymbol{\rho}')\delta(\boldsymbol{\rho} - \boldsymbol{\rho}')dS' = \sum_\alpha F_\alpha \Phi_\alpha(\boldsymbol{\rho}) \tag{2.3.31}$$

or alternately,

$$F(x,y) = \int\int_S F(x',y')\delta(x-x')\delta(y-y')dx'dy' = \sum_\alpha F_\alpha \Phi_\alpha(\boldsymbol{\rho}) \tag{2.3.32}$$

which implies that the modal coefficients, F_α, are given by

$$F_\alpha = \int\int_S F(\boldsymbol{\rho}')\Phi_\alpha(\boldsymbol{\rho}')dS' \tag{2.3.33}$$

2.3.3 Observations

The summation in (2.3.31) is an eigenfunction expansion representation of a permissible function $F(\boldsymbol{\rho})$ with a discrete mode spectrum and proper eigenfunctions. The separable geometry of the rectangular waveguide has enabled one- and two-dimensional eigenfunctions and their eigenvalues to be simply related. The geometry itself is responsible for the discrete eigenvalue spectrum and the form of the eigenfunctions. Variations in geometry are considered later.

Considering the more general problem of an eigenfunction expansion, the signal of interest is again represented by a summation of eigenfunctions, weighted by the "Fourier" coefficients. The particular problem of the rectangular cavity exhibits discrete eigenvalues, which may be interpreted in the same way as the $k\omega_0$ terms in the complex exponential eigenfunctions of the standard Fourier series. An eigenvalue spectrum is also used in representing the "spectral content" of some signal. The spectral representation of the delta function at some point x' is obtained through a modal coefficient which is the inner-product of the eigenfunction with the delta function, which evaluates to the same eigenfunction evaluated at x' (the sifting theorem). The representation of the delta function by the completeness relation is not obvious, requiring a short discussion of how the delta function is obtained. Consider the one-dimensional eigenfunctions in the x-domain $0 \leq x \leq a$ for representing $\delta(x - x')$. From (2.3.24), with

$x' = a/2$,

$$\delta(x - a/2) = \frac{2}{a}\sum_{m=1}^{\infty} sin\frac{m\pi}{2} sin\frac{m\pi x}{a} \tag{2.3.34}$$

$$\approx \frac{2}{a}\sum_{m=1}^{J} sin\frac{m\pi}{2} sin\frac{m\pi x}{a} \tag{2.3.35}$$

$$= \frac{2}{a}\left(sin\frac{\pi x}{a} - sin\frac{3\pi x}{a} + sin\frac{5\pi x}{a} \ldots sin\frac{J\pi x}{a}\right) \tag{2.3.36}$$

where a finite summation to J terms is used to computationally verify the representation. The spectral representation of the delta function at $x' = a/2$, for $a = 4$ units is approximated in figure 2.1. Note that as $J \to \infty$, the central lobe at $a/2$ will become infinitely high and infinitely narrow, with an area of 1: this defines the dirac-delta function, according to Laurent Schwarz' Theory of Generalized Distributions [15].

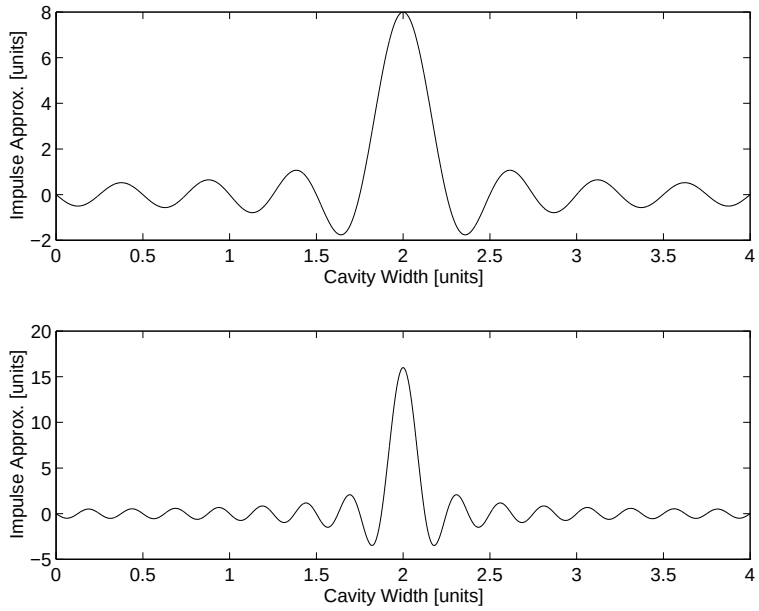

Figure 2.1: Spectral Representation of the dirac-delta function, per the finite summation in (2.3.36). Top figure: J = 15. Bottom figure: J = 31.

2.3.4 Open Region Generalizations

An open region exists when one or more of the domain endpoints of the formulation are at infinity. For an operator L and these boundary conditions, the eigenvalue problem is more complicated, specifically as the discrete eigenvalue spectra become a continuous spectrum. Eigenfunctions are then known as *improper*, since the normalization procedure of the mode

set admits an undefined integral [16, 13]. Solution of the problem requires a characteristic Green's function procedure (c.f. section B.1).

A Semi-Infinite Rectangular Region

The treatment of the semi-infinite rectangular region problem presented by Felsen *et al* [13], Rozzi [17] and Collin [18, pp. 800-830] are comprehensive in their treatment of continuous eigenvalue spectra introduced by open region boundary conditions. A brief explanation derived from this reference provides a suitable introduction to the problem of continuous eigenfunction expansions.

For the rectangular region bounded in both the x and y dimensions, the eigenvalues were discrete (c.f. equations (2.3.19) and (2.3.20)). Considering the differential equation in the x-dimension alone, the discrete eigenvalues were given by $k_p = p\pi/a$. Using the notation of Felsen *et al* [13], the m-th eigenvalue is denoted ξ_m, with the separation between 2 consecutive eigenvalues $\Delta\xi_m = \xi_{m+1} - \xi_m = \pi/a$. For an open region in the x-dimension defined as $a \to \infty$, the separation between consecutive eigenvalues tends to 0. The eigenvalue spectrum thus tends to a continuous form.

The completeness relation for the mode set of the semi-infinite problem in the x-domain is derived from the rectangular boundary problem completeness relation given in (2.3.24) as

$$\delta(x - x') = \lim_{\Delta\xi_m \to 0} \frac{2}{\pi} \sum_{\xi_m = \Delta\xi_m}^{\infty} \sin(\xi_m x) \sin(\xi_m x') \Delta\xi_m \tag{2.3.37}$$

$$= \frac{2}{\pi} \int_0^{\infty} \sin(\xi x) \sin(\xi x') d\xi \quad \text{for} \quad 0 < x, x' < \infty \tag{2.3.38}$$

Comparing this with (2.3.23), the continuous eigenfunctions are

$$\Phi_\xi(x) = \Phi(\xi, x) = \sqrt{\frac{2}{\pi}} \sin \xi x \quad \text{for} \quad 0 < \xi < \infty \tag{2.3.39}$$

The interpretation of the spectral representation of the delta function for the semi-infinite rectangular region is a logical extension of that of the bounded rectangular cavity. Since the eigenvalue spectrum is now continuous, the summation becomes an integral over the eigenvalue range.

2.4 Prior Work on Spectral Representation/Expansion Methods

This chapter has presented a systematic, intuitive development of expansion representations for required signals, functions or observables. The heuristic approach to system responses, and more specifically, fields defined by Maxwell's equations enables us to comprehend the significance of the underlying physics of a problem being useful in some reduced-order mathematical model. We know that superpositions of modes can be used to define fields within a rectangular cavity, and that our discrete eigenvalues "become continuous" as we open our waveguide boundary. The spectral characteristics of eigenvalues and eigenfunctions, such as completeness relations and Fourier-type expansions are clearly useful in field approximations.

We now look to the specific literature on Model-Based Parameter Estimation (MBPE), Transfer Function Estimation (TFE), Eigenfunction Expansion Methods (EEM) and the Singularity Expansion Method (SEM); these methods are in fact inextricably linked. It is known that SEM and EEM are related, as discussed later. MBPE, however, exists as a standalone application or methodology in the literature - a fact that is exploited in this document.

2.4.1 MBPE - an Abstract Tool

Model Based Parameter Estimation (MBPE), a term introduced by Miller and Burke [19], involves "fitting physically motivated approximations to accurately computed or measured electromagnetic quantities from which unknown coefficients (the model parameters) are numerically obtained".

Most EM problems are formulated in the time or frequency domain, with generic descriptions of pole and exponential series related by a Laplace transform pair. Miller [7] extended this transform pair to generalized Spectral domain and Waveform domain forms, with defining equations,

$$\begin{array}{rrcl} & F(X) = F_p(X) + F_{np}(X) & = & \sum_\alpha \frac{R_\alpha}{X - s_\alpha} + F_{np}(X) \quad \text{for} \quad \alpha = 1, 2, \ldots, P \\ \text{and} & f(x) = f_p(x) + f_{np}(x) & = & \sum_\alpha R_\alpha e^{s_\alpha x} + f_{np}(x) \quad \text{for} \quad \alpha = 1, 2, \ldots, P \end{array}$$

respectively. 'x' represents the waveform domain independent variable, and 'X' the spectral domain equivalent. The 'p' subscript denotes the component of the response which contains poles and residues alone. The 'np' subscript denotes the non-pole components, which are typically constants or a combination of zeros [2]. In most applications in the literature, only the pole components are considered, in which case, we can write a simple rational function

[2] Derived from the Mittag-Leffler expansion and are often referred to as entire function contributions.

expression

$$H(s) = \frac{N(s)}{D(s)} = \frac{b_0 + b_1 s + \ldots + b_n s^n}{a_0 + a_1 s + \ldots + a_d s^d} \tag{2.4.1}$$

where the a_n and b_n coefficients are to be determined. Both the spectral and waveform domain MBPE formulation has seen specific application within the computational electromagnetic literature, however, the former is of primary interest in this document. The spectral domain formulation is recognized as an abstract spectral representation or expansion method.

Application in the Literature

A variant of MBPE, using Cauchy's method has been presented by several authors [20, 21, 22], to extrapolate and/or interpolate a narrowband set of system data to a broadband set of data. Kottapalli [22] considered scattering from a perfectly conducting cylinder using a Method of Moment (MoM) formulation. Frequency derivative data and Cauchy's technique were applied to the rational function approximation of the MBPE; this work utilized a basic analytic continuation principle. Traditional MBPE implements a Taylor-series, Padé expansion near a singularity. Cauchy's method differs from "traditional MBPE methods" in that the unknowns are determined using a singular value decomposition (SVD) and a method of least squares.

Application of MBPE to several types of problems, including the following, has been published:

- Radar Cross Section (RCS) of a sphere and a flat plate in frequency domain [21].
- Scattered far fields from square and slit cylinders [22, 23].
- Dipole, monopole (on a ground plane) and forked monopole [24].
- Modelling far-field angle variations, using a Prony Method in the spatial domain [25].
- An approximation of the input impedance of a helical antenna [26, 27].
- Acoustic backscattering problems from a circular cylinder [26, 28].
- A three-element Yagi array for calculating radiation patterns in the spatial domain [29].
- Design of a corrugated horn [30], and
- Estimation of a dielectric resonator input impedance and radiation patterns [31].

In general it was observed that accuracy was good, with a significant reduction in calculation time for large computational domains and reduced memory overhead for storage of matrix entries. With papers published as recently as 2006, it is clearly a popular contemporary

technique. As a point of reference with respect to unique contributions of this work, the papers [31], [32] and [33], together present results that are comparable in complexity to the work presented by this author in Chapter 8.

Critical Review/Observations

MBPE has seen considerable application in the literature in the last 15 years, a small subset of which was listed earlier. This author also performed theoretical and numerical analysis on the topic [8, 34] for complex real-world problems, as opposed to the simple and canonical problems listed in the prior section. What is interesting is that MBPE, in its abstracted form has been separated from its mathematical roots. Consider the following questions and observations:

1. For the approximation shown in figure 2.2, an MBPE implementation by this author [8], using a Prony technique. What caused the spike? Was this due to an ill-conditioned matrix that is an artifact of the Padé method? Or perhaps the MoM discretization of the underlying integral equations being used?

2. Would a frequency-domain rational function approximation be valid for an EFIE and/or an MFIE? More specifically, would the approximation be valid when applied to the thin-wire kernel electric field equations used in Method of Moments (MoM) solutions in SuperNEC?

3. Certain authors have used Singular Value Decompositions (SVD) [20, 21, 22] - is this a requirement, and if so, under what mathematical condition?

4. Is there a relation between pole/zero locations and the nonuniqueness problems of integral equations used to formulate frequency-domain Method of Moment solutions?

5. No reference is made to the Singularity Expansion Method (SEM) in any MBPE paper since and including that of Miller and Burke [19]. It will be shown in this document that the SEM is in fact a key component of the underlying mathematical basis of MBPE.

6. If this truly is a "smart curve fit", based on the physics of the underlying problem [35], then how is it the we take that into account. This author contends that MBPE as applied in the literature is truly just a curve-fit, with as much insight into the underlying problem as would be used in applying a spline fit.

The application of a frequency-domain rational function method requires that additional questions be answered, including:

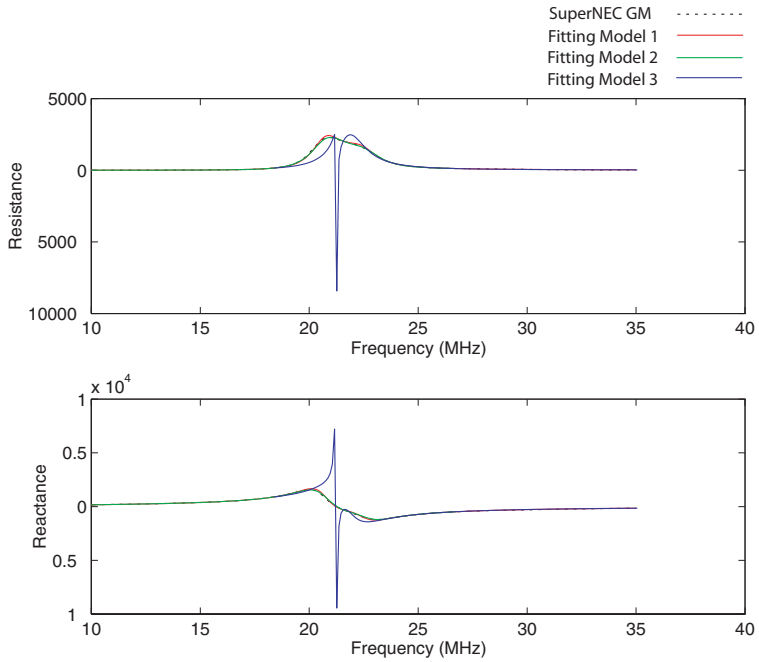

Figure 2.2: An attack helicopter segmented at 25 MHz. Multiple MBPE Models applied

- The suitability and optimization of a rational function approximation for complex and highly resonant structures.
- The relationship between numerator and denominator orders and their impact on the accuracy of a matrix-based solution for the rational function unknowns.
- The suitability of an adaptive sampling technique for evaluating a response over an arbitrarily large bandwidth.
- The effectiveness of incorporating a complex frequency domain method into a frequency domain MoM code, such as SuperNEC.
- The scope for extending the rational function approximation from a 2-dimensional frequency domain optimization problem to that of a segment by segment N-dimensional rational function approximation.
- The exact relations between MBPE and the Singularity Expansion Method, w.r.t multiple poles, entire function contributions and frequency dependence of coefficients.

The design instrument which emerges after the resolution of these issues that is capable of calculating a feasible model over any frequency band is referred to as the Transfer Function Estimation (TFE) module (see Chapter 7).

2.4.2 Transfer Function Estimation

The rational function approximation in equation (2.4.1) is similar to that used in control and systems theory for pole-zero analysis and begs the question as to whether this method can be used as a Transfer Function Estimation (TFE) technique. We can therefore adopt a system response perspective, as in section 2.1.3, where the transfer function embodies the effect of the electromagnetic field perturbation created by some structure. In this case, $H(s)$ is a Generalized System Function or Transfer Function.

TFE allows for the modelling of the complex frequency response of an electromagnetic structure [3], given a set of real frequency data, by a representation of poles and residues in rational function form. The subject of a Generalized System Function being constructed by MBPE is not new. This author, in previous work considered the application of MBPE (as part of a much broader analysis) for the wideband approximation of electromagnetic responses for scattering from complex structures. A dissertation on Transfer Function Estimation [34] was submitted and examined in 2003. A subsequent paper by Li [33] presents the generalized system function, $H(s)$, associated with radiated and scattered fields, using it to analyze interior and exterior resonances of antenna and scattering systems. Li [33] contends that accurate scattered fields are calculated by eliminating poles corresponding to interior resonances from H(s).

The interior resonance problem addressed by Li *et al* in their recent paper [33] raises the same questions of the mathematical origins of the MBPE as mentioned in the prior section. The focus of that paper is to eliminate poles due to interior resonances - this sounds correct in principle, however, since the underlying equations are not examined, the conclusions are incorrect. The ill-posedness of the equations at hand are fundamental, and discussed at length in the literature. The uniqueness problem is one component of a larger issue on ill-posedness of the integral equations related to the scattering and radiation problems. Section 4.5 analyzes the electric and magnetic field integral equations that are derived in chapter 3. Li doesn't qualify that the specific uniqueness issue is in fact dependent on the nature of the integral equation formulation; it only applies to the EFIE (c.f. section 4.5). Canning has presented solutions based on a Singular Value Decomposition (SVD) where "troublesome" interior modes can be eliminated; SVD is considered in relation to other expansions in Chapter 5. Reference earlier questions on the necessity of using SVD (c.f. section 2.4.1). The reader should appreciate that there is a possibility of common theoretical bases here.

This chapter has been framed from two perspectives; firstly, we have considered abstract system identification approaches, the MBPE and Transfer Function Estimation methods. Secondly, we reviewed an abstract eigenfunction approach where spectral expansions could

[3] A structure which contains or subtends an electromagnetic radiating element is referred to as an *electromagnetic structure*, in this document.

be used to provide a reduced-order model. It is appropriate, as part of a review on prior work, that we consider the specific techniques of the Eigenmode Expansion Method (EEM) and the Singularity Expansion Method (SEM), which follow from our intuitive spectral approach. The next two sections explore these methods in the literature.

2.4.3 The Eigenmode Expansion Method

The heuristic introductions of sections 2.1 through 2.3 used linear superposition of basis functions, such as complex exponential terms, giving eigenfunction expansions for a desired signal or system response. Modal theory, a small slice of which was reviewed in our rectangular cavity example, is used extensively, with many famous text books authored on the subject. With this generic framework in place, we look to a subset of the theory that applies to our scattering problem, and the body of literature that applies to this specialization, known as the Eigenmode Expansion Method (EEM). A term first coined by Baum [9] for the electromagnetic literature in 1971, the EEM eigenfunction expansion was applied in various engineering applications in the 1970s before becoming subject to more rigorous mathematical analysis. Ramm, the most noted contributor [36, 37, 38], presented more rigorous mathematical theory of the scalar EEM for the scalar scattering problem.

Baum [39] introduced the Eigenmode Expansion Method (EEM) of the general form

$$\langle \Gamma(\mathbf{r}, \mathbf{r}'; s); \mathbf{R}_\beta(\mathbf{r}, s) \rangle = \lambda_\beta(s) \mathbf{R}_\beta(\mathbf{r}, s) \tag{2.4.2}$$

$$\text{and} \quad \langle \mathbf{L}_\beta(\mathbf{r}, s); \Gamma(\mathbf{r}, \mathbf{r}'; s) \rangle = \lambda_\beta(s) \mathbf{L}_\beta(\mathbf{r}, s) \tag{2.4.3}$$

where β is the eigenmode index, as in (5.2.18) and $\mathbf{R}_\beta(\mathbf{r}, s), \mathbf{L}_\beta(\mathbf{r}, s)$ the complex frequency-dependent eigenmodes, corresponding to eigenvalue $\lambda_\beta(s)$. The Fourier integral and Fourier series forms developed earlier in this chapter are clearly analogous to these equations. Baum [39] has presented relationships between the SEM and EEM., showing relationships between groupings of natural frequencies to eigenvalues and natural modes to eigenmodes. The EEM is explored in much more detail in section 5.2.3.

The methodology for representing eigenmode expansions follows that of sections 2.2 and 2.3 very closely, and we can deduce that the EEM method proposed by Baum in [9] is a specialization of the modal techniques used by many authors, including Collin [18] and Felsen [13]. The assumptions used expose the potential limitations of the method, and will require validation before use.

The EEM has been under some mathematical scrutiny due to its formulation lacking mathematical rigor. In particular, Ramm [37, 38] criticized the weak mathematical footing of this method, calling into question the validity of the expansion given the nature of nonselfadjoint

operators. In analyzing the scalar radiation problem, Ramm made astute observations regarding this method. For finite dimensional spaces $\mathbf{R}^N$, the root system of a linear operator forms a basis. The general expansion of the form $\sum_j \lambda_j^{-1} c_j \, f_j$ may not be valid for an operator on some Hilbert Space, because root vectors are not taken into account. Ramm, in previous work [38], pointed out that if the operator of interest is nonselfadjoint, that it is not obvious that the operator has any eigenvalues.

Questions that arise, needing to be addressed, are:

1. Does EEM using Picard's method, apply to the integral equation form used in SuperNEC? Given that series of basis functions form a complete set for a selfadjoint operator, and require root vectors (and more analysis) for the nonselfadjoint case, which approach applies?
2. Assuming the operator of interest is nonselfadjoint on a Hilbert Space H, does it have a root system which forms a basis of H?
3. When does the set of eigenvectors of our operator form a Riesz basis of H?
4. If the set of eigenvectors does not form a Riesz basis, what about a Riesz basis with brackets? Is this of any significance?
5. How do Riesz bases relate to the concepts we have already discussed, such as orthonormal bases, or Schauder bases?

Clearly, the observations Ramm has made, and the questions we ask are applicable to the specific operators and integral equations defined for our scattering problem. It is more complex, in that we have first and second kind equations admitting vector and dyadic terms, with more complex kernels.

2.4.4 The Singularity Expansion Method

The History of the SEM

The SEM method was first presented by Dr.Carl Baum [9] and later formalized by Marin *et al* [40] in May 1972, who proposed a representation of transient scattered fields in terms of free oscillations of bodies. This formulation of magnetic field intensity, in integral operator form, showed the operator inverse to be an analytic function of the complex wavenumber k, except at certain singularities, where it had poles. The approach found its origins in 2 places:

- The theoretical analyses of canonical problems, with the aim being to determine natural oscillations particular to the structures considered. Pocklington [41] calculated the

oscillations of a thin wire bent into a circular ring. Oseen [42] calculated oscillations of a straight thin wire, and Hállen [43] the fundamental oscillation of a thin wire represented by an integral equation of the first kind. Prolate spheroids and perfectly conducting spheres were solved analytically by Abraham [44] and Stratton [45], respectively.

- *Observations* of induced currents and scattered fields seemingly describable by exponentially damped sinusoidal oscillations. Experimental observations of the transient response of complicated scatterers, such as missiles and aircraft led to the development of the SEM formalism [9]. Experimental results to excitations of antennas were presented by Ross [46] and Schmitt *et al* [47].

Compounding analytical difficulties in finding these oscillations, the response to an arbitrary excitation had proved intractable.

Applications of the SEM

The first canonical problem used in the numerical validation of SEM, as presented in the open literature, was that of the thin wire, analyzed by Tesche [48]. He calculated the exterior natural resonant frequencies of the thin wire from an integral equation formulation of the scattering problem. Umashankar *et al* [49] extended this work to the case of an L-shaped wire, which was characterized by a Hállen-type integral. It was observed that the pole patterns for the L-shaped wire closely followed those of the original thin wire. It was also noted that the bend had relatively small effect on the distribution of the currents on the wire. To test the SEM in its application to image-type problems, Umashankar *et al* [50] considered the problem of scattering by a thin wire parallel to a ground plane. The natural frequencies were found to be very close to the natural frequencies of the same thin wire in free space. As the wire was moved closer to the ground plane, the poles were found to spiral around the free space pole.

SEM has been applied to many problems from as early as the 1970s till today. A very few of these, that were more significant are:

- The SEM applied to perpendicular crossed wires (a basic aircraft model) [51]
- Thin wire transient analysis with types of coupling coefficients [52].
- The transient response of cylindrical dipole antennas [53].
- In the application to target detection [54].
- Radar cross-sections of thin-wire targets [55]

- Far-field responses of step-excited linear antennas [56].
- Representation of the early and late time fields scattered from wire targets [57].
- Application to a matrix-pencil method for both time and frequency domain representations for antennas [58]

Critical Review and Observations

SEM builds on the concept of natural frequencies and natural modes corresponding to "free oscillations". We consider therefore, the homogeneous equations for the scattering problem, defined in terms of an impedance (dyadic) operator, $\Gamma(\mathbf{r}, \mathbf{r}'; s_\alpha)$ and mode vectors, $\mathbf{M}_\alpha, \mathbf{C}_\alpha$.

$$\langle \Gamma(\mathbf{r}, \mathbf{r}'; s_\alpha); \mathbf{M}_\alpha(\mathbf{r}') \rangle = 0 \tag{2.4.4}$$

and

$$\langle \mathbf{C}_\alpha(\mathbf{r}); \Gamma(\mathbf{r}, \mathbf{r}'; s_\alpha) \rangle = 0 \tag{2.4.5}$$

where $\Gamma(\mathbf{r}, \mathbf{r}'; s_\alpha)$ is the kernel of the Fredholm integral equation defined in chapter 3, evaluated at $s = s_\alpha$. $\langle \cdot, \cdot \rangle$ is the usual inner product, as defined in chapter 4. This follows of course from the general integral equation for the excitation $\mathbf{V}(\mathbf{r}, s)$

$$\langle \Gamma(\mathbf{r}, \mathbf{r}'; s_\alpha); \mathbf{I}(\mathbf{r}', s) \rangle = \mathbf{V}(\mathbf{r}, s) \tag{2.4.6}$$

Expanding this integral equation near $s = s_\alpha$ using the Taylor and Laurent series formula, the required spatial current distribution is

$$\mathbf{I}(\mathbf{r}, s) = \sum_\alpha \frac{\eta_\alpha(s)\mathbf{M}_\alpha(\mathbf{r})}{(s - s_\alpha)^{m_\alpha}} + \mathbf{I}'(\mathbf{r}, s) \tag{2.4.7}$$

The second term, $\mathbf{I}'(\mathbf{r}, s)$, corresponds to the analytic power series expansion of (B.7.8), often referred to as the *entire function contribution.* $\eta_\alpha(s)$ is the coupling coefficient, defining the strength of the natural oscillation in terms of the object and incident wave parameters. Detailed derivations are provided in Appendix B.7. m_α defines the multiplicity of the poles.

A number of key observations can be made and questions posed regarding the SEM in this electromagnetic application.

- Dolph [59] observed that many of the papers on SEM were difficult to interpret mathematically, since neither the properties of the integral operators, nor the space in which solutions are sought were specified.

- Solutions and SEM representations for integral equations of the first kind were purported to facilitate easier numerical solution, without considering the ill-posed nature of the equations of the first kind.
- There are questions regarding compactness of first-kind integral operators and therefore the applicability of solution methods. This suggests the possible need for regularization prior to analysis by Fredholm methods.
- Dolph [59] showed that the natural frequencies in the SEM consisted of 2 non-intersecting sets of "wavenumber parameters"; the interior resonant frequencies on the negative imaginary axis and a set in the left-hand half plane.
- Dolph and Ramm [37, 38] found solutions for current components tangential to the surface and in an L^2 space, i.e. they are Lebesgue-square integrable. In other applications, Hölder-continuous spaces are required. Do these requirements/spaces differ for the EFIE and MFIE? Furthermore, would these spaces lend themselves to a viable computation scheme?
- Is there a practical integration approach for applying an SEM approach within SuperNEC, while still maintaining the integrity of the SuperNEC formulation?
- What is the relationship between SEM and other expansion methods in modes, eigenfunctions and singular functions?
- Are there specific requirements on the integral operator for a valid SEM to apply? Does it need to be of the first kind, second kind, Hilbert-Schmidt, Carleman?
- Is the SEM approach a feasible method for complex structures, as opposed to the simple problems reviewed in the previous section? Does application of a Method of Moments discretization or a wire-grid segmentation corrupt the solution, or is this incidental to the underlying sound mathematical basis?

We can clearly conclude that attention to the mathematical basis of MBPE, SEM and EEM is required. The choice of functional space for analysis is important, as are the operator characteristics of the integral and differential operators. The characteristics of integral equations with respect to uniqueness and ill-posedness have been considered in the literature and need to be addressed as part of the mathematical basis for integration of spectral expansion methods into SuperNEC.

2.5 Conclusions

Sections 2.1 to 2.3 of this chapter presented an intuitive development of "expansions" being used in the approximation of a signal or the response of a system. Section 2.2 discussed a guided wave eigen-representation, derived from a source-free consideration of Maxwell's equations. One of the best recognized canonical problems for the analysis of modes is the rectangular cavity. The discrete eigenvalue spectrum was noted to become continuous for a domain end point stretching to infinity, for the guided wave rectangular cavity problem in section 2.3. Eigenfunction expansions are suitable for the description of the characteristic radiation and scattering properties of a much larger class of structures than those separable geometries presented in section 2.3. This chapter presented an extension of these concepts to a general formulation suitable for a description in terms of singularities and natural modes; these would clearly be dependent on the geometry itself. Structures modeled by thin wire segments in an unbounded homogeneous space are considered; the separable geometry and bounded domain spaces no longer apply.

In section 2.4, we reviewed the existing literature with respect to 4 methodologies or formulations that would be applicable to reduced-order approximations for this electromagnetic problem. The review includes applications of these technologies and presents series of questions regarding applicability and implementation. Model Based Parameter Estimation (MBPE) was introduced in section 2.4.1 as an estimation platform containing 2 generic forms: a spectral and waveform domain approximation. MBPE has seen widespread application in the electromagnetic community, though typically for "simple" implementations and canonical problems. In the critical review of section 2.4.1, we explored the contention that MBPE has largely been applied as a mathematical curve-fit, having lost its link to the underlying physics. Relations to EEM, SVD, SEM and a sound mathematical basis are not explored in the literature; these issues are addressed in this document. Transfer Function Estimation is another abstraction, based on the rational-function approximation used for the spectral domain MBPE. TFE was used by other authors in identifying poles and zeros that produce spurious resonances - and eliminating them. The topic of ill-posedness of the integral equations used for our scattering problem will be considered in more detail in chapter 4, however, it was noted that faulty conclusions were presented by at least one author, due to the weak mathematical basis in the equation formulation.

The linear superposition of basis functions, presented in the early sections of the chapter, was evolved into the Eigenmode Expansion Method (EEM) in section 2.4.3. A formal analysis for the exterior scalar scattering problem was presented with questions regarding existence, completeness and orthonormality of bases for the case of nonselfadjoint operators. This method has significant question related to applicability to EFIE and MFIE (nonselfadjoint) operator equations.

The Singularity Expansion Method (SEM) was presented in section 2.4.4; it is a formulation that is based on the analytical properties of the electromagnetic response as a function of the two-sided Laplace Transform variable s, the complex frequency. The SEM formulation is defined in terms of natural modes and coupling coefficients which are numerically obtained using the methods discussed later, in section 6.2.3. The observations of induced currents and scattered fields being described by linear combinations of exponentially damped sinusoidal oscillations, supported by the theoretical representations of canonical problems in terms of natural frequencies, formed the origins of the SEM.

Chapter 3 is largely dedicated to the integral equation theory necessary for the analysis of the radiation and scattering problems for complex structures modeled with perfectly conducting surfaces. Green's methods form the foundation with a logical development from the basic static problem, through the scalar, vector and dyadic inhomogeneous wave equations problems.

Chapter 3

Integral Equation Methods

In addressing the key issues of a weak theoretical and mathematical foundation of spectral representations, in this chapter we derive the relevant integral equation formulations for our scattering and radiation problem. The separation of variables approach, used in the prior chapter for the rectangular cavity guided wave formulation is not helpful for the general radiation and scattering problem. The solution of partial differential equations by Integral Equation Methods is an extensive field of study; this chapter addresses the solution by Green's Function methods, for the scalar, vector and dyadic cases, respectively. In section 3.1 we introduce the Green's function method with potential theory as the basis, considering the fundamental problem of electrostatics, solving Poisson's equation. Dirichlet and Neumann conditions are defined and multiple subdomains considered. We build on these foundations in section 3.1.3 with the solution of the scalar wave problem, defined as an inhomogeneous scalar wave integral equation; the mathematics of Green's functions and Green's theorem are evolved. The surfaces and regions constructed are consistent with those in all radiation and scattering problems reviewed in this document.

Section 3.2 reviews derivations of frequency-domain (time harmonic) integral equations in vector and dyadic form specific to the general radiation and scattering problem for a perfectly conducting body; specific reduction of these equations to the magnetic field integral equation (MFIE) and electric field integral equation (EFIE) form used in SuperNEC is given. The Direct integration method, leading to a Stratton-Chu representation is also given. This is used extensively in chapters 4 and 5 for Spectral Expansion methods. A review of integral equation theory applied to the Electromagnetics field would not be complete without dyadic analysis. As the chapter develops, Green's formula is used in successively complex form, from the scalar through to the dyadic form. The dyadic form does present problems related to the so-called *source dyadic*, due to the dyadic mathematics near the source singularity. The dependency on the shape of the source region, and a treatment of the dyadic approach is given in section 3.2.2.

3.1 Potential Theory, Green's Theorem, Scalar Wave and Helmholtz Equations

This section presents a progressive analysis of integral equation theory from the static case, through the scalar wave equation and to the vector wave equation. Dyadic analysis is also applied, with particular attention paid to the different formulation paths and the complications associated with the source dyadic.

3.1.1 Potential Theory Preliminaries

Consider a homogeneous medium, bounded by a closed surface, S_{inf}, enclosing a volume V_{inf}. The set of all points within V_{inf} are considered interior points, and the complement set, exterior to V_{inf} (i.e. outside bounding surface S_{inf}).

At arbitrary interior points we have a distribution of charge, specified in terms of charge per unit volume. We use scalar function of position (scalar point-function), charge density $\varrho(\mathbf{r})$, defined at a point $\mathbf{r} \in V_{inf}$ with respect to an arbitrary origin. This charge distribution results in some static electric field, $\mathbf{E}(\mathbf{r})$ throughout V_{inf}. The scalar potential function, $\phi(\mathbf{r})$, defines the potential in terms of the work required to bring a positive test charge from infinity to point $\mathbf{r}$ against the effect of the electric field, $\mathbf{E}(\mathbf{r})$.

$$\phi(\mathbf{r}) = \int_{-\infty}^{\mathbf{r}} \mathbf{E}(\mathbf{r}).\ d\mathbf{l} \tag{3.1.1}$$

Stratton [45, p.162] defines the fundamental problem of electrostatics to be that of determining a function $\phi(\mathbf{r})$ that satisfies *Poisson's equation* for every point in space, $\mathbf{r} \in V_{inf}$. In a homogeneous medium, the scalar potential $\phi(\mathbf{r})$ is related to charge density $\varrho(\mathbf{r})$ by Poisson's equation,

$$\nabla^2\phi(\mathbf{r}) = -\frac{\varrho(\mathbf{r})}{\epsilon} \tag{3.1.2}$$

where ϵ denotes the permittivity of the homogeneous medium. This equation requires that $\phi(\mathbf{r})$ be twice continuously-differentiable, and $\varrho(\mathbf{r})$ bounded and piecewise continuous. In source-free regions, this inhomogeneous partial differential equation can be reduced to the homogeneous *Laplace's equation*

$$\nabla^2\phi(\mathbf{r}) = 0 \tag{3.1.3}$$

The requirement is to find $\phi(\mathbf{r})$ for all $\mathbf{r} \in V_{inf}$. This basic problem in Potential Theory has been thoroughly analyzed in the literature for most of the last century, with some of the foremost works being those of Kellogg [60] and Stratton [45, p. 554-563]. In elementary electrostatics, we enclose all charge within the homogeneous medium by a surface S_T, enclosing

V_T. It is well known that the solution to this equation is

$$\phi(\mathbf{r}) = \frac{1}{4\pi\epsilon}\int_{V_T}\frac{\varrho(\mathbf{r}')}{|\mathbf{r}-\mathbf{r}'|}\,dv' \tag{3.1.4}$$

where the integration is performed over all source volumes, dv'. The singularity at $\mathbf{r} = \mathbf{r}'$ is addressed later, in section 3.1.2, where integration over an exclusion volume is used. In the limit, as the observation point tends to infinity, the charge distribution of $\varrho(\mathbf{r})$ confined within surface S_T tends to a point charge of magnitude q. The resulting Coulomb field is defined by

$$\phi(\mathbf{r}) = \frac{q}{4\pi\epsilon R} \tag{3.1.5}$$

where $R = |\mathbf{r}-\mathbf{r}'|$, with $\mathbf{r}'$ defining the source point.

For advanced analysis, we are concerned with the boundary value problems created by enclosing logical "sub-domains" within V_{inf}. For example, surfaces S_2, S_3 and S_4 enclosing volumes V_2, V_3 and V_4, respectively. The general problem thus requires any defining surface to be specified, allowing the potential function to be correctly defined within its interior volume. Intuitively, we would expect the potential for $\mathbf{r} \in V_4$ to be due to the charge density at all source points, $\mathbf{r}' \in V_4$, with boundary conditions on S_4 encompassing the effects of all charges $\varrho(\mathbf{r}) \in (V_{inf}/V_4)$. Stratton [45, pp.165-193] shows how this bounding surface reduces the field outside to zero, by introducing a single- and double-layer distribution on the surface, to take into account all external charges.

From elementary differential equation analysis, we would expect the solution $\phi(\mathbf{r})$ of Poisson's equation to consist of a particular solution and a general solution,

$$\phi(\mathbf{r}) = \phi_{ps}(\mathbf{r}) + \phi_{gs}(\mathbf{r}) \tag{3.1.6}$$

Intuitively, the solution of Poisson's equation would involve integration over the volume of interest, surface integration over the boundary surface(s) and taking into account the respective boundary conditions. For the general mixed conditions, specifying for surface points, $\mathbf{r}^s \in S$:

$$\phi_{bc}(\mathbf{r}^s) = \alpha\phi(\mathbf{r}^s) + \beta\frac{\partial\phi(\mathbf{r}^s)}{\partial n} \tag{3.1.7}$$

The first term is recognized as a Dirichlet condition, the second a Neumann condition, also specified as $\nabla\phi(\mathbf{r}^s).\ \hat{\mathbf{n}}$ where $\hat{\mathbf{n}}$ is the outward normal vector on the surface at $\mathbf{r}^s$. For any $\phi_{bc}(\mathbf{r}^s) \neq 0$, the boundary conditions are inhomogeneous, while $\phi_{bc}(\mathbf{r}^s) = 0$ are homogeneous boundary conditions. The number subscript, used to identify surfaces has been dropped, for these general derivations.

The solution to the inhomogeneous Poisson's equation is [45, p.167]

$$\phi(\mathbf{r}) = \frac{1}{4\pi\epsilon}\int_V \frac{\varrho(\mathbf{r}')}{R}\, dv' + \frac{1}{4\pi}\int_S \left[\frac{1}{R}\frac{\partial\phi(\mathbf{r}')}{\partial n} - \phi(\mathbf{r}')\frac{\partial}{\partial n}\left(\frac{1}{R}\right)\right] da' \tag{3.1.8}$$

where $\partial/\partial n$ denotes the directional derivative in the direction of $\hat{\mathbf{n}}(\mathbf{r})$ and $R = |\mathbf{r} - \mathbf{r}'|$, as before. Note that the first term is identical to (3.1.4) and is identified as the particular solution. The second term is the general (complimentary) solution and recognized as the solution of Laplace's equation, the homogeneous equation.

3.1.2 Green's Theorem

A key body of mathematics is useful for analysis of Electromagnetics; Green's identities and Green's theorem in its scalar, vector and dyadic forms are the foundation of the integral equation methods used in the Computational Electromagnetics field. Not just an abstract tool for relating integral terms, Green's work is based on the original potential theory investigations carried out in the late 1700s and early 1800s, including the work of such greats as Poisson, Gauss and Laplace. This section builds on the preliminaries of the potential theory just reviewed and lays the foundations for the integral theory used in calculating fields radiated or scattered from complex structures.

Gauss' theorem, also known as the Divergence Theorem, relates the divergence of a vector out of a volume to the normal "outflow" vector from the surface enclosing that volume. The Divergence Theorem integral equation formulation for vector $\mathbf{F}$ defined in volume V, enclosed by surface S is

$$\int_V \nabla.\mathbf{F}\; dv = \int_S \mathbf{F}.d\mathbf{A} \tag{3.1.9}$$

The axial vector, $d\mathbf{A}$, can also be interpreted as $\hat{\mathbf{n}}\, dA$, where $\hat{\mathbf{n}}$ is the usual outward normal on surface S. The solution of the electrostatic problem, $\phi(\mathbf{r})$, is a scalar function of position, and for this analysis a function of source and observation coordinates. The notation $\phi(\mathbf{r}, \mathbf{r}')$ is used. The divergence theorem relates vector field characteristics over a volume and the enclosing surface. Introducing another scalar field of position, denoted $\psi(\mathbf{r}, \mathbf{r}')$ and using the gradient symbolic vector with respect to the source coordinates, ∇', we can introduce 2 vector fields, $\psi(\mathbf{r}, \mathbf{r}')\nabla'\phi(\mathbf{r}, \mathbf{r}')$ and $\phi(\mathbf{r}, \mathbf{r}')\nabla'\psi(\mathbf{r}, \mathbf{r}')$. Substituting these 2 vector fields for $\mathbf{F}$ in (3.1.9) and using the identity

$$\nabla'.\left(\phi\nabla'\psi\right) = \nabla'\phi.\nabla'\psi + \phi\nabla'^2\psi$$

we establish the first Green's identities for vectors $\psi(\mathbf{r},\mathbf{r}')\nabla'\phi(\mathbf{r},\mathbf{r}')$ and $\phi(\mathbf{r},\mathbf{r}')\nabla'\psi(\mathbf{r},\mathbf{r}')$,

$$\int_V \nabla'\psi(\mathbf{r},\mathbf{r}').\nabla'\phi(\mathbf{r},\mathbf{r}')\ dv' + \int_V \psi(\mathbf{r},\mathbf{r}')\nabla'^{\,2}\phi(\mathbf{r},\mathbf{r}')\ dv' = \int_S \psi(\mathbf{r},\mathbf{r}')\frac{\partial\phi(\mathbf{r},\mathbf{r}')}{\partial n}\ da' \quad (3.1.10)$$

$$\int_V \nabla'\phi(\mathbf{r},\mathbf{r}').\nabla'\psi(\mathbf{r},\mathbf{r}')\ dv' + \int_V \phi(\mathbf{r},\mathbf{r}')\nabla'^2\psi(\mathbf{r},\mathbf{r}')\ dv' = \int_S \phi(\mathbf{r},\mathbf{r}')\frac{\partial\psi(\mathbf{r},\mathbf{r}')}{\partial n}\ da' \quad (3.1.11)$$

The term on the right hand side is given by

$$\frac{\partial\phi(\mathbf{r},\mathbf{r}')}{\partial n} = \nabla'\phi(\mathbf{r},\mathbf{r}').\hat{\mathbf{n}}$$

Subtracting (3.1.10) and (3.1.11), we have Green's theorem

$$\int_V \left[\psi(\mathbf{r},\mathbf{r}')\nabla'^2\phi(\mathbf{r},\mathbf{r}') - \phi(\mathbf{r},\mathbf{r}')\nabla'^2\psi(\mathbf{r},\mathbf{r}')\right] dv' = \int_s \left[\psi(\mathbf{r},\mathbf{r}')\frac{\partial\phi(\mathbf{r},\mathbf{r}')}{\partial n} - \phi(\mathbf{r},\mathbf{r}')\frac{\partial\psi(\mathbf{r},\mathbf{r}')}{\partial n}\right] da' \quad (3.1.12)$$

Comparing terms of the right hand side of this equation with (3.1.7), it is clear how the Neumann and Dirichlet boundary conditions at surface S are included. Green's theorem, (3.1.12), requires potential functions $\phi(\mathbf{r},\mathbf{r}')$ and $\psi(\mathbf{r},\mathbf{r}')$ and their first and second derivatives to be continuous throughout V and on S [45, pp. 165-171]. An appropriate choice of the solution $\psi(\mathbf{r},\mathbf{r}')$ to Laplace's equation reduces the left hand side of (3.1.12) to a form involving the Laplacian on $\psi(\mathbf{r},\mathbf{r}')$. The $\phi(\mathbf{r},\mathbf{r}')$ function includes a dependence on the source and observation coordinates. For

$$\psi(\mathbf{r},\mathbf{r}') = \frac{1}{|\mathbf{r}-\mathbf{r}'|} = \frac{1}{r}\ , \quad (3.1.13)$$

$$\nabla'^2\psi(\mathbf{r},\mathbf{r}') = 0 \quad (3.1.14)$$

The discontinuity at $\mathbf{r} = \mathbf{r}'$ requires introduction of a singularity exclusion volume, V_s, such that volume V is bounded internally by S_s. Stratton [45, p.167] showed that for a spherical exclusion volume, the contribution of the surface integral of (3.1.12) tends to $-4\pi\phi(\mathbf{r})$, as the sphere radius tends to zero.

$$\int_{V+V_s} \frac{\nabla'^2\phi(\mathbf{r},\mathbf{r}')}{r}dv' = \int_{S+S_s}\left[\frac{1}{r}\frac{\partial\phi(\mathbf{r},\mathbf{r}')}{\partial n} - \phi(\mathbf{r},\mathbf{r}')\frac{\partial}{\partial n}\left(\frac{1}{r}\right)\right] da' \quad (3.1.15)$$

$$\phi(\mathbf{r}) = -\frac{1}{4\pi}\int_V \frac{\nabla'^2\phi(\mathbf{r},\mathbf{r}')}{r}dv' + \frac{1}{4\pi}\int_S\left[\frac{1}{r}\frac{\partial\phi(\mathbf{r},\mathbf{r}')}{\partial n} - \phi(\mathbf{r},\mathbf{r}')\frac{\partial}{\partial n}\left(\frac{1}{r}\right)\right] da' \quad (3.1.16)$$

3.1.3 Inhomogeneous Scalar Wave Problem

Solutions to the scalar wave problem have been dated to Fresnel in his mathematical investigations of Huygen's principle [61, pp. 20-31], as well as the body of literature that covers acoustic wave propagation [62, 63]. Having analyzed the potential theory problem of Poisson's equation in section 3.1, we have the mathematical tools for the solution of the inhomogeneous scalar wave equation, as defined in terms of Green's theorems, and surface boundary conditions of the Neumann and Dirichlet variety.

Section 3.2 deals with the theory and derivations of the vector wave problem and the application of the vector Green's Theorems; this section is a primer for that, showing the basic geometries and the derivations for the separable case where scalar wave equations are defined.

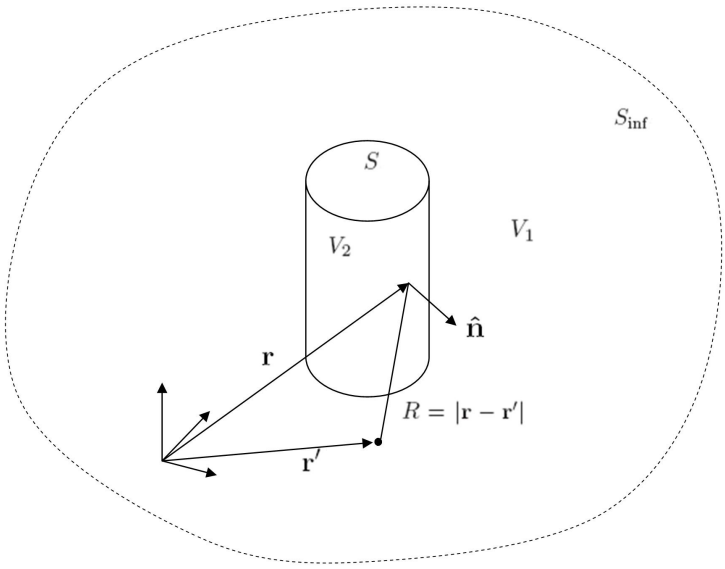

Figure 3.1: Surface S enclosing volume V_2, embedded in volume V_1

Consider a 3-dimensional region in space V_2 bounded by a surface S, with an outward-directed normal vector, $\hat{\mathbf{n}}$. We are interested in two cases, with a point of observation within the region V_2, bound by S, and the case of a point outside S. We consider another region V_1, internally bound by S and in turn enclosed by a distant surface S_{inf}.

The scalar field of interest (an acoustic or electric potential field), defined as $\phi_2(\mathbf{r})$ with respect to position vector $\mathbf{r}$ exists within region V_2. There is also the question of the influence of an excitation, $s(\mathbf{r})$, which may be internal or external to S. The work of Green, Fresnel and Huygens centered on the analysis of the effect of a point charge, with respect to a surface of interest.

Proceeding with the case of the source external to S, i.e. in region V_1. The potential function in this region is obviously $\phi_1(\mathbf{r})$. Constants k_1 and k_2 encapsulate material properties in the 2 regions.

From the vector wave equation for region 1, for a homogeneous, isotropic medium, we can derive the well-known vector Helmholtz equations, $\forall\ \mathbf{r} \in V_1$

$$\nabla^2\mathbf{E}(\mathbf{r}) + \omega^2\epsilon_1\mu_1\mathbf{E}(\mathbf{r}) = i\omega\mu_1\mathbf{J_e}(\mathbf{r}) + \nabla\times\mathbf{J_m}(\mathbf{r}) + \frac{\nabla\rho_e}{\epsilon_1} \tag{3.1.17a}$$

$$\nabla^2\mathbf{H}(\mathbf{r}) + \omega^2\epsilon_1\mu_1\mathbf{H}(\mathbf{r}) = i\omega\mu_1\mathbf{J_m}(\mathbf{r}) - \nabla\times\mathbf{J_e}(\mathbf{r}) + \frac{\nabla\rho_m}{\mu_1} \tag{3.1.17b}$$

Introducing magnetic vector potential $\mathbf{A}(\mathbf{r})$ and Lorenz gauge $\nabla\cdot\mathbf{A}(\mathbf{r}) = -i\omega\mu_1\epsilon_1\phi$, we have:

$$\nabla^2\mathbf{A}(\mathbf{r}) + k_1^2\mathbf{A}(\mathbf{r}) = -\mu_1\mathbf{J_e}(\mathbf{r}) \tag{3.1.18}$$

The analysis of the separation of variables for various problems in different coordinate systems is nontrivial, and of particular interest in path integral theory a la Feynman in Quantum Mechanics and QED. The reader is referred to a text such as Grosche [64]. It can be shown that a three-dimensional Euclidean space can be separable in up to 11 different coordinate systems (Cartesian, polar, spherical, paraboloid, etc). A separable scalar equation can be written, for $\nabla^2\mathbf{A}(\mathbf{r}) = \hat{\mathbf{x}}\nabla^2A_x + \hat{\mathbf{y}}\nabla^2A_y + \hat{\mathbf{z}}\nabla^2A_z$, giving scalar Helmholtz equation

$$\left(\nabla^2 + k_1^2\right)\psi_1(\mathbf{r}) = -s(\mathbf{r}) \tag{3.1.19}$$

For a unit point-source excitation at fixed point $\mathbf{r}'$, we can write this Helmholtz equation in terms of a Green's function, relating source point $\mathbf{r}'$ and observer's or field point $\mathbf{r}$, denoted $G(\mathbf{r},\mathbf{r}')$,

$$\left(\nabla^2 + k_1^2\right)G(\mathbf{r},\mathbf{r}') = -\delta(\mathbf{r}-\mathbf{r}') \tag{3.1.20}$$

Clearly at point $\mathbf{r}'$, the Green's function is used to solve the inhomogeneous equation; it is the field response to an impulse excitation. At all other points, the homogeneous equation is satisfied. Note also that the ∇ operator is acting on observational coordinates, $\mathbf{r}$.

For the two regions depicted in figure 3.1, we have

$$\left(\nabla^2 + k_1^2\right)\psi_1(\mathbf{r}) = -s(\mathbf{r}), \quad \forall\ \mathbf{r}' \in V_1 \tag{3.1.21a}$$

$$\left(\nabla^2 + k_1^2\right)\psi_2(\mathbf{r}) = 0, \quad \forall\ \mathbf{r}' \in V_2 \tag{3.1.21b}$$

corresponding to sources in V_1 and V_2 respectively. The respective Green's functions are

solutions to

$$\left(\nabla^2 + k_1^2\right) G_1(\mathbf{r}, \mathbf{r}') = -\delta(\mathbf{r} - \mathbf{r}'), \quad \forall\ \mathbf{r}' \in V_1 \tag{3.1.22a}$$

$$\left(\nabla^2 + k_1^2\right) G_2(\mathbf{r}, \mathbf{r}') = -\delta(\mathbf{r} - \mathbf{r}'), \quad \forall\ \mathbf{r}' \in V_2 \tag{3.1.22b}$$

Function $G_1(\mathbf{r}, \mathbf{r}')$ must satisfy radiation condition

$$\lim_{R\to\infty} R\left(\frac{\partial G_1(\mathbf{r}, \mathbf{r}')}{\partial R} - ik\, G_1(\mathbf{r}, \mathbf{r}')\right) = 0 \tag{3.1.23}$$

where $R = |\mathbf{r} - \mathbf{r}'|$. Multiplying (3.1.21a) by $G_1(\mathbf{r}, \mathbf{r}')$, (3.1.22a) by $\psi_1(\mathbf{r})$, subtracting and integrating over volume V_1,

$$\int_{V_1} \left[\, G_1(\mathbf{r}, \mathbf{r}')\nabla^2\psi_1(\mathbf{r}) - \psi_1(\mathbf{r})\nabla^2 G_1(\mathbf{r}, \mathbf{r}')\right] dV = -\int_{V_1} G_1(\mathbf{r}, \mathbf{r}')\, s(\mathbf{r})\, dV + \psi_1(\mathbf{r}'), \quad \forall\ \mathbf{r}' \in V_1 \tag{3.1.24}$$

By the Divergence Theorem, the volume integral can be reduced to a surface integral, per (3.1.9), such that, with an interchange of $\mathbf{r}$ and $\mathbf{r}'$,

$$-\int_{S+S_{\text{inf}}} \hat{\mathbf{n}}\cdot\left[\, G_1(\mathbf{r}, \mathbf{r}')\nabla'\psi_1(\mathbf{r}') - \psi_1(\mathbf{r}')\nabla' G_1(\mathbf{r}, \mathbf{r}')\right] dS' = -\psi_{\text{inc}}(\mathbf{r}) + \psi_1(\mathbf{r}), \quad \forall\, \mathbf{r} \in V_1 \tag{3.1.25}$$

where the minus sign on the first term is due to the normal vector being directed into volume V_1 from surfaces S and S_{inf}, and incident field, $\psi_{\text{inc}} = \int_{V_1} G_1(\mathbf{r}, \mathbf{r}')\, s(\mathbf{r}')dV'$ is generated by source distribution $s(\mathbf{r}')$. For the source-free region, V_2,

$$+\int_{S+S_{\text{inf}}} \hat{\mathbf{n}} \cdot \left[\, G_2(\mathbf{r}, \mathbf{r}')\nabla'\psi_2(\mathbf{r}') - \psi_2(\mathbf{r}')\nabla' G_2(\mathbf{r}, \mathbf{r}')\right] dS' = 0, \quad \forall\ \mathbf{r} \in V_2 \tag{3.1.26}$$

The interchange of variables in (3.1.25) and (3.1.26) allows the interpretation of the integral over all source points $\mathbf{r}'$, as observed at field point $\mathbf{r}$; the partial differential ∇ operator is applied to source-point coordinates. Note that for region V_2, the normal is directed outward, as is consistent with the definition for the Divergence Theorem, thus, giving a positive term on left-hand-side of (3.1.26).

In summary, by (3.1.12)

$$-\int_{S+S_{\text{inf}}} \left[G_1(\mathbf{r}, \mathbf{r}')\frac{\partial\psi_1(\mathbf{r}')}{\partial n} - \psi(\mathbf{r}')\frac{\partial G_1(\mathbf{r}, \mathbf{r}')}{\partial n}\right] dS' \;=\; \psi_{\text{inc}} + \psi_1(\mathbf{r}),\ \forall\, \mathbf{r} \in V_1 \tag{3.1.27}$$

$$\int_{S+S_{\text{inf}}} \left[G_2(\mathbf{r}, \mathbf{r}')\frac{\partial\psi_2(\mathbf{r}')}{\partial n} - \psi(\mathbf{r}')\frac{\partial G_2(\mathbf{r}, \mathbf{r}')}{\partial n}\right] dS' \;=\; 0,\ \forall\, \mathbf{r} \in V_2 \tag{3.1.28}$$

This derivation, based on Green's theorem is of course predicated on continuous first and second derivatives on surfaces S and S_{inf}. $\nabla'\varphi(\mathbf{r}, \mathbf{r}') = \partial\varphi(\mathbf{r}, \mathbf{r}')/\partial n$ where $\partial/\partial n$ is the directional

derivative in the direction of the normal to surfaces S and S_{inf}.

3.2 Inhomogeneous Vector Wave Problem

In this section, we seek the solution of the inhomogeneous vector wave problem where no separability in a coordinate system is assumed. The scalar wave equation form, in equation (3.1.19) was predicated on separation of variables, a dependency on the geometry of the problem (as in the rectangular cavity problem of section 2.3) and the chosen coordinate system. Both direct and indirect methods exist. The direct integration method, leading to a Stratton-Chu representation follows.

3.2.1 Direct Integration Method - Stratton Chu approach

The Stratton-Chu [65, 45] formulation is an application of the 2nd vector's Green's theorem to the solution of the inhomogeneous vector wave equations; it is essentially a direct integration method. The medium considered is of zero conductivity, homogeneous and isotropic. The field equations are defined as follows,

$$\nabla \times \mathbf{E}(\mathbf{r}) - i\mu\omega\mathbf{H}(\mathbf{r}) = -\mathbf{J_m}(\mathbf{r}) \tag{3.2.1a}$$

$$\nabla \times \mathbf{H}(\mathbf{r}) + i\epsilon\omega\mathbf{E}(\mathbf{r}) = \mathbf{J_e}(\mathbf{r}) \tag{3.2.1b}$$

$$\nabla.\mathbf{H}(\mathbf{r}) = \frac{\rho_m}{\mu} \tag{3.2.1c}$$

$$\nabla.\mathbf{E}(\mathbf{r}) = \frac{\rho_e}{\epsilon} \tag{3.2.1d}$$

where ρ_m is magnetic charge density and $\mathbf{J_m}(\mathbf{r})$ is magnetic current. We can state, based on simple identity manipulations, the vector wave equations

$$\nabla \times \nabla \times \mathbf{E}(\mathbf{r}) - k^2\mathbf{E}(\mathbf{r}) = i\omega\mu\mathbf{J_e}(\mathbf{r}) - \nabla \times \mathbf{J_m}(\mathbf{r}) \tag{3.2.2a}$$

$$\nabla \times \nabla \times \mathbf{H}(\mathbf{r}) - k^2\mathbf{H}(\mathbf{r}) = i\omega\epsilon\mathbf{J_m}(\mathbf{r}) - \nabla \times \mathbf{J_e}(\mathbf{r}) \tag{3.2.2b}$$

where $k^2 = \omega^2\mu\epsilon$ for the homogeneous, isotropic medium. The mechanism used to perform integration is the vector Green's theorem. This equation, derived from Gauss' Divergence Theorem is essentially a statement of reciprocity between 2 vector fields, the field of interest, say $\mathbf{E}(\mathbf{r})$, and an appropriate Green's function.

The same methodology evolved in section 3.1.3 for the scalar wave problem is used here: the second vector Green's theorem, relating expressions in two vector functions of position, $\mathbf{P}$

and $\mathbf{Q}$ in a volume V bounded by surface S.

$$\int_V [(\nabla \times \nabla \times \mathbf{P}) \cdot \mathbf{Q} - \mathbf{P} \cdot \nabla \times \nabla \times \mathbf{Q}]\, dv = \oint_S \hat{\mathbf{n}} \cdot [\mathbf{P} \times (\nabla \times \mathbf{Q}) + (\nabla \times \mathbf{P} \times \mathbf{Q})]\, dS \quad (3.2.3)$$

Let $\mathbf{P} = \mathbf{E}$ and $\mathbf{Q} = \hat{\mathbf{a}}\, G(\mathbf{r}, \mathbf{r}')$ where free-space Green's function $G(\mathbf{r}, \mathbf{r}') = e^{ikR}/R$, a scalar function of position, with $R = |\mathbf{r} - \mathbf{r}'|$ and $\hat{\mathbf{a}}$ is an arbitrarily directed unit vector. Using the vector wave equations and standard vector identities, it is trivial to show that $\nabla \times \mathbf{Q} = (\nabla G(\mathbf{r}, \mathbf{r}')) \times \hat{a}$ and $\nabla \times \nabla \times G(\mathbf{r}, \mathbf{r}')\, \hat{\mathbf{a}} = \nabla(\hat{\mathbf{a}} \cdot \nabla G(\mathbf{r}, \mathbf{r}')) - k^2 G(\mathbf{r}, \mathbf{r}')\, \hat{\mathbf{a}}$. It follows in (3.2.3),

$$\begin{aligned} &\int_V [(\nabla \times \nabla \times \mathbf{P}) \cdot \mathbf{Q} - \mathbf{P} \cdot \nabla \times \nabla \times \mathbf{Q}]\, dv \\ &= \int_V \Big[\hat{\mathbf{a}} \cdot G(\mathbf{r}, \mathbf{r}')(i\omega\mu \mathbf{J_e}(\mathbf{r}) - \nabla \times \mathbf{J_m}(\mathbf{r})) + \hat{\mathbf{a}} \cdot (\nabla G(\mathbf{r}, \mathbf{r}'))\frac{\rho}{\epsilon}\Big]\, dv + \oint_S \big[\hat{\mathbf{a}} \cdot (\nabla G(\mathbf{r}, \mathbf{r}'))\mathbf{E}(\mathbf{r})\big] \cdot \hat{\mathbf{n}}\, dS \end{aligned} \quad (3.2.4)$$

by noting that

$$\mathbf{E}(\mathbf{r}) \cdot \nabla(\hat{\mathbf{a}} \cdot \nabla G(\mathbf{r}, \mathbf{r}')) = \nabla \cdot (\hat{\mathbf{a}} \cdot \nabla G(\mathbf{r}, \mathbf{r}'))\mathbf{E}(\mathbf{r}) - (\hat{\mathbf{a}} \cdot \nabla G(\mathbf{r}, \mathbf{r}'))\nabla \cdot \mathbf{E}(\mathbf{r}) \quad (3.2.5)$$

that $\nabla \cdot \mathbf{E}(\mathbf{r}) = \rho_e/\epsilon$, and by invoking Gauss' Theorem relating the volume and surface integrals. For the surface integral in the second vector Green's Theorem, (3.2.3),

$$\begin{aligned} &\oint_S \hat{\mathbf{n}} \cdot [\mathbf{P} \times (\nabla \times \mathbf{Q}) + (\nabla \times \mathbf{P} \times \mathbf{Q})]\, dS \\ &\qquad = \oint_S \big[(\nabla \times G(\mathbf{r}, \mathbf{r}')\hat{\mathbf{a}}) \cdot (\hat{\mathbf{n}} \times \mathbf{E}(\mathbf{r})) - G(\mathbf{r}, \mathbf{r}')\ \hat{\mathbf{a}} \cdot (\nabla \times \mathbf{E}(\mathbf{r}) \times \hat{\mathbf{n}})\big]\, dS \\ &\qquad\qquad = \oint_S \big[\hat{\mathbf{a}} \cdot (\hat{\mathbf{n}} \times \mathbf{E}(\mathbf{r}) \times \nabla G(\mathbf{r}, \mathbf{r}')) - \hat{\mathbf{a}} \cdot G(\mathbf{r}, \mathbf{r}')(\nabla \times \mathbf{E}(\mathbf{r}) \times \hat{\mathbf{n}})\big]\, dS \end{aligned} \quad (3.2.6)$$

By Maxwell's equation, $\nabla \times \mathbf{E}(\mathbf{r}) = i\omega\mu\mathbf{H}(\mathbf{r}) - \mathbf{J_m}(\mathbf{r})$ and the identity $(\mathbf{a} + \mathbf{b}) \times \mathbf{c} = -(\mathbf{c} \times \mathbf{a}) - (\mathbf{c} \times \mathbf{b})$, the right hand side of equation (3.2.6) is

$$\oint_S \big[\hat{\mathbf{a}} \cdot (\hat{\mathbf{n}} \times \mathbf{E}(\mathbf{r})) \times \nabla G(\mathbf{r}, \mathbf{r}') + (\hat{\mathbf{n}} \times \mathbf{H}(\mathbf{r}))i\omega\mu G(\mathbf{r}, \mathbf{r}') - (\hat{\mathbf{n}} \times \mathbf{J_m}(\mathbf{r}))G(\mathbf{r}, \mathbf{r}')\big]\, dS \quad (3.2.7)$$

Eliminating the arbitrary vector $\hat{\mathbf{a}}$ from the equation, we have

$$\begin{aligned} &\int_V \Big[G(\mathbf{r}, \mathbf{r}')i\omega\mu \mathbf{J_e}(\mathbf{r}) - G(\mathbf{r}, \mathbf{r}')(\nabla \times \mathbf{J_m}(\mathbf{r})) + (\nabla G(\mathbf{r}, \mathbf{r}'))\frac{\rho_e}{\epsilon}\Big]\, dv \\ &\qquad = \oint_S \big[\hat{\mathbf{n}} \times \mathbf{E}(\mathbf{r}) \times \nabla G(\mathbf{r}, \mathbf{r}') + (\hat{\mathbf{n}} \times \mathbf{H}(\mathbf{r}))\, i\omega\mu G(\mathbf{r}, \mathbf{r}') - (\hat{\mathbf{n}} \times \mathbf{J_m}(\mathbf{r}))\, G(\mathbf{r}, \mathbf{r}') \\ &\qquad\qquad + (\nabla G(\mathbf{r}, \mathbf{r}'))\mathbf{E}(\mathbf{r}) \cdot \hat{\mathbf{n}}\big] dS \end{aligned} \quad (3.2.8)$$

The identity

$$\int_V (\nabla \times \mathbf{J_m}(\mathbf{r}))G(\mathbf{r},\mathbf{r}')\,dv = \oint_S (\hat{\mathbf{n}} \times \mathbf{J_m}(\mathbf{r}))G(\mathbf{r},\mathbf{r}')\,dS + \int_V \mathbf{J_m}(\mathbf{r}) \times (\nabla G(\mathbf{r},\mathbf{r}'))\,dv \quad (3.2.9)$$

followed by an interchange of independent variables $\mathbf{r}$ and $\mathbf{r}'$, and using the reciprocity of the Green's function, gives

$$\begin{aligned}&\int_V \left[i\omega\mu\, G(\mathbf{r},\mathbf{r}')\mathbf{J_e}(\mathbf{r}') - \mathbf{J_m}(\mathbf{r}') \times \nabla' G(\mathbf{r},\mathbf{r}') + (\nabla' G(\mathbf{r},\mathbf{r}'))\frac{\rho_e}{\epsilon}\right] dv' \\ &= \oint_S \left[\hat{\mathbf{n}} \times \mathbf{E}(\mathbf{r}') \times \nabla G(\mathbf{r},\mathbf{r}') + i\omega\mu\,(\hat{\mathbf{n}} \times \mathbf{H}(\mathbf{r}'))G(\mathbf{r},\mathbf{r}') + (\nabla G(\mathbf{r},\mathbf{r}'))\mathbf{E}(\mathbf{r}') \cdot \hat{\mathbf{n}}\right] dS' \quad (3.2.10)\end{aligned}$$

the Stratton-Chu representation [65]. Using the same spherical exclusion volume technique as demonstrated for the scalar problem in section 3.1.2, we can find the value of $\mathbf{E}(\mathbf{r})$ at an interior point of V.

$$\begin{aligned}\mathbf{E}(\mathbf{r}) = &\frac{1}{4\pi}\int_V \left[i\omega\mu\, G(\mathbf{r},\mathbf{r}')\mathbf{J_e}(\mathbf{r}') - \mathbf{J_m}(\mathbf{r}') \times \nabla' G(\mathbf{r},\mathbf{r}') + (\nabla' G(\mathbf{r},\mathbf{r}'))\frac{\rho_e}{\epsilon}\right] dv' \\ &- \frac{1}{4\pi}\oint_S \left[\hat{\mathbf{n}} \times \mathbf{E}(\mathbf{r}') \times \nabla G(\mathbf{r},\mathbf{r}') + i\omega\mu\,(\hat{\mathbf{n}} \times \mathbf{H}(\mathbf{r}'))G(\mathbf{r},\mathbf{r}') + (\nabla G(\mathbf{r},\mathbf{r}'))\mathbf{E}(\mathbf{r}') \cdot \hat{\mathbf{n}}\right] dS'\end{aligned} \quad (3.2.11)$$

For $\mathbf{r}$ external to V, the left-hand side equals zero. The electric field at point $\mathbf{r}$ is thus given in terms of the sum of a volume integral over actual sources and a surface integral over fields regarded to be the equivalent sources on a surface [66, p.67]. By duality, we can state the magnetic field equivalent

$$\begin{aligned}\mathbf{H}(\mathbf{r}) = &\frac{1}{4\pi}\int_V \left[i\omega\epsilon\, G(\mathbf{r},\mathbf{r}')\mathbf{J_m}(\mathbf{r}') + \mathbf{J_e}(\mathbf{r}') \times \nabla' G(\mathbf{r},\mathbf{r}') + (\nabla' G(\mathbf{r},\mathbf{r}'))\frac{\rho_m}{\mu}\right] dv' \\ &+ \frac{1}{4\pi}\oint_S \left[-\hat{\mathbf{n}} \times \mathbf{H}(\mathbf{r}') \times \nabla G(\mathbf{r},\mathbf{r}') + i\omega\epsilon\,(\hat{\mathbf{n}} \times \mathbf{E}(\mathbf{r}'))G(\mathbf{r},\mathbf{r}') - (\nabla G(\mathbf{r},\mathbf{r}'))\mathbf{H}(\mathbf{r}') \cdot \hat{\mathbf{n}}\right] dS'\end{aligned} \quad (3.2.12)$$

This takes into account sources external to surface S, as boundary conditions, hence the $\hat{\mathbf{n}} \times \mathbf{E}$ and $\hat{\mathbf{n}} \times \mathbf{H}$ terms.

For an observation, or field point inside surface S, we construct a sphere of radius r_1, with normal $\mathbf{r_1}$ directed into the sphere, with surface area $4\pi r_1^2$. Consider the limit as $r_1 \to 0$. Noting that the gradient of the scalar green's function is

$$\nabla G(\mathbf{r},\mathbf{r}') = \left(\frac{1}{r_1} - ik\right)\frac{e^{ikr_1}}{r_1}\mathbf{r_1} \quad (3.2.13)$$

The first term in equation (3.2.11), of the form $\int_S G(\mathbf{r},\mathbf{r}')\psi(\mathbf{r}')ds'$ is continuous across S; this is an improper integral, with weakly singular kernel, for continuous ψ. The gradient operator terms in $G(\mathbf{r},\mathbf{r}')$ require more scrutiny, due to the $1/R$ term. In the limit as $\mathbf{r}' \to S^{\pm}$, for Hölder-continuous $\hat{\mathbf{n}} \times \mathbf{E}(\mathbf{r})$ [67],

$$\lim_{\mathbf{r}\to S^{\pm}} \frac{1}{4\pi}\int_S \nabla' G(\mathbf{r},\mathbf{r}') \times [\hat{\mathbf{n}} \times \mathbf{E}(\mathbf{r},\mathbf{r}')]\, ds' = \frac{1}{4\pi}\!\!\int\!\!\!\!\!\!-_S \nabla' G(\mathbf{r},\mathbf{r}') \times [\hat{\mathbf{n}} \times \mathbf{E}(\mathbf{r},\mathbf{r}')]\, ds' \pm \frac{1}{2}\,\hat{\mathbf{n}}(\mathbf{r}) \times [\hat{\mathbf{n}}(\mathbf{r}) \times \mathbf{E}_{\pm}(\mathbf{r})] \quad (3.2.14)$$

$\int\!\!\!\!\!\!-$ denotes a Cauchy principal value integral. For Hölder-continuous $\hat{\mathbf{n}} \cdot \mathbf{E}(\mathbf{r})$

$$\lim_{\mathbf{r}\to S^{\pm}} \frac{1}{4\pi}\int_S \nabla' G(\mathbf{r},\mathbf{r}')\, \hat{\mathbf{n}} \cdot \mathbf{E}_{\pm}(\mathbf{r}')\, ds' = \frac{1}{4\pi}\!\!\int\!\!\!\!\!\!-_S \nabla' G(\mathbf{r},\mathbf{r}')\hat{\mathbf{n}} \cdot \mathbf{E}_{\pm}(\mathbf{r}')\, ds' \pm \frac{1}{2}\hat{\mathbf{n}}(\mathbf{r})\big[\hat{\mathbf{n}}(\mathbf{r}) \cdot \mathbf{E}_{\pm}(\mathbf{r})\big] \quad (3.2.15)$$

Recognizing E_- as the incident field, and E_+ as the scattered field, with total field $\mathbf{E}(\mathbf{r}) = \mathbf{E}^{inc}(\mathbf{r}) + \mathbf{E}^{S}(\mathbf{r})$, we obtain

$$\frac{1}{4\pi}\!\!\int\!\!\!\!\!\!-_S \big\{ i\omega\mu\, G(\mathbf{r},\mathbf{r}')\,[\hat{\mathbf{n}}(\mathbf{r}') \times \mathbf{H}(\mathbf{r}')] + \nabla' G(\mathbf{r},\mathbf{r}')[\hat{\mathbf{n}}(\mathbf{r}')\cdot\mathbf{E}(\mathbf{r}')] - \nabla' G(\mathbf{r},\mathbf{r}') \times [\hat{\mathbf{n}}(\mathbf{r}') \times \mathbf{E}(\mathbf{r}')]\big\} = \frac{1}{2}\mathbf{E}(\mathbf{r}) - \mathbf{E}^{inc}(\mathbf{r}) \quad (3.2.16)$$

Recalling surface divergence and curl operators, such that

$$\hat{\mathbf{n}}(\mathbf{r}') \cdot \nabla' \times \mathbf{H}(\mathbf{r}') = -\nabla'_t \cdot \hat{\mathbf{n}}(\mathbf{r}') \times \mathbf{H}(\mathbf{r}') \quad (3.2.17)$$

and using Maxwell's equations, equation (3.2.16) becomes

$$\frac{1}{4\pi}\!\!\int\!\!\!\!\!\!-_S \big\{ i\omega\mu\, G(\mathbf{r},\mathbf{r}')[\hat{\mathbf{n}}(\mathbf{r}') \times \mathbf{H}(\mathbf{r}')] - \frac{i\omega\mu}{k^2}\nabla' G(\mathbf{r},\mathbf{r}')\nabla'_t \cdot [\hat{\mathbf{n}}(\mathbf{r}') \times \mathbf{H}(\mathbf{r}')] - \nabla' G(\mathbf{r},\mathbf{r}') \times [\hat{\mathbf{n}}(\mathbf{r}') \times \mathbf{H}(\mathbf{r}')]\big\}\, ds' = \frac{1}{2}\,\mathbf{E}(\mathbf{r}) - \mathbf{E}^{inc}(\mathbf{r}) \quad (3.2.18)$$

Similarly, we can derive an expression for $\mathbf{H}(\mathbf{r})$.

$$\frac{1}{4\pi}\int_S -i\omega\epsilon G(\mathbf{r},\mathbf{r}')[\hat{\mathbf{n}}(\mathbf{r}') \times \mathbf{E}(\mathbf{r}')] + \frac{i\omega\epsilon}{k^2}\nabla' G(\mathbf{r},\mathbf{r}')\nabla'_t \cdot [\hat{\mathbf{n}}(\mathbf{r}') \times \mathbf{E}(\mathbf{r}')] - \nabla' G(\mathbf{r},\mathbf{r}') \times [\hat{\mathbf{n}}(\mathbf{r}') \times \mathbf{H}(\mathbf{r}')]\, ds' = \frac{1}{2}\,\mathbf{H}(\mathbf{r}) - \mathbf{H}^{inc}(\mathbf{r}) \quad (3.2.19)$$

The boundary conditions for a perfect conductor, $\hat{\mathbf{n}} \times \mathbf{E} = 0$ and $\hat{\mathbf{n}} \cdot \mathbf{H} = 0$, with an applied

$\mathbf{E}^{inc}(\mathbf{r})$, yields

$$\frac{i\omega\mu}{4\pi}\oint_S G(\mathbf{r},\mathbf{r}')[\hat{\mathbf{n}}(\mathbf{r}')\times\mathbf{H}(\mathbf{r}')]-\frac{1}{k^2}\nabla' G(\mathbf{r},\mathbf{r}')\nabla'_t\cdot[\hat{\mathbf{n}}(\mathbf{r}')\times\mathbf{H}(\mathbf{r}')]\,ds' = -\hat{\mathbf{n}}(\mathbf{r})\times\mathbf{E}^{inc}(\mathbf{r}) \quad (3.2.20)$$

and

$$-\frac{\hat{\mathbf{n}}(\mathbf{r})}{4\pi}\times\int_S \nabla' G(\mathbf{r},\mathbf{r}')\times[\hat{\mathbf{n}}(\mathbf{r}')\times\mathbf{H}(\mathbf{r}')]\,ds' = \frac{1}{2}\hat{\mathbf{n}}(\mathbf{r})\times\mathbf{H}(\mathbf{r})-\hat{\mathbf{n}}(\mathbf{r})\times\mathbf{H}^{inc}(\mathbf{r}) \quad (3.2.21)$$

These vector equations for unknown current $[\hat{\mathbf{n}}(\mathbf{r})\times\mathbf{H}(\mathbf{r})]$ are the Electric Field Integral Equation (EFIE) and Magnetic Field Integral Equation (MFIE). This particular form, usually attributed to Maue [68] is the same version used by Poggio *et al* [6].

3.2.2 Classical Delta Function Dyadic Approach

Dyadic representations enable solutions of electromagnetic problems to be more compactly written. Common representations of the dyadic Green's function used in EM problems include: spatial representation in terms of derivatives of the common scalar Green's function and the eigenfunction representation in terms of vector wave functions of the geometry. Recall that the Green's function of a wave equation is a solution of the wave equation for a point source. When the solution due to a point source is known, the solution to the general source can be obtained by the principle of linear superposition [69, p.24].

The prior section performed a direct integration of the vector wave equation using the second vector Green's theorem. This section considers a method based on the use of Dyadic analysis, known to give more compact representations for complex scattering problems.

Recall the vector wave equation as

$$\nabla\times\nabla\times\mathbf{E}(\mathbf{r})-k^2\,\mathbf{E}(\mathbf{r}) = i\omega\mu\mathbf{J}_\mathbf{e}(\mathbf{r}) \quad (3.2.22)$$

The Dyadic Green's function satisfies

$$\nabla\times\nabla\times\overline{\mathbf{G}}(\mathbf{r},\mathbf{r}')-k^2\,\overline{\mathbf{G}}(\mathbf{r},\mathbf{r}') = \overline{\mathbf{I}}\delta(\mathbf{r}-\mathbf{r}') \quad (3.2.23)$$

In similar fashion to earlier, we use the Second Vector-Dyadic Green's theorem, written

$$\int_V\big[(\nabla\times\nabla\times\mathbf{P})\cdot\overline{\mathbf{Q}}-\mathbf{P}\cdot(\nabla\times\nabla\times\overline{\mathbf{Q}})\big]dV = \int_S\hat{\mathbf{n}}\cdot\big[\mathbf{P}\times(\nabla\times\overline{\mathbf{Q}})+(\nabla\times\mathbf{P})\times\overline{\mathbf{Q}}\big]dS \quad (3.2.24)$$

Substituting (3.2.22), (3.2.23) in (3.2.24) and applying the singularity exclusion approach,

$$\mathbf{E}(\mathbf{r}) = \lim_{\delta\to 0}\int_{V-V_\delta}\left(\nabla^2\mathbf{E}(\mathbf{r}') + k^2\mathbf{E}(\mathbf{r}')\right)\cdot\bar{\mathbf{I}}G(\mathbf{r},\mathbf{r}')\,dV + \oint_S\left[\hat{\mathbf{n}}(\mathbf{r})\times\mathbf{E}(\mathbf{r}')\cdot(\nabla\times G(\mathbf{r},\mathbf{r}')\right]dS'$$
$$+\oint_S\left\{(\hat{\mathbf{n}}(\mathbf{r}')\times\nabla\times\mathbf{E}(\mathbf{r}'))\cdot\bar{\mathbf{I}}G(\mathbf{r},\mathbf{r}') + \left[\hat{\mathbf{n}}(\mathbf{r}')\cdot\mathbf{E}(\mathbf{r}')\nabla\cdot\bar{\mathbf{I}}G(\mathbf{r},\mathbf{r}')\right.\right.$$
$$\left.\left.-\,\hat{\mathbf{n}}(\mathbf{r}')\cdot\bar{\mathbf{I}}G(\mathbf{r},\mathbf{r}')\nabla\cdot\mathbf{E}(\mathbf{r}')\right]\right\}dS' \quad (3.2.25)$$

Recognizing that for any $\mathbf{r}\in V$,

$$\nabla^2\mathbf{E}(\mathbf{r}') + k^2\mathbf{E}(\mathbf{r}') = i\omega\mu\left[\bar{\mathbf{I}} + \frac{\nabla\nabla}{k^2}\right]\cdot\mathbf{J}_\mathbf{e}(\mathbf{r}) \quad (3.2.26)$$

and the conventional electric field Green's dyadic, $\overline{G}_{ee}$ is the solution of

$$\overline{G}_{ee}(\mathbf{r},\mathbf{r}') = \frac{1}{4\pi}\left[\overline{I} + \frac{\nabla\nabla}{k^2}\right]G(\mathbf{r},\mathbf{r}'),\ \text{for}\ \mathbf{r}'\neq\mathbf{r} \quad (3.2.27)$$

where $G(\mathbf{r},\mathbf{r}')$ is the usual free space scalar Green's function. We can reduce the volume integral term to the key electric field equation of interest [70],

$$E(\mathbf{r}) = i\omega\mu_0\int_V\mathbf{J}(\mathbf{r}')\cdot\overline{G}_{ee}(\mathbf{r},\mathbf{r}')\,dV' \quad (3.2.28)$$

known to be valid for $\mathbf{r}$ outside of V and is valid inside V as well. If we let the surface S extend to infinity and apply the radiation condition, the surface integrals in (3.2.25) disappear, leaving the volume integral of the form in equation (3.2.28).

In deriving the equation for the electric field in terms of the electric dyadic Green's function, two methods of solution exist, one integral formula approach using a classical delta-function approach, and one without. Historically, there has been much confusion in that different solution approaches yielded differing results, where uniqueness requires the same result [71, 72, 70, 73, 74]. The fundamental difference involved the specification of the principal volume, and the associated manipulation of integral and differential operators in the field derivations. At the source point, this interchange becomes invalid [74].

For a differential operator L, its inverse is an integral operator, which can be assumed to have a kernel $g(\mathbf{r};\mathbf{r}')$. The integral operator is defined as [14, pp. 45-51]

$$L^{-1}u(\mathbf{r}) = \int g(\mathbf{r},\zeta)u(\zeta)d\zeta \quad (3.2.29)$$

By interchanging the order of integration and differentiation

$$u(\mathbf{r}) = L^{-1}Lu(\mathbf{r}) = \int Lg(\mathbf{r},\zeta)d\zeta \tag{3.2.30}$$

which implies that

$$Lg(\mathbf{r},\mathbf{r}') = \delta(\mathbf{r},\mathbf{r}') \tag{3.2.31}$$

In a rigorous sense, the operator interchange above could not be performed, however, the dirac-delta function is a symbolic function, and has special properties that enable such treatment. These properties were investigated by Schwarz in the Theory of Distributions, presented by Dirac [15]. In the strictest sense, however, special accommodations needs to be made if dyadic functions or operators are involved. This is the equivalent of a special treatment for the handling of the exclusion volume. Van Bladel [70] concluded that this dyadic Green's function is insufficient at the source point to determine the correct value of $E(\mathbf{r})$, requiring the addition of a dyadic representing a source contribution. Another name for depolarizing dyadic $\overline{L}$ is "normalized dyadic solid angle".

Yaghjian [74] reformulated equation (3.2.28) to take this source dyadic into account,

$$E(\mathbf{r}) = i\omega\mu_0 \lim \delta \to 0 \int_{V-V_\delta} \overline{G}_{ee} \cdot J \; dV' + \frac{\overline{L} \cdot J}{i\omega\epsilon_0} \tag{3.2.32}$$

where

$$\overline{L} = \frac{1}{4\pi} \int_{S_\delta} \frac{\hat{\mathbf{n}}\, \mathbf{e}_{\mathbf{R}'}}{R^2} dS' \tag{3.2.33}$$

Note that $\hat{\mathbf{n}}$ is the unit normal out of the principal volume and $\mathbf{e}_{\mathbf{R}'}$ is the unit vector from $\mathbf{r}'$ to $\mathbf{r}$. As Yaghjian points out [74, p. 252], the dyadic $\overline{L}$, which depends on the geometry of the the principal volume compensates exactly to produce the unique $E(\mathbf{r})$, regardless of the geometry of said volume.

3.3 Conclusions

In section 3.1 we introduced the Green's function method with potential theory as the basis; Poisson's equation is solved, giving a particular and complimentary solution that accommodate Dirichlet and Neumann boundary conditions on the surface of a region of interest. A progressive introduction of Green's theorem is given, with the initial focus on the scalar static problem. We build on these foundations in section 3.1.3 with the solution of the scalar wave problem, defined as an inhomogeneous scalar wave integral equation; the mathematics of Green's functions and Green's theorem are evolved. The surfaces and regions constructed are consistent with those in all radiation and scattering problems reviewed in this document.

The discontinuity, where source equals observation point, is handled by use of a singularity exclusion volume and limit calculations. For the scalar wave equation, it was shown that the vector problem was reduced to a simplified scalar form, due to separation of variables.

Section 3.2 reviews derivations of frequency-domain (time harmonic) integral equations in vector and dyadic form specific to the general radiation and scattering problem for a perfectly conducting body. A direct integration method, considered equivalent to that of Stratton and Chu was presented. The second vector Green's theorem is applied, with the typical singularity exclusion surface used. With the application of boundary conditions for perfect electric conductors, the Stratton-Chu representation is reduced to the well-known magnetic field integral equation (MFIE) and electric field integral equation (EFIE) form. This form is used extensively in chapters 4 and 5 for Spectral Expansion methods.

A review of integral equation theory applied to the Electromagnetics field would not be complete without dyadic analysis and the electric Green's dyadic. Two approaches were presented, the classical delta function dyadic approach, and Yaghjian's "combined integral formula" approach. Some of the contention surrounding these two methods was discussed; Yaghjian's formulation, which introduces the source dyadic has stood the test of time. The root cause of the problem in the delta function approach was shown to be in the interchange of operators and the handling of the principal volume. The dependency on the shape of the source region, and a treatment of the dyadic approach is given in section 3.2.2.

Chapter 4

Operator Analysis of EFIE and MFIE

This chapter draws together a diverse range of topics in integral theory and functional analysis with a cohesive treatment in preparation for the application of spectral expansion and resolvent methods. In chapter 3, a progressive development of integral equation theory for the scalar, vector and dyadic inhomogeneous equations was presented. In this chapter, we define an operator theory framework for EFIE and MFIE equations, study operator properties, the space on which the operators act, and its topological and algebraic structure.

The focus of the latter part of this thesis is on the EFIE and MFIE, with emphasis on numerical application of appropriate spectral expansions. This form is later discretized for numerical evaluation. The fundamental theories and formulations that require investigation are the properties of the (integral) operators considered, the spaces in/on which they are applied, and the expansion of points in the function space in terms of its basis elements. This chapter presents directed analyses particular to the external radiation and scattering problem from complex structures.

The mathematics of function spaces used throughout the document are introduced in section 4.1, starting with Hilbert space. A primer on algebraic and topological structure applied to function spaces is presented, including definitions of continuity, completeness and convergence. For the reader familiar with functional analysis, this section can be skipped. To facilitate handling of derivatives and integral equations, we review Lebesgue integrability, generalized distributions and Sobolev Spaces. More attention is given to Sobolev space in the region and on the boundary of a region, with a motivation for its use tied to power considerations in electromagnetic problems.

In section 4.3, we define accurate (mathematically justifiable) representations of integral equations for scattering from a complex body within a function space with the appropriate structure, including domains, norms and inner products. Application of the Stratton-Chu integral equations to the complex structures in this document, as appropriate for generic complex structures is included. Operator forms of the EFIE and MFIE are defined, followed by an analysis of the operator characteristics.

The mathematical constructs of bases are discussed in section 4.2, beginning with Schauder bases on Banach spaces to orthonormal bases and root vectors for Hilbert spaces. Derivation of operator properties used for later spectral analysis are reviewed in section 4.4. Compactness and nonselfadjointness are the 2 key characteristics that will be utilized in spectral expansion methods in chapter 5. The characteristics of the integral operator L, and in particular, the case of nonselfadjoint, compact and complete operators will be defined. Manipulations of nonselfadjoint operators to Hilbert-Schmidt forms as used in certain cases will be evolved. The theoretical analysis of nonselfadjoint operators and the applicability of orthonormality, Riesz basis with brackets and techniques for handling root vectors and Jordan Chains are also discussed in section 4.4.

Hadamard's properties for well-posed solutions to partial differential equations are given in section 4.5, with a pointed analysis of cause and effect. Known deficiencies with respect to ill-posedness and nonuniqueness of the solutions of the integral equations are discussed. In section 4.6.2, we review regularization methods as potential stabilization mechanisms for these ill-posed problems, discussing analytical techniques as well as discretization approaches, suitable for a SuperNEC integral equation solution.

4.1 Function Space for our Problem

This section provides some of the basic mathematical constructs of the *spaces* used throughout this document. The mathematical literature dealing with real, complex and functional analysis is voluminous and varies in level of complexity. The electromagnetics literature uses these tools, often without clear definitions and typically not explaining why these mathematical tools are used. Lengthy and abstract definitions can be provided for Hilbert spaces, Banach spaces, inner-product, normed, linear, metric, function, sequence and topological spaces. We summarize the most useful constructs here.

4.1.1 The Hilbert space and its Elements

Hilbert space contains a level of algebraic and topological structure that is useful for engineering problems; it will be defined in an abstract form, as given by Riesz and Von Neumann.

We can then examine each of its constituents as building blocks for the structure of the space.

Given a set of abstract elements, $f, g, h, \ldots$, an abstract Hilbert space, denoted H, possesses the following properties [75]:

1. H is a *linear space*. The operations of addition and multiplication by real and complex numbers are defined for its elements and obey the usual rules of the algebra of vectors.
2. H is a *metric space*, whose metric is derived from an inner product. This means that to every pair of elements, f and g, there is an associated real or complex number, called the inner product, denoted (f, g) or $\langle f, g \rangle$. The choice of the exact form of inner product is considered later.
3. H is a *complete space* in the sense that if a sequence of elements $\{f_n\}$ of H satisfies the condition $\|f_n - f_m\| \to 0$ for $m, n \to \infty$, then there exists an element f^* of H such that $\|f_n - f^*\| \to 0$ for $n \to \infty$.

The linear and metric spaces provide the algebraic and topological structure required to specify a problem. The definitions are built on an underlying set-theoretic structure, such as ZFC set theory [76], that includes unions, intersections, closure and subsets, to name but a few. Possible elements of these sets are scalar fields (such as $\mathcal{R}$ and $\mathcal{C}$), functions and sequences.

4.1.2 Algebraic Structure

A linear space over a scalar field $\mathbb{F}$ is a nonempty set X with structure allowing mappings of addition and scalar multiplication of elements. The usual rules of vector algebra such as commutation, distribution, etc. are used to define the additional structure of the space. The linear space structure does not provide mechanisms for dealing with infinite series and their convergence; this requires topological constructs.

Algebraic axioms allow more structure to be built on the basic "simple" structure. We can construct group-like structures, ringoids and modules. Even more complex are composite structures, such as vector spaces that are defined over 2 sets, with multiple binary operations. For further detail on Universal Algebra, consult Birkhoff [77] or Burris [78]. While normed vector spaces and inner products can be defined with algebraic structure alone, it is the introduction of the concept of the distance function, commensurate with metric spaces, that brings topological structure.

A metric space (M, d) is defined as a set M, together with a distance function $d : M \times M \to R$, a metric satisfying four conditions [79], including nonnegativity, symmetry and the triangle inequality. The set M includes the set of all real numbers, $\mathbf{R}$, the finite dimensional Euclidean

space $\mathbf{R}^n$, $\mathbf{C}$, and allows continuous or discrete metrics such as $d(x,y) = |x-y|$ for $x, y \in M$ and $M = \mathbf{C}$. The metric, as a distance function, is a measure of the distance between elements of the space, as well as the size of the space. The abstract metric space theory presented by Fréchet in his thesis [79] is built on point-set topology where each abstract element represents a point in the space. We consider this topological structure in more detail.

4.1.3 Topological Structure

Topology introduces concepts of "closeness", with properties such as convergence, continuity and completeness, to name but a few structural building blocks. The distance function introduced in the metric space, discussed above, enables the engineer to define a neighborhood of one point (or element), how "close" one element of the set is to another - continuity intuitively follows as a mechanism where two functions, or points are "close" to within some *error distance*. The norm combines the topological structure of metric spaces with the algebraic structure of linear spaces. A norm incorporates the concept of length and distance and is of course related to the distance metric. The norm, a real-valued function $\|x\|$ where $x \in H$, a linear space, satisfies properties of positivity, homogeneity, positive-definiteness and the triangle inequality. Topology provides the structure to take these vague, intuitive ideas and create useful mathematical constructs.

We state here, without proof, several definitions which are used throughout this text.

Continuity [80, pp.88-90]
Let $f : S_i \to S_j$ be a mapping of metric space (S_i, d_i) to metric space (S_j, d_j). The mapping f is said to be continuous at point $t_0 \in S_i$ if for every $\epsilon > 0$ there exists a number $\delta(t_0, \epsilon)$ such that

$$d_j(f(t), f(t_0)) < \epsilon$$

whenever $d_i(t, t_0) < \delta$. A mapping that is continuous at every point in its domain is continuous. We also use specialized types of continuity, such as Lipschitz, Hölder and Uniform continuity. See Appendix A.2 for definitions.

Convergence [80, pp. 90-94]
Convergence describes limiting behavior of a series or set to some point, the limit. There are several types of convergence suitable to various applications, including Cauchy convergence (discussed below), pointwise, uniform and mean-square convergence. A sequence of elements $\{x_n\}$ in metric space S are said to converge to an element $x \in S$, if for real $\epsilon > 0$, integer $N(\epsilon)$ exists, such that $|x - x_n| < \epsilon$ for all $n \geq N$.

Completeness
Intuitively, completeness of a set or domain means that no points are "left out". For metric

spaces, the space is complete if every Cauchy sequence converges to a point in that space. A sequence is Cauchy if for each $\epsilon > 0$, there exists an N such that $d(x_n, x_m) \leq \epsilon$ for $n, m \geq N$. Alternately, that $\lim_{n,m\to\infty} d(x_n, x_m) = 0$.

The space of real and complex numbers are complete, as is the Euclidean space. By contrast, the set of rational numbers with the standard metric is not complete. We can consider sequences in the open interval $(0, 1)$ that converge to 0 - the open interval is therefore not complete. The closed interval $[0, 1]$ is!

A *Banach space* is a complete normed linear space.

4.1.4 Generalized Derivatives and Continuous Function Spaces

The space of k-times differentiable continuous functions on domain Ω is $C^k(\Omega)$; the larger k implies the smoother function. We recognize the space of infinitely-differentiable, continuous functions as $C^\infty(\Omega)$, and the inclusions $C^\infty(\Omega) \subset C^k(\Omega) \subset C^0(\Omega)$. When defined with compact support, we use $C_0^\infty(\Omega)$. For n-dimensional multi-index $\alpha = (\alpha_1, \alpha_2, \ldots \alpha_n)$ and $|\alpha| = \alpha_1 + \alpha_2 + \ldots + \alpha_n$, the generalized derivative $D^\alpha \equiv D_1^{\alpha_1} D_2^{\alpha_2} \ldots D_n^{\alpha_n}$, with $D_i^j \equiv \partial^j / \partial x_i^j$ gives the familiar

$$D^\alpha f = D_1^{\alpha_1} D_2^{\alpha_2} \ldots D_n^{\alpha_n} = \frac{\partial^{|\alpha|} f}{\partial^{\alpha_1} x_1 \ldots \partial^{\alpha_n} x^n} \tag{4.1.1}$$

Noting the inclusions

$$C(\Omega) \equiv C^0(\Omega) \subset C(\overline{\Omega}) \subset L^2(\Omega) \tag{4.1.2}$$

we also observe that $L^2(\Omega)$ is the completion of $C(\Omega)$, where $L^2(\Omega)$ as defined below is the space of Lebesgue-square integrable functions on Ω.

In later parts of this text, domain D or volume V are used, or a volume V_1 enclosed by a surface S. Clearly D or V correspond to the domain term, Ω, while the boundary of the region, denoted $\partial\Omega$ is synonymous with surface S.

4.1.5 Lebesgue-Integrable Functions and Spaces

Riemann integrals are not applicable to the class of all measurable functions. In particular, those functions that exhibit discontinuous behavior such as the generalized functions, which include the Dirichlet delta function. For the Riemann integral being the limit of the summation, $\sum_k f(x_k)\Delta x_k$, it requires $f(x)$ at points that are close enough together, or with a set of discontinuities that are not too large. Per Kolmogorov [81, p. 48], a bounded function $f(x)$ is Riemann integrable if and only if its set of discontinuities has measure zero. The measure of a set A, denoted $\mu(A)$ is the natural extension of concepts such as length, area, volume. Computation of the Riemann integral of function f requires that the domain $[a, b]$

be partitioned into subintervals, while in the Lebesgue integral, the range of f is in effect partitioned [82, p. 56]. In this way, the notion of the integral can be extended to a much larger class of functions. The preference of Lebesgue integration versus Riemann integration is due to its ability to handle this larger class of measurable functions. For further details on measure theory and measurable functions, see Kolmogorov [81].

The space L^p is the set of functions f on the domain Ω such that $|f|^p$ is integrable, in a Lebesgue sense. As usual, $1 \leq p < \infty$. The most common space, $L^2(\Omega)$, is the set of functions that are square-integrable on Ω.

4.1.6 Sobolev Space

In practical problems, the requirement for functions to satisfy a finite energy criterion introduces a restriction of the (Banach) function space of p-integrable functions. The work of Sobolev and Schwartz (independently) on generalized, or weak, derivatives demonstrated its use in distributions as applied to engineering applications. In this text, we apply these techniques to integral equations used to describe Maxwell's equations in a Boundary Value form; the EFIE and MFIE derived in section 3.2 are used. A cursory introduction of Sobolev spaces, trace theorems and fractional order spaces are given in this section.

Since a norm is one measure of closeness between two elements or points in a function space, it follows that for a practical problem where we are interested in closeness from an "energy perspective", that the norm be modified. As before, a Banach space is a complete, normed space. A Sobolev space is a normed space of functions obtained by imposing on a function f and its generalized weak derivatives $D^\alpha f$, up to some order $|\alpha|$, the condition of finite L^p norm, for $p \geq 1$. Clearly $f, D^\alpha f \in L^p(\Omega)$. In section 6.1.2 we show how application of the Poynting vector is consistent with a Sobolev norm.

For $s \in \mathbf{N}$, $p \in [1, \infty)$, Ω an open subset of $\mathbf{R}^N$, a Lipschitz domain (see A.2 for definition), $N \geq 1$, $N \in \mathbb{N}^+$. We can define Sobolev space, $W^{s,p}(\Omega)$,

$$W^{s,p}(\Omega) = \{f \in L^p(\Omega) : \forall\, |\alpha| \leq s, D^\alpha f \in L^p(\Omega)\} \tag{4.1.3}$$

A Sobolev norm, $\|\cdot\|_{W^{s,p}(\Omega)}$ can be defined,

$$\|f\|_{W^{s,p}(\Omega)} = \sum_{|\alpha| \leq s} \|D^\alpha f\|_{L^p(\Omega)} \tag{4.1.4}$$

Assuming this norm is induced by a typical scalar product on the space, the resulting (non-Banach) Sobolev space scalar product would be given by

$$\langle f_1, f_2 \rangle_{W^{s,p}(\Omega)} = \sum_{|\alpha| \leq s} \left\{ \int_\Omega D^\alpha f_1 \cdot \overline{D^\alpha f_2}\, dV(\mathbf{x})\, dV(\mathbf{y}) \right\} \tag{4.1.5}$$

where $dV(\mathbf{x})$ is differential unit in $\mathbb{R}^N$ defined in terms of vector $\mathbf{x}$. For a complete space with this linear, conjugate-linear inner (scalar) product, we recognize the space as a Hilbert Space. There are different notations used in the literature; $W_p^s(\Omega)$ is identical to $W^{s,p}(\Omega)$. $H^s(\Omega) = W^{s,2}(\Omega)$ for $0 \leq s \leq 1$, is also common. For the particular case of $p = 2$, we note that $H^0(\Omega) \equiv L^2(\Omega)$. It follows that for $f \in H^0(\Omega)$, there is a Cauchy sequence $\{f_n\} \in C(\Omega)$ or $C^0(\Omega)$, such that $f \to f_n$ in that norm [83, p. 40].

4.1.7 Sobolev Spaces on the Boundary of a Region

Consider a hypersurface $\partial\Omega$, defined by $\partial\Omega = \{(x_1, x_2 \ldots x_{N-1}, 0)\} \subset \mathbb{R}^N$, that is a boundary of a region Ω defined by $\{(x_1, x_2 \ldots x_N) \in \mathbb{R}^N : x_N > 0\}$. This is of interest in defining a function f, near $\partial\Omega$ on $\partial\Omega$ itself, as applied in boundary values problems in electromagnetics where we are interested in tangential field components on some surface. The mapping $\gamma : C^\infty(\Omega) \to C^\infty(\partial\Omega)$ implies $\gamma \mapsto \gamma|_{\partial\Omega}$ where the final term notes a restriction to $\partial\Omega$. For $s > 1/2$, for a bounded operator, this can be extended to a mapping from $H^s(\mathbb{R}^N)$ to $H^{s-1/2}(\mathbb{R}^{N-1})$, for a Lipschitz domain Ω. This is known as the Sobolev Trace Theorem, and is a derived from a more general Restriction Theorem. An extension theorem for Sobolev spaces is also applicable and follows in a straight-forward derivation.

Trace theorems enable us to relate Sobolev spaces on a region Ω to the Sobolev spaces on a boundary Γ. Per Monk [84, pp. 36-46], for $\sigma = s - [s]$, where $[s] \in \mathbb{N}$ and $0 \leq \sigma < 1$,

$$\int_\Omega \int_\Omega \frac{|D^\alpha f(\mathbf{x}) - D^\alpha f(\mathbf{y})|^p}{|\mathbf{x} - \mathbf{y}|^{N+\sigma p}}\, dV(\mathbf{x})\, dV(\mathbf{y}) < \infty \;\; \forall \;\; |\alpha| = [s] \tag{4.1.6}$$

where $\sigma \in \mathbb{R}$. The norm for this fractional order Sobolev Space of p-integrable functions is defined by

$$\|f\|_{W^{s,p}(\Omega)} = \left[\|f\|_{W^{[s],p}(\Omega)} + \sum_{|\alpha|=[s]} \int_\Omega \int_\Omega \frac{|D^\alpha f(\mathbf{x}) - D^\alpha f(\mathbf{y})|^p}{|\mathbf{x} - \mathbf{y}|^{N+\sigma p}} dV(\mathbf{x}) dV(\mathbf{y}) \right]^{1/p} \tag{4.1.7}$$

The boundary of our domain Ω is denoted $\partial\Omega$; assume we have a Lipschitz-continuous boundary, admitting a proper subset $\Gamma \subseteq \partial\Omega$. Toselli [85] demonstrated that for functions defined on $\partial\Omega$, a space $H^s(\partial\Omega), 0 \leq s < 1$ could be defined, with a finite norm that is modified by

inclusion of a semi-norm [1]. For Lebesgue-square integrable functions, we can show that

$$\|f\|^2_{H^s(\partial\Omega)} = \int_{\partial\Omega} |f|^2 \, d\Omega + \int_{\partial\Omega}\int_{\partial\Omega} \frac{|D^\alpha f(\mathbf{x}) - D^\alpha f(\mathbf{y})|^2}{|\mathbf{x}-\mathbf{y}|^{2\sigma+N-1}} \, dS_x \, dS_y \tag{4.1.8}$$

The algebraic and topological structure inherited from Banach and Hilbert spaces is useful in engineering problems. Note that a Sobolev space is a complete space [86, p. 66]. A frequent mistake is made by assuming that if a field quantity is defined in an L^2-space, that it remains so under the operation of grad, curl and div operators. In addition, that if field quantities are specified in a space, that the quantities defined on the boundaries of the scattering domain are in the same space. Intuitively, successive derivatives of an element (function) reduces "smoothness" and therefore integrability will be impacted.

4.2 Bases and Eigensystems

4.2.1 Basis for Banach space

A sequence of vectors $\{x_1, x_2, x_3, \ldots\}$ in an infinite dimensional Banach space X is said to be a Schauder basis for X if to each vector x in the space there corresponds a unique sequence of scalars $\{c_1, c_2, c_3, \ldots\}$ such that [87, p.1]

$$x = \sum_{n=1}^{\infty} c_n x_n \tag{4.2.1}$$

The convergence of the series is understood to be with respect to the strong norm topology of X, i.e. for all x,

$$\left\| x - \sum_{i=1}^{n} c_i x_i \right\| \to 0 \quad \text{as} \quad n \to \infty \tag{4.2.2}$$

For an infinite-dimensional Banach space, the term *basis* shall refer to a Schauder basis; a Banach space with a basis must be separable. While almost all infinite dimensional separable Banach spaces are known to have bases, this is not always the case, as demonstrated by Per Enflo [88]. For practical purposes, and certainly this text, separability is assumed. The coefficients are linear functionals of the element $x \in X$ such that $c_i = \Psi_i(x)$, where $\Psi_i(x)$ describes the required function.

[1] A norm $\|f\|$ is a semi-norm $|f|$ with the additional property that it is zero if and only if f is the zero vector (positive definiteness)

4.2.2 Basis for Inner-Product and Hilbert Space

Banach Space does not include the structure provided by an inner product, i.e. for the case of an inner-product space. It has a norm, and hence, the topology required to define "closeness" of elements. Intuitively, inner-product is a measure of orthogonality between two points in the space. Various forms can be used and are typically a linear combination of the products of elements (points in the space). Though not required, inner-products and norms are often simply related, for instance, $\|f,g\|^2 = \langle f,g\rangle$ (the norm is induced by the inner-product). The definition of the inner-product is chosen for convenience, but is usually stated as a linear combination of weighted element products, such as

$$\langle f,g\rangle = \sum_i w_i f_i \overline{g_i} \quad \text{or} \quad \int w_i f_i(x)\overline{g_i(x)}dx$$

where $\{w_i\}$ denotes a set of weighting coefficients, appropriately selected [89, pp. 307-318]. Inner-product spaces are also known as Pre-Hilbert spaces (inner-product spaces that are not complete). An inner product space that is complete in the norm $\|x\| = \langle x,x\rangle^{1/2}$ is a Hilbert Space (c.f. section 4.1.1). Orthogonality of two elements f and g requires $\langle f,g\rangle = 0$ for $f \neq g$. If in addition, $f = g$, orthonormality requires $\|f\| = 1$ and $\langle f,g\rangle = 1$. In a distributional sense, $\langle x_i,x_j\rangle = \delta_{ij}$ for $x_i,x_j \in X$.

For an orthonormal set of points, $\{x_i\}$ in an inner product space X, the set $\{x_i\}$ is linearly independent. There is a maximal orthonormal set B in X with $x_i \subset B$ [89, p. 306]. Of course, X generalizes to Hilbert Spaces.

It follows that an orthonormal set $B = \{x_i\}$ in an inner product space X is maximal if and only if $x \perp x_i$ for all i implies that $x = 0$. A maximal orthonormal set B in a Hilbert Space H is referred to as an orthonormal basis for H. We also note that a Hilbert Space H has a countable orthonormal basis if and only if it is separable [89, p. 314].

A basis for a Hilbert space is a Riesz basis if it is equivalent to an orthonormal basis, that is, if it is obtained from an orthonormal basis by means of a bounded invertible operator [87, p.26]. In this section, we have addressed Q5 on the Eigenmode Expansion Method, from chapter 2, namely: **How do Riesz bases relate to the concepts we have already discussed, such as orthonormal bases, or Schauder bases?**

4.2.3 Eigensystems and Root Systems

For a linear operator T, with domain $\mathcal{D}(T)$ and range $\mathcal{R}(T)$ contained in linear space X. A scalar $\lambda \in \mathbf{C}$ such that there exists an $x \in \mathcal{D}(T), x \neq 0$ satisfying the equation $Tx = \lambda x$ is an *eigenvalue* of T. The x is an eigenvector or eigenfunction of T corresponding to eigenvalue λ.

The null space of the transformation $(T - \lambda I)$, $\mathcal{N}(T - \lambda I)$ is the eigenmanifold or eigenspace corresponding to eigenvalue λ. Note that this definition applies to linear operators, whether continuous or not.

The complex spectral theorems for finite dimensional Hilbert spaces are well-understood; for $T : H^n \to H^n$, n-dimensional space H^n has an orthonormal basis of eigenvectors $\{x_n\}$ if and only if T is normal (c.f section 4.4.2). If $T : H^n \to H^n$ admits a diagonal representation then any nondiagonal representation (i.e. in terms of a basis that is not an eigenbasis) can be diagonalized. That is,

$$[T]_{\mathbf{e}} = diag[\lambda_1, \lambda_2 \cdots \lambda_n] \text{ for eigenbasis } \mathbf{e} = \{x_n\}$$

The Spectral Theorem, for the finite-dimensional case is thus a generalization of the familiar theorem from linear algebra that a self-adjoint matrix can be diagonalized. Furthermore, that there is a diagonal matrix D and a unitary matrix U such that $T = UDU^{-1}$. Diagonal components of D are eigenvalues of T listed in some order, repeated according to their multiplicity [90, p. 52].

Extended to infinite-dimensional spaces, where $T : H \to H$ is a compact, self-adjoint (or normal) linear operator acting on Hilbert Space H. There exists an orthonormal system of eigenvectors $\{u_n\}$ corresponding to nonzero eigenvalues $\{\lambda_n\}$ such that every $x \in H$ can be uniquely represented as

$$x = x_0 + \sum_{n=1}^{\infty} \langle x, u_n \rangle u_n \tag{4.2.3}$$

where x_0 satisfies $Tx_0 = 0$. Furthermore, if $\{\lambda_n\}$ is an infinite set of distinct eigenvalues, then $\lim_{n\to\infty} \lambda_n = 0$. The Hilbert-Schmidt theorem for compact self-adjoint operators [91, pp. 179-180] defines expansion

$$Tx = \sum_n \lambda_n \langle x, x_n \rangle x_n \tag{4.2.4}$$

An isolated eigenvalue λ is called a *normal eigenvalue* if its algebraic multiplicity is finite and the Hilbert space can be decomposed into the direct sum of subspaces $H = L_\lambda \dotplus R_\lambda$. L_λ is the root subspace of A and R_λ is an invariant subspace for A in which $(T - \lambda I)^{-1}$ exists. The root space L_λ is the space of all eigen and root vectors of T corresponding to λ [92, p.10].

If the elements $\{u_k\}$ correlate with

$$Tu_p = \lambda_0 u_p + u_{p-1}, \quad p = 1, 2, \ldots, k \tag{4.2.5}$$

then element u_k is called a k-associated vector to the eigenvector u_0. The number $k + 1$ is the length of the chain $u_1, u_2, \ldots, u_k$. The element u_0 is called an eigenvector of rank r if the longest chain corresponding to u_0 has length r. The chain $u_0, u_1, \ldots, u_{r-1}$ is called the *Jordan*

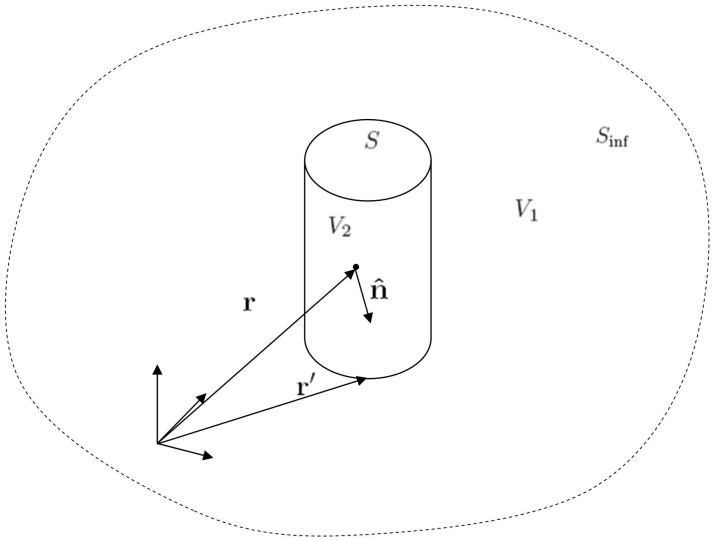

Figure 4.1: Surface S enclosing volume V_2, embedded in volume V_1

chain, and the elements are linearly independent [92, p.1-10]. Eigenvectors and associated vectors are joined under the common name of *root vectors*.

In the case of the nonselfadjoint, compact linear operator T, it is not clear if the operator has root vectors. Furthermore, it is not clear whether either the eigenvectors, the root vectors, both or neither are complete and form a basis in H. In the case where operator T is normal, the spectral theorem in equation (4.2.4) applies. We consider the nonnormal case in section 4.4.2.

4.3 Problem Geometry and Defining Equations

In the most general sense, for the scattering problem, we use the same problem geometry as defined in section 3.1. A 3-dimensional region in space V_2 is bounded by a surface S, with an outward-directed normal vector, $\hat{\mathbf{n}}$. Another region, V_1, is internally bound by S and in turn enclosed by a distant surface S_{inf}. The regions are depicted in figure 4.1.

The vector wave equations for homogeneous, isotropic region V_1, with the source external to S are

$$\nabla \times \nabla \times \mathbf{E}(\mathbf{r}) - k^2 \mathbf{E}(\mathbf{r}) = i\omega\mu \mathbf{J}_{\mathbf{e}}(\mathbf{r}) - \nabla \times \mathbf{J}_{\mathbf{m}}(\mathbf{r}) \tag{4.3.1a}$$

$$\nabla \times \nabla \times \mathbf{H}(\mathbf{r}) - k^2 \mathbf{H}(\mathbf{r}) = i\omega\epsilon \mathbf{J}_{\mathbf{m}}(\mathbf{r}) - \nabla \times \mathbf{J}_{\mathbf{e}}(\mathbf{r}) \tag{4.3.1b}$$

As before, constant $k_1 = \omega_1\sqrt{\mu_1\epsilon_1}$ encapsulates material and medium properties in the region, at the frequency of interest. Furthermore, the medium in region V_1 has zero conductivity ($\sigma = 0$). We are interested in region V_1 for the exterior scattering and radiation problem and therefore drop the subscripts of all medium and geometry parameters. Green's theorem shows that sources in V_2 can be captured as boundary conditions for V_1 on S. See section 3.1.

This abstract characterization of our problem geometry enables our 2 structures of interest, the helicopter and the LPDA (the subjects of chapter 8) to be simply characterized by a surface S, the exterior envelope of the structure, enclosing volume V_2, embedded in a medium V_1 with defined attributes.

Figure 4.2 depicts a real-world application where electromagnetic observables such as radiation patterns, input impedances and radar cross-sections are required for the electronics system design of an attack helicopter. Complex surface S, the exterior envelope of the helicopter needs to be approximated by a wire-grid structure for a Method of Moment solution using SuperNEC, depicted on the right in figure 4.2. The segmented structure is required for the numerical solution of the problem in SuperNEC. The details of this domain discretization are discussed in section 8.3.2.

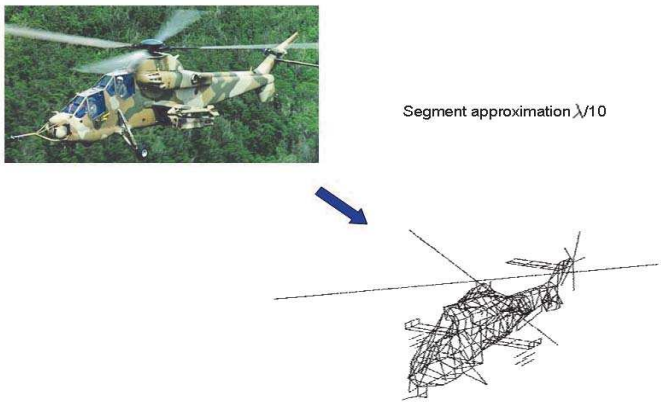

Figure 4.2: Wire-grid model approximation of an attack helicopter at 25 MHz

4.3.1 Equations for the Radiation and Scattering Problem

The Stratton-Chu representation, defined in section 3.2.1, is the direct method approach to the solution of the inhomogeneous vector wave equation, based on application of 2nd vector

Green's theorem. The equation is repeated here for convenience,

$$\int_V \left[G(\mathbf{r},\mathbf{r}')i\omega\mu\mathbf{J_e}(\mathbf{r}) - G(\mathbf{r},\mathbf{r}')(\nabla\times\mathbf{J_m}(\mathbf{r})) - (\nabla G(\mathbf{r},\mathbf{r}'))\frac{\rho_e}{\epsilon}\right] dv$$
$$= \oint_S \big[\hat{\mathbf{n}}\times\mathbf{E}(\mathbf{r})\times\nabla G(\mathbf{r},\mathbf{r}') + (\hat{\mathbf{n}}\times\mathbf{H}(\mathbf{r}))i\omega\mu G(\mathbf{r},\mathbf{r}') \qquad (4.3.2)$$
$$- (\hat{\mathbf{n}}\times\mathbf{J_m}(\mathbf{r}))G(\mathbf{r},\mathbf{r}') + (\nabla G(\mathbf{r},\mathbf{r}'))\mathbf{E}(\mathbf{r})\cdot\hat{\mathbf{n}}\big] dS$$

In section 3.2 we considered the vector wave equations derived from Maxwell's equations. Applying the Direct Integration Method (Stratton-Chu Approach) of section 3.2.10 and our problem geometry in figures 4.1 and 4.2, we find solutions to the vector wave equations (c.f. eqns (3.2.20) and (3.2.21)) as

$$i\omega\mu\oint_S G(\mathbf{r},\mathbf{r}')[\hat{\mathbf{n}}(\mathbf{r}')\times\mathbf{H}(\mathbf{r}')] - \frac{1}{k^2}\nabla' G(\mathbf{r},\mathbf{r}')\nabla'_t\cdot[\hat{\mathbf{n}}(\mathbf{r}')\times\mathbf{H}(\mathbf{r}')]\, ds' = -\hat{\mathbf{n}}(\mathbf{r})\times\mathbf{E}^{inc}(\mathbf{r}) \quad (4.3.3)$$

and

$$-\hat{\mathbf{n}}(\mathbf{r})\times\oint_S \nabla' G(\mathbf{r},\mathbf{r}')\times[\hat{\mathbf{n}}(\mathbf{r}')\times\mathbf{H}(\mathbf{r}')]\, ds' = \frac{1}{2}\hat{\mathbf{n}}(\mathbf{r})\times\mathbf{H}(\mathbf{r}) - \hat{\mathbf{n}}(\mathbf{r})\times\mathbf{H}^{inc}(\mathbf{r}) \qquad (4.3.4)$$

4.3.2 Operator Form of EFIE/MFIE

For a perfect electric conductor, the integral equations in (4.3.3) and (4.3.4) can be written in operator form as,

$$T\mathbf{J} = -\hat{\mathbf{n}}\times\mathbf{E}^i = \mathbf{M}^i \qquad (4.3.5)$$
$$\left(\frac{1}{2}I + K\right)\mathbf{J} = Z\hat{\mathbf{n}}\times\mathbf{H}^i = \mathbf{J}^i \qquad (4.3.6)$$

where Z is the characteristic impedance and I denotes the identity operator. The operators are defined as

$$T\mathbf{J} = i\omega\mu\oint\left[G(\mathbf{r},\mathbf{r}')\mathbf{J}(\mathbf{r}') - \frac{1}{k^2}\nabla' G(\mathbf{r},\mathbf{r}')\nabla'_t\cdot\mathbf{J}(\mathbf{r}')\right] ds' \qquad (4.3.7)$$
$$K\mathbf{J} = -\hat{\mathbf{n}}(\mathbf{r})\times\oint\nabla' G(\mathbf{r},\mathbf{r}')\times\mathbf{J}(\mathbf{r}')ds' \qquad (4.3.8)$$

Using an indirect method [67], we can show that an equivalent MFIE can be written, namely:

$$\left(\frac{1}{2}I - K\right)\mathbf{J} = \mathbf{J}^i \qquad (4.3.9)$$

$\mathbf{J}^i \in L^2(\Omega)^3$ and the MFIE domain is $D_K = \{\mathbf{J} : \mathbf{J}(\mathbf{r}),\, K\mathbf{J}(\mathbf{r}) \in L^2(\Omega)^3\}$. Similarly, the EFIE domain is $D_T = \{\mathbf{J} : \mathbf{J}(\mathbf{r}),\, T\mathbf{J}(\mathbf{r}) \in L^2(\Omega)^3\}$. The Riesz Representation theorem guarantees bounded linear functionals on $L^2(\Omega)^3$ [80, p. 144] of the form

$$l(x(\mathbf{r})) = \langle KJ, x\rangle = \int_\Omega K\mathbf{J}(\mathbf{r},\mathbf{r}')\,\overline{x(\mathbf{r}')}\,d\Omega' \tag{4.3.10}$$

and for the adjoint operator,

$$l(x(\mathbf{r})) = \langle KJ, x\rangle = \langle J, K^*x\rangle = \int_\Omega \mathbf{J}(\mathbf{r}')\,\overline{K^*x(\mathbf{r}')}\,d\Omega' \tag{4.3.11}$$

with the domain $D_{K^*} = \{\mathbf{J} : \mathbf{J}(\mathbf{r}),\, K\mathbf{J}(\mathbf{r}) \in L^2(\Omega)^3\}$. This representation theorem facilitates the usual inner product relation between and operator, and its adjoint.

The Riesz Representation theorem does not require compactness, but boundedness. The relation (4.3.11) still applies in the unbounded case, however the domains are different and uniqueness may not apply.

4.4 Operator Characteristics

In the application of spectral theorems, applicability of expansion types and use of bases, the characteristics of the operator need to be considered. Our Fourier series representations in chapter 2 are an expansion in a complex exponential basis, with Fourier coefficients based on minimization of a 2-norm. Many questions can be asked as to the applicability of such expansions, for instance, those of Ramm [37] on the EEM. In addition to considerations of the type of functional space considered, as discussed earlier, key operator details are relevant. For a full treatment of linear transformation theory, the reader is referred to Naylor[89] or Riesz [75]. Details of compact, selfadjoint vs nonselfadjoint and normal vs nonnormal operators are considered here.

4.4.1 Properties of Compact Operators

Let H be a Hilbert space and let $T : H \to H$ be a bounded linear operator (transformation). "A linear operator is said to be compact if and only if every infinite sequence $\{y_j\}$ of bounded elements (i.e. $\|y_j\| \le c$ for all j) of the sequence $\{Ty_j\}$ has a convergent subsequence, where $T : H \to H$. A compact operator is necessarily bounded." [93, p.129]. Effectively, compact (completely continuous) operators have near finite-dimensional ranges.

Alternatively, we can satisfy one of the two following conditions [93, p.133]:
First, that if for every $\epsilon > 0$ there is a compact operator T_ϵ such that $\|Tx - T_\epsilon x\| \le \epsilon\,\|x\|$,

for all $x \in H$, then T is compact. Second, that if T is a bounded operator on H and y_j, z_k are two complete orthonormal sets, then T is compact if

$$\sum_{j=1}^{\infty}\sum_{k=1}^{\infty}|(Ty_j, z_k)|^2$$

is finite. Compact operators exist and are defined in both Banach and Hilbert space. For the former case, where an inner-product is not defined, we use alternate definitions, given elsewhere [75, 79].

Given the similarity between compact operators in infinite-dimensional Hilbert spaces, and the more simplistic finite dimensional operators, the foundational mathematics for the infinite-dimensional compact operator are familiar to many readers. Common terms such as resolvent sets, discrete, continuous and residual spectra and the properties of the null space follow logically from finite-dimensional analysis. Linear operators with a finite-dimensional range are also known as finite-rank operators. A useful property of compact operators is that they can be represented as the sum of a finite-rank operator and an operator with a small norm. Compact operators map weakly convergent sequences into strongly convergent sequences, and are thought of a strongly bounded, or strongly continuous operators [80, p. 171]. Note also that the inverse of a compact operator is unbounded. Other key properties, particularly related to spectral representations are given in Appendix B.4.

4.4.2 Properties of Normal and Selfadjoint Operators

As before, let H be a Hilbert space and let $T : H \to H$ be a bounded linear transformation (operator). T is said to be normal if $TT^* = T^*T$; that is, T commutes with its adjoint [89, p. 367]. An operator T is normal if and only if $\|Tx\| = \|T^*x\|$ for all $x \in H$. It also follows that if T is normal, that $(T - \lambda I)$ is normal as well, where λ is a complex parameter, used later. T is said to be self-adjoint if $T = T^*$. It also follows that $\langle Tx, y\rangle = \langle x, Ty\rangle$ where $\langle\cdot,\cdot\rangle$ denotes the inner-product of the space H. Furthermore, if T is self-adjoint, it is normal.

Normal operators are operators that commute with their adjoint. We stated in section 4.2.3 that the Spectral Theorem for the infinite-dimensional Hilbert space for the normal operator was defined by the Hilbert-Schmidt Theorem. Recall from equation (4.2.4) that we have a weighted sum of projections using the inner-product mechanism,

$$Tx = \sum_n \lambda_n \langle x, x_n\rangle x_n \tag{4.4.1}$$

For the case of compact operators that are not normal, a weighted sum of projections is no

longer valid. Moreover, the eigenfunctions (eigenvectors) do not necessarily form an orthonormal (complete) set [89, pp. 476-482]. It is important to note that normal operators provide for a simplified expansion in terms of eigenvalues and eigenfunctions. The nonnormal operator case requires additional mechanics based on the theory of Schmidt. We elaborate on this in section 4.2.3. What is extremely useful is an expansion valid for every compact operator T, mapping Hilbert space H into itself, such that:

$$Tx = \sum_n \mu_n \langle x, x_n \rangle y_n \tag{4.4.2}$$

where $\{x_n\}$ and $\{y_n\}$ are two orthonormal systems and $\{\mu_1, \mu_2, \ldots\}$ are a non-negative sequence. Convergence is in the sense of the uniform topology [2], such that, $\|T - S_N\| \to 0$ as $N \to \infty$, where

$$S_N(x) = \sum_{n=1}^{N} \mu_n \langle x, x_n \rangle y_n \tag{4.4.3}$$

The eigenvalues of TT^* are μ_n^2 and the eigenvectors (eigenfunctions) are y_n^2. These spectral expansions are used in section 5.3.

4.5 Well-Posed Solutions of Fredholm Integral Equations for Surface Integral Equations (EFIE and MFIE)

Hadamard considered three properties in the solution of initial and boundary value partial differential equations [94, 95]:

1. Existence of a solution
2. Uniqueness of a solution
3. Continuous dependence of a solution on data

A problem satisfying all three requirements is considered well-posed. The numerical solution of an integral equation is typically a solution with perturbed data, as in property 3 above; this is of particular relevance to this body of work. The existence of solutions to integral equations of the first and the second kind are well known, and considered given for this analysis. For further detail, see Kress [94], Green [96], Mikhlin [97], Colton and Kress [98]. We address non-uniqueness and ill-posedness in sections 4.5.1 and 4.5.2, respectively.

[2] If $\|T_n - T\|$, that is, the supremum of $T_n x - Tx$ converges to 0, where x ranges over the unit ball in H, we say that $T_n \to T$ in the uniform operator topology. [75, p. 127]

4.5.1 Non-Uniqueness of EFIE, MFIE

For the scattering problem, there is a complication with the MFIE and EFIE surface integral equations. When the frequency of the incident wave equals an interior resonance frequency of the closed body, the EFIE does not present a unique solution [99, 100]. The MFIE is actually invalid at these frequencies [101, 102]. Canning [103, 104, 105] addressed possible solutions to the EFIE "breakdown" at resonant frequencies, which he equates to the observation that the current does not have a unique solution. Other researchers documented failures of Method of Moments solutions to the EFIE at these resonant frequencies [101, 106]. Sarkar and Rao [107] proposed an iterative minimum 2-norm solution applicable for a "numerically singular" moment matrix formulation.

The predisposition of closed bodies to present solutions at an interior resonance creates numerical problems in the calculation of the scattered exterior fields. It has been observed [103, 104] that as the frequency of the resonance is approached, that in theory the cavity (interior resonance) mode contributes less and less to the externally scattered field. Theoretically, it has been established that the correct external field is determined by the EFIE [101, 102, 103, 108]. In numerical calculation, the opposite is observed - an artifact of the formulation causes a strong scattered field. Cavity modes can occur in the interior and have associated cavity mode electric currents on the surface of the conductor, however, they do not cause radiation external to the cavity. We can deduce that they are purely numerical in nature. Furthermore, the numerical instabilities occur in narrow frequency ranges adjacent to these resonant modes. The mechanics of this instability lie in the ill-conditioning of the matrix approximation used to discretize the integral equation. There is an inextricable link to the ill-posedness of the integral equation here.

To restate, the scattered fields are sensitive to errors made in arriving at the matrix equation, a statement of the ill-posedness of the EFIE due to the method of discretization.

A survey of solutions was compiled by Peterson [106]; these include a linear combination of the MFIE and EFIE to form a Combined Field Integral Equation Formulation (CFIE) [101], a combined source method and a source simulation method to deal with the nonuniqueness [109, 99]. Boundary condition modification including the extended boundary condition (EBC) formulation [110, 111] and an augmented boundary condition [102] have also been proposed. The CFIE, in particular, is discussed in more detail in section 4.6.1.

4.5.2 Ill-posedness of the EFIE

The first kind integral equation is known to be be ill-posed, in the sense of Hadamard. Formally, for function spaces X and Y, Kress [112] defines a well-posed problem for integral

equation $LI = e$: if for any $e \in Y$, the problem has a unique solution $I \in X$, such that

$$\|I\|_X \leq C \|e\|_Y \tag{4.5.1}$$

for a constant $C > 0$. This implies that small variations in e result in limited excursions in I. By (4.5.1), $\left\|L^{-1}e\right\| \leq C \|e\|$, and $\|LI\| \geq (1/C) \|I\|$ for all $I \in X$; we can conclude that L is bounded below. As a result, it possesses a continuous (bounded) inverse that depends continuously on e. As established in the prior section, the second kind compact-plus-identity MFIE operator has a bounded inverse and is therefore well-posed. The EFIE, on the other hand is not. This fact has been exploited in several different approaches, including the Method of Analytical Regularization (MAR) [113], also known as Nosich' semi-inversion technique [114], and the method of Burton and Miller [115]. The latter is particular interesting, being applied to the scalar scattering problem and Singular Function Expansions [116, 117].

Strictly speaking, ill-posed problems must be infinite-dimensional. We use the term *discrete ill-posed problem* for the finite-dimensional problem having properties similar to the ill-posed, infinite dimensional problem. For these discrete ill-posed problems, the condition number of the matrix is typically large. Also characteristic of these problems is that replacement of the matrix by a well-conditioned derivative may not help. In practice, errors caused by discretization (or truncation), and numerically singular behavior can be difficult to isolate.

Yaghjian [118] and others have explored the ill-conditioning caused by the so-called mesh instabilities, due to discretization errors resulting from the ill-posed nature of the parent equations. It has been observed [119] that standard finite-element methods used to discretize the EFIE lead to an unbounded increase in the condition number of the resulting linear system as mesh resolution is increased.

Canning [103] observed that the moment-method equations, expressed in terms of a finite number of basis functions already contained the error; that the significant error came from the discretization operation applied from the exact integral equation to the approximate matrix equation. Furthermore, it can be shown that the moment method matrix does not come close enough to being singular to create a problem in its numerical solution. Direct matrix solution methods, such as LU decomposition and matrix inversion have limited tolerance for higher condition numbers and are generally more stable than iterative methods. The conditioning of the MFIE is independent of the discretization interval as $\delta \to 0$, whereas the EFIE sees an unbounded increase in condition number under the same limit condition [120].

The numerical consequences of iterative algorithms applied to the poorly conditioned matrices are more pronounced; Adams [119] shows that as the discretization interval tends to zero that it leads to an unbounded increase in condition number for Krylov subspace algorithms, including the conjugate-gradient method. It is also worth noting that published methods

for addressing these problems have been focussed on canonical problems, such as the PEC cylinder, or simple planar surfaces in space.

Discretization of integral equations by subdomain or entire domain basis functions produces meaningful results, however, there are no general theorems proving convergence [114]. As a result, numerical experimentation and rules of thumb are used. Dudley [121] points out that the results of solving these matrix equations are in fact numerical approximations and not solutions. Specific analysis of plane wave scattering from a circular cylinder showed errors of up to 1000% generated by a Moment-Method solution [122, 114].

4.6 Well-Posed Solutions

The EFIE implementation discussed in chapter 6 forms the core of the SuperNEC engine; commensurately, we focus our attention on questions regarding the validity of this formulation, given the question of ill-posedness and ill-conditioning of its discrete representation.

4.6.1 Stabilization of EFIE

Adams [119] and Hsiao [67] presented insightful analyses into the cause of the ill-posedness of the EFIE operator, in contrast to its MFIE counterpart. The EFIE imposes a boundary condition on magnetic currents in terms of electric sources, an impedance-type mapping, i.e. operation $T\mathbf{J}$ maps the electric current $\mathbf{J}$ into a magnetic current $\mathbf{M}$. The MFIE maps electric current into electric current. Recent developments [119, 120, 123, 124] have shown that the impedance-type mapping effected by T can be stabilized by using an admittance pre-multiplier, a preconditioning approach. The net effect is that the preconditioning causes the first kind operator T to be converted to a second kind operator mapping electric current into electric current, as is the case with the MFIE.

We explore stabilization through preconditioners, creating composite operators. Consider the Helmholtz decomposition of the EFIE operator, as follows:

$$T = T_s + T_h \tag{4.6.1}$$

$$T_s\mathbf{J} = i\omega\mu \int\!\!\!\!\!\!- G(\mathbf{r},\mathbf{r}')\mathbf{J}(\mathbf{r}')ds' \tag{4.6.2}$$

$$T_h\mathbf{J} = -\frac{i\omega\mu}{k^2} \int\!\!\!\!\!\!- \nabla' G(\mathbf{r},\mathbf{r}')\nabla'_t \cdot \mathbf{J}(\mathbf{r}')ds' \tag{4.6.3}$$

T_s is a smoothing operator and T_h a hypersingular operator, given the differential operator acting on the singular Green's function. The EFIE, as stated earlier is given as $T\mathbf{J} = \mathbf{M}^i$, where $\mathbf{J} = \eta\hat{\mathbf{n}} \times \mathbf{H}$ and $\mathbf{M}^i = -\hat{\mathbf{n}} \times \mathbf{E}^i$. Composite operators can provide smoothing effects,

or the reverse. A smoothing operator applied to another operator has a stabilizing effect, suggesting a method where ill-posedness could be eliminated.

Adams [119] proposed a stabilized form of the EFIE based on minimizing the effects of the impedance operation by pre-multiplying with an admittance operator; it is motivated by an integral identity relating the EFIE and MFIE forms. Pre-multiplication by T of the EFIE, $T\mathbf{J} = \mathbf{M^i}$ yields $T^2\mathbf{J} = T\mathbf{M^i}$. The application of the composite operator T^2, as opposed to "just" T, provides a well-posed formulation of the EFIE, in contrast to that of the ill-posed representation of the T operator. Adams claimed this as the MEFIE (Modified EFIE) form. Hsiao [67] and Roach [125] independently established the operator relationships

$$\left(-\frac{1}{2}\,I + K\right)\left(\frac{1}{2}\,I + K\right)\mathbf{J} = T^2\mathbf{J} \tag{4.6.4}$$

with the operator relation

$$\frac{1}{4}\,I - K^2 = -T^2 \tag{4.6.5}$$

Adams [119] used these relations as the key to conditioning the ill-posed EFIE, as discussed earlier, on account of the equivalence of $\left(1/4\,I - K^2\right)$ to bounded $-T^2$. In [120], the techniques of Roach [125] and Hsiao [67] were applied to give the general form of $1/4 - P_1^2 = -P_2P_3$, for abstract operators P_1, P_2 and P_3. Where P_2 is a smoothing operator acting on P_3, the composite operator P_2P_3 behaves much better than P_3 alone. The problem of non-uniqueness, on the other hand, is exacerbated by this formulation, as the "interior" resonances particular to $1/2 - P_1$ and $1/2 + P_1$ are now both present. The numerical implementation of MEFIE for certain canonical problems and details of the discretization of the operator product, the T^2 operator, based on Helmholtz decompositions are considered in [118, 119, 124, 126]. The theory of Calderon projectors [127] is also useful in the derivation of the unique operator relation used for pre-condition.

The MEFIE equation can be written as $(I - 4K^2)\mathbf{J} = -4T\mathbf{M}^i$, with the left-hand side operator representing a bounded perturbation of the identity operator. It contains the resonances of both the $(I - 2K)$ and $(I + 2K)$ operators. For this reason, Adams claims that the internal resonance problem cannot be solved using the linear summation of the MFIE and MEFIE equations in the form of a new combined-field integral equation.

The Helmholtz decomposition of T^2 as $(T_sT_s + T_sT_h + T_hT_s + T_hT_h)$ can be used to understand how discretization can maintain stabilization properties. The square of the hypersingular operator T_h needs to be removed, i.e. $T_h^2 = 0$ to ensure a stable (well-conditioned) solution. The composite operators that remain have been demonstrated to smooth the resulting second kind equation. It has been shown that the low-order divergence conforming RWG (Rao-Wilton-Glisson) basis elements provide an adequate subspace for discretization of T^2 [124]. The particular challenges for convergence of iterative solutions using RWG and other bases,

such as Buffa-Christiansen bases on barycentric meshes, are considered elsewhere [128, 129, 130]. Anrdiulli et al [128] identified challenges with Calderon preconditioning that have limited its application in practice.

- Direct discretization of the T^2 operator is infeasible as $T(f_n)$ is not available in closed form, where $T(f_n)$ denotes the integral operator evaluated at a basis function f_n.
- A variety of techniques exist for discretizing each factor in the product T^2 using ad hoc integration rules or operatorial manipulations.
- Using the expansion in singular and hypersingular components, a computationally expensive technique was proposed by Adams [124], but argued by Andriulli [128] to introduce errors in the discretized $T_h T_h(\mathbf{J})$ term.
- Finally, modification of the impedance matrix Z produced by the standard EFIE code eliminates ease of integration of a preconditioner into existing software.

These considerations were published in 2008, some time after work on this thesis first began - the fact that a broadband solution easily integrated into SuperNEC (an EFIE code) is presented herein is of much interest to the community. Preconditioning in general has seen considerable attention - a related solution was presented in Dreyer and Clark [131] where preconditioning was applied to the Sparse Iterative Method (SIM).

Internal resonances can be handled using various techniques. A localized stabilization through a localized preconditioning operator $T(local)$ allows internal resonances to be excluded, [132, 126], though must be formulated to ensure nonphysical interactions are not included. Domain limitations methods can be used, where the problem is formulated over some subdomain. An alternate technique is a modified combined-field integral equation method (MCFIE), based on a linear combination of an MEFIE and EFIE equation. This is variation of the CFIE technique pioneered by Mautz *et al* [101]. The CFIE, is a viable solution to the uniqueness problem, however, it also exhibits the discretization or mesh instability issues [123]. Even with renormalization schemes applied [133, 134], accounting for physically dominant behaviors, the CFIE can still produce poor results. This is due to the non-physical mechanisms at work in the EFIE. The MFIE, a second kind equation does not exhibit the discretization problems of its first kind counterpart, and therefore does not have the ill-conditioning problems of the EFIE. This fact is exploited later, as we consider preconditioning mechanisms to stabilize the equations.

Form of CFIE proposed by Adams [123] is $C_T\mathbf{J} = Y\mathbf{M}^i + \mathbf{J}^i$ with $C_T = (YT + 1/2I + K)$ where Y is an arbitrary nonlocal operator. Typical applications use $Y = \alpha I$ with $\alpha \in \mathbb{C}$, a complex constant. With simple norms to discretize the CFIE, it exhibits instability, caused by the EFIE kernel, T. Adams coins term MCFIE, as a combination of the MEFIE and MFIE:

it provides discretization stability, giving a stable condition number for low frequencies and high mesh resolution.

Canning [103] proposed the application of the Singular Value Decomposition (SVD) to diagonalize the (moment matrix) problem and isolate the contribution of the cavity mode. See the next section and section 5.3.2 for additional detail.

Canning's approach [103, 104] has a dependency on the number of basis functions used and requires user interaction / analyses to the define the "near-resonance". There has been some contention in the literature about the definitions of "resonance" used [135], and the fact that the resonant term may or may not correspond to the smallest singular value. Marks [116, 117, 135] showed that the singular values of the first kind equation accumulate at zero and that there are a large number accumulating there, as opposed to a single "smallest one". This challenges the methodology espoused by Canning [103, 104] that uses a SVD and orthogonalizing and eliminating the resonance term that corresponds to the smallest singular value. This author agrees with the observations of Marks, concluding that the user intervention required to define the 'near-resonance" term, as well as the tailoring of basis functions precludes it from natural integration into the SuperNEC tool.

4.6.2 Regularization

Nashed [136] presented a comprehensive review of operator-theoretic and computational approaches to regularization of ill-posed equations. He groups these methods into 3 categories;

1. Regularization methods in function spaces, including Tikhonov regularization, the method of quasi-reversibility, and the method of generalized inverses, using reproducing kernel Hilbert space (RKHS).

2. Resolution of ill-posedness by control of dimensionality, including projection methods, truncated singular-value expansions and discretization methods.

3. Iterative and filteration methods applied to the problem in function space, or to its discrete equivalent. These methods will not be discussed further. For their application, see Nashed [136].

The most common principle of regularization is to balance the minimum residual norm with a so-called side-constraint norm. The concept is that the unknown solution to an unperturbed problem is approximated by a "regularized solution" of the perturbed problem, with a small side constraint norm and a suitably small residual norm. For the ill-posed problem, while a solution can be found, it is extremely sensitive to perturbations. We look to minimize the

norm $\|\mathbf{Ax}-\mathbf{b}\|$ and introduce a side constraint constructed from an estimate of the solution, say $\Lambda(\mathbf{x}) = \|L(\mathbf{x}-\mathbf{x}^*)\|$, where L could be an identity matrix or operator.

A Sobolev norm side-constraint is also common in the literature:

$$\Lambda(\mathbf{x}) = \alpha_0 \|\mathbf{Ax}-\mathbf{b}\|^2 + \sum_{i=1}^{q} \alpha_i^2 \|L_i(\mathbf{x}-\mathbf{x}^*)\|^2 \tag{4.6.6}$$

where L_i is the ith derivative operator [137, p. 7].

The most common form of regularization is Tikhonov Regularization [138, 139, 140]; it is a logical extension of the rationale already discussed, where the goal is to minimize parameter ξ.

$$\mathbf{x}_\xi = \text{argmin}\ \{\|\mathbf{Ax}-\mathbf{b}\|^2 + \xi^2 \|L(\mathbf{x}-\mathbf{x}^*)\|^2\} \tag{4.6.7}$$

Large ξ favors the side constraint at the cost of larger residual norm, and vice-versa.

The Singular Value Decomposition (SVD) of $\mathbf{Ax}=\mathbf{b}$ and $\min_{\mathbf{x}} \|\mathbf{Ax}-\mathbf{b}\|$ are both given by

$$\mathbf{x} = \sum_{i=1}^{n} \frac{\mathbf{u}_i^T\mathbf{b}}{\sigma_i}\mathbf{v}_i \tag{4.6.8}$$

where $\mathbf{u}_i$ and $\mathbf{v}_i$ are left and right singular vectors. SVD is discussed in more detail in section 5.3.2, particularly as related to other spectral expansion methods. Fourier coefficients $\left|\mathbf{u}_i^T\mathbf{b}\right|$ corresponding to smaller singular values σ_i do not decay as fast as singular values. It follows that the solution is dominated by terms corresponding to smaller values of σ_i. Regularization dampens out the small σ_i terms that distort the solution. The generalized form for $L \neq I$, where I denotes the identity matrix, is

$$\mathbf{x}_{reg} = \sum_{i=1}^{P} f_i \frac{\mathbf{u}_i^T\mathbf{b}}{\sigma_i}\mathbf{x}_i + \sum_{i=p+1}^{n} (\mathbf{u}_i^T\mathbf{b})\ \mathbf{x}_i \tag{4.6.9}$$

The f_i are filters that vary from one regularization method to the next. For Tikhonov's method [137, 138],

$$f_i = \frac{\gamma_i^2}{\gamma_i^2+\xi^2} \tag{4.6.10}$$

The Method of Analytical Regularization (MAR), sometimes also referred to as semi-inversion, has also seen recent application in the electromagnetic literature [113, 114]. The MAR converts a first-kind linear operator equation into a second kind equation, by applying a "regularizing" operator and inverting part of the equation (typically the problematic part, such as a high frequency contributor). This lends itself to the type of regularization that the preconditioner of section 4.6.1 creates. The Identity plus Compact form thus lends itself to the

application of the Fredholm theory.

For the general first kind operator equation

$$GX = Y \text{ or } (G_1 + G_2)X = Y \tag{4.6.11}$$

the MAR transforms this into the second-kind equation

$$(I + G_1^{-1}G_2)X = G_1^{-1}Y \tag{4.6.12}$$

by applying regularizer G_1^{-1}, where it is noted that $G_1^{-1}G_2$ is compact [113]. This method of analytical regularization is very interesting, and is the subject of ongoing work by this author, but is not treated in any further detail in this document.

In closing, we remark on regularization of ill-posed problems by "Control of Dimensionality" through discretization. More primitive than the methods already discussed, this approach seeks an approximation of a solution by a linear combination of judiciously chosen basis functions. The problem is then reduced to a best approximation with a few parameters [136]. This method is used by default in the formulation of the impedance matrix by the application of the Method of Moments solution to the first kind (ill-posed) integral equation in SuperNEC. This will be discussed in some detail in chapter 6, based on the judicious application of the sine-cosine-constant basis functions for the thin-wire kernel formulation in section 6.1.

4.7 Conclusions

Hilbert space was shown, in section 4.1, to be a complete inner-product space constructed from the combined algebraic and topological structure of linear and metric spaces. In a brief primer on algebraic and topological space, we considered the axioms of linear space defined over some fields, and such topological concepts as continuity, convergence and completeness. A more detailed treatment of Sobolev space was given, by placing restrictions of finite L^p norm on the function and its generalized derivatives. For a function defined in a region of a (Sobolev) space, it was shown that in a region of that space, a Trace restriction theorem is required to define the projection of that function onto the boundary of that region. In so doing, fractional order Sobolev spaces are defined for boundaries of regions.

Section 4.2 provided a brief overview of bases, evolved from the structure of the Banach space, through to the more structured Hilbert spaces, allowing orthogonality in terms of projections. The spectral theorem for the finite and infinite dimensional cases was reviewed, linking the finite-dimensional concepts of diagonalization to an infinite-dimensional equivalent. The Hilbert-Schmidt theorem was noted to apply to the selfadjoint or normal operator

cases, requiring more complicated expansions to be used for the nonselfadjoint operator; based on the method of Schmidt. For the case where there is a dependency of multiple eigenvectors on a single eigenvalue, associated eigenvectors and Jordan chains were shown to apply.

Moving from concepts to application, section 4.3 considers the analysis of the integral equation for both the electric field and magnetic field cases, derived in chapter 3 as solutions of the inhomogeneous vector wave equations. The operator form of the EFIE and MFIE derived from the Stratton-Chu representation were stated, with all appropriate definitions of domains and ranges.

Section 4.4 focusses on analyzing the integral operators derived earlier, paying particular attention to compactness and selfadjointness. These two characteristics are fundamental to the use of spectral expansions and the applicability of various types of bases and their use in approximating solutions. Both EFIE and MFIE are shown to be nonselfadjoint. For this case, the spectral theorems presented earlier no longer apply. The nonnormal case requires the use of a modified Spectral Theorem using the method of Schmidt; the theory of root vectors and Jordan chains become applicable.

Interior resonance problems and uniqueness of solutions of the MFIE and EFIE formulations were reviewed in section 4.5, in consideration of the well-posedness of the operator equations for the scattering and radiation problems. Other mathematical and physical complications arise due to the integral equation formulation of the boundary value problem; resonances and uniqueness constraints are discussed. The behavior of the integral equations under the operation of discretization is also analyzed, as the numerical approximation of the solution of these equations can introduce instabilities.

Producing a well-posed solution using a stabilization of the ill-posed problem, or a regularization technique were considered in section 4.6. Recent techniques, based on a preconditioner for the EFIE were reviewed. A Helmholtz decomposition of the EFIE showed the impact of the smoothing and hypersingular components of the integral operator. The preconditioner, used to create a Modified EFIE (MEFIE) or a Modified Combined FIE (MCFIE) was shown to migrate the first kind operator to a more stable second kind operator. In chapter 5, this technique is linked to the fundamental mathematics of the SEM. Regularization, reviewed in section 4.6.2, presents a stabilization mechanism by allowing the unknown solution to an unperturbed problem to be approximated by a "regularized solution" of the perturbed problem. A number of techniques, including Tikhonov's method and the Method of Analytical Regularization (MAR) were presented; a solution using discretization will be applied in practice, and is discussed further in chapter 6.

Chapter 5

Spectral Expansions Applied to EFIE, MFIE

In the previous chapter we presented representations of integral equations for scattering from a complex body, within a function space with appropriate norms and inner products. The EFIE and MFIE operators were defined based on Stratton-Chu representations; they were analyzed for compactness and selfadjointness. The complications introduced by nonnormal operators were reviewed; simple eigenfunction expansions no longer apply, since basis sets are incomplete and generally non-orthogonal. The theoretical analysis of Riesz basis with brackets and techniques for handling root vectors and Jordan Chains were discussed.

With the theoretical foundations assembled in the previous chapters, solution paths in terms of spectral expansions can be determined. Functional analysis enables the practitioner to explore the solution space more easily than traditional calculus and integral equation theory permits. This chapter considers relations between various prevalent spectral theory techniques, applied specifically to a Fredholm integral equation formulation suitable for the scattering/radiation problem. In section 5.1, it will be demonstrated that there is a common theoretical basis for the Singularity Expansion Method (SEM) and stabilized (preconditioned) electric field and magnetic field integral equations (EFIE, MFIE). The significance of this is that it provides a mathematically justifiable link between a well-posed boundary integral equation and a practical operator inverse technique that has seen extensive analysis in the literature. A formal analysis of both an EFIE and MFIE solution using Fredholm's Determinant Theory (Carleman's method) is provided. For a finite-sized object admitting only pole singularities, the solution of the preconditioned EFIE and MFIE is equivalent to the frequency-domain SEM solution. The common SEM representation differs only in the coupling coefficient terms. Coupling coefficients for the MFIE are known, however, explicit formulations for the EFIE, and the modified coupling coefficients for the MEFIE and MMFIE are new contributions.

In section 5.2, two solution paths to the EFIE and MFIE are considered, based on Fredholm's alternative. First is integral equation based, an expansion of the resolvent, leading to an SEM form. The second is based on a traditional Eigenfunction (EEM) or Singular Function expansion (SFM). Based on the Fredholm Alternative and known spectral theorems, the relationship between the Singularity Expansion Method (SEM), the Eigenmode Expansion Method (EEM) and the Singular Function Expansion Method (SFM) are examined. Manipulation of the field equations with preconditioning operators enables valid SEM, EEM and SFM expansions to be written.

Section 5.3 presents an analysis of spectral expansions valid for the electric and magnetic field integral equations, suitable for the approximation of radiation and scattering from complex structures. The study of spectral expansions is completed with a review of the Singular Value Expansion (SVE) and the Singular Value Decomposition (SVD), considering their application in the electromagnetic literature, and their relation to techniques reviewed earlier.

The theoretical analyses presented in this chapter are substantial contributions to the field, published by the author in several papers [141, 142, 143]. Disparate topics in electromagnetic theory, developed over a 40 year period are shown to be inextricably linked. This same analysis provides the basis for a practical implementation in SuperNEC, developed in Chapters 6-8. We also identified earlier that a key issue with the application of spectral expansion methods was that in losing the link to the fundamental theory, any user or compiler of a black box tool, technique or algorithm would likely be subjected to anomalous behavior, with no understanding of root cause. This work goes a long way to alleviate this problem, by providing the theoretical evolution.

The MBPE abstraction and its relation to SEM is considered in the next chapter.

5.1 A Common Theoretical Basis

The Singularity Expansion Method (SEM) [39], as discussed in chapter 2, is a formal procedure for analysis of linear initial boundary value problems, resulting in a series representation for the description of a transient field. The series is defined in terms of "natural modes" of position, with time-dependent complex-exponential "natural frequencies", determining the decay of these oscillations. Most theoretical and practical work on this topic was published in the 1970s and 1980s. Interestingly, little mention is made in the literature of a key piece of work by Marin [144] based on an MFIE formulation. He concluded that the operator inverse is an analytic operator-valued function in the complex frequency plane, except at a few points (where it has poles) was the mathematical foundation of the subsequent SEM body of literature. This author demonstrated that there is a common theoretical basis for the Singularity Expansion Method (SEM) and stabilized (preconditioned) electric field and magnetic field

integral equations [141]. A review of this theory follows.

5.1.1 Field Integral Equations

Our geometry and the defining field equations have been incrementally developed in chapters 3 and 4 and are briefly restated here. Consider a perfectly conducting closed body of arbitrary shape and finite extent, with surface S, embedded in a homogeneous medium. We use the Stratton-Chu representation, a direct approach to the solution of the inhomogeneous vector wave equation based on application of the 2nd vector Green's theorem.

The total electric field in the space D_+, external to surface S is $\mathbf{E}(\mathbf{r}) = \mathbf{E}^i(\mathbf{r}) + \mathbf{E}^S(\mathbf{r}),\ \mathbf{r} \in D_+$. For notational ease, we use $\mathbf{E}_- \equiv \mathbf{E}^i$ and $\mathbf{E}_+ \equiv \mathbf{E}^S$ for certain combined forms. Similarly, for magnetic field $\mathbf{H}(\mathbf{r})$. For Hölder-continuous $\hat{\mathbf{n}} \cdot \mathbf{E}_\pm$, and tangential derivatives of $\hat{\mathbf{n}} \times \mathbf{E}_\pm$ that are Hölder continuous on S (a condition stronger than mere continuity), where $\hat{\mathbf{n}} \equiv \hat{\mathbf{n}}(\mathbf{r})$ is the outward-directed normal at $\mathbf{r}$, in the limit $\mathbf{r} \to S^\pm$ we write the Stratton-Chu representation

$$\oint\!\!\!\!\!\!-_S \left\{ i\omega\mu\, G(\mathbf{r},\mathbf{r}')\, [\hat{\mathbf{n}}(\mathbf{r}') \times \mathbf{H}(\mathbf{r}')] + \nabla' G(\mathbf{r},\mathbf{r}')[\hat{\mathbf{n}}(\mathbf{r}') \cdot \mathbf{E}(\mathbf{r}')] - \nabla' G(\mathbf{r},\mathbf{r}') \times [\hat{\mathbf{n}}(\mathbf{r}') \times \mathbf{E}(\mathbf{r}')] \right\} ds' = \mathbf{E}(\mathbf{r}) - \frac{1}{2}\mathbf{E}^i(\mathbf{r}) \quad (5.1.1)$$

where $\oint\!\!\!\!\!\!-$ denotes a Cauchy principal value integral. Hölder continuity imposes smoothness conditions on the problem that may be limiting in certain engineering applications. The scalar free-space Green's function is defined as $G(\mathbf{r},\mathbf{r}') = \exp(ik\,|\mathbf{r}-\mathbf{r}'|)/4\pi\,|\mathbf{r}-\mathbf{r}'|$. For the homogenous medium the wavenumber is $k = \omega(\mu\epsilon)^{1/2}$, where μ is the permeability and ϵ the permittivity of the medium. Characteristic impedance, $Z = 1/Y = \sqrt{\mu/\epsilon}$. $\mathbf{r}$ and $\mathbf{r}'$ are position vectors, at source and field points, respectively. Following [6]; note that $\mathbf{E}(\mathbf{r}') = (iZ/k)[\nabla' \times \mathbf{H}(\mathbf{r}')]$ and the identity $\hat{\mathbf{n}}(\mathbf{r}') \cdot [\nabla' \times \mathbf{H}(\mathbf{r}')] = -\nabla'_t \cdot [\hat{\mathbf{n}}(\mathbf{r}') \times \mathbf{H}(\mathbf{r}')]$. ∇'_t denotes the surface nabla operator with respect to source coordinates $\mathbf{r}'$. Applying the tangential electric field boundary conditions for a perfect conductor, $\hat{\mathbf{n}} \times E = 0$, expression (5.1.1) reduced to Maue's form [68], is the Electric Field Integral Equation (EFIE),

$$(i\omega\mu)\,\hat{\mathbf{n}}(\mathbf{r}) \times \oint\!\!\!\!\!\!-_S \left\{ G(\mathbf{r},\mathbf{r}')[\hat{\mathbf{n}}(\mathbf{r}') \times \mathbf{H}(\mathbf{r}')] - \frac{1}{k^2} \nabla' G(\mathbf{r},\mathbf{r}') \nabla'_t \cdot [\hat{\mathbf{n}}(\mathbf{r}') \times \mathbf{H}(\mathbf{r}')] \right\} ds' = -\hat{\mathbf{n}}(\mathbf{r}) \times \mathbf{E}^i(\mathbf{r}) \quad (5.1.2)$$

Similarly, following Stratton-Chu for deriving the magnetic field equivalent,

$$\int_S \left\{ -i\omega\epsilon G(\mathbf{r},\mathbf{r}')[\hat{\mathbf{n}}(\mathbf{r}')\times\mathbf{E}(\mathbf{r}')] + \frac{i\omega\epsilon}{k^2}\nabla' G(\mathbf{r},\mathbf{r}')[\hat{\mathbf{n}}\cdot\mathbf{H}(\mathbf{r}')] - \nabla' G(\mathbf{r},\mathbf{r}')\times[\hat{\mathbf{n}}(\mathbf{r}')\times\mathbf{H}(\mathbf{r}')] \right\} ds'$$
$$= \mathbf{H}(\mathbf{r}) - \frac{1}{2}\mathbf{H}^i(\mathbf{r}) \quad (5.1.3)$$

Applying Maxwell's equations and the surface Nabla operator as above, Maue's form of the Magnetic Field Integral Equation (MFIE) follows

$$-\hat{\mathbf{n}}(\mathbf{r})\times\int_S \nabla' G(\mathbf{r},\mathbf{r}')\times[\hat{\mathbf{n}}(\mathbf{r}')\times\mathbf{H}(\mathbf{r}')]\,ds' = \frac{1}{2}\hat{\mathbf{n}}(\mathbf{r})\times\mathbf{H}(\mathbf{r}) - \hat{\mathbf{n}}(\mathbf{r})\times\mathbf{H}^i(\mathbf{r}) \quad (5.1.4)$$

5.1.2 Operator Representation

It should be noted that the high-order or infinitely-differentiable continuous function spaces, such as $C^\infty(S)$ are not valid for practical problems, in general. The (complete) Hilbert space of Lebesgue-square-integrable functions, $L^2(S)$ in generic region of space $S \in \mathbf{R}^n, n \in \mathbf{N}$ is useful. For rigorous derivations, we consider the Sobolev space of tangential field components, a subset of the larger L^2 space.

For a perfect electric conductor, operator representations in terms of unknown tangential surface current $\mathbf{J}(\mathbf{r}) = [Z\mathbf{n}(\mathbf{r})\times\mathbf{H}(\mathbf{r})]$ of the integral equations (5.1.2) and (5.1.4) can be used (in shorthand notation) [67, 119],

$$T\mathbf{J} = -\mathbf{n}\times\mathbf{E}^i = \mathbf{M}^i \quad (5.1.5)$$
$$\left(\frac{1}{2}I + K\right)\mathbf{J} = Z\mathbf{n}\times\mathbf{H}^i = \mathbf{J}^i \quad (5.1.6)$$

where Z is the characteristic impedance and I the identity operator. Using an indirect (layer ansatz or source) approach [67], we can show that an equivalent MFIE can be written, namely

$$\left(\frac{1}{2}I - K\right)\mathbf{J} = \mathbf{M}^i \quad (5.1.7)$$

Tangential representations of (5.1.1) and (5.1.3) in matrix form can be written as

$$\begin{pmatrix} I/2 \mp K & \pm T \\ \mp T & I/2 \mp K \end{pmatrix}\begin{pmatrix} \mathbf{n}\times\mathbf{E}_\pm \\ Z\mathbf{n}\times\mathbf{H}_\pm \end{pmatrix} = \begin{pmatrix} \mathbf{n}\times\mathbf{E}_\pm \\ Z\mathbf{n}\times\mathbf{H}_\pm \end{pmatrix} \quad (5.1.8)$$

whereby the matrix term on the left, the Calderon projector, projects the tangential components of the boundary values of the interior and exterior solutions onto themselves. Through

a series of algebraic manipulations, following [67],

$$\mp \begin{pmatrix} I/4 - K^2 + T^2 & (KT + TK) \\ -(TK + KT) & I/4 - K^2 + T^2 \end{pmatrix} \begin{pmatrix} \mathbf{J} \\ \mathbf{M} \end{pmatrix} = \begin{pmatrix} \mathbf{0} \\ \mathbf{0} \end{pmatrix} \tag{5.1.9}$$

For a zero coefficient matrix, two operator relations follow (c.f. section 4.6.1),

$$TK = -KT \tag{5.1.10}$$

and

$$\frac{1}{4} I - K^2 = -T^2 \tag{5.1.11}$$

which has been termed the Calderon preconditioning relation [128]. We elaborate on its application in the next section.

It is well-known that operator $K : L^2(S) \to L^2(S)$ in (5.1.6) is compact [93, p.346], and hence bounded [80, p. 140]. Since $KK^* \neq K^*K$, thanks to the $\exp(ik|\mathbf{r}-\mathbf{r}'|)/(4\pi|\mathbf{r}-\mathbf{r}'|)$ term in the scalar free space Green's function $G(\mathbf{r}, \mathbf{r}')$, operator K is also nonselfadjoint and nonnormal. The identity operator in (5.1.6) is bounded, but not compact. The relevance of compact operators is that they have useful properties in the "forward direction", but are problematic in the "reverse direction". The inverse of a compact and invertible operator is unbounded. The compact-plus-identity operator, like (5.1.6), behaves well due to the noncompact identity operator.

The (complete) Hilbert space of Lebesgue-square-integrable functions, $L^2(S)$ in $S \subset \mathbf{R}^2$, is the appropriate function space for this application. Therefore, $\mathbf{J}^i \in L^2(S)$ and the MFIE domain is $D_K = \{\mathbf{J} : \mathbf{J}(\mathbf{r}),\, K\mathbf{J}(\mathbf{r}) \in L^2(S), \mathbf{r} \neq \mathbf{r}'\}$.

The Cauchy singular integral in the EFIE is more difficult to characterize in function space. Per Dolph [59], integral $T : C^{1+\lambda}(S) \to C^{1+\lambda}(S)$ if $S \in C^2$, where $C^{1+\lambda}$ is the space of continuous functions with continuous first derivative, i.e. Hölder continuous with exponent λ. C^2 is the space of twice continuously differentiable functions. Since not every bounded sequence will converge in $C^{1+\lambda}(S)$, T is not compact. This can be useful; if T is invertible, it has a bounded inverse. However, as Dolph noted, regularization is required before the Fredholm Alternative can be invoked to establish uniqueness. Since T is not bounded from below, the inverse is also not continuous; as $\mathbf{M}^i$ varies, $T^{-1}\mathbf{M}^i$ does not vary continuously. This problem of ill-posedness is addressed in section 4.6.1.

In the sections to follow, it will be shown that the Calderon preconditioner converts the EFIE to a second kind equation in K^2 (or T^2) which operates on $L^2(S)$. As discussed above, the resulting compact-plus-identity operator behaves well in both forward and reverse directions.

5.1.3 Solving MFIE and EFIE

Marin presented a comprehensive analysis of the solution to the MFIE based on the Fredholm Determinant theory and Carleman's method [40, 144, 1]. This work is recognized to have given the SEM a stronger mathematical foundation. The method is reviewed in this section and extended to the EFIE case as well, by first preconditioning the EFIE per operator relation (5.1.11), yielding the MEFIE. It will also be revealed that Marin's approach includes a preconditioning of the MFIE, for different reasons than those of the EFIE. We term this form the Modified MFIE (MMFIE).

Through the identical Calderon preconditioner, both the (M)EFIE and (M)MFIE can be shown to be stable integral equations with solutions that can be approximated by a Singularity Expansion Method (SEM), giving series of poles and residues in the frequency domain form and series of damped exponentials in time domain form.

As discussed above and in section 4.4, the compact-plus-identify MFIE has desirable properties, namely being well-posed with a bounded inverse, i.e. readily solvable. To apply Carleman's method, based on the Fredholm Determinant theory, an additional property is required of the operator, namely to be Hilbert-Schmidt. While the compact-plus-identity operator equation is readily solvable, this additional property is needed to ensure that the recursive series expansions of the Fredholm Determinant method apply and that the series converges. For integral operator $K : L^2(S) \rightarrow L^2(S)$ to be Hilbert-Schmidt it requires a finite norm-squared, defined by

$$\|K\|^2 \leq \int_S \int_S |k(\mathbf{x}, \mathbf{y})|^2 \, ds_x \, ds_y < \infty \tag{5.1.12}$$

where surface $S \subset \mathbf{R}^2$, and $k(\mathbf{x}, \mathbf{y})$ is the integral kernel corresponding to operator K. While K in the MFIE is bounded and compact, it does not satisfy (5.1.12) and therefore is not Hilbert-Schmidt [145, pp.162-165]; it can be shown that operator K^2 and T^2 are. It is noteworthy that Hilbert-Schmidt operators are compact, but that the reverse does not apply [146].

Multiplying both sides of (5.1.6) by $(1/2\, I - K)$, the tangential current density is the solution of the equation

$$(-1/4I + K^2)\mathbf{J} = [(-1/2I + K)]\, \mathbf{J}^i \tag{5.1.13}$$

which we refer to as the Modified MFIE (MMFIE). Multiplying both sides of (5.1.5) by T and applying (5.1.11), we have the Modified EFIE (MEFIE)

$$(-1/4I + K^2)\mathbf{J} = T\mathbf{M}^i \tag{5.1.14}$$

The solutions of the MMFIE and MEFIE are therefore

$$\mathbf{J} = \left(-1/4\, I + K^2\right)^{-1} \left[\left(-1/2\, I + K\right) \mathbf{J}^i\right] \tag{5.1.15}$$

$$\text{and } \mathbf{J} = \left(-1/4\, I + K^2\right)^{-1} \left[T\mathbf{M}^i\right] \tag{5.1.16}$$

We briefly (and formally) explore the Fredholm approach to solving these integral equations, requiring similar recursive determinant terms. Consider a one-dimensional (in space) "structure" in some medium such that $S = [u_1, u_n]$ with n equispaced subdivisions. There is a scalar current distribution on S written in matrix notation $\mathbf{x} = [x(u_1), x(u_2), \ldots x(u_n)]$ and a modified excitation $\mathbf{y} = [y(u_1), y(u_2), \ldots y(u_n)]$. We have already established that the same integral kernels are used for both MMFIE and MEFIE and use a common matrix approximation $Z = 4K^2$. Further, the kernel is an $n \times n$ matrix $\mathbf{Z} = \mathbf{Z}(u_i, u_j)$ with $i, j = 1, 2, \ldots n$. The differential length in our integral equation is approximated by the subdivision of width δ_n, The infinite-dimensional MxFIE integral equation (c.f. eqn (5.1.13) or (5.1.14)) is therefore approximated by the finite-dimensional matrix equation

$$\mathbf{x} = \mathbf{y} + \lambda\delta_n \mathbf{Z}\mathbf{x} \tag{5.1.17}$$

which has a unique solution if determinant

$$d_n(\lambda) = \det(\mathbf{I} - \lambda\delta_n \mathbf{Z}) \neq 0 \tag{5.1.18}$$

A review of the Fredholm Determinant Theory applicable to this derivation is contained in Appendix A.7. Consistent with Cramer's theorem, this solution is

$$\mathbf{x} = \frac{1}{d_n(\lambda)} \text{ adj } (\mathbf{I} - \lambda\delta_n \mathbf{Z})\mathbf{y} \tag{5.1.19}$$

The determinant can be expanded in polynomial terms, which in the limit as $n \to \infty$ is

$$\begin{aligned} d(\lambda) = \lim_{n\to\infty} d_n(\lambda) = 1 - \lambda \int_S Z(u,u)\, du + \frac{\lambda^2}{2!} \int_S \int_S \begin{vmatrix} Z(u,u) & Z(u,v) \\ Z(v,u) & Z(v,v) \end{vmatrix} du\, dv \\ - \frac{\lambda^3}{3!} \int_S \int_S \int_S \begin{vmatrix} Z(u,u) & Z(u,v) & Z(u,w) \\ Z(v,u) & Z(v,v) & Z(v,w) \\ Z(w,u) & Z(w,v) & Z(w,w) \end{vmatrix} du\, dv\, dw + \ldots \end{aligned} \tag{5.1.20}$$

The adjoint is determined as usual by using the minors of the matrix. We can therefore derive a similar expression for $D_\lambda(s,t)$. For this one-dimensional example, the solution in the limit

is [147, pp.67-68]

$$x(u) = y(u) + \lambda \int_S H_\lambda(u,v)\, y(v)\, dv = y(u) + \frac{\lambda}{d(\lambda)} \int_S D_\lambda(u,v)\, y(v)\, dv \tag{5.1.21}$$

If $d(\lambda) \neq 0$, λ is a regular value of $Z(u,v)$ and the resolvent $H_\lambda(u,v)$ is given by:

$$H_\lambda(u,v) = \frac{D_\lambda(u,v)}{d(\lambda)} \tag{5.1.22}$$

The successive approximation method used in the determinant theory shows that the solution can be written

$$x(u) = y(u) + \sum_{m=1}^{\infty} \lambda^m \int_S Z_m(u,v) y(v)\, dv \tag{5.1.23}$$

where $Z_m(u,v)$ is defined recursively,

$$Z_m(u,v) = \int_S Z(u,w) Z_{m-1}(w,v)\, dw \tag{5.1.24}$$

For the second kind integral in (5.1.17), it is the integral kernel operator Z that needs to be Hilbert-Schmidt. The identity operator does not contribute to the series convergence, instead giving the first term on the right hand side of (5.1.23). Therefore, the identity-plus-compact operator solved using the determinant theory requires the compact operator be Hilbert-Schmidt to ensure convergence of the solution.

By the Fredholm Determinant theory and Carleman's method, we can define the modified Fredholm determinant, $\delta(\lambda)$, and the modified first Fredholm minor of $Z(u,v)$, denoted $D_\lambda(u,v)$

$$d(\lambda) = \sum_{n=0}^{\infty} d_n \lambda^n \tag{5.1.25}$$

$$D_\lambda(u,v) = \sum_{n=0}^{\infty} D_n(u,v) \lambda^n \tag{5.1.26}$$

Smithies [147, pp. 65-105] showed that the series were convergent for all complex λ; Carleman's contribution was in proving that these expansions applied under the sole assumption that the operator Z was Hilbert-Schmidt. We can extend this one-dimensional approach to the solution of the general MEFIE and MMFIE in terms of modified Fredholm minors and determinants; we now consider functions in $L^2(S)$ where S is now a surface in a three-dimensional space. The validity of this extension from a scalar case to a higher-dimensional function space was established by Marin in the appendix of his paper, based on a technique

developed by Goursat [148, pp. 152-165]. For the MMFIE the solution is written in the form

$$\mathbf{J} = \left(I + \frac{D}{d}\right)\left[\left(-\frac{1}{2}\,I + K\right)\mathbf{J}^i\right] \tag{5.1.27}$$

where $D \equiv D(\mathbf{r}, \mathbf{r}'; s)$ is the modified first Fredholm minor and $d \equiv d(s)$ the modified Fredholm determinant with complex frequency, s and we set $\lambda = 1$. The tangential current density solution for the MEFIE can be written in the same way as earlier,

$$\mathbf{J} = \left(I + \frac{D}{d}\right)\left[T\mathbf{M}^i\right] \tag{5.1.28}$$

Clearly, the $(-1/2I + K)$ preconditioner applied to the MFIE can be interpreted as the Calderon preconditioner $(-1/4I + K^2)$ applied to a modified excitation term, namely $(-1/2I + K)\mathbf{J}^i$ versus $\mathbf{J}^i$. The Calderon preconditioner, creating the MEFIE and MMFIE forms, establishes a common mathematical basis; following the approach of Marin, this leads to an SEM formulation, as demonstrated in the next section. We also examine the details of the Fredholm minor and determinant terms for both MEFIE and MMFIE forms, leading to this result.

5.1.4 The Common SEM Solution

The resolvent operator $d(s)^{-1}D(\mathbf{r}, \mathbf{r}'; s)$ is common to both MMFIE and MEFIE with recursive Fredholm minor and determinant terms having been generated by recursive integrals using the analytical Fredholm integral theory (and forming a Neumann series). Formally, the modified determinant and minor are [147, pp. 71-101], [144], [149, pp. 257-286]

$$d(s) = \sum_{n=0}^{\infty} d_n(s) \tag{5.1.29}$$

$$D(\mathbf{r}, \mathbf{r}'; s) = \sum_{n=0}^{\infty} D_n(\mathbf{r}, \mathbf{r}'; s) \tag{5.1.30}$$

where

$$d_n(s) = \frac{(-1)^n}{n!}\int_{S_{\tau_n}} \dots \int_{S_{\tau_1}} \begin{vmatrix} 0 & Z(\tau_1,\tau_2) & \dots & Z(\tau_1,\tau_n) \\ Z(\tau_2,\tau_1) & 0 & \dots & Z(\tau_2,\tau_n) \\ \dots & \dots & \dots & \dots \\ Z(\tau_n,\tau_1) & Z(\tau_n,\tau_2) & \dots & 0 \end{vmatrix} d\tau_1\, d\tau_2\, \dots d\tau_n \tag{5.1.31}$$

and

$$D_n(\mathbf{r},\mathbf{r}';s)=\frac{(-1)^n}{n!}\int_{S_{\tau_n}}\dots\int_{S_{\tau_1}}\begin{vmatrix} Z(s,t) & Z(s,\tau_1) & \dots & Z(s,\tau_n)\\ Z(\tau_1,t) & 0 & \dots & Z(\tau_1,\tau_n)\\ \dots & \dots & \dots & \dots\\ Z(\tau_n,t) & Z(\tau_n,u_1) & \dots & 0\end{vmatrix} d\tau_1\, d\tau_2\, \dots d\tau_n \tag{5.1.32}$$

$d_0(s)=1$ and $D_0(\mathbf{r},\mathbf{r}';s)=4K^2(\mathbf{r},\mathbf{r}';s)$, where

$$4K^2\mathbf{J}=4\int_S\int_S K(\mathbf{r},\mathbf{r}'';s)K(\mathbf{r}'',\mathbf{r}';s)\cdot\mathbf{J}(\mathbf{r}')\,ds''ds' \tag{5.1.33}$$

with

$$K\mathbf{J}=-\frac{\mathbf{n}(\mathbf{r})}{4\pi}\times\int_S\nabla' g(\mathbf{r},\mathbf{r}')\times\mathbf{J}\,ds' \tag{5.1.34}$$

We exclude the singular point at $\mathbf{r}=\mathbf{r}'$. These formal representations are of limited value in their application to engineering problems, however, can be suitably approximated due to their interesting properties as functions in the complex plane.

The analytic Fredholm theorem states that for the family of compact operators $A(s)$ on an open, connected subset of the complex plane S; either $(I-A(s))$ is nowhere invertible in S or $(I-A(s))^{-1}$ is meromorphic in S [150, 59]. In a finite region of the complex plane, there are a finite number of poles. $D(\mathbf{r},\mathbf{r}';s)$ is an operator-valued analytic function of s, and $d(s)$ an analytic function of s; both are convergent for all s [147, pp.30-31]. It follows that $(-1/4I+K^2)^{-1}$ is an analytic operator valued function, except at the zeros of $d(s)$, where it has poles. The Mittag-Leffler theorem asks the question: is a function uniquely specified by its singular points and the coefficients of its Laurent series? The theorem statement is essentially that one can always construct a meromorphic function $f(z)$ with principal parts $G_n(z)$ of the Laurent expansion at an infinite sequence of prescribed poles provided that the sequence of poles approaches infinity [151]. Any such function can be written as

$$f(z)=\phi(z)+\sum_1^\infty(G_n(z)+Q_n(z)) \tag{5.1.35}$$

where $\phi(z)$ is an entire function and $\{Q_n(z)\}$ are polynomials that guarantee the convergence of the expansion. For the scattering problem, the entire function contributions are required to ensure convergence of the series for the early time/ high-frequency components. This accounts for transient effects during the interval in which the object is responding to the leading edge of an incident field traversing it. Baum grouped the polynomial summands and $\phi(z)$ together into a single entire function term, appended to the SEM pole series. Pearson raised concerns regarding convergence due to separating polynomial terms from their respective poles [151], making this approach questionable for the early time case. Two classes of coefficients for

accommodating the entire function are detailed below.

We can also construct this series representation in terms of the Fredholm Alternative (following from Fredholm Analytic Theorem). At the singularity points, $s = s_n$, a nontrivial solution to our integral equation with no "forcing function", implies the existence of interior or exterior resonances from structure Ω. Therefore,

$$\left(\frac{1}{2}I - K(s_n)\right)\mathbf{J}_n = 0 \tag{5.1.36}$$

$$\text{and} \quad \left(\frac{1}{2}I - K^*(s_n)\right)\mathbf{J}^*{}_n = 0 \tag{5.1.37}$$

Certain authors identify these functions $\mathbf{J}_n, \mathbf{J}^*{}_n$ as natural mode and coupling functions, respectively, corresponding to natural frequency s_n. For the case of an incident pulse, the desired tangential current density $\mathbf{J}$ in the neighborhood of S_n is [144]

$$\mathbf{J} = \sum_{p=1}^{P}\sum_{m=1}^{M} C_{npm}(s - s_n)^{-p}\mathbf{J}_{npm} + \mathbf{J}'_n \tag{5.1.38}$$

where C_{npm} are constants, $\mathbf{J}_{npm}$ are nontrivial solutions of (5.1.37), and $\mathbf{J}'_n$ is a bounded function. Taylor and Laurent series expansions around s_n, with a Mittag-Leffler expansion enable the solution of $\left(\frac{1}{2}I - K\right)^{-1}$ to be found anywhere in the plane. We now derive more explicit coefficients.

As demonstrated in Appendix B.7, the class 2 coupling coefficients for both the MFIE and EFIE forms can be derived by Laurent and Taylor series expansions around $s = s_n$. The tangential current distribution therefore follows for these two cases as

$$\mathbf{J}^{e,m}(\mathbf{r}, s) = \sum_{\alpha}\left[\frac{\Psi_\alpha^{e,m}(s)\mathbf{N}_\alpha^{e,m}(\mathbf{r})}{(s - s_\alpha)^{m_\alpha}} + \mathbf{J}_\alpha^{e,m}(\mathbf{r}, s)\right] + \mathbf{J}_{np}^{e,m}(\mathbf{r}, s) \tag{5.1.39}$$

$$\text{with} \quad \Psi_\alpha^{e,m}(s) = \frac{\langle \mathbf{C}_\alpha^{e,m}(\mathbf{r}); \mathbf{I}^{e,m}(\mathbf{r}, s)\rangle}{\langle \mathbf{C}_\alpha^{e,m}(\mathbf{r}); \Gamma_{1_\alpha}^{e,m}(\mathbf{r}, \mathbf{r}'); \mathbf{N}_\alpha^{e,m}(\mathbf{r}')\rangle} \tag{5.1.40}$$

where we use the e, m superscript to denote the EFIE and MFIE forms, respectively. Excitation terms are given by $\mathbf{I}^e(\mathbf{r}, s) = \mathbf{M}^i(\mathbf{r}, s)$ and $\mathbf{I}^m(\mathbf{r}, s) = \mathbf{J}^i(\mathbf{r}, s)$. $\Gamma_{1_\alpha}^{e,m}(\mathbf{r}, \mathbf{r}')$ is the derivative in s of the applicable kernel (c.f. eqns (5.1.2) and (5.1.4)). The coupling coefficients are stated explicitly in (B.7.19) through (B.7.23). Comparing to (5.1.35), the $\mathbf{J}_\alpha^{e,m}(\mathbf{r}, s)$ term is the polynomial entire function ensuring convergence of the series, and $\mathbf{J}_{np}^{e,m}(\mathbf{r}, s)$ corresponding to entire function $\phi(z)$.

The solution of the MMFIE coincides with the solution of the MFIE for all values of s for which the inverse operators exist. By the analytic Fredholm theorem; $(1/2I - K)^{-1}$ and $(-1/4I + K^2)^{-1}$ are analytic operator-valued functions of s, except at finite $s = s_n$ where

they have the same poles. The coupling coefficients, as determined by Marin and Baum, are based on the "original" integral equation, namely the MFIE. Its denominator is a function of the MFIE kernel. The EFIE coupling coefficient, $\Psi^e_\alpha(s)$ in (5.1.40), still contains a singular integral and may possibly present numerical instability. Modified coupling coefficients can be derived that are based on series expansions of the modified kernels (after application of the preconditioner).

Let $P(\mathbf{r},\mathbf{r}';s) \equiv [-1/4I + K^2](\mathbf{r},\mathbf{r}';s)$ denote the preconditioning operator. Its derivative with respect to s, evaluated at s_α is

$$P_{1\alpha}(\mathbf{r},\mathbf{r}') = \frac{\partial}{\partial s} P(\mathbf{r},\mathbf{r}';s)\Big|_{s=s_\alpha} \tag{5.1.41}$$

As detailed in Appendix B.7, the class 2 modified coupling coefficients for the MMFIE and MEFIE are

$$\Phi^m_\alpha(s) = \frac{\langle \mathbf{U}_\alpha(\mathbf{r}); [-1/2I + K]_\alpha(\mathbf{r},\mathbf{r}'); \mathbf{J}^i_\alpha(\mathbf{r},s)\rangle}{\langle \mathbf{U}_\alpha(\mathbf{r}); P_{1\alpha}(\mathbf{r},\mathbf{r}'); \mathbf{V}_\alpha(\mathbf{r}')\rangle} \tag{5.1.42}$$

$$\Phi^e_\alpha(s) = \frac{\langle \mathbf{U}_\alpha(\mathbf{r}); T_\alpha(\mathbf{r},\mathbf{r}'); \mathbf{M}^i_\alpha(\mathbf{r},s)\rangle}{\langle \mathbf{U}_\alpha(\mathbf{r}); P_{1\alpha}(\mathbf{r},\mathbf{r}'); \mathbf{V}_\alpha(\mathbf{r}')\rangle} \tag{5.1.43}$$

where $[-1/2I + K]_\alpha(\mathbf{r},\mathbf{r}') \equiv [-1/2I + K](\mathbf{r},\mathbf{r}';s)\big|_{s=s_\alpha}$ and $T_\alpha(\mathbf{r},\mathbf{r}') = T(\mathbf{r},\mathbf{r}';s)\big|_{s=s_\alpha}$. As demonstrated in Appendix B.7, the natural modes and coupling vectors are derived from the homogeneous solution of the integral equations (c.f. (B.7.25) and (B.7.26)) and their adjoints at $s = s_\alpha$. Since the LHS of both of these equations is the same, the natural modes of the MEFIE and MMFIE are equal, denoted $\mathbf{U}_\alpha(\mathbf{s})$. The same applies to the coupling vectors, $\mathbf{V}_\alpha(\mathbf{s})$. This differs from the EFIE and MFIE coupling coefficients where natural mode and coupling vectors are not common (the superscripts in (5.1.40) denote the different term for EFIE and MFIE case).

For the class 2 coefficients in (5.1.40), the frequency dependence of the $\Psi^{e,m}_\alpha(s)$ comes from $\mathbf{I}^{e,m}(\mathbf{r},s)$. In the time domain, this corresponds to smoothing out the rise time of the α-th pole by convolution [152]. For incident radiation or an applied source, Baum introduced the "turn-on time" t' at which the pole series is allowed to begin contributing to the representation of the surface current induced on a scattering object. If the turn-on time is chosen later than the time at which the actual response begins, then the entire function contribution must "fill the gap" between the time that the response begins and the time that the pole series contributions are allowed to contribute to the representation [152, 151]. The EFIE and MFIE class 1 coefficient is thus

$$\Psi^{e,m}_\alpha(s_\alpha) = \frac{\langle \mathbf{C}^{\mathbf{e,m}}_\alpha(\mathbf{r}); \mathbf{I}^{e,m}_{0_\alpha}(\mathbf{r})\rangle}{\langle \mathbf{C}^{e,m}_\alpha(\mathbf{r}); \Gamma^{e,m}_{1_\alpha}(\mathbf{r},\mathbf{r}'); \mathbf{N}^{e,m}_\alpha(\mathbf{r})\rangle} e^{(s_\alpha - s)t'} \tag{5.1.44}$$

where the current term $\mathbf{I}_{0_\alpha}^{e,m}(\mathbf{r})$ is evaluated at the pole. The same expression holds for the modified coupling coefficients, $\Phi_\alpha^{e,m}(s_\alpha)$. Various asymptotic techniques have been suggested for handling the early time contributions, including physical optics methods [153] and Geometrical Theory of Diffraction [154]. The entire function is not needed for the late-time description due to the early time effects having subsided. Class 2 coupling coefficients are more complicated to calculate than class 1 coefficients, however give smoother early-time results for a finite number of poles when included in the numerical summation, due to the smoother rise of resulting pole terms in the time domain [57].

Application of Laplace or Fourier Transformation, as required, gives the late-time form equivalent of (5.1.39) [152],

$$\mathbf{J}(\mathbf{r},t) = u(t-t')\sum_\alpha \Psi_\alpha^{e,m}(s_\alpha)\mathbf{N}_\alpha^{e,m}(\mathbf{r})e^{s_\alpha t} \tag{5.1.45}$$

where $u(t-t')$ is a Heaviside unit step function at $t=t'$.

Since operator $(-1/4I + K^2)$ applies to both the MMFIE and MEFIE case, with different modified excitation terms, the only difference between the MEFIE-based solution and the MMFIE-based one is the coupling coefficient, $\Psi_\alpha^{e,m}(s_\alpha)$. The solution is stable, in the sense of Hadamard, with the ill-posed first kind EFIE removed by the Calderon preconditioning, and both MEFIE and MMFIE forms having bounded norm-square on L^2.

In many applications, an abstracted form is used, where the numerator is denoted $R(s_\alpha)$ such that

$$\mathbf{J}(\mathbf{r},s) = \sum_\alpha \frac{R(s_\alpha)}{(s-s_\alpha)} \quad = \frac{b_0 + b_1 s + \ldots + b_n s^n}{a_0 + a_1 s + \ldots + a_d s^d} \tag{5.1.46}$$

Applications in the frequency domain employ this reduced order model to approximate some system response, or transfer function by poles and residues (numerator and denominator coefficients, b_k, a_k). The order of the rational function polynomials, or the commensurate number of poles and residues, are examined in other documents [34, 155, 24]. Model-based parameter estimation techniques arise from this abstract form [19].

Most recent (last 15 years) applications of the SEM do not typically calculate coupling coefficients in terms of the complex underlying recursive determinant integrals. Instead, the abstracted form is used, and poles and residues found using standard techniques of Prony, Cauchy and Newton-Raphson. Prony's methods, in the time or frequency domain are most popular. Sensitivity to input time or frequency samples have been handled by the modified LS-Prony [156] and TLS-Prony [157] methods, and other techniques based on the use of the singular value decomposition [158]. The Matrix Pencil Method (MPM) [159] has also been used for applications in low signal-to-noise ratio environments. Iterative search methods based on Newton-Raphson methods are also applied [48].

5.2 Solution Paths for EFIE and MFIE

It has just been demonstrated that the solution of the MFIE and EFIE (with preconditioning, as required) based on a SEM approach was one path of the solution of a Fredholm integral equation using Fredholm's Alternative. We extend this methodology to the other alternative presented by this theorem. Operator characteristics require other methods, such as that of Schmidt, to enable valid expansions to be given. This section addresses the formal relationships between the various spectral expansion methods, building on the intuitively satisfying approaches of chapters 2 and 3, and linking known methods in the literature. More than just adding completeness to the landscape of viable solutions considered, some of these methods continue to be used in the most recent literature [160].

5.2.1 Resolvent expansions and SEM

Using Fredholm's alternative for bounded, linear equations, we consider the first case, namely: for bounded linear Fredholm operator $A : H \to H$, adjoint operator $A^\dagger$ and for every $y, g \in H$ the corresponding nonhomogeneous and homogeneous equations,

$$Ax = y, \qquad \text{and} \qquad Ax = 0 \tag{5.2.1}$$

$$A^\dagger f = g, \qquad \text{and} \qquad A^\dagger f = 0 \tag{5.2.2}$$

have unique solutions x, f for the nonhomogeneous equation and trivial solutions for its homogeneous variant [80, p. 205]. For the second kind equation, the set of all λ such that $A = \lambda I - T$ is dense in H, and with continuous inverse (i.e one-to-one) defined on the range is the resolvent set of T, $\rho(T)$. The continuous spectrum, $C\sigma(T)$ and residual spectrum, $R\sigma(T)$, apply when the inverse is not continuous, and the range is not dense, respectively. In general, the spectrum is given by $\sigma(T) = P\sigma(T) \cup C\sigma(T) \cup R\sigma(T)$, where the term $P\sigma(T)$, the point spectrum, corresponds to the nonzero eigenvalues, the "second case" of the Fredholm Alternative. For a compact operator T, it follows that $\lambda \in P\sigma(T)$ or $\lambda \in \rho(T)$ [89].

We briefly restate one of the results from the previous section; for the second-kind MFIE,

$$\mathbf{J} = \left(\frac{1}{2} I + K\right)^{-1} \mathbf{J}^i \tag{5.2.3}$$

using the Fredholm Determinant Theory to calculate the resolvent $\left(\frac{1}{2} I + K\right)^{-1}$ of the operator equation. The resulting series approximation of the current density distributed on the structure of interest is a result of the Singularity Expansion Method, written in abstract form. We also demonstrated that this technique could be extended to an EFIE, through

self-regularization using a Calderon preconditioner. Where necessary, the full coupling coefficients could be calculated for either EFIE or MFIE. The abstract form, suitable for a Prony method is used later in this document. The pole series expansion is

$$\mathbf{J} = \sum_{p=1}^{P} \sum_{m=1}^{M} C_{npm}(s - s_n)^{-p} \mathbf{J}_{npm} \tag{5.2.4}$$

where C_{npm} are constants and $\mathbf{J}_{npm}$ are the natural mode functions (c.f eqn (5.1.37)). The entire function produced by the Mittag-Leffler expansion is ignored here. Application to practical examples is given elsewhere [34].

Intuitively, it is clear that this type of analytical broadband description of the desired tangential current density is of considerable less computational expense than the direct solution calculated at a single frequency in a frequency domain code, such as NEC.

5.2.2 Eigenfunction, Singular Function Expansions

For the "second case" of the Fredholm Alternative, the homogeneous equations $Ax = 0$ and $A^\dagger f = 0$ have nontrivial linearly independent solutions $x_1, x_2, \ldots, x_n$ and $f_1, f_2, \ldots, f_n$, with $n \geq 1$. The corresponding nonhomogeneous equations $Ax = y$ and $A^\dagger f = g$ are not solvable for all y, g [80, p. 205].

Recall that the Spectral Theorem (c.f. section 4.2.3) is a generalization of a familiar theorem from linear algebra asserting that a self-adjoint $n \times n$ matrix A, in a finite dimensional Hilbert space, can be diagonalized. This diagonalization procedure is an efficient mechanism to calculate the unknown in the matrix equation. The logical extension of this concept, and its promise of a computationally efficient alternative to a "brute-force" MoM solution, to the infinite dimensional Hilbert space is considered here.

For a compact, normal operator K, in an infinite dimensional Hilbert space, $K : H \to H$, with orthonormal basis $\{x_n\}$. Eigenfunctions $\{u_n\}$ form a basis for the range of K, R_K, and $\{v_n\}$ a basis for the null space of K, N_K. Clearly $\{u_n\} \subseteq \{x_n\}$ and $\{x_n\} = \{u_n\} \cup \{v_n\}$. By application of the (Hilbert-Schmidt) spectral theorem, admitting an operator representation, for $\lambda \neq 0$, we have

$$Ax = \sum_n \lambda_n \langle x, u_n \rangle u_n \tag{5.2.5}$$

where $\langle \cdot, \cdot \rangle$ denotes the usual integral inner product on H. The equations of the first and

second kind, respectively, with eigenvalue λ_m, have solutions

$$x = x_0 + \sum_n \frac{1}{\lambda_n}\langle y, u_n\rangle u_n \tag{5.2.6}$$

$$x = -\frac{y_0}{\lambda_m} + \sum_{n\neq m} \frac{1}{(\lambda_n - \lambda_m)}\langle y, u_n\rangle + \langle x_m, u_m\rangle u_m \tag{5.2.7}$$

where we assume $N_K \neq \{0\}$ [91, pp. 179-180], [80, p. 258]. Terms x_0 and y_0 satisfy $Kx_0 = 0$ and $Ky_0 = 0$ respectively. For an infinite set of distinct eigenvalues, $\lim_{n\to\infty} \lambda_n = 0$.

Considering the scalar radiation equation, discussed in chapter 3,

$$\left(\nabla^2 + k^2\right) u = 0 \ \text{ in } \ \Omega = \mathbb{R}/D \ \ k^2 > 0 \tag{5.2.8}$$

where Ω is the region exterior to finite obstacle D, with enclosing surface Γ. The boundary conditions are $u|_\Gamma = f$ and scalar radiation condition, $r\left(\frac{\partial u}{\partial r} - iku\right) \to 0$ as $r \to \infty$. Note that equation (5.2.8) is the exterior scalar scattering equivalent of (2.3.11) used for the interior problem of the rectangular cavity.

The solution is of the form

$$u = \int_\Gamma G_0(x, s, k)\, g(s)\, ds \tag{5.2.9}$$

$$\text{where} \quad G_0(x, y, k) = \frac{\exp(ik\,|x - y|)}{4\pi\,|x - y|} \tag{5.2.10}$$

and $g(s)$ is unknown. $G_0(x, y, k)$ is recognized as a scalar Green's function.

The inhomogeneous integral equation (of the first kind) is thus

$$Ag = \int_\Gamma G_0(x, s, s', k)\, g(s')ds' = f, \qquad s \in \Gamma \tag{5.2.11}$$

Supposing operator A satisfying equation $Ag = f$ has eigenvectors, then

$$Af_j = \lambda_j f_j \ \text{ and } \ |\lambda_1| \geq |\lambda_2| \geq \ldots \tag{5.2.12}$$

and the set $\{f_j\}$ forms a basis of Hilbert Space $H = L^2(\Gamma)$. Based on these assumptions, any element $f \in H$ can be represented by a convergent in H series,

$$f = \sum_{j=1}^{\infty} c_j\, f_j \tag{5.2.13}$$

where $c_j = \langle f, f_j\rangle$, consistent with (5.2.5). Also resulting from these assumptions is the

representation of the solution g by the linear combination of basis functions, f_j,

$$g = \sum_{j=1}^{\infty} g_j \, f_j \tag{5.2.14}$$

Using Picard's method, $g_j = \lambda_j^{-1} c_j$, such that the unknown can be defined by series

$$g = \sum_{j=1}^{\infty} \lambda_j^{-1} c_j \, f_j = \sum_{j=1}^{\infty} \lambda_j^{-1} \langle f, f_j \rangle f_j \tag{5.2.15}$$

This is a scalar equivalent of the the eigenmode expansion method (EEM). This methodology follows that of sections 2.2 and 2.3 very closely, and we can deduce that the EEM method proposed by Baum [9] is a specialization of the modal techniques used by many authors, including Collin [18] and Felsen [13]. The assumptions used expose the potential limitations of the method, and will require validation before use.

For finite dimensional spaces $\mathbf{R}^N$, the root system of a linear operator forms a basis. The general expansion of the form $\sum_j \lambda_j^{-1} c_j \, f_j$ may not be valid for A on H, because root vectors are not taken into account. Ramm, in previous work [38], pointed out that operator A is nonselfadjoint, and therefore, it is not obvious that A has eigenvalues. He also proved that nonselfadjoint operator A satisfies $A^{-1} \in R_b(H)$ and $A \in R_b(H)$ where $A \in R_b(H)$ states that the root system of linear operator A on H form a Riesz basis of H with brackets, invoking the theory of frames. By representing operator $A = A_0 + A_1$ where $A_0 > 0$ is a compact operator, and A_1 a nuclear and dissipative operator, Ramm proved that the root system of A is complete.

Normal operators are operators that commute with their adjoint, satisfying $AA^\dagger - A^\dagger A = 0$. The requirement for an operator to be normal for the scalar radiation problem is a requirement on the shape of the obstacle - it can be shown that the operator is normal for spherical surfaces and linear antennas [161]. For the case of compact operators that are not normal, a weighted sum of projections is no longer valid. Moreover, the eigenfunctions do not necessarily form an orthonormal (complete) set [89, pp. 476-482]. What is extremely useful is an expansion valid for every compact operator A, mapping Hilbert space H into itself, such that:

$$Ax = \sum_n \mu_n \langle x, x_n \rangle y_n \tag{5.2.16}$$

where $\{x_n\}$ and $\{y_n\}$ are two orthonormal systems, the left and right singular functions, and $\{\mu_1, \mu_2, \ldots\}$, the singular values, a non-negative sequence. The eigenvalues of AA^* are μ_n^2 and the eigenfunctions y_n^2. The eigenvalues of A^*A are μ_n^2 corresponding to eigenfunctions x_n^2. Comparing (5.2.16) with (5.2.5), the choice and application of spectral theorems to different operator types is clear; further detail was presented in section 4.2.3. The key to the choice of

spectral expansion is whether or not the operator of interest is normal or nonnormal.

Questions 1 through 4 on the Eigenmode Expansion Method in chapter 2 have been addressed in this section and the next.

5.2.3 Application to EEM and SFM

In the guided wave formulation of Maxwell's equations in section 2.2, an eigenproblem was constructed in the plane transverse to the direction of uniform wave propagation. The eigenfunctions were recognized to be wave vectors of an electric or magnetic intensity type, corresponding to mode wavenumber eigenvalues (c.f. equation (2.2.8)). The simplified scalar eigenvalue problem with a set of boundary conditions provided was shown to have eigenfunctions which were geometry dependent.

For the general EFIE formulation which is discussed in this chapter, the matrix equation of (6.1.12) is used. Since the natural frequencies are defined at some $s = s_\alpha$ when $\det[\mathbf{Z}(s_\alpha)] = 0$, there must be a relationship between the eigenvalues and natural frequencies inherent in the $\mathbf{Z}(s)$ system impedance matrix. Since

$$Z_{mn} = \int_{\Delta_n} f'(\mathbf{r}_m, \mathbf{r}')\Gamma(\mathbf{r}_m, \mathbf{r}')d\mathbf{r}' \tag{5.2.17}$$

equation (6.1.12) is a discretization of an "impedance" integral equation. The eigenvalues of the system impedance matrix are given by

$$\det[\mathbf{Z}(s)] = \prod_{\beta=1}^{N} \lambda_\beta(s) \tag{5.2.18}$$

where the eigenvalues are a continuous function of complex frequency, in general. An eigenvalue of the impedance matrix is referred to as an *eigenimpedance* by Baum [39]. At a natural frequency, $\det[\mathbf{Z}(s)] = 0$, implying by (5.2.18) that at least one of the eigenvalues must be zero at this frequency. It follows that 1 zero eigenvalue may correspond to several natural frequencies; the natural frequencies of a perfectly conducting sphere occur in layers similar to those of the dipole in figure 6.1, which are grouped in orthogonal "arcs" according to their corresponding eigenvalue [1].

This representation using eigenimpedances differs from that of sections 2.2 and 2.3 in that the eigenvalue is of a different type (impedance vs wavenumber) due to the different form of the eigenvalue equation. Baum [39] introduced the Eigenmode Expansion Method (EEM) of

the general form

$$\langle \Gamma(\mathbf{r}, \mathbf{r}'; s); \mathbf{R}_\beta(\mathbf{r}, s) \rangle = \lambda_\beta(s) \mathbf{R}_\beta(\mathbf{r}, s) \tag{5.2.19}$$

$$\text{and } \langle \mathbf{L}_\beta(\mathbf{r}, s); \Gamma(\mathbf{r}, \mathbf{r}'; s) \rangle = \lambda_\beta(s) \mathbf{L}_\beta(\mathbf{r}, s) \tag{5.2.20}$$

where β is the eigenmode index, as in (5.2.18). Despite the impedance vs wavenumber difference, the eigenfunction approach in section 2.3.2 which discussed transverse eigenfunctions, has the same form as (5.2.19) and (5.2.20). In the heuristic developments of section 2.1, the Fourier integral and Fourier series forms are clearly analogous to these equations. In the same way in which several natural frequencies are grouped by 1 eigenvalue, several natural modes as defined by (6.2.4) are grouped by 1 eigenmode $\mathbf{R}_\beta(\mathbf{r}, s)$ and several coupling vectors by 1 eigenmode $\mathbf{L}_\beta(\mathbf{r}, s)$. Baum [39] has presented relationships between the SEM and EEM.

Baum's equations for the Eigenmode Expansion Method as presented in (5.2.19) and (5.2.20), are clearly based on an assumption of compactness and self-adjointness of operator $\Gamma(\mathbf{r}, \mathbf{r}'; s)$ (c.f. eqn (5.2.6)). In the case of the scalar scattering problem, Ramm [37] showed that the scalar integral operator was in fact nonselfadjoint, and went on to prove that the eigenfunctions used in such an expansion may not be complete, not orthogonal and may not even exist, under certain circumstances. The types of bases and analyses of root systems versus eigensystems is given in section 4.2.

Application of the spectral theorem of eqn (5.2.5) to the MFIE, in equation (5.1.6), is not valid; operator $K : L^2(\Omega) \to L^2(\Omega)$ in (5.1.6) is compact, and hence bounded. It can also be shown to be nonselfadjoint and nonnormal. Marks [116, 117] presented a solution for the scalar scattering problem for which he coined the term Singular Function Expansion (SFM). He used the technique of Burton [115] to convert the scalar Helmholtz equation to a Fredholm integral equation of the second kind, then applying the Method of Schmidt to find a spectral (singular function) expansion.

For the case of the nonselfadjoint operator, K, in MFIE operator equation (5.1.6), we can define $U = I + 2K$ such that $U = 2\mathbf{J}^i$. The eigenvalue equation

$$U^\dagger U \psi_n = |\Lambda|^2 \psi_n \tag{5.2.21}$$

has Hermitian operator $U^\dagger U$ and eigenvalues $|\Lambda|^2$ that are real and nonnegative with eigenfunctions forming an orthonormal set. For eigenfunctions with eigenvalue equal to zero, the basis for the null space $\{v_n\}$ exists, such that $\{\psi_n\} \cup \{v_n\}$ form a complete set. The spectral form given in (5.2.16) is therefore applicable and the solution is given using Picard's method, in the form

$$\psi = \sum_n \frac{\langle \phi_n, \mathbf{J}^i \rangle}{\Lambda_n} \psi_n \tag{5.2.22}$$

ϕ_n are the complementary functions, satisfying $\phi_n = \lambda_n^{-1} U\psi_n$. The SFM is simply an application of the spectral theorem for compact, nonselfadjoint operators. Incidentally, the impact of the (compact + identity) operator in the eigenvalue equation is to offset and scale the eigenvalues. Specifically,

$$(I + 2K)\left(I^\dagger + 2K^\dagger\right)\psi_n = |\Lambda|^2 \psi_n \tag{5.2.23}$$

$$\therefore \left(K^\dagger + K + 2KK^\dagger\right)\psi_n = \frac{1}{2}\left|\Lambda^2 - 1\right|\psi_n \tag{5.2.24}$$

Using the preconditioning operator [141, 119], the representation in terms of Hilbert-Schmidt operator K^2 in (5.1.15) is simplified. Considering tangent vectors spanning the tangent plane at $\mathbf{r}$ on S, we can represent the kernel of our integral operator K as $\overline{K}(\mathbf{r}, \mathbf{r}'; s)$, a 2×2 matrix having elements $K_{ij}(\mathbf{r}, \mathbf{r}'; s)$, $i, j = 1, 2$. The integral operator expression for K follows [144]:

$$K\mathbf{J}(\mathbf{r}) = \int_S \overline{K}(\mathbf{r}, \mathbf{r}'; s) \cdot \mathbf{J}(\mathbf{r}') dS' \tag{5.2.25}$$

K^2 is given in terms of iterated kernels, such that

$$K^2\mathbf{J}(\mathbf{r}) = \int_S \overline{K_2}(\mathbf{r}, \mathbf{r}'; s) \cdot \mathbf{J}(\mathbf{r}') dS' \tag{5.2.26}$$

$$= \int_S \int_S \overline{K}(\mathbf{r}, \mathbf{r}''; s)\overline{K}(\mathbf{r}'', \mathbf{r}'; s) \cdot \mathbf{J}(\mathbf{r}') dS'' dS' \tag{5.2.27}$$

Kernel operator $K(\mathbf{r}, \mathbf{r}')$ is defined

$$K(\mathbf{r}, \mathbf{r}')\mathbf{J} = -\frac{\mathbf{n}(\mathbf{r})}{4\pi} \times \int_\Omega \nabla' G(\mathbf{r}, \mathbf{r}') \times \mathbf{J} dS' \tag{5.2.28}$$

as a function of scalar Green's function $G(\mathbf{r}, \mathbf{r}') = \exp\left(-ik\left|\mathbf{r} - \mathbf{r}'\right|\right)/4\pi\left|\mathbf{r} - \mathbf{r}'\right|$. Noting that $K^2 = KK^\dagger = K^\dagger K$, it is clear that operator K^2 is compact Hermitian, i.e. normal and selfadjoint. The Spectral Theory of compact, normal operators suffices for expansion of operator K. The Eigenmode Expansion Method is therefore valid for the preconditioned MFIE in (5.1.15). Equation (5.1.27) is therefore applicable in the expansion of required current density in terms of eigenmodes $R_\beta(\mathbf{r}; s)$ and $L_\beta(\mathbf{r}; s)$. This same analysis applies to the EFIE, since we have already proven [141] that the EFIE can be reformulated as an equation of the second kind using (5.1.11).

5.3 Relating Other Spectral Expansions

This chapter has already reviewed the Singularity Expansion Method, the Singular Function Method and the Eigenmode Expansion Method, providing a critical review of their application

to the vector integral equation problem for the electric and magnetic field cases. We complete the review of common spectral expansions in this section with a review of the Singular Value Expansion (SVE) and the Singular Value Decomposition (SVD).

5.3.1 The Singular Value Expansion (SVE)

The Singular Value Expansion (SVE) was formulated by E. Schmidt in 1907-1908 [162]; the algebraic Singular Value Decomposition (SVD) was formulated much later in 1936-1939 by Eckhart and Young. Smithies [147] extended the theory of Schmidt for a Hermitian kernel, with a system of complex numbers, the characteristic values and corresponding characteristic functions. In an L^2 space, with inner product

$$\langle u, v\rangle = \int_S u^\dagger(\mathbf{r}')v(\mathbf{r}')ds' \tag{5.3.1}$$

and non-null kernel with adjoint kernel, $K^\dagger(\mathbf{r}, \mathbf{r}')$ satisfying the usual relation,

$$K^\dagger(\mathbf{r}, \mathbf{r}') = \overline{K(\mathbf{r}', \mathbf{r})} \tag{5.3.2}$$

For $u, v \in L^2$ satisfying

$$u(\mathbf{r}) = \mu K(\mathbf{r}, \mathbf{r}')v(\mathbf{r}) \tag{5.3.3}$$

$$v(\mathbf{r}) = \mu K^\dagger(\mathbf{r}, \mathbf{r}')u(\mathbf{r}) \tag{5.3.4}$$

Schmidt identified a system of singular functions $[u, v]$ and corresponding singular value μ. In the literature, the singular values are often referred to as "s-numbers". Other authors [162] use the term, left and right singular functions for u and v respectively. The composite kernels $KK^\dagger$ and $K^\dagger K$ satisfy the relationship $(K^\dagger K)^\dagger = (K^\dagger)^\dagger K^\dagger = KK^\dagger$ - it follows that both $KK^\dagger$ and $K^\dagger K$ are Hermitian kernels. Substituting equation (5.3.3) in (5.3.4), and vice-versa,

$$u(\mathbf{r}) = \mu K(\mathbf{r}, \mathbf{r}')[\mu K^\dagger(\mathbf{r}, \mathbf{r}')u(\mathbf{r})] = \mu^2 K(\mathbf{r}, \mathbf{r}')K^\dagger(\mathbf{r}, \mathbf{r}')u(\mathbf{r}) \tag{5.3.5}$$

$$v(\mathbf{r}) = \mu K^\dagger(\mathbf{r}, \mathbf{r}')(\mu K(\mathbf{r}, \mathbf{r}')v(\mathbf{r})) = \mu^2 K^\dagger(\mathbf{r}, \mathbf{r}')K(\mathbf{r}, \mathbf{r}')v(\mathbf{r}) \tag{5.3.6}$$

Recognizing the standard characteristic value-eigenfunction relation, it is clear that we can define eigensystems $(u_n; 1/\mu_m^2)$ and $(v_n; 1/\mu_n^2)$. These of course correspond to $KK^\dagger$ and $K^\dagger K$, respectively. Also, $\mu_n > 0$ and $n \geq 1$. For some $x(\mathbf{r}) \in L^2(\Omega)$,

$$K(\mathbf{r}, \mathbf{r}')x(\mathbf{r}) = \sum_{i=1}^{\infty} \frac{\langle x, v_i\rangle}{\mu_i} u_i \tag{5.3.7}$$

Comparing equations (5.3.5) and (5.3.6) with (5.2.21), it is clear that the Singular Function Method (SFM) and the Singular Value Expansion Method (SVE) are in fact identical, and based on the theory of Schmidt. It is worth noting that in the older literature, the term characteristic value was used in favor of eigenvalue, and that they are the reciprocal of each other. Hence in comparing these equations, we note that $\Lambda^2 = 1/\mu^2$ is simply this interpretation.

5.3.2 The Singular Value Decomposition

Given a set of simultaneous equations, with matrix $A \in \mathbf{R}^{m\times n}$, where the raised dot indicates matrix multiplication,

$$\mathbf{A} \cdot \mathbf{x} = \mathbf{b}$$

Matrix $\mathbf{A}$ has a Singular Value Decomposition (SVD) defined by

$$\mathbf{A} = \mathbf{U} \cdot \Sigma \cdot \mathbf{V}^T \tag{5.3.8}$$

where $\mathbf{U} = (\mathbf{u}_1, \ldots, \mathbf{u}_N)$ and $\mathbf{V} = (\mathbf{v}_1, \ldots, \mathbf{v}_N)$ are matrices with orthonormal columns. Diagonal matrix $\Sigma = \text{diag}(w_j)$ with w_j entries corresponding to the singular values of $\mathbf{A}$, such that $w_1 \geq \ldots \geq w_n \geq 0$. $\mathbf{U}$ and $\mathbf{V}$ are square matrices for a square matrix $\mathbf{A}$: the columns of $\mathbf{U}$ whose same-numbered elements w_j are non-zero form an orthonormal set of basis vectors that span the range; the columns of $\mathbf{V}$ whose same-numbered elements w_j are zero form an orthonormal basis for the nullspace [163]. The solution of the linear system can be expressed in terms of a linear combination of basis functions, the singular vectors.

$$\mathbf{x} = \sum_{i=1}^{N} \left(\frac{\mathbf{U}_i \cdot \mathbf{b}}{w_i} \right) \mathbf{V}_i \tag{5.3.9}$$

The smallest singular values thus dominate the solution by scaling the corresponding singular vectors most. *Condition number* is defined as the ratio of the largest to the smallest singular values of a given matrix, in this case, $\text{Cond}(A) = w_1/w_n$. An excessive spread of singular values, giving a large condition number, distorts the solution. Small perturbations in $\mathbf{b}$ and $\mathbf{A}$, or rounding and precision errors in w_i, cause significant variations in $\mathbf{x}$. Errors introduced during the solution of the linear system result in a decrease in accuracy as the condition number increases. It is well-known that the singular values decay gradually to zero with no marked gap in the spectrum.

Clearly the Singular Value Decomposition and the Singular Value Expansion are closely related, seen by comparing (5.3.9) to (5.3.7). P.C. Hansen [162] characterizes the SVD as a discretization of the SVE, with similar properties as depicted in table 5.1 The matrix norm

Singular Value Expansion	Singular Value Decomposition
$\mu_1 \geq \mu_2 \geq \mu_3 \geq \ldots$	$w_1 \geq w_2 \geq w_3 \geq \ldots$
$\|K\|^2 = \sum_{i=1}^{\infty} \mu_i^2$	$\|A\|_F \sum_{i=1}^{n} w_i^2$
$\left.\begin{array}{rcl} \langle u_i, u_j \rangle & = & \delta_{ij} \\ \langle v_i, v_j \rangle & = & \delta_{ij} \end{array}\right\} i,j = 1,2,\ldots$	$\left.\begin{array}{rcl} \mathbf{u}_i^T \mathbf{u}_j & = & \delta_{ij} \\ \mathbf{v}_i^T \mathbf{v}_j & = & \delta_{ij} \end{array}\right\} i,j, = 1,2,\ldots,n$
$\begin{array}{rcl} \int_\Omega K(s,t)\, v_i(t)\, dt & = & \mu_i\, u_i(s) \\ \int_\Omega \overline{K(s,t)}\, u_i(s)\, ds & = & \mu_i\, v_i(t) \end{array}$	$\begin{array}{rcl} A\mathbf{v}_i & = & w_i\, \mathbf{u}_i \\ A^T \mathbf{u}_i & = & w_i\, \mathbf{v}_i \end{array}$

Table 5.1: Comparison of Properties of the SVD and SVE

$\|A\|_F$ is a Frobenius norm defined by

$$\|A\|_F = \sum_{i=1}^{n} \sum_{j=1}^{n} a_{ij}^2 = \sum_{i=1}^{n} w_i^2 \tag{5.3.10}$$

Using the so-called MoM-SVD approach, P.C. Hansen [162] showed that if a Fredholm integral equation of the first kind was discretized using a Method of Moments technique, that a singular value decomposition of the resulting matrix approximated the singular value expansion of the kernel.

As discussed in section 4.6.1, Canning [103, 104, 105] has proposed the use of the Singular Value Decomposition for the isolation and elimination of modes that are numerical artifacts of the EFIE formulation. The method is based on the SVD of the Impedance Matrix, and elimination of the (near) resonant mode. As will be demonstrated in the next chapter, the Impedance Matrix is derived from the EFIE using a MoM approach. This SVD method therefore is equivalent to Hansen's MoM-SVD approach [162]. In turn it is equivalent to the SFM approach discussed in section 5.2.2 and 5.2.3.

5.4 Conclusions

The integral equations for radiation and scattering from a perfectly conducting object in a homogeneous medium were stated based on the Stratton-Chu representations as EFIE and MFIE operator representations. The Calderon projectors were used to expose the linkage between the operator EFIE and MFIE, through operator relation $(1/4I - K^2) = -T^2$. When applied to the EFIE, giving Adams' MEFIE, this operator preconditions the ill-posed first kind equation, mapping it to a second kind form. It is also the same operator applied by Marin in the mathematical foundations for the SEM.

The operator relation also enables both the MFIE and EFIE to be written as Hilbert-Schmidt operators and solved using the Fredholm Determinant Theory. Through the Calderon preconditioning relation, both the MEFIE and MMFIE can be shown to be stable integral equations with solutions that can be approximated by a Singularity Expansion Method (SEM), giving series of poles and residues in the frequency domain form and series of damped exponentials in time domain form. Abstract time and frequency domain methods based on Prony's method or Model-Based Parameter Estimation (MBPE) are therefore valid approaches.

For the EFIE and MFIE compact operators, the Fredholm Alternative presents two solution paths. The first, for the resolvent set, where λ is not an eigenvalue, was shown to yield a solution through the SEM. The integral equations were first modified using the preconditioning operator established elsewhere. This enabled the Fredholm Determinant Theory to be applied in calculating the resolvent.

The second solution path, with nontrivial solutions to the homogeneous first and second kind equations, is used to analyze the Eigenmode Expansion Method and Singular Function Expansion Method. The EEM, requiring selfadjoint operators to be valid, can be replaced by the SFM, which uses singular function expansions, based on the Method of Schmidt, to calculate an expansion valid for nonselfadjoint operators. However, using the preconditioning operator again, we showed that the integral equations could be written in a Hermitian form, allowing the EEM to be used. The SFM technique is therefore not required.

As part of our analysis on spectral expansions, we also considered the Singular Value Expansion (SVE) and Singular Value Decomposition (SVD) in section 5.3. Demonstrated to be identical to the SFM, SVE is based on the Method of Schmidt where Hermitian composite kernels are constructed and simple relations between eigenvalues and singular values defined. The similarities between the SVD and SVE were highlighted in 5.3.2, where it was shown that the SVD may be considered to be a discretized version of the SVE. A known technique in the applied mathematics literature is relevant to this electromagnetic application, namely Hansen's Mom-SVD approach. The MoM application to the EFIE yields the SVE of the Fredholm equation of the first kind; since the EFIE is a nonselfadjoint operator, this is a useful representation. However, since it was noted earlier in the chapter that the preconditioner approach eliminated the need for the SVE/SFM approach, the MoM-SVD is not specifically applied.

Chapter 6

Application of Spectral Expansion Methods to SuperNEC

Chapter 5 evaluated spectral expansions suitable for the EFIE and MFIE. Common theoretical grounds were established and appropriate expansions defined for various operator types. Conclusions to theoretical questions were formed; this chapter considers a shift from the theoretical integral equations to the specific integrals and solution techniques used within SuperNEC. A key contribution of this work is that theoretical methods are presented with sufficient rigor to stand up to mathematical scrutiny, while still offering practical solutions that demonstrate the effectiveness of the techniques. When all is said and done, the goal of dramatically reducing computational expense in modelling radiation and scattering from a complex structure needs to be achieved.

Integration of a solution into SuperNEC implies that a subset of the expansion methods discussed in chapter 5 will be applicable; the fundamental architecture of this frequency domain code limits practical application. An EEM solution, for instance, does not lend itself to reasonable integration effort into SuperNEC, while an SVD method would. SuperNEC also addresses certain aspects of the discretization problem associated with ill-posedness of the first kind EFIE, due to its original formulation.

Of the spectral expansions reviewed thus far, noticeably missing is the discussion of Transfer Function Estimation and the relationship between the spectral expansions and MBPE (see chapter 2). These details are considered in this chapter. Also considered is the specific choice of a method based on the Singularity Expansion Method (SEM), using a frequency domain Prony method that addresses our requirement of reducing computational expense.

Another focal point of this chapter is to take the spectral expansion methods presented in chapter 5 and to apply them to structures comprised of wire segments. The EFIE implementation in SuperNEC is known to give accurate results, provided the design engineer complies

with modelling guidelines.

Section 6.1 reviews the thin-wire kernel equations, derived from the general EFIE already discussed. Hilbert spaces, Lebesgue-square integrability and Sobolev spaces are applied to the electromagnetics problems. The z-directed EFIE, a Fredholm equation of the first kind is solved using a Method of Moments (MoM) technique, consistent with the solution using SuperNEC. Posedness of the thin-wire kernel MoM solution is considered in some detail, using first an exact kernel and later a reduced kernel form. The analyses of the general EFIE presented in chapter 4 are extended to the specific case applicable to SuperNEC. We cast these forms in Lebesgue-square integrable function spaces, in section 6.1.2, moving on to ill-posedness considerations (section 6.1.3) with Sobolev space analysis using boundary conditions and tangential field components, creating formulations suitable for solving first kind EFIE equations. The impact of Sobolev formulations on SuperNEC integration for the exact and reduced kernels is given in section 6.1.4. For review of preliminaries on ill-posedness, see section 4.5.

In section 6.2 we consider spectral expansions applied to SuperNEC. Being an existing code, with suites of numerical implementations in place, based on underlying theoretical derivations, it is logical that our solution space of spectral expansion methods will not all be practically useful within SuperNEC. The SEM is - we view the solution at a single frequency as "expanded" through application of Taylor and Laurent series using an SEM methodology. We explore the link to the resolvent expansions of chapter 5 and techniques for evaluation of SEM parameters.

Section 6.3 presents solutions based on Prony's method for both the time- and frequency-domain case. The Frequency Domain Prony Method (FDPM), in particular, is of interest as it is suitable for analytical representation of frequency-domain models, effectively presenting a wideband model derived from SuperNEC data/simulation results. We conclude the section with an analysis of the MBPE abstraction, showing its relation to the SEM, its theoretical underpinnings and we answer questions asked in chapter 3 of this method.

6.1 A Thin Wire Solution for SuperNEC

As demonstrated in section 4.5.2, the discretization of the analytical integral equation representation for Maxwell's partial differential equations creates an ill-posed formulation. Our attempt to calculate scattered fields from a complex structure is therefore critically linked to the nature of this discretization. Independently, we know that a SuperNEC formulation, and its predecessor NEC2 used either thin-wire or extended thin-wire kernel forms of the Pocklington's (EFIE) Integral equation [41]. A series of guidelines have been empirically determined which ensure stable numerical performance. One therefore can question whether

there is a theoretical basis for validating these guidelines.

We begin this section with a formal derivation of the Method of Moment impedance matrix used within SuperNEC. Notations for Lebesgue-square integrability and Sobolev spaces for the scattering problem are stated in section 6.1.2. Section 6.1.3 considers the ill-posedness of the z-directed EFIE for the exact kernel formulation, drawing on the theoretical analyses of section 4.5.2. This is extended to the reduced form, with an evaluation of its applicability to SuperNEC thereafter.

6.1.1 The Method of Moment Formulation

While indepth derivations are not provided, this section will consider the SuperNEC formulation - an application of the integral equation theory covered in chapter 3. The inverse (integral) operator used in the approximation of a thin, cylindrical wire has been the subject of much analysis for over 60 years, with its origins traced back to the works of Pocklington, more than a century ago. The methods of Pocklington [41] and Hállen [43] form the first rigorous analysis of the linear cylindrical antenna problem; the texts "The Theory of Linear Antennas" by King [164] and "Advanced Antenna Theory" by Schelkunoff [165] are considered catalysts to the development of antenna theory in the later half of the twentieth century.

Consider a thin, conducting cylindrical wire segment in free space. Using Maxwell's equations, and the theory developed in chapter 3, we can state without further proof the z-directed form of the EFIE, known as Pocklington's integral equation. For radiation from a wire of length L [166], with surface S:

$$\int_L I(z') \left[\frac{\partial^2}{\partial z^2} G(z,z') + k^2 G(z,z') \right] dz' = -i\ \omega\epsilon E_z^{inc}(z) \quad z \in L \tag{6.1.1}$$

where k is the wavenumber, $G(z,z')$, the free-space Green's function and E_z^{inc} the z-directed field produced by the generator. For the exact formulation,

$$G(u) = \frac{1}{2\pi} \int_0^{2\pi} \frac{\exp\left[-ik\left(u^2 + 4a^2 \sin^2\left(\frac{1}{2}\theta\right)\right)\right]}{u^2 + 4a^2 \sin^2\left(\frac{1}{2}\theta\right)}\, d\theta \quad u \in \mathbf{R} \tag{6.1.2}$$

where a denotes the radius of the wire, and θ the cross-sectional angle. The simplification presented here, as derived by Schelkunoff [165] is the z-directed formulation of the Electric Field Integral Equation (EFIE), eqn (5.1.2). While a full derivation is not given here, some analysis of the inverse operator problem with respect to Green's functions is given in section B.1. Mei [166] provides a pedestrian prescription for a general curved wire in terms of a distance parametric independent variable.

For the thin-wire approximation, we generate the reduced-kernel form. This approximation assumes that the current can be represented by a filament on the z-axis. Transverse currents and circumferential variations are ignored and the required boundary conditions are only enforced in the axial region. The free space Green's function, $G(z, z')$ that is consistent with these assumptions, is given by

$$G(z, z') = \frac{e^{-jkR}}{4\pi R} \quad \text{where} \quad R = ((z - z')^2 + a^2)^{1/2} \tag{6.1.3}$$

Let $l(z, z') = \left[\frac{\partial^2}{\partial z^2} G(z, z') + k^2 G(z, z')\right]$, denote the kernel. This approximation is valid for wire radii significantly less than wire length and wavelength.

For these derivations, the reader is referred to the work of Poggio *et al* [6]. For brevity, discussions relating to the Numerical Electromagnetic Code (NEC2) in this document will be limited to the SuperNEC implementation, which formed the basis of this work. The electromagnetic framework presented in the Fortran code, NEC2, is still present, in a more advanced object-oriented form in SuperNEC [5].

The formulation of (6.1.1) as well as the equations to follow are valid at a single frequency. Viewing (6.1.1) as a general linear operator equation

$$Lh = e \tag{6.1.4}$$

with h the unknown response and e the excitation vector. Consistent with the definitions of section 4.1, $h, e \in L^2(S)^1$, where S is the surface of the cylindrical wire segment; the z-directed formulation integral is evaluated over the length of the wire segment. The unknown function h, in (6.1.4), the z-directed current density, is a point in an infinite dimensional Lebesgue square-integrable function space. A projection of the function from an infinite-dimensional space to a finite P-dimensional "approximation", can be represented as a sum of P basis functions, such that

$$h = \sum_{p=1}^{P} \alpha_p h_p \tag{6.1.5}$$

where α_p is a scalar coefficient. The kernel of (6.1.1), $l(z, z') \in L^2(S \times S)^{1\times 1}$ has corresponding integral operator $L : L^2(S)^1 \rightarrow L^2(S)^1$. Authors often drop the superscript "1", the spatial dimension of the geometry.

Performing an inner product of (6.1.4) and substituting (6.1.5) with N weighting functions,

w_m, we have

$$\begin{aligned} \sum_{p=1}^{P} \alpha_p \langle w_m, Lh_p \rangle &= \langle w_m, e \rangle \quad \text{for} \quad m = 1, 2, \ldots, N \\ \text{where} \quad \langle x, y \rangle &= \int_S x(\mathbf{r}) y(\mathbf{r})\, dS \quad \text{for SuperNEC} \end{aligned} \tag{6.1.6}$$

$\langle x, y \rangle$ defines the inner product of vectors x and y. For the Fredholm integral equation used in the EFIE formulation, a wire of length L, divided into N segments of length Δ_n, with dirac-delta weighting functions applied at $\mathbf{r}_m$ is given by

$$\int_{-L/2}^{L/2} \sum_{p=1}^{P} \alpha_{np} h_{np}(\mathbf{r}_m, \mathbf{r}'; s_\beta) \Gamma(\mathbf{r}_m, \mathbf{r}'; s_\beta) d\mathbf{r}' = -E_{\tan}(\mathbf{r}_m; s_\beta) \quad \text{for} \quad m = 1, 2, \ldots, N \tag{6.1.7}$$

where $\Gamma(\cdot)$ is the kernel of the Fredholm equation and s_β the frequency at which the integral is formulated. $E_{\tan}$ is the tangential electric field at the surface of the wire segment[1]. Sub-sectional bases [3] have been used, implying that P basis functions are defined over each of the N segments with different coefficients α_{pn} for each segment. Equation (6.1.5) becomes

$$h_n = \sum_{p=1}^{P} \alpha_{pn} h_{pn} \tag{6.1.8}$$

on segment n. Applying the weighting functions at the midpoints of each of the segments comprising the wire gives N equations in N unknowns. The SuperNEC basis functions are represented by 3 terms: a sine, cosine and constant term, viz. on segment n [4],

$$h_n(d) = A_n + B_n \sin k(d - d_n) + C_n \cos k(d - d_n) \quad \text{and} \quad |d - d_n| < \Delta_n/2 \tag{6.1.9}$$

where d is a distance parameter along the wire axis at $\mathbf{r}$, d_n the distance parameter at the centre of the n-th segment and k the wavenumber. The amplitudes of the 3 terms are related such that their sum satisfies physical conditions on the local behaviour of current and charge on segment ends; it allows the 3 coefficients in (6.1.9) to be reduced to 1 unknown [4]. Expressing (6.1.9) in terms of the single unknown as

$$h_n(d) = I_n h'(d, d_n) = I_n h'(\mathbf{r}, \mathbf{r}') \tag{6.1.10}$$

the integral equation of (6.1.7) is then

$$\sum_{n=1}^{N} I_n \int_{\Delta_n} h'(\mathbf{r}_m, \mathbf{r}') \Gamma(\mathbf{r}_m, \mathbf{r}') d\mathbf{r}' = -E_{\tan}(\mathbf{r}_m) \quad \text{for} \quad m = 1, 2, \ldots, N \tag{6.1.11}$$

[1]The explicit dependence of frequency, s_β is implied in the equations that follow.

where the integrand is now completely known and for each Δ_n, the integration of $\mathbf{r}'$ is performed over the length of the nth segment. This representation is also given as

$$\sum_{n=1}^{N} Z_{mn} I_n = V_m \quad \text{for} \quad m = 1, 2, \ldots, N \tag{6.1.12}$$

Z_{mn} is the *system impedance matrix* and V_m, the excitation vector. Clearly, $V_m = -E_{\tan}(\mathbf{r}_m)$ and $Z_{mn} = \int_{\Delta_n} f'(\mathbf{r}_m, \mathbf{r}')\Gamma(\mathbf{r}_m, \mathbf{r}')d\mathbf{r}'$.

The derivations of equations (6.1.1) through (6.1.7) are based on a time-harmonic representation of the electric field, current and Green's function, implying that the equations are defined at a single frequency only.

The general derivations in Appendix B.7 use the complete representation. The frequency dependence of a segmented structure in SuperNEC is discussed in section 7.1.1, in the interest of completeness.

6.1.2 Lebesgue-Integrability and Sobolev Spaces for the Scattering Problem

For a general region in space, Ω, with boundary $\partial\Omega$, we consider electromagnetic fields as generalized m-tuples in n dimensions. For instance, a field $\mathbf{f}(\tau)$ typically consists of a triple (i.e. $m = 3$), $\mathbf{f}(\tau) = (f_1(\tau), f_2(\tau), f_3(\tau))$, corresponding to 3 field components in the direction of unit vectors $\mathbf{u_1}, \mathbf{u_2}, \mathbf{u_3}$. Independent variable τ is typically a position vector with time coordinate, such that $\tau = (x, y, z, t) \in \Omega \subset R^4$, or for position only, $\tau = (x, y, z) \in \Omega \subset R^3$. The differential "volume" is $d\mathbf{\Omega} = dx\, dy\, dz\, dt$ or $d\mathbf{\Omega} = dx\, dy\, dz$, respectively. It follows that for finite integrability to the p-th power (for the former case), of these functions, we have:

$$\int_{\Omega} |\mathbf{f}(\tau)|^p \, dx\, dy\, dz\, dt < \infty \tag{6.1.13}$$

for $1 \leq p < \infty$.

It should be noted that the high-order or infinitely-differentiable continuous function spaces, such as $C^{\infty}(\Omega)$ are not valid for practical problems, in general. The (complete) Hilbert space of Lebesgue-square-integrable functions, $L^2(\Omega)$ in generic region of space $\Omega \in \mathbf{R}^n, n \in \mathbf{N}$ is useful; in common applications, the finite $\int_{\Omega} |f(t)|^2 \, d\Omega$ is a finite energy consideration. In electromagnetics, to satisfy Poynting's finite energy criterion, we place requirements on $\mathbf{E}$ and $\mathbf{H}$, $\int_{\Omega} \epsilon |\mathbf{E}|^2 + \mu |\mathbf{H}|^2 \, d\Omega < \infty$, which can of course be represented in terms of $\mathbf{E}$ and $\nabla \times \mathbf{E}$. Similarly with $\mathbf{H}$.

Consider electric and magnetic fields in the vicinity of subdomain $\partial\Omega_1$; denote these fields as

$\mathbf{E}_{loc}(\mathbf{r})$ and $\mathbf{H}_{loc}(\mathbf{r})$. We can define a function space where both the field quantity and the range generated by curl and div operators on that field quantity are square-integrable; i.e. $\mathbf{E}$, $\nabla \times \mathbf{E}$ and $\nabla \cdot \mathbf{E}$ are elements of $L^2(D_+)$. It follows that both the field quantity and its first derivatives are square-integrable. Therefore,

$$\mathbf{E}^1_{loc}(\text{curl}, \Omega) \equiv \{ \mathbf{f} \,|\, \mathbf{f} \in L^2(\Omega), \nabla \times \mathbf{f} \in L^2(\Omega)\} \tag{6.1.14}$$

$$\mathbf{E}^1_{loc}(\text{div}, \Omega) \equiv \{ \mathbf{f} \,|\, \mathbf{f} \in L^2(\Omega), \nabla \cdot \mathbf{f} \in L^2(\Omega)\} \tag{6.1.15}$$

where $\mathbf{E}^1_{loc}(\text{div}, \Omega), \mathbf{E}^1_{loc}(\text{curl}, \Omega) \in L^2(\Omega)$.

For complex-valued triples, such as $\mathbf{E}(\mathbf{r}, t) = (E_x(x, y, z, t), E_y(x, y, z, t), E_z(x, y, z, t))$ and $\mathbf{H}(\mathbf{r}, t) = (H_x(x, y, z, t), H_y(x, y, z, t), H_z(x, y, z, t))$, the space $L^p(\Omega)^3$ denotes the set of all functions Lebesgue-integrable to p-th power.

The typical L^2-norm is

$$\|\mathbf{f}\|_{L^2(\Omega)} = \int_\Omega |\mathbf{f}(\mathbf{x})|^2 \, d\mathbf{x} \tag{6.1.16}$$

The norms for the curl- and div- field spaces are

$$\|\mathbf{f}\|^2_{\text{curl},\Omega} = \|\mathbf{f}\|^2_{L^2(\Omega)} + \|\nabla \times \mathbf{f}\|^2_{L^2(\Omega)} \tag{6.1.17}$$

$$\|\mathbf{f}\|^2_{\text{div},\Omega} = \|\mathbf{f}\|^2_{L^2(\Omega)} + \|\nabla \cdot \mathbf{f}\|^2_{L^2(\Omega)} \tag{6.1.18}$$

6.1.3 Ill-posedness Considerations

In this section, we ask several questions regarding the well-posedness of the integral equations used in SuperNEC and the function spaces applicable to accurate characterization of the thin-wire problem. Having reviewed the general ill-posedness and uniqueness challenges in section 4.5, we discuss both exact and reduced kernel formulations in preparation for a SuperNEC implementation. Note that in section 4.6, it was shown that ill-posed equations could be "treated" by stabilization methods and various regularization techniques. This section aims to identify whether the problem really is ill-posed in the spaces of interest and thereafter we evaluate whether that is practical for implementation in SuperNEC.

Considering the exact form of the Pocklington integro-differential equation (c.f. eqn (6.1.1)), written in operator form as $Lh = e$, as in the previous section. For convenience, define the interval as $S = (-1, 1)$, with $G : \mathbf{R} \to \mathbf{C}$ given by [167]

$$G(u) = -\frac{1}{a\pi} \ln |u| + Ru, \quad u \in \mathbf{R} \tag{6.1.19}$$

where R is continuous with bounded measurable derivative on $\mathbf{R}$. For a thin wire, the current at the ends satisfies the boundary condition $h(\pm 1) = 0$. The solution is written $h = \Gamma e$, where

Γ is the resolvent of the integral operator. Recall that the problem is well-posed if for every $e \in L^2(S)$, there exists a solution $h = \Gamma e$ and that the solution depends continuously on e (i.e. the continuous linear operator is bounded). In the literature, as reviewed in section 4.5.2, it is generally perceived that the solution h does not depend continuously on e and therefore that the problem is not well-posed. We show here that there are in fact formulations, based on the use of Sobolev spaces, that enable a well-posed description to be found.

The most basic concept of smoothness is continuity; differentiability is a stronger notion and the requirement for the derivative to be continuous stronger yet. In defining the appropriate spaces for considering well-posedness of the exact kernel integral equations for the thin-wire z-directed case, particularly for application of Galerkin or Moment-Methods, we deal with functions of varying characteristics. Basis functions are usually piecewise C^0, such as "constant" or pulse basis functions or piecewise C^1, such as the piecewise linear basis functions [2]. We go on to consider the set of Lebesgue measurable functions L^p where $p \geq 1$, as defined in section 4.1.5. These increasing "requirements" for differentiability/integrability, smoothness and continuity require different norms and function spaces to be used.

Based on the uniqueness result of Jones [167] for the straight wire problem, stating that if e is continuous on $\overline{S} = [1, 1]$, the problem is shown to be unique. The problem can be shown to be well-posed, if cast in the appropriate function spaces [168, 67]. We explore appropriate representations here.

As defined in section 4.1.6, let $W^{1,p}(S)$ be the set of functions $f \in L^p(S)$ with a weak (or generalized) derivative $Df \in L^p(S)$ and define a norm on $W^{1,p}(S)$ by $\|f\|_{1,p} = \|f\|_p + \|Df\|_p$. By Hutson [169, p. 289], for basis function $f(z)$, if $f'(z)$ exists for all $z \in S$ and $f' \in L^p(S)$ then $f' \in W^{1,p}(S)$ [3]. As before, inclusions of spaces of the form $H^m(S) \subset H^k(S) \subset L^2(S)$ for $m \geq k \geq 0$ apply. We augment these spaces to accommodate additional functions, for instance Sobolev space $W^{1,p}(S) \subset C(\overline{S})$, does not contain pulse basis functions. As is customary, $W_0^{1,p}(S)$ denotes compact support on S, incorporating the boundary conditions.

For the case of $1 < p < 2$; Rynne [170] showed that for any $e \in L^p(S)$ that there exists a solution $h = Se \in W_0^{1,p}(S)$ with a bounded operator $S : L^p(S) \to W_0^{1,p}(S)$ is bounded, and hence, well-posed. For $p > 2$, it is necessary to "add" functions to the space to deal with the singular characteristics at the wire end-points. For the case when $p > 2$, for most $e \in L^p(U)$, the functions $\xi_\pm$ are necessary to describe solution Se. These functions account for the discontinuity at the wire ends where the boundary condition $I(\pm 1) = 0$. Since these functions don't belong to $W_0^{1,p}(U)$, they must be added to it, giving the augmented space $W_{0,a}^{1,p}(U) = W_0^{1,p}(U) \oplus [\xi_\pm]$ [171]. Rynne [170] showed that for $p > 2$, for $e \in L^p(U)$ there

[2] Recall that $C^0(\Omega)$ is the space of continuous functions and $C^1(\Omega)$ the space of continuously differentiable functions on domain Ω.

[3] Recall that $H^s(S) = W^{s,2}(S)$.

exists a unique solution $I = Se \in W^{1,p}_{0,a}(U)$ and operator $S : L^p(U) \to W^{1,p}_{0,a}(U)$ is bounded. Solution has the form $Se = \psi(e) + \beta_-(e)\xi_- + \beta_+(e)\xi_+$ where $\psi : L^p(U) \to W^{1,p}_0(U)$ and $\beta_\pm : L^p(U) \to \mathbf{C}$.

In section 4.1.7, we reviewed the Sobolev Trace theorem, showing that it was a restriction theory that could be used to define the functions on the boundary of a region, noting that a different space applies there than in the region itself; specifically, $H^s(\Omega) \to H^{s-1/2}(S)$ where S is the boundary of region Ω. This norm, of the form in equation (4.1.8) is defined for the fractional order Sobolev space. The Sobolev Trace Theorem enables us to consider the field quantities projected onto their trace; in practical application, it gives us field quantities described in one space with a trace (its projection) in another space. The appropriate energy space for the fields scattered by a perfect conducting surface S is $H^1_{loc}(S_+)$ and the boundary values of the fields will lie in $H^{1/2}(S)$, a subspace of L^2 [67]. This is discussed in more detail later in this section. The case $s = 1/2$, for $H^{1/2}(S)$ requires the mechanics of fractional order Sobolev spaces, with the norm given by (4.1.8). This space accommodates norms between the $s = 0$ and $s = 1$ cases, using an interpolation approach. For further details on fractional order Sobolev spaces, see [172].

As we look to deal with different basis functions, from constant and pulse-type basis functions, to piece-wise linear and in general, p-integrable functions, we invoke successively more complex function spaces to include the necessary additional functions.

With respect to notation, consistent with section 6.1.2, $f \in H(\text{curl}, D_-)$ is defined by $\{f : f \in L^2(D_-) \text{ and } \nabla \times f \in L^2(D_-)\}$. Region D_- is enclosed by surface S, while region D_+ is external to the surface. We use the notation $D_\pm$ to indicate that either region is considered in the formulations. When referring to square-integrability over a region external to S, it implies a localized region. Some authors use $H_{loc}(D_+)$, as in section 6.1.2, when referring to Lebesgue-integrability in an external region. In the discussions that follow, we drop the *loc* subscript, noting that it is implied.

In constructing function spaces for thin-wire analyses, many questions can be asked. As additional features or constraints are added, including normal derivatives, square integrability, curl and divergence operators, we modify our spaces. Below is a table showing how these requirements define the spaces.

We conclude, consistent with Hsiao [67], that functions with locally square-integrable curls and divergences, having normal or tangential components in $H^{1/2}(S)$ are vector functions whose components and derivatives are square integrable with boundary values in $H^{1/2}(S)$.

Rynne [170, 171] proved that for $s \in [1/2, 1)$ that for any $e \in H^{s-1}$ there exists a unique solution $I = Se \in W^{s,2}_0$ and that operator $S : H^{s-1}(U) \to W^{s,2}_0$ is bounded. For $s \in (0, 1)$, the generalized functions, such as the Dirac delta are accommodated. For $e \in L^2(U)$, it follows

Function with Requirement	**Function Space**
For scalar $f = f(\mathbf{r})$	
$\{f : f$ and $\nabla f \in L^2(D_\pm)$	$f \in W^{1,2}(D_\pm) = H^1(D_\pm)$
$f\big\vert_S$, where $\{f : f, \nabla f \in L^2(D_\pm)\}$	$f\big\vert_S \in W^{1/2,2}(S) = H^{1/2}(S) \subset L^2(S)$
$\{f : f \in L^2(D_\pm), \nabla^2(f) \in L^2(D_\pm)\}$	$f \in H^1(\nabla^2, D_\pm) = W^{1,p}(D_\pm) \oplus C(D_\pm)$, where $C(D_\pm)$ are non-square integrable functions.
For vector $\mathbf{f} = f(\mathbf{u_1}, \mathbf{u_2}, \mathbf{u_3})$	
$\mathbf{f} \in H(\text{curl}, D_-),\ \hat{\mathbf{n}} \times \mathbf{f}\big\vert_S \in H^{1/2}(S)$ and $f \in H(\text{div}, D_-),\ \hat{\mathbf{n}} \cdot f\big\vert_S \in H^{-1/2}$	Space of normal derivatives is $H^{-1/2}(S)$. Note : $L^2(D_\pm) \subset H^1(\nabla^2, D_\pm)$
$\{\mathbf{f}\big\vert\hat{\mathbf{n}} \cdot \mathbf{f} = 0, \mathbf{f} \in H^{-1/2}(S), \nabla_t \cdot \mathbf{f} \in H^{-1/2}(S)\}$	$H^{-1/2}_{div}(S)$
$\{\mathbf{f}\big\vert\hat{\mathbf{n}} \cdot \mathbf{f} = 0, \mathbf{f} \in H^{-1/2}(S), \nabla_t \nabla \mathbf{f} \in H^{-1/2}(S)\}$	$H^{-1/2}_{curl}(S)$
Perfect Electric Conductor	
$f \in H(\text{curl}, D_-),\ \hat{\mathbf{n}} \times f\big\vert_S \in H^{1/2}(S)$ and $f \in H(\text{div}, D_-),\ \hat{\mathbf{n}} \cdot f\big\vert_S \in H^{1/2}$	$f \in H^1(D_\pm)$ Trace of f on S is in $H^{1/2}(S)$

Table 6.1: Function space definitions for scalar and vector field components. The special case of the perfect electric conductor is also given.

that solution I belongs to $W^{1,2}_0(U)$; the well-posedness results are delicate for this $p = 2$ case. It is assumed to apply for the scope of this work; for further analysis, see Rynne [168, 170].

In summary, applying the the work of Rynne [173, 170, 168, 171] and Hsiao [67] we have demonstrated the following:

- For defining the function spaces needed to describe the well-posed solution of the linear integral equation of interest, we need to consider the impact of normal vs tangential components, derivatives of functions, curls, divergences and the projection of these functions onto the surface enclosing some region.
- Table 6.1 summarizes the elaboration of the basic Lebesgue-square integrable space to accomodate these additional requirements.
- Field components in the exterior region, for the scattering problem, were shown to be in Sobolev space $H^1(D_+)$.
- The projection of these field components onto the boundary of the region, surface S, is effected through the Sobolev trace theorem, giving $H^s(D_+) \to H^{s-1/2}(S)$, where $s = 1$ for this example.

- The tangential components exist in the same space as the functions on the surface S, i.e. they lie in $H^{1/2}(S)$.
- It was demonstrated that for the cases of $1 < p < 2$, that the problem was well-posed for the excitation in an L^p-space, with the solution defined in a Sobolev space, $W_0^{1,p}(D_\pm)$. The $p > 2$ case was shown to be a superset of L^2 since it had to accommodate the boundary condition wire "end-point" conditions. The $p = 2$ case was noted to be a delicate case, requiring special attention.
- For the exact kernel, the surface field components used in the boundary value formulations of Chapter 3 belong to $H^{1/2}(S)$, derived from field components in $H^1(D)$ through the Sobolev trace theorem. It was shown that the integral equation is well-posed when cast in these function spaces.

In the next section, the application of this theory to the thin-wire kernel form and integration into the SuperNEC application is considered.

6.1.4 Thin-Wire Kernel Formulation in SuperNEC

One of the fundamental requirements for candidate methods to be integrated into the SuperNEC application was that they should minimize impact to the core code. The preceding analyses on solutions to the ill-posed nature of the EFIE, in its general, exact or reduced kernel z-directed form, must therefore adhere to this premise. In this section, we begin with a brief review of the thin-wire kernel and proceed to an evaluation of the revised formulations in Sobolev spaces.

The exact kernel formulation and its well-posed nature, when cast in the appropriate function space were considered in section 6.1.3. Many applications of frequency-domain MoM codes, including SuperNEC, use a simplification of this exact formulation to the thin-wire kernel, or extended thin-wire kernel. The thin-wire kernel is based on the scalar Green's function written

$$G(z, z') = \frac{e^{-jkR}}{4\pi R} \quad \text{where} \quad R = ((z - z')^2 + a^2)^{1/2} \tag{6.1.20}$$

Davies *et al* [174] showed that the Pocklington integral equation (of the first kind) with the reduced kernel is not mathematically well-posed. Small perturbations in the right-hand side of the matrix equation can cause large oscillatory components; perturbations as small as the machine precision of the computer being used can cause these instabilities. Observation of this principle for the frequency domain is documented [175]. The solution is not "sensible" unless the segment mesh size used in discretization is large compared to the radius of the thin-wire. Though not characterized as such, this is a regularization method, identical to those described in section 4.6.2.

In section 6.1 we considered the exact solution of the z-directed Pocklington equation derived for the EFIE. It was shown that the ill-posed equation could be shown to be well-posed, if formulated in the correct function space. We invoked the theory of Sobolev spaces to accommodate the culprit operators and their associated boundary conditions. Trace theorems enabled fractional order Sobolev spaces to be used for these well-posed formulations.

Recasting equation (6.1.6) in fractional order Sobolev space, we modify the Method of Moments projection based on the Sobolev norm.

$$\sum_{p=1}^{P} \alpha_p \langle w_m, Lh_p \rangle_{H^{1/2}} = \langle w_m, e \rangle_{H^{1/2}} \quad \text{for} \quad m = 1, 2, \ldots, N \tag{6.1.21}$$

where for Lebesgue-square integrable functions, from equation (4.1.8), the inner-product for the Sobolev space satisfies

$$\langle \mathbf{f}, \mathbf{f} \rangle_{H^{1/2}} = \|\mathbf{f}\|^2_{H^{1/2}}(\partial\Omega) = \int_{\partial\Omega} |f|^2 \, d\Omega + \int_{\partial\Omega} \int_{\partial\Omega} \frac{|D^\alpha \mathbf{f}(\mathbf{x}) - D^\alpha \mathbf{f}(\mathbf{y})|^2}{|\mathbf{x} - \mathbf{y}|^N} \, dS_x \, dS_y \tag{6.1.22}$$

The discretized integral equation of (6.1.7) will therefore require modification to support the inner-product in a fractional order Sobolev space. The result will be modified and additional integral terms will be required for calculating matrix elements of the impedance matrix. The impact on implementation within SuperNEC is nontrivial, since this requires a change to the matrix fill algorithms as well as the computational expense of additional numerical integration required for each element. For an $N-$dimensional structure, the fill expense is of $\mathcal{O}(N^2)$; introducing additional computational overhead in each of these N^2 elements is undesirable. It can be concluded that the analysis demonstrates a mathematically justifiable theoretical method for creating a well-posed variant of the exact kernel Pocklington's equation integral solution; furthermore, that its implementation into SuperNEC presents unacceptable increases in computational overhead.

We conclude that the thin-wire kernel approach admits an ill-posed form that can not practically be adjusted by modification of the inner-products and norms used to construct the Method of Moment discretization. The Sobolev formulations are recognized to be mathematically sound, but are destined for future software integration, given that they require modifications to SuperNEC core software that are too extensive. Recognizing the ill-posedness as given, then, we are forced to apply a regularization approach or stabilization using preconditioners. It will be demonstrated in upcoming sections that the SEM approach embeds a preconditioner, while the segmentation empirical rules and the sine-cosine-constant basis functions create a form of regularization that render meaningful solutions.

6.2 SuperNEC and Spectral Expansions

Not all the spectral expansions identified in chapter 5 can be practically integrated into SuperNEC. The architecture of the frequency-domain code lends itself to integration of certain techniques more readily than others. These matters are considered in this section. We also reconnect with the abstract MBPE and our systems concepts of transfer functions and impulse responses, as we move toward the goal of a practical technique integrated into SuperNEC that has a sound mathematical foundation.

6.2.1 SEM Related to SuperNEC Formulations

Using the MoM formulation for an N segment wire-grid model presented in the previous section, the impedance matrix for the N-segment wire-grid structure is (c.f. (6.1.12))

$$\sum_{n=1}^{N} Z_{mn} I_n = V_m \quad \text{for} \quad m = 1, 2, \ldots, N \tag{6.2.1}$$

This is otherwise represented as

$$\mathbf{Z}(s_\alpha) \cdot \mathbf{I}(s_\alpha) = \mathbf{V}(s_\alpha) \tag{6.2.2}$$

where the raised dot denotes matrix multiplication and $\mathbf{Z}(s_\alpha)$ is the $N \times N$ system impedance matrix, a complex frequency dependent quantity. $\mathbf{I}(s_\alpha)$ and $\mathbf{V}(s_\alpha)$ denote the frequency dependent current and excitation vectors, respectively. The formulation is compiled at frequency $s = s_\alpha$. For evaluating natural modes we consider the nontrivial $N \times 1$ vector $\mathbf{I}(s)$ from the source free representation (homogeneous equation)

$$\mathbf{Z}(s) \cdot \mathbf{I}(s) = 0 \tag{6.2.3}$$

The general operator formulation of section 2.2 gives the same formulation in the general sense for Maxwell's equations, specifically reduced to give a guided wave representation. Baum [39] and Tesche [48] indicate that for the nontrivial solution of this equation at some $s = s_\alpha$,

$$\mathbf{Z}(s_\alpha) \cdot \mathbf{M}(s_\alpha) = 0 \tag{6.2.4}$$

where the vector $\mathbf{M}(s_\alpha)$ is known as the *natural mode vector*. The *coupling vector*, $\mathbf{C}(s_\alpha)$ is given by

$$\mathbf{Z}(s_\alpha)^T \cdot \mathbf{C}_\alpha = 0 \tag{6.2.5}$$

For a source-free system, described by a homogeneous equation, any nontrivial solution implies that the system impedance matrix is overdetermined. The solutions therefore contain dependent components. Intuitively, this implies that the current corresponding to a natural mode has amplitudes on certain segments which are dependent on the amplitudes of other segments. In the same way in which the modes of the rectangular cavity were dependent on the geometry of the cavity itself, the natural mode currents distributed on the structure being modeled are determined by the geometry of that structure. It is this dependence of currents at different locations which encapsulates the concept of a natural mode, that being the natural state in which the structure can resonate, if suitable excitation is provided. Garbacz [176] purports that resonance of a scattering obstacle must somehow take into account the obstacle shape as an integrated whole. Its contribution to the description of the overall current on a structure is determined by the source vector, in the same manner as (B.5.9). The inverse of (6.2.2) gives

$$\mathbf{I}(s_\alpha) = \mathbf{Z}(s_\alpha)^{-1} \cdot \mathbf{V}(s_\alpha) \tag{6.2.6}$$

Using Cramer's theorem [11],

$$\mathbf{Z}(s_\alpha)^{-1} = \frac{\mathbf{A}(s_\alpha)}{\Delta(s_\alpha)} \tag{6.2.7}$$

where $\mathbf{A}(s_\alpha)$ is the adjoint matrix of $\mathbf{Z}(s_\alpha)$ and $\Delta(s_\alpha)$ the s-dependent determinant.

Since the natural mode vectors represent homogeneous solutions of (6.2.2), this implies that

$$\det(\mathbf{Z}(s_\alpha)) \equiv \Delta(s_\alpha) = 0 \tag{6.2.8}$$

Whenever the determinant of the system impedance matrix is 0, at some $s = s_\alpha$, a singularity in the complex plane is introduced. At these natural frequencies, s_α, the admittance matrix defined in the complex frequency plane has a singularity. Tesche [48] assumed as an approximation to the inverse of the system impedance matrix, a linear combination of simple poles of the form

$$\mathbf{Z}(s_\alpha)^{-1} = \sum_\alpha \frac{\mathbf{R}(s_\alpha)}{s - s_\alpha} \tag{6.2.9}$$

where

$$\mathbf{R}(s_\alpha) = \mathbf{M}(s_\alpha) \cdot \mathbf{C}(s_\alpha)^T \tag{6.2.10}$$

The residue matrix, $\mathbf{R}(s_\alpha)$ is hence the outer product of the natural mode and coupling vectors, respectively. Note that for a symmetric residue matrix, the coupling and natural mode vectors are the same, hence

$$\mathbf{R}_\alpha = \mathbf{C}_\alpha \cdot \mathbf{C}_\alpha^T \tag{6.2.11}$$

Note that (6.2.9) is not calculated at some $s = s_\alpha$, but a function of s. This analytical description would have to be evaluated at multiple frequencies to approximate with a frequency

domain code, such as NEC2 or SuperNEC. The assumption of a series of poles weighted by a suitable residue is based on the series expansion of a function in the complex frequency plane. Where no singularities exist, a Taylor series expansion is suitable, however the more general Laurent series is required for regions admitting singularities. It is this expansion in the region of a singularity which led to the term *Singularity Expansion Method*. A review of Taylor and Laurent series expansions in the complex plane is given in Appendix A.5.

The theoretical derivations which form the basis of the sum of weighted simple poles are not considered in matrix form, but using inner product relations, as given in Appendix B.7. Since the Laurent series approximation of $\mathbf{I}(\mathbf{r}, s)$ at $s = s_\alpha$ gives

$$\mathbf{I}(\mathbf{r}, s) = \sum_{n=1}^{\infty} \frac{b_n}{(s - s_\alpha)^n} + \mathbf{I}'(\mathbf{r}, s) \tag{6.2.12}$$

it is clear that b_n must include some information specific to the geometry. Since the approximation is at $s = s_\alpha$, the corresponding natural mode vector would incorporate the geometrical information in the natural state of the system. In the same way in which eigenfunctions of a system need to be excited by some forcing function, a "Fourier"-type coefficient can be used to represent the weighting of that particular mode. This coefficient, known as the coupling coefficient is derived in Appendix B.7. The first term in (6.2.12) is the principal part of the Laurent series expansion. The second term, the entire function contribution, is discussed in more detail in section 5.1.4.

The series expansions comprising the SEM are given in Appendix B.7 where it is shown that the coupling coefficient at $s = s_\alpha$ is

$$\eta_\alpha(s_\alpha) = \frac{\langle \mathbf{C}_\alpha(\mathbf{r}); \mathbf{V}_{0\alpha}(\mathbf{r}) \rangle}{\langle \mathbf{C}_\alpha(\mathbf{r}); \Gamma_{1\alpha}(\mathbf{r}, \mathbf{r}'); \mathbf{M}_\alpha(\mathbf{r}') \rangle} \tag{6.2.13}$$

where

$$\Gamma_{1\alpha}(\mathbf{r}, \mathbf{r}') = \frac{\partial}{\partial s} \Gamma(\mathbf{r}, \mathbf{r}'; s) \bigg|_{s=s_\alpha} \tag{6.2.14}$$

and

$$\mathbf{V}_{0\alpha}(\mathbf{r}) = \mathbf{V}(\mathbf{r}, s)|_{s=s_\alpha} \tag{6.2.15}$$

The terms in (6.2.14) and (6.2.15) are introduced by the derivative terms in the Taylor series approximation to $\Gamma(\mathbf{r}, \mathbf{r}', s)$ and $\mathbf{V}(\mathbf{r}, s)$. For $s \neq s_\alpha$, various functional dependencies of η_α on s are possible. Two successful options, known as *class 1* and *class 2* approximations are used. The former (and most common) introduces a time delay component, and corresponds to a frequency independent residue, for some pole:

$$\eta_\alpha(s) = \left[e^{(s_\alpha - s)t'} \right] \times \eta(s_\alpha) \tag{6.2.16}$$

Marin [40, 144, 1] went on to show that the response of an object to a delta function excitation is given by:

$$\mathbf{I}(\mathbf{r}, s) = \sum_{\alpha} \frac{\eta_\alpha(s)\mathbf{M}_\alpha(\mathbf{r})}{(s - s_\alpha)^{m_\alpha}} + \text{entire function contributions} \tag{6.2.17}$$

The numerator is noted to be the residue defined in matrix form in (6.2.9). For the purpose of all these papers, it was proposed, but not theoretically verified that for conducting bodies, the poles were simple, i.e. $m = 1$ for all α. The class 1 and class 2 coefficients are different when $s \neq s_\alpha$ because of the difference introduced by the entire function contributions. This contribution is due to the left-hand term in (A.5.1), noted to be the effect of the analytic function *near* a singularity at $s = s_\alpha$.

6.2.2 The Resolvent Expansion Link

We conclude that the solution of the impedance matrix equation (6.2.2) can therefore be written as an expansion series in terms of pole terms, as given by equations (6.2.12) and (6.2.17). We have thus shown the inherent compatibility of the SEM formulation with the SuperNEC impedance matrix form. What remains to be defined is a methodology for finding the unknowns, both poles and residues. The next section addresses some of the techniques in the literature, followed by alternative approaches in section 6.3 for both time and frequency domain consumption.

The assumption of the pole series form in (6.2.9) is interesting. This assumption drives the form of the solution for the SuperNEC impedance matrix. We revisit our resolvent expansions of chapter 5 for direction and to substantiate this assumption. In section 5.2, it was demonstrated through use of the Fredholm Alternative that unique solutions of the inhomogeneous equations can be determined, and furthermore that this resolvent could be defined in terms of a Singularity Expansion Method. It was shown that by invoking the Fredholm Determinant Theory we could define the unknown current solution in terms of the recursive determinants and Fredholm minors. By comparing (6.2.12) with (5.2.4) it follows that the meromorphic nature of the resolvent justifies our approximation and assumption.

6.2.3 Evaluation of SEM parameters for Radiation and Scattering Problems

To evaluate natural frequencies, use the determinant of the system matrix, since

$$\det(\mathbf{Z}(s_\alpha)) \equiv \Delta(s_\alpha) = 0 \tag{6.2.18}$$

at some natural complex frequency s_α. A Taylor series expansion, limited to 2 terms in the neighborhood of s_α, evaluated at a point s_0, gives

$$\Delta(s_\alpha) = \Delta(s_0) + \Delta'(s_0)(s_\alpha - s_0) = 0 \tag{6.2.19}$$

Therefore,

$$(s_\alpha - s_0) = -\frac{\Delta(s_0)}{\Delta'(s_0)} \tag{6.2.20}$$

This iterative method for finding s_α is similar to a Newton-Raphson approach. For a thin wire scatterer, these natural resonances appear to occur in layers. It should be noted that this iterative search implies s_α is near s_0. Without mathematical rigor; the Taylor series is an M term approximation to a function $f(x)$ near $x = x_0$. The greater the distance between x and x_0, the less accurate the approximation. It can be concluded that the iterative search requires an "educated" starting point for the Newton-Raphson iterative search.

These results are similar to the layers of natural frequencies of a perfectly conducting sphere, found by Stratton [45]. The first layer of poles are clearly most significant, as they have the smallest magnitude real component. The residue matrix was found using a limit approach [48]; for the residue at the kth pole,

$$\lim_{s\to s_k}(s - s_k)\mathbf{Z}(s)^{-1} = \lim_{s\to s_k}(s - s_k)\sum_\alpha \frac{\mathbf{R}_\alpha}{s - s_\alpha} = \mathbf{R}_k \tag{6.2.21}$$

Given that $s = s_k + \epsilon$;

$$\mathbf{R}_k = \lim_{\epsilon\to 0}\epsilon[Z_k(s_k + \epsilon)]^{-1} \tag{6.2.22}$$

The numerical approach that Tesche [48] advocated for evaluating this limit required choosing several values of ϵ which were suitably small that $\mathbf{R}_k$ in (6.2.22) did not change appreciably. The natural mode vectors and coupling vectors are determined from the residue matrix, if necessary.

Marin [1] used a similar procedure, also based on the determinant. His approach hinged on the Householder triangularisation method [177] of the system matrix. For $t_{NN}(s)$the last element in the triangular matrix, solving (6.2.18) reduced to satisfying $t_{NN}(s) = 0$, for some s_α. Again, an iterative method based on Newton-Raphson, with some initial guess was used.

6.3 Estimation Models Using Transient Data

In section 2.1.3, we reviewed the solution of $h(t)$ or $H(s)$ from a system perspective. Recall that in the case where the samples used for the signal reconstruction were taken from the response of a system to an impulse input, the approximation is viewed as an *Impulse*

Response Estimation (IRE) technique. Clearly, for a general input, which in a discrete system is given by an impulse convolved with some signal, the system response is given by the convolution of the impulse response with the input signal. The complex frequency domain equivalent of impulse response estimation is *Transfer Function Estimation (TFE)*. The time and frequency domain Prony methods, TDPM and FDPM are impulse response and transfer function estimation methods, respectively. These two estimation models are defined below. The MBPE abstraction, also an IRE or TFE method, depending on the domain of application, is considered later.

6.3.1 The Time Domain Method

The iterative search for all possible poles in the s-plane using the determinant of the system impedance matrix was superseded by an analytical method of obtaining the unknown coefficients in the impulse response representation directly from transient data.

Van Blaricum and Mittra [178] applied Prony's algorithm [93, pp. 428-431], [179] to transient data, resulting in a systematic approach for deriving the complex poles and zeros of a structure. Following the derivations of the SEM, the impulse response for a system has a representation given by

$$h(t) = \sum_{\alpha=1}^{N} R_\alpha e^{s_\alpha t} + h_{np}(t) \tag{6.3.1}$$

The poles, s_α must occur in conjugate pairs if the function $h(t)$ is to be real. R_α are the residues, and $h_{np}(t)$ corresponds to the non-pole (entire function) components of the response. The time domain response of the source excitation is typically responsible for non-pole components. Causality is also assumed. The true representation of the impulse response of the system requires the summation in (6.3.1) to extend to infinity, as is observed in practical systems. For example, the natural frequencies of the dipole, depicted in figure 6.1, occur in an infinite number of pole layers. Other canonical problems such as the conducting sphere [45], have natural frequencies determined by the zeros of Hankel or Bessel functions, which are infinite in number. Computationally, the number of poles must be limited: achieving this requires limiting the solution to a particular spectral range of interest, hence the summation to N terms in (6.3.1). This assumes that the effect of the poles outside this range is negligible.

Neglecting the non-pole component, for $2N$ discrete samples,

$$h(t_n) = h_n = \sum_{\alpha=1}^{N} R_\alpha e^{s_\alpha n \Delta t} \qquad \text{for} \qquad n = 0, 1, \ldots, 2N-1 \tag{6.3.2}$$

where Δt is the constant interval between time samples, and $t_n = n\Delta t$. The interpolation of a function using a series of complex exponentials, is known as Prony's Algorithm [93,

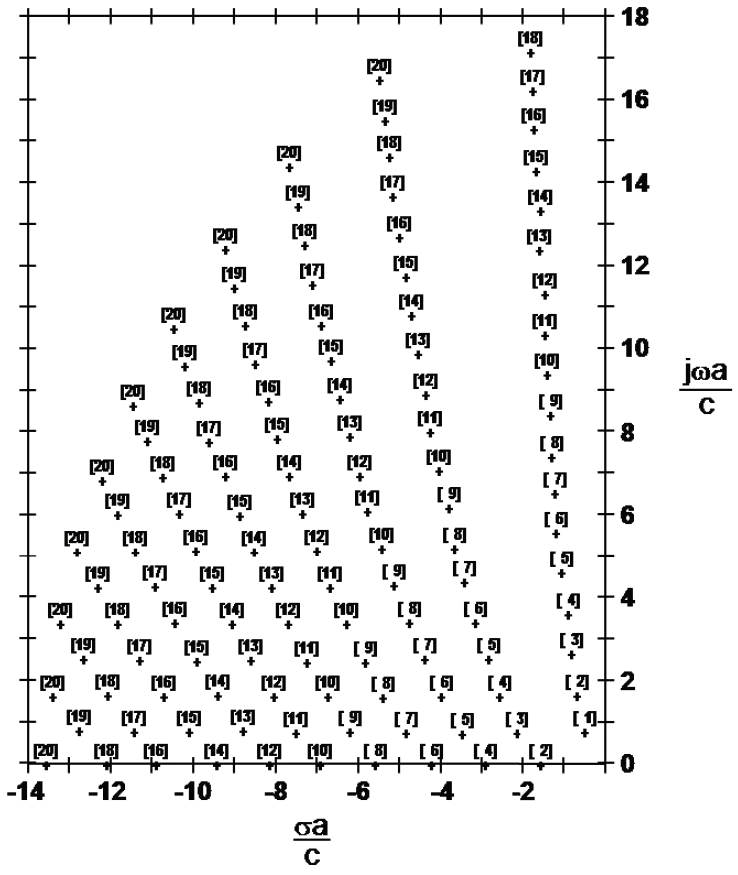

Figure 6.1: The layers of natural frequencies for a dipole [1]

pp. 428-431], [179], or alternatively, the Time Domain Prony Method (TDPM). The nonlinear equation (6.3.2) of $2N$ unknowns in $2N$ equations is,

$$\begin{aligned} h(t_0) &= R_1 + R_2 + \ldots + R_N \\ h(t_1) &= R_1 e^{s_1 \Delta t} + R_2 e^{s_2 \Delta t} + \ldots + R_N e^{s_N \Delta t} \\ \ldots &= \ldots \\ h(t_{(2N-1)}) &= R_N e^{s_1 (2N-1) \Delta t} + R_2 e^{s_2 (2N-1) \Delta t} + \ldots + R_N e^{s_N (2N-1) \Delta t} \end{aligned}$$

Jones [93, pp. 428-431] showed that

$$\sum_{p=1}^{N} b_p h_{n+N-p} = h_{n+N} \tag{6.3.3}$$

provided that $z_\alpha = \exp s_\alpha \Delta t$ satisfies

$$z_\alpha^N + \sum_{p=1}^{N} b_p z_\alpha^{N-p} = 0 \tag{6.3.4}$$

Equation (6.3.3) is noted to be a linear prediction of the $(n+N)$th data point, as calculated by weighted summation of the previous N data points. As related to Prony's original problem of characterization of heat propagating through some conductor, it follows that a linear prediction approach, given some window of N points, would be used. The particular significance of using the complex exponential basis functions is that they satisfy the polynomial expression of (6.3.4). Equation (6.3.3) is solved as a standard matrix equation, to find b_p. Once they are known, the roots of the polynomial equation, (6.3.4), must be found (typically using Newton's, Muller's or Cauchy's method [163]). The s_n are hence calculated and the matrix solution of (6.3.2) gives the a_n.

If the function approximation in (6.3.2) is not strictly valid, the results may exhibit instability due to extreme sensitivity to small alterations [93]. A feasible solution is obtained by a singular value decomposition (SVD) of (6.3.3) to yield the so-called SVD-Prony method. More specific details of matrix conditioning and the SVD are given in section 7.2.4. Singular values which are zero or comparatively smaller than the others indicate that the full-rank approximation of (6.3.3) should be re-formulated with the rank reduced by the number of zero singular values. Intuitively, this implies that the number of previous information samples required to estimate the $(n+N)$th sample must be reduced, as the extra samples used are degrading the approximation. The SVD-Prony method as well as methods to reduce computational effort have been discussed by Younan *et al* [180].

6.3.2 The Complex Frequency Domain Method

The *transfer function*, as defined by Oppenheim *et al* [10], is the frequency domain equivalent of the impulse response, as discussed earlier. In the complex frequency plane, it is obtained using the bilateral Laplace Transform, whereas for the real frequency plane, the Fourier Transform is used. The impulse response, from (6.3.1) is

$$h(t) = \sum_{\alpha=1}^{N} R_\alpha e^{s_\alpha t} + h_{np}(t) \tag{6.3.5}$$

Note that these equations consider only 1-dimension of the n-dimensional formulation presented in section 2.4.4. The representation is thus suitable for any electromagnetic quantity observed on 1 segment, in a MoM formulation. Therefore, by the Laplace Transform,

$$H(s) = \int_{\sigma_0+j\infty}^{\sigma_0-j\infty} \left[\sum_{\alpha=1}^{N} R_\alpha e^{s_\alpha t} + h_{np}(t) \right] e^{-st} dt \tag{6.3.6}$$

$$= \sum_{\alpha=1}^{N} \frac{R_\alpha}{s - s_\alpha} + H_{np}(s) \tag{6.3.7}$$

$$\text{where} \quad H_{np}(s) = \int_{\sigma_0+j\infty}^{\sigma_0-j\infty} h_{np}(t) e^{-st} dt \tag{6.3.8}$$

$$\approx \sum_{\beta=-P}^{Q} c_\beta s^\beta \tag{6.3.9}$$

Miller and Burke [19] suggested that the non-pole components would be limited to 0 or 1, in practice. Therefore,

$$H(s) = \sum_{\alpha=1}^{N} \frac{R_\alpha}{s - s_\alpha} + \sum_{\beta=0,1} c_\beta s^\beta \tag{6.3.10}$$

The non-pole components have their origins in the entire function contributions, presented in section 6.2. Considering only the pole components,

$$H(s) = \frac{R_1}{s - s_1} + \frac{R_2}{s - s_2} + \ldots + \frac{R_N}{s - s_N} \tag{6.3.11}$$

$$= \frac{R_1(s - s_2)\ldots(s - s_N) + \ldots + R_N(s - s_1)\ldots(s - s_{N-1})}{(s - s_1)(s - s_2)\ldots(s - s_N)} \tag{6.3.12}$$

Therefore,

$$H(s) \prod_{i=1}^{N} (s - s_i) = \sum_{i=1}^{N} R_i \prod_{j=1, j\neq i}^{N} (s - s_j) \tag{6.3.13}$$

Given a number of real frequency samples, $s_\alpha = j\omega_\alpha$, where $\alpha = 0, 1, \ldots (P-1)$, a matrix

equation can be formed.

$$\sum_{i=0}^{N-1} X_{\alpha i} a_i - Y_{\alpha i} b_i = -s_\alpha^N H_\alpha \tag{6.3.14}$$

where

$$X_{\alpha i} = s_\alpha^i H_\alpha \tag{6.3.15}$$

$$Y_{\alpha i} = s_\alpha^i \tag{6.3.16}$$

Unlike the time domain equivalent, this frequency domain technique does not require equi-spaced samples, making it ideal for integration into software such as SuperNEC, which can optimally choose sample placing for convergence of the approximation of the system transfer function. In this document, the matrix is referred to as the *transfer function matrix*. A general representation of this transfer function has the form:

$$H(s) = \frac{N(s)}{D(s)} = \frac{b_0 + b_1 s + \ldots + b_n s^n}{a_0 + a_1 s + \ldots + a_d s^d} \tag{6.3.17}$$

For a homogeneous equation formulation, set $a_d = 1$. There are $n+d+1$ unknowns, requiring thus at least $2N$ samples of real frequency information.

The concept of using a Laplace Transform method for obtaining a complex frequency domain representation of the time domain Prony estimation method was presented by Van Blaricum *et al* [178]. The matrix formulation, given in (6.3.14) is an identical representation to that given by Brittingham *et al* [155, 7], and has been referred to as the Frequency Domain Prony Method (FDPM). The matrix in (6.3.14) can be solved directly if $P = 2N$ transient data samples are available. For $P > 2N$ samples, a least squares approach or Moore-Penrose pseudo-inverse could be used.

If the rational function is restricted to *diagonal* form, with the degrees of numerator and denominator equal[4] (for P odd), or the degree of the denominator larger by 1 (for P even), the Bulirsch-Stoer recurrence algorithm can be used [163, 181].

We now consider the MBPE abstraction, also an IRE or TFE method, depending on the domain of application.

6.3.3 The MBPE Abstraction

Recall from chapter 2 that MBPE is an abstract tool used to provide a physically-motivated approximation to some response over a frequency band or time slice of interest. Touted as

[4]The odd or even no. of samples for the diagonal form is different to that in Press *et al* [163], since the FDPM method assumes 1 known coefficient to obtain a homogeneous equation.

accomodating the physics of the underlying problem, this author contends that it has largely been used as a mathematical curve fit, losing the link to this underlying basis. Review of the literature suggested in chapter 2 is insightful in this regard. In this document, we do show that this underlying physical basis is intact for our radiation and scattering problems.

The generic descriptions of pole and exponential series related by a Laplace transform pair were extended by Miller [7] to generalized Spectral domain and Waveform domain forms, with defining equations,

$$\begin{array}{rrcl} & F(X) & = & F_p(X) + F_{np}(X) \quad = \quad \sum_\alpha \frac{R_\alpha}{X - s_\alpha} + F_{np}(X) \quad \text{for} \quad \alpha = 1, 2, \ldots, P \\ \text{and} & f(x) & = & f_p(x) + f_{np}(x) \quad = \quad \sum_\alpha R_\alpha e^{s_\alpha x} + f_{np}(x) \quad \text{for} \quad \alpha = 1, 2, \ldots, P \end{array}$$

Comparing with equations (6.2.12) and (6.2.17), the abstract spectral domain MBPE formulation is clearly equivalent. At this point, we can also answer some of the questions from section 2.4.1 on the MBPE:

Q6. If this truly is a "smart curve fit", based on the physics of the underlying problem [35], then how is it the we take that into account. This author contends that MBPE as applied in the literature is truly just a curve-fit, with as much insight into the underlying problem as would be used in applying a spline fit. The following "chain" of derivations thus follow. In chapter 3 we derived the EFIE for the perfectly conducting surface; reducing the solution of the inhomogeneous vector wave equation to the Stratton-Chu representation. Applying the requisite boundary conditions, we reduce to EFIE and MFIE forms known in the literature today. Applying preconditioners to represent the kernels of the integral equations in Hilbert-Schmidt form, we showed that the Fredholm Determinant Theory was applicable, giving rise to a meromorphic resolvent. The resolvent, written in pole-residue form, can be represented as a series of pole terms leading to a rational function model of unknown order. We then look to a Prony method, in the applicable time or frequency domain to solve for the unknown coefficients. This "chain" of theoretical development suggests that the rational function model, as an abstract mechanism, is in fact linked to the underlying theory of the physics at hand.

Q2. Would a frequency-domain rational function approximation be valid for an EFIE and/or an MFIE? More specifically, would the approximation be valid when applied to the thin-wire kernel electric field equations used in Method of Moments (MoM) solutions in SuperNEC? The derivations and logic of section 6.2.1 validate the use of the rational function for the approximation of the current distribution on a structure in the frequency domain. The focus of the application to SuperNEC is centered around the EFIE; Nitch [182] suggested that the MFIE implementation in NEC2 and SuperNEC was found to be exceedingly sensitive to patch configuration and yielded inconsistent results. Having shown the theoretically (formal) validity of the approximation, we turn to the validity

of the MoM solution in practice. This is the subject of chapter 8, where the Transfer Function Estimation method is shown to yield accurate results with a given error criterion.

Q5. No reference is made to the Singularity Expansion Method (SEM) in any MBPE paper since and including that of Miller and Burke [19]. It will be shown in this document that the SEM is in fact a key component of the underlying mathematical basis of MBPE. Given the derivations in the last 3 chapters, MBPE in its spectral domain form, is inextricably linked to the SEM. If it were published as such in the literature, this author believes that its occasionally anomalous behavior could be better understood, by modifying the formulation consistent with the underlying physics.

6.4 Conclusions

The general vector EFIE evolved in chapter 3 is reduced to a z-directed form with a known technique derived by Schelkunoff; this form is used in SuperNEC. In section 6.1, a generic Method of Moment technique in P basis functions was used to reduce the first kind z-directed EFIE to matrix form. For the SuperNEC implementation, using a sine-cosine-constant basis, current and charge boundary conditions were used to reduce the current term to a single unknown, leading to the system impedance matrix. This matrix is defined at a single frequency; a broadband description of the current on some structure would require a large number of these system impedance matrices to be formed, and solved - as determined by the desired resolution. Lebesgue-integral considerations and application of Sobolev space methods were reviewed in section 6.1.2. The function spaces necessary to describe the tangential field components on a surface enclosing a region were reviewed: the Sobolev Trace theorem was used to demonstrate that field components in the Sobolev space $H^1(D_+)^3$, for the 3-dimensional case, were projected onto the surface S, in space $H^{1/2}(S)^3$, a fractional order Sobolev space. Attention was paid to the various function spaces that could be constructed from a requirement set that was presented in table 6.1. Well-posedness of the EFIE forms was proven for the exact form of the z-directed Pocklington equation. The reduced, thin-wire kernel, in contrast, is known to be ill-posed. The merits of these formulations were reviewed in section 6.1.4. While it was noted that the formulations were mathematically sound, they were not practical for integration into SuperNEC, due to the computational impact on the matrix fill operation. The ill-posed form of the SuperNEC thin-wire EFIE is therefore handled by a combination of pre-conditioning and a regularization method based on segmentation criteria.

The application of spectral expansions to SuperNEC was considered in section 6.2. Applying the concepts of natural modes and coupling vectors, we define an expression for the inverse of the system impedance matrix as a sum of pole terms, with residues. Note that this defines a solution which has complex frequency as an independent variable - a broadband description

over a frequency band of interest is conceivable. In section 6.2.2, we show the link back to the resolvent expansion derivations for solution of the EFIE and MFIE in chapter 5. The Fredholm Determinant Theory was shown to justify the pole-residue summation form being used for the current term required in the system impedance matrix equation. It clearly follows that a Singularity Expansion Method approach for resolvent expansion can be used for a wideband description of the current distribution over a structure. Other spectral expansions derived earlier, including EEM and SFM/SVE are not immediately useful to integrate into SuperNEC, even though their mathematical and theoretical foundations have been validated. A brief overview, in section 6.2.3, of methods for finding poles and residues using Newton-Raphson or Householder triangularization was presented. Not ideal for SuperNEC application, we consider Prony methods instead.

Prony's algorithms, useful as a systematic approach to finding complex poles and zeros, are used in section 6.3 for both the time and frequency domain cases, and referred to as the TDPM and FDPM, respectively. They are also consistent with our earlier nomenclature of Impulse Response Estimation (IRE) and Transfer Function Estimation (TFE) techniques, as introduced in section 2.1.3. Recognize that MBPE can also be viewed as an abstract IRE or TFE tool, depending on the domain of application.

The abstract MBPE method is revisited in section 6.3.3. The link to SEM and the underlying physics of the scattering and radiation problem are reviewed. Many of the questions asked in the critical review of MBPE in chapter 2 were answered. We can conclude that the rational function approach derived through the SEM from Maxwell's equations, by way of Stratton-Chu integral equations is valid. The key theory on resolvent expansions, showing that the inverse of the system impedance matrix was a meromorphic function allows a pole-residue series to be used; a rational function approximation follows. The Fredholm determinant theory is fundamental in arriving at these conclusions, and requires analysis of the integral operators, noting that a Hilbert-Schmidt kernel is required for this theory to be used. Preconditioning is therefore necessary to stabilize the nonselfadjoint integral operators.

Chapter 7

Frequency Domain Model Estimation in SuperNEC

The complex frequency domain estimation technique, introduced as the FDPM in the previous chapter, was conceived due to the difficulty in obtaining a meaningful broadband description of some system response. Traditional methods use a linear or low-order polynomial interpolation of a number of discrete samples of the response, with the choice of samples primarily satisfying aesthetic criteria. Resonant behaviour which is often characteristic of the geometry of a scatterer or radiating structure is often missed by the designer due to undersampling that particular frequency band [30]. Furthermore, the placement of samples in the region of an anticipated resonance may require considerably more samples than the minimum required by information theory stipulations. The transition of methodology from a "curve-fitting exercise" to a physically-motivated approximation enables the designer to build a priori information about the system into the broadband modelling rationale. This argument draws parallels with that of section 2.1 where the signal was described with a minimum number of unknowns by a Fourier series, if the signal was known to be periodic, i.e. a description using complex sinusoidal basis functions.

The application of frequency domain methods to the SuperNEC implementation, based on the electric field integral equation (EFIE), is discussed in section 7.1. The Method of Moment formulation for solution of an operator equation using matrix equation methods is explored in some detail.

The capacity of the complex frequency domain method to construct a physically-motivated model using real frequency information has the freedom of sample placement, but does not define a sampling strategy which optimizes the approximation with minimal computational effort. Furthermore, it is obvious that some low-order rational function cannot describe the entire usable frequency range; a practical modelling approach which exhibits the ability to

model any operational frequency band of a structure needs to be assessed.

This chapter addresses the practical application of the complex frequency domain parameter estimation technique by presenting an adaptive sampling strategy which allows FDPM to be applied over an arbitrarily wide frequency range in the HF, VHF and UHF bands. A number of issues central to the effective design of a technique suitable for integration in SuperNEC have been identified; section 7.2 introduces these modelling details which range from restrictions in the number of poles in a rational function to the computational implications of an adaptive sampling architecture. Section 7.3 addresses the design of the iterative successive-approximation process for finding the optimal wideband description of a system. Continuous error measures and an implementation architecture which makes it suitable for integration into SuperNEC are proposed with validation experiments performed on the simulation platform given in section 7.2.1.

7.1 SuperNEC Frequency Domain Implementation

7.1.1 FDPM Applied to a Single Variable Response

Using the MoM formulation in SuperNEC, a wire segment approximation to the structure is needed [4]. The EFIE integral equation used originally in NEC2, and subsequently, in SuperNEC, is a Fredholm equation of the first kind (c.f. equation (6.1.1)). This is an equation of the general form

$$\int_a^b K(s,t)f(t)dt = g(s) \quad c \leq s \leq d \tag{7.1.1}$$

where K, the kernel and g, the excitation, are known functions, with f required. Hansen [183] and Kress [112, pp.47-53] showed that Fredholm integral equations of the first kind are inherently ill-posed, as discussed earlier. Discretization of the Fredholm integral equation, by MoM or any other method, to a matrix formulation of the problem has limitations. Specific criteria need to be applied to the discretization and matrix solution, be it LU-decomposition, Cholesky factorisation or an iterative method (stationary or nonstationary), to obtain valid results. For the SuperNEC and NEC2 formulation, this intuitively implies setting constraints on segmentation sizes and thickness-to-length ratio [184] such that the sine-cosine-constant basis functions can reasonably reconstruct the current distribution over 1 segment. Trueman *et al* [184] published a set of empirical segmentation criteria for use in NEC2.

As the frequency of incident radiation or that of an applied source increases, the spatial current distribution over the structure varies more rapidly, hence requiring smaller segments to describe it. The posedness of the problem is frequency dependent, and it follows that the

segmentation criteria of Trueman *et al* [184] are as well.

Returning to the system impedance matrix of (6.1.12) defined at a specific frequency, it is clear that the N segments are defined using Trueman-type (or similar) criteria. The MoM discretization used in SuperNEC, based on the sine-cosine-constant basis functions, discussed in section 7.1 reduces the EFIE formulation to the system impedance matrix

$$\sum_{n=1}^{N} Z_{mn} I_n = V_m \quad \text{for} \quad m = 1, 2, \ldots, N \tag{7.1.2}$$

for an N-segment wire-grid model. A single variable response, such as tangential electric field component, or input impedance at the source segment can be found through the solution of this matrix equation.

At the source segment, the input impedance is calculated from

$$Z_{input} = \frac{E_{tan} \times \Delta_{input}}{I_{input}} \tag{7.1.3}$$

where Δ_{input} is the length of the source segment, E_{tan} is the tangential electric field on the structure segment and I_{input} the current evaluated at the midpoint of that segment. The single independent variable response can be written in terms of a general rational transfer function representation, from (6.3.17),

$$H(s) = \frac{N(s)}{D(s)} = \frac{b_0 + b_1 s + \ldots + b_n s^n}{a_0 + a_1 s + \ldots + a_d s^d} \tag{7.1.4}$$

such that for the input impedance, as a function of frequency,

$$Z_{input}(s) = \frac{b_0 + b_1 s + \ldots + b_n s^n}{a_0 + a_1 s + \ldots + a_d s^d} \tag{7.1.5}$$

Given M samples of input impedance Z_m, $m = 1 \ldots M$, the transfer function matrix equation, from (6.3.14) with $H_m = Z_m$,

$$\begin{bmatrix} s_0^0 Z_0 & \ldots & s_0^{d-1} Z_0 & -s_0^1 & \ldots & -s_0^n \\ s_1^0 Z_1 & \ldots & s_1^{d-1} Z_1 & -s_1^1 & \ldots & -s_1^n \\ \cdot & \cdot & \cdot & \cdot & \cdot & \cdot \\ \cdot & \cdot & \cdot & \cdot & \cdot & \cdot \\ \cdot & \cdot & \cdot & \cdot & \cdot & \cdot \\ \cdot & \cdot & \cdot & \cdot & \cdot & \cdot \\ s_{M-1}^0 Z_{M-1} & \ldots & s_{M-1}^{d-1} & -s_{M-1}^1 & \ldots & -s_{M-1}^n \end{bmatrix} \begin{bmatrix} a_0 \\ a_1 \\ \cdot \\ a_{d-1} \\ b_0 \\ \cdot \\ b_n \end{bmatrix} = \begin{bmatrix} -s_0^N Z_0 \\ -s_1^N Z_1 \\ \cdot \\ \cdot \\ \cdot \\ \cdot \\ -s_{M-1}^N Z_{M-1} \end{bmatrix} \tag{7.1.6}$$

This transfer function matrix should not be confused with the system impedance matrix;

the transfer function matrix relates rational function coefficients to the response observable, evaluated at $M = n+d+1$ discrete frequencies, with n and d corresponding to numerator and denominator orders. The system impedance matrix of this section relates current distribution to tangential electric field component at a single frequency, based on the segmented wire-grid model satisfying Trueman-type criteria at that frequency.

For the single variable response, in this case input impedance, the wire-grid structure is segmented and solved using SuperNEC at M frequencies: an analytical expression for the input impedance over some frequency range spanning the M frequencies is given using the frequency domain Prony method (FDPM). A number of pertinent questions arise related to the applicable frequency range for the model, the number of samples required, the order and form of the rational function, to name but a few (c.f. section 2.4.1). Section 7.2 deals with the statement of these questions and the design details relevant to the use of low-order frequency domain models within SuperNEC.

7.1.2 Terminology

The terminology used by Miller in his general treatment of MBPE in electromagnetic applications [185] has been adopted for the discussions in this chapter.

Any limiting assumptions made during the modelling process degrade the effectiveness of the first-principle model in describing the actual physical problem or process; the resulting model is known as the *generating model* (GM). Within the context of this document, the Fredholm integral equation of the first kind, used to describe the current distribution on a structure submitted to an electric field excitation, using a thin-wire approximation, is a generating model.

Real frequency GM samples are used to construct the transfer function matrix of (7.1.6), the solution of which defines the coefficients of the rational function model of (7.1.5). The representation of (7.1.5) gives a large number of possible rational functions or *fitting models* (FMs), each model dependent on the GM samples used in the matrix formulation. The FM may thus be viewed as a reduced-rank parametric model which attempts to accurately describe some GM, given a number of samples of that GM.

The *Data Fit* (DF) is a measure of the difference between the GM samples used to fill the transfer function matrix, and the FM rational function evaluated at those same frequencies [186]. The *Model Fit* (MF) is found by evaluating the FM at all GM samples not already used to generate the FM. An average MF for each FM is typically calculated.

7.2 Design Details for Wideband Modelling

The integration of a frequency domain estimation method into the frequency domain code, SuperNEC, necessitates a comprehensive analysis of the FDPM, with core issues including:

- The restrictions imposed by sampling theory on sampling rates and hence the description of frequency responses.
- The specific form of the rational function; relationships between numerator and denominator polynomial orders.
- The limitations on the maximum number of poles which can be used to describe a system response, due to the matrix formulation.
- Determining the number of poles required to accurately describe the system as well as error measures suitable for describing convergence. The effects of over- or undersampling of the system response.
- A measure of the effectiveness of this method in characterizing responses of varying degrees of resonance, and the frequency ranges/bandwidth which can be accurately modeled using a complex frequency domain estimator.
- The computational implications of an iterative strategy for successive-approximation.

The optimal system which can find an accurate, analytical representation of some electromagnetic parameter over an arbitrary frequency range, has been designed for integration into SuperNEC: it is known as a *Transfer Function Estimation* (TFE) module.

7.2.1 A Simulated Transfer Function

For illustrative purposes, a highly resonant, simulated response is suitable to investigate performance limitations associated with the frequency domain estimation technique, presenting a test platform for algorithms suitable for TFE. The GM is a simulated pole series, similar to that used by Miller [185], having poles and residues defined by

$$s_i = \frac{\sqrt{i}}{15} - ji \quad \text{and} \quad R_i = \frac{\sqrt{i}}{15} \quad \text{for} \;\; i = 1, 2, \ldots 15 \tag{7.2.1}$$

where $j = \sqrt{-1}$ s_i and R_i are poles and residues, respectively. The GM is defined by

$$\begin{aligned} G(s) &= \frac{1/15}{s - 1/15 + j} + \frac{\sqrt{2}/15}{s - \sqrt{2}/15 + 2j} + \ldots + \frac{\sqrt{15}/15}{s - \sqrt{15}/15 + 15j} \\ &= \sum_{i=1}^{15} \frac{\sqrt{i}/15}{s - \sqrt{i}/15 + ji} \end{aligned} \tag{7.2.2}$$

Each term in the series contributes a resonance at $\omega = i$ (where $s = j\omega$): the result is a GM which has 15 resonant peaks in the real component. This chosen series highlights the applicability of representing resonant structures and responses with a rational function approximation. It is also noted that the response is similiar to that of the dipole over a wide frequency band [178]. The generating model is defined by (7.2.2) and shown in figure 7.1. Note that some response characterized by many resonant peaks will result in a higher order rational function, implying more response "samples" and generating a larger and more ill-conditioned transfer function matrix.

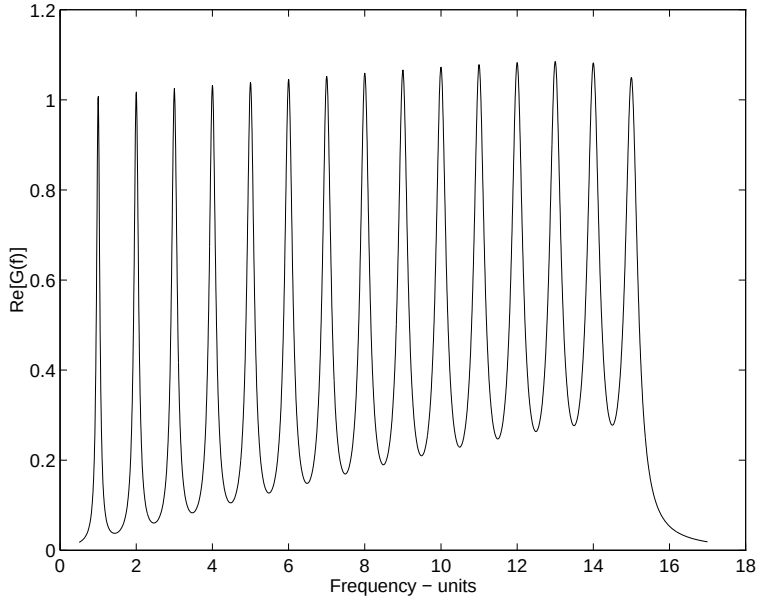

Figure 7.1: The real component of a simulated resonant system defined in (7.2.2)

7.2.2 Sampling Theory Restrictions

The representation of the time or frequency response of a system with a set of discrete data points requires a sampling process. The inherent limitations introduced by the sampling

process restrict accuracy in the characterization of a response by a Fourier[1] transform pair between 2 domains. The impact of these limitations on the design process is dependent on whether information of both transient and spectral characteristics is required. Although this chapter addresses issues related to the FDPM, the information theory sampling criteria are first presented in the time domain; for more indepth discussion, see [10].

The generic spectral domain-waveform domain pair is based on a finite number of samples, $P = 2N$ in the formulations of sections 6.3.1 and 6.3.2. For the time-domain representation of (6.3.2) to fully describe the frequency content of some response, the $2N$ equispaced samples require a minimum sample interval known as the *Nyquist interval*. Shannon's Sampling Theorem states that for a band-limited signal of finite energy, with bandwidth W, the Nyquist interval of $1/2W$ is required to completely describe the signal. There are two implications of the Time Domain Prony Method:-

- A truncation to $2N$ samples may be viewed as multiplying the actual infinite extent time signal by a rectangular window. The frequency domain implication is the convolution of a sinc function with the frequency response of the infinite time signal.
- The largest bandwidth, W, of a signal that can be described is equal to $1/2$ the sampling rate (Nyquist rate); this can impose serious computational limitations. For example, to describe the response of some structure at the lowest frequency in the UHF range (300MHz) requires a Nyquist interval spacing of $< 1/(600 \times 10^6) = 1{,}67$ ns.

The duality between time and frequency domains, effected by a Fourier transform, gives a mirror argument for sampling of frequency domain parameters to fully characterize a transient response. Transient scattering and radiation problems for general structures were first treated by numerical inverse Fourier Transforms of frequency domain solutions [39]. The primary use of the complex frequency domain estimator discussed in this chapter is for the wideband description of some parameter. At present, facilities for numerical inverse Fourier Transform calculations are not planned for SuperNEC; transient time domain codes, such as the Finite Difference Time Domain (FDTD) codes [187] are more useful. The sampling theory presented here is purely in recognition of the limitations introduced by the formulations of chapter 2.4.4, if Fourier Transforms (and inverses) were to be performed.

7.2.3 The Form of the Rational Function

A frequency domain representation derived from (6.3.13), with non-pole components ignored, maps to a rational function with the degree of the denominator 1 larger than the numerator.

[1] This argument also applies to Laplace Transforms in general.

A general rational function used for interpolation does not have this limitation [163]. Non-pole terms can be included into the rational function, causing the degrees of the numerator and denominator to be equal ($n = d$), for $\beta = 0$ in (6.3.13), or the degree of the numerator larger by 2 ($n = d + 2$) for a unit step contribution.

The NEC4 post-processor [188] limited the form of the rational function to $n = d$ for an odd number of total samples, P, or $n = d+1$ for P even. An increase by 1 of the numerator order accounts for a constant non-pole component, whereas a linear term in s causes the numerator order to be 1 greater than that of the denominator.

A given bandwidth, say 3:1, cannot necessarily be described using 1 rational function. The interaction between radiating elements on a structure and the structure itself may result in the EM observable, say input impedance, being highly resonant. Conversely, the structure may be nonresonant over its entire frequency range of interest. The broadband log-periodic antenna and the HF antenna on an attack helicopter are examples of structures at each end of the so-called "resonance scale". These specific structures are considered for evaluation of frequency domain estimation methods in SuperNEC evaluated in the next chapter.

7.2.4 Matrix Conditioning and its Effect

The rational function approximation of the transfer function of some electromagnetically-excited structure reduces to a linear system of equations, with the unknowns being the numerator and denominator coefficients (c.f section 6.3.2). The transfer function matrix, which is constructed from at least $2N$ real frequency samples of some parameter, has a structure very similar to that of a Vandermonde matrix, which is particularly well known for its ill-conditioned structure. This section discusses measurements of matrix conditioning, the causes of ill-conditioning and the effects of conditioning on the accuracy of the pole and residue solutions. This analysis is limited to the forms of the rational function used in the electromagnetic literature, for MBPE implementations, as discussed in section 7.2.3. While this investigation uses a simulated resonant response, it should be noted that the order of the simulated system is higher than the systems encountered in practice. It may therefore be viewed as an appropriate practical asymptote, defining a maximum model order for use in the successive approximation method (see section 7.3). Condition numbers of transfer function estimation matrices for specific wire-grid structures in SuperNEC are examined in section 8.4.1.

Given a set of simultaneous equations, where the raised dot indicates matrix multiplication,

$$\mathbf{A} \cdot \mathbf{x} = \mathbf{b}$$

Matrix **A** has a singular value decomposition (SVD) defined by

$$\mathbf{A} = \mathbf{U} \cdot \mathrm{diag}(w_j) \cdot \mathbf{V}^T \tag{7.2.3}$$

where the w_j entries of the diagonal matrix correspond to the singular values of **A**. **U** and **V** are square matrices for a square matrix **A**: the columns of **U** whose same-numbered elements w_j are non-zero form an orthonormal set of basis vectors that span the range; the columns of **V** whose same-numbered elements w_j are zero form an orthonormal basis for the nullspace [163]. The solution of the linear system can be expressed in terms of a linear combination of basis functions, the singular vectors.

$$\mathbf{x} = \sum_{i=1}^{N} \left(\frac{\mathbf{U}_i \cdot \mathbf{b}}{w_i} \right) \mathbf{V}_i \tag{7.2.4}$$

The smallest singular values thus dominate the solution by scaling the corresponding singular vectors most. *Condition number* is defined as the ratio of the largest to the smallest singular values of a given matrix. An excessive spread of singular values, giving a large condition number, distorts the solution. Small perturbations in **b** and **A**, or rounding and precision errors in w_i, cause significant variations in **x**. Errors introduced during the solution of the linear system result in a decrease in accuracy as the condition number increases.

The general representation, given in (7.1.5) presents a large number of possible rational functions, or fitting models (FMs), for any P points. With the restrictions to diagonal form, particular algorithms can be used, as mentioned in section 6.3. Non-pole terms must also be considered, with appropriate simplifications given in section 7.2.3. Using the simulated transfer function of section 7.1.2, the effects of numerator and denominator polynomial degrees on the condition number of the transfer matrix (c.f. section 7.1.2) and accuracy of solution can be quantified.

The condition number of the transfer function matrix grows with an increasing number of sample points for a fitting model (FM) spanning a fixed frequency range. The data fit (DF) decreases monotonically as a function of numerator order for all denominator orders. This is caused by the increasing condition number of the matrix: a matrix is ill-conditioned if the reciprocal approaches the machine's floating point precision, typically 10^{-6} for single and 10^{-12} for double precision [163]. High condition numbers manifest in small pivot elements in solvers like Gauss-Jordan: rounding errors and precision problems propagate through to give a meaningless solution.

CN and DF are plotted in figure 7.2a as a function of N, using D as a parameter. The

results are specified in digits, evaluated as

$$\text{CN} = \text{abs } [\log_{10}(\text{Condition Number})] \tag{7.2.5}$$

$$\text{DF} = \text{abs } [\log_{10}(\text{Data Fit})] \tag{7.2.6}$$

Miller noted [186] that $CN + DF \approx CP$, where CP is the computing precision, specified in digits. The precision calculation used to reproduce this result was CP = abs $[\log_{10}(\text{eps})]$, where *eps* is the relative floating point accuracy and is defined to be the distance from 1.0 to the next largest floating point number. The author could not concur with Miller's observation, noting only that $CN + DF$ was limited between 15.5 and 19. The CN was found to vary as $\approx 10^{n+d}$ with n and d being the numerator and denominator degrees in (6.3.17).

In figure 7.3a, the model fit curves of figure 7.2b are used to generate a surface (using the denominator parameterization). Figure 7.3a depicts what could best be described as a parabolic cylinder, the parabolic section symmetrical about a plane corresponding to $N+D = 13$. This corresponds to a maximum dimension, full rank transfer function matrix of dimension 13, before the inaccuracy introduced by the ill-conditioned matrix sets in (manifesting in rank-deficiency). The maximum MF illustrates that the best case accuracy of 10^{-4} coincides with the plane, $N + D = 13$. The data fit plot in figure 7.2a is also used to generate a surface, using a denominator parameterization as depicted in figure 7.3(b). The intersection of the plane $N+D = 13$ indicates the accuracy tradeoff in the data fit corresponding to a maximum model fit.

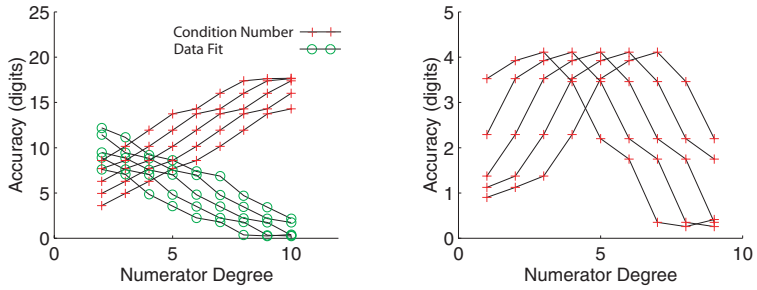

Figure 7.2: (a) CN and DF as a function of numerator degree, using a denominator parameterization. (b) Model Fit Accuracy as a function of numerator degree, using a denominator parameterisation.

7.2.5 An Over- or Underdetermined System Formulation

Given $2N$ samples, FDPM solves for the N poles and their associated residues. An obvious question is thus highlighted by this formulation, namely, whether the system under scrutiny

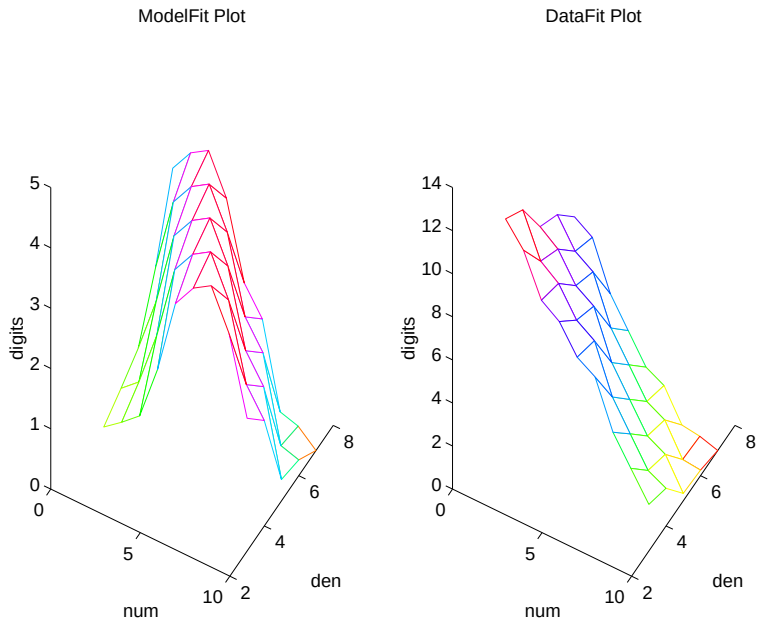

Figure 7.3: (a) A surface generated from figure 7.2(b) using a denominator parameterization. (b) A surface generated from the data fit of figure 7.2(a), using a denominator parameterization.

is accurately characterized by N poles. The TDPM, or MBPE in its waveform domain form, states that the impulse response of the system can be characterized by $2N$ evenly spaced time samples, defining the same N poles. If N is chosen incorrectly, the system being described is either over- or underdetermined.

If the system being described has M unknowns and the number of GM samples $P < M$; the system is undersampled and the poles and residues are incorrect. A simple analogy of this effect is the approximation of a cubic polynomial with a quadratic. Different placement of samples will yield different rational functions. For $P = M$, the solution will be correct, irrespective of sample placement, provided that the condition number of the matrix is reasonable. For $P > M$; the matrix representation at the P points will be extremely ill-conditioned. Even if the condition number had no marked increase, a deduction could be made as to the accuracy of a particular FM if it agreed with another FM describing the same band, which had 1 less sample. An error tolerance is typically used to measure agreement.

If there is no definite oversampling, manifesting in an increase in condition number, then the interpolation method does not correctly model the underlying problem. Referring to the earlier analogy of the approximation of a cubic; if 5 samples were used, the matrix being solved would be overdetermined, with a massive condition number. The condition number (CN) dependence on numerator and denominator orders, as given in section 7.2.4, provides no indication of the order of the system, as is the case with a polynomial model. The limitation

in this formulation is suspected to be that complex conjugate poles were not used. This topic is currently being investigated.

7.3 Successive Approximation for Model Optimization

The discussions in previous sections of the form of the rational functions, the conditioning of the transfer function matrix and the under- or overdetermination of the system refer to 1 FM over some frequency range. As highlighted earlier, 1 FM cannot be expected to provide an accurate model over a large bandwidth, necessitating a more comprehensive strategy. The discussions that follow address the necessary details.

Unlike Prony's method applied to the time domain problem, frequency domain parameter estimation does not require equispaced samples. Freedom in the placement of samples lends itself to an iterative successive-approximation process of obtaining an optimum model of the system. Miller [185] advocated several possible approaches with origins in variable step width numerical quadrature methods, such as Romberg's method. Miller's favored approach involves generating an error measure which is a continuous function of the independent variable, in this case, frequency. New samples are added wherever this measure is a maximum.

7.3.1 Continuous Error Measures

Consider a structure which has been sampled at N different frequency points. Noting the limitation of 13 samples, as discussed in section 7.2.4, an arbitrary frequency range will generally need several models. Given X different FMs spanning the P points (the forms of the models are discussed in detail in sections 7.2.5 and 7.2.3), with each model constructed from at least 3 and at most N samples, i.e.

$$FM_i(f) = \frac{b_0 + b_1 s + \ldots + b_n s^n}{a_0 + a_1 s + \ldots + a_d s^d} \quad \text{for} \quad i = 1, 2, \ldots, X \tag{7.3.1}$$

The mismatch between overlapping FMs, as used by Miller [185] is

$$\Delta MM_{ij} = \frac{|FM_i(f) - FM_j(f)|}{|FM_i(f)| + |FM_j(f)|} \tag{7.3.2}$$

This continuous mismatch error function can be evaluated with the number of samples chosen to obtain the necessary resolution. At the maximum mismatch error, the next frequency sample required from the GM is chosen. Note that the denominator is a normalization function chosen to include the relative magnitudes of both FMs. Instead of this global, approximation error criterion, an exact point-wise error measure can be used. For this measure, the mismatch

is calculated between the FMs and the GM evaluated at some frequency f_i, i.e. consider $G(f_i)$, the exact, normalized error between the GM and the kth FM, evaluated at f_i is

$$\Delta GM_{ik} = \frac{|G(f_i) - FM_k(f_i)|}{|G(f_i)| + |FM_k(f_i)|} \tag{7.3.3}$$

For particularly large problems, typically requiring a segmentation number in excess of 1000, evaluating the generating model at some frequency is extremely costly in computational effort. It therefore supports maximum inference of error characteristics from successive comparisons and approximations of fitting models. Consequently, the global mismatch error function of (7.3.2) is used.

7.3.2 An Iterative Strategy

FDPM as defined in section 6.3.2 is purely capable of filling a transfer function matrix based on a number of samples and solving for the numerator and denominator coefficients. This solution gives a rational function analytical approximation to the system defined by those P points. Since $P = 2N$ defines N poles and associated residues, this assumes that there are N poles required to correctly characterise the frequency response of the given structure (c.f. section 7.2.5). By using the continuous error measure of section 7.3.1, a relative error in the two FM approximations is given; specific problems related to this global approximation are given in section 7.3.4. Each continuous mismatch error function ΔMM_{ij} has 1 error maximum; it is thus deduced that the GM is least accurately defined at that frequency. The GM therefore needs to be evaluated at that frequency and new, more accurate FMs defined. Each new GM sample regenerates at *least* 2 FMs. The iterative successive-approximation method, otherwise known as *adaptive sampling* is hence defined. For the implementation discussed in this document, the frequency corresponding to the largest error across all mismatch functions defines the new sample to be obtained from the GM.

A minimum of 4 GM samples is required to allow 2 FMs to be generated. The maximum number of samples permitted for any FM is limited by the condition number of its matrix; for the target system used in this investigation, the largest condition number is roughly 9×10^{13}. At the GM samples used for developing the FMs, the mismatch error will be approximately zero (c.f. section 7.1.2). Due to the large condition numbers of the matrices used to calculate the rational function coefficients, the coefficients are limited in accuracy by computational precision. The cumulative error in the entire rational function polynomial expansion may result in numerical errors at the original GM samples.

The *sample selection and update* strategy based on the global, approximate error measure of section 7.3.1 is iteratively performed until the mismatch error floor is reached. The error floor, typically of the order of 10^{-3} indicates that the maximum mismatch error between all

overlapping models is less than the floor, in this case 10^{-3}.

The output of the adaptive sampling TFE module is thus 1 or several FMs defined over the frequency band of interest, which accurately describes the system response for the parameter concerned. The accuracy is of course determined by the chosen error floor and the total number of iterations required to reach this floor; it is thus dependent on the degree of resonance of the response.

7.3.3 Validation on a Simulated Structure

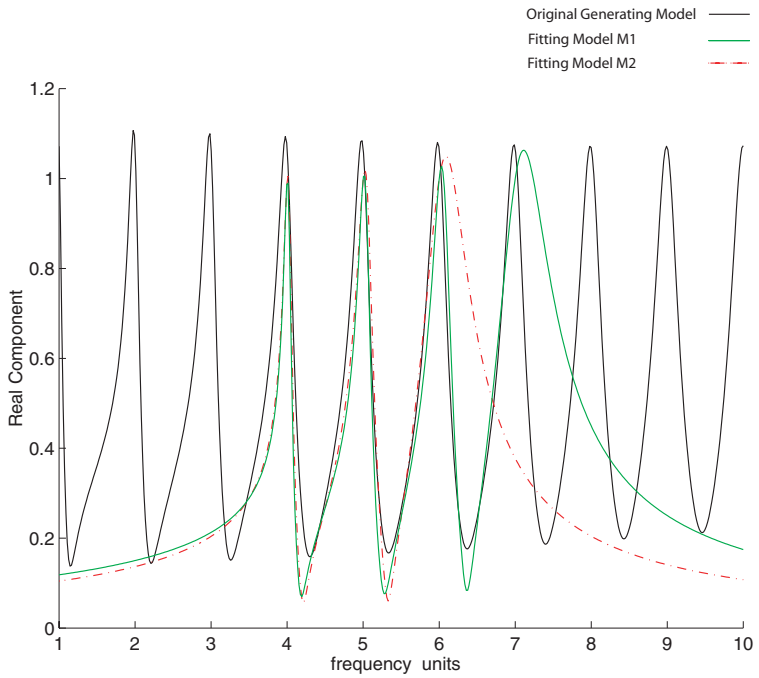

Figure 7.4: The original GM with continuous fitting models M_1 and M_2 superimposed

The error measures of section 7.3.1 are developed using comparisons of overlapping models over some frequency range. The simulated transfer function of section 7.2.1 was used as the platform for this evaluation. The known, real frequency information is at $f_i = 3.5 + i0.5$ for $i = 0, 1, \ldots, 14$. For discussion purposes, consider 2 models, M_1 and M_2, characterized by the frequency samples f_i at which the parameter information is used to construct the FMs:

$$\begin{aligned} M_1 &= \{3.5 \;\; 4 \;\; 4.5 \;\; 5 \;\; 5.5 \;\; 6\} \\ M_2 &= \{3.5 \;\; 4 \;\; 4.5 \;\; 5 \;\; 5.5 \;\; 6 \;\; 6.5 \;\; 7 \;\; 7.5 \;\; 8\} \end{aligned}$$

The overlapping region is the closed interval [3.5 6]. Figure 7.4 depicts the approximation of fitting models M_1 and M_2 to the actual GM, where both fitting models are evaluated

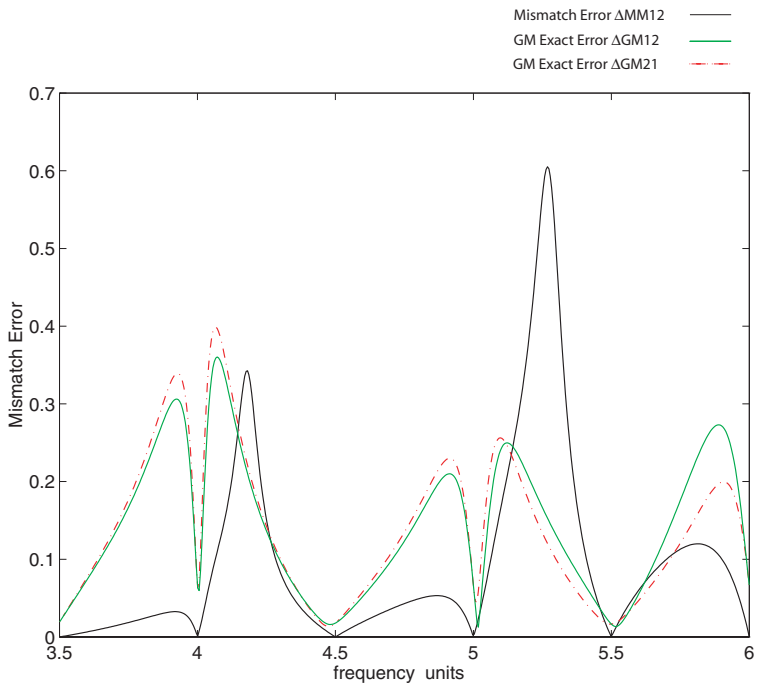

Figure 7.5: The mismatch error function ΔMM_{12} is compared with the exact, point-wise approximations of ΔGM_{12} and ΔGM_{21}

over the range [1 10]. Both the exact point-wise and global approximate error measures of section 7.3.1 are evaluated. In figure 7.5, the green (–) and red (-.) curves are ΔGM_{12} and ΔGM_{21} respectively, while the black (–) curve is ΔMM_{12}. For the mismatch error function, ΔMM_{12}, the next sample is required at frequency 5.27. Hence, the new models have samples -

$$\begin{aligned} M_1 &= \{3.5 \;\; 4 \;\; 4.5 \;\; 5 \;\; 5.27 \;\; 5.5 \;\; 6\} \\ M_2 &= \{3.5 \;\; 4 \;\; 4.5 \;\; 5 \;\; 5.27 \;\; 5.5 \;\; 6 \;\; 6.5 \;\; 7 \;\; 7.5 \;\; 8\} \end{aligned}$$

Similarly, for two models overlapping the range [8.5 11], the error measures are given in figure 7.6. The fitting models generated after the first iteration have significantly improved accuracy (comparing figures 7.4 and 7.7). Performing a further iteration, accuracy is still further improved. As at the second iteration, the mismatch error function is depicted in figure 7.8. The impact of the effectiveness of this algorithm is obvious by comparing the mismatch error function of the initial models (figure 7.5) with those of the FMs after 2 iterations (figure 7.8).

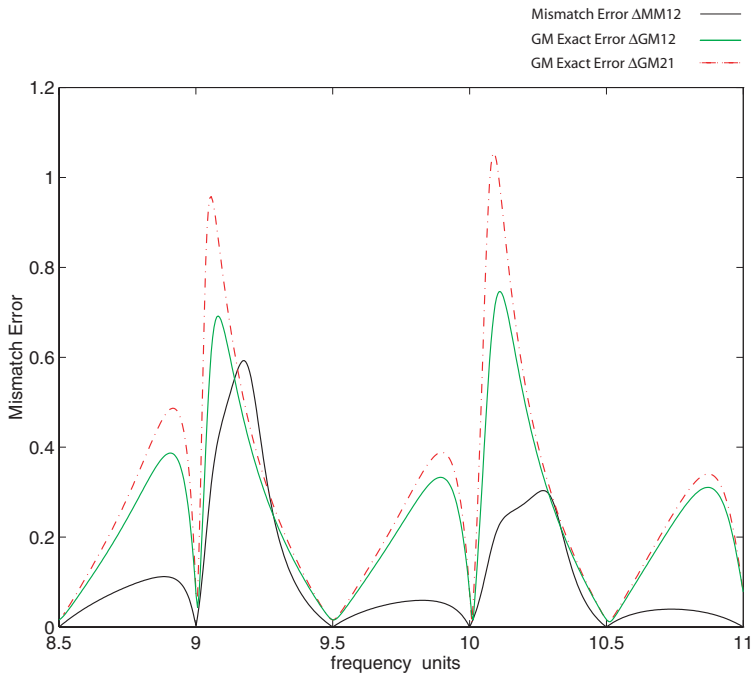

Figure 7.6: The error measures of the ΔGM_{12}, ΔGM_{21} and ΔMM_{12} after 1 iteration

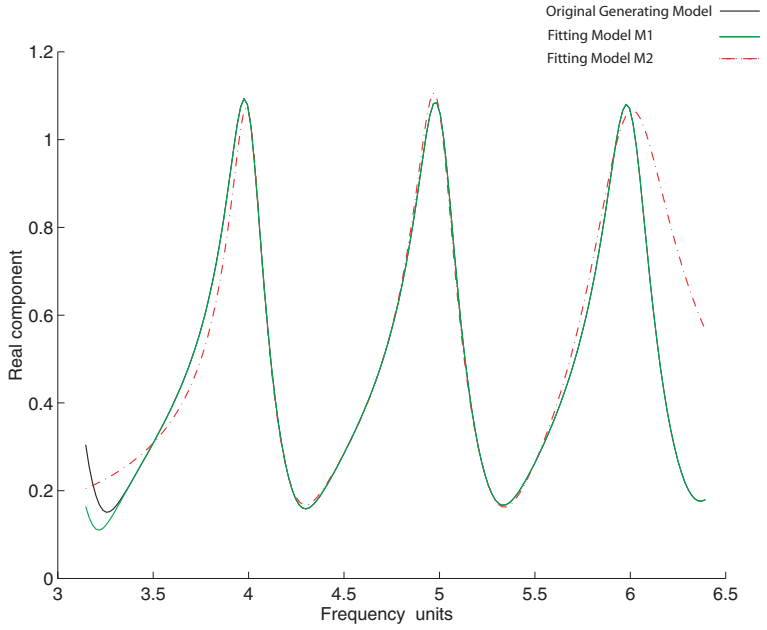

Figure 7.7: The original GM with continuous fitting models M_1 and M_2 superimposed, after 1 iteration

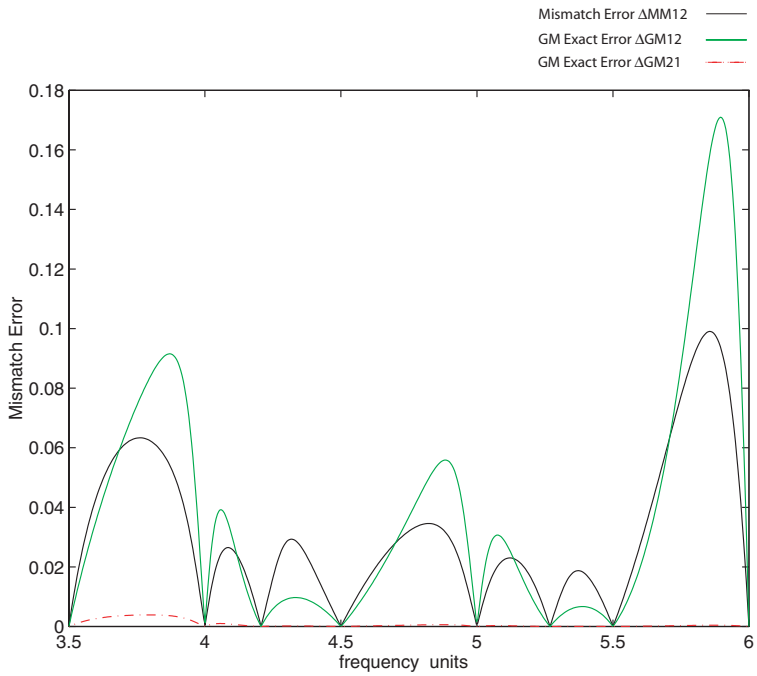

Figure 7.8: The error measures of the ΔGM_{12}, ΔGM_{21} and ΔMM_{12} after 2 iterations

7.3.4 Problems with Adaptive Sampling

Two problems have been identified:

- The primary problem is that of insufficient spacing between samples used to generate a FM; for a slowly varying function, closely spaced samples can create a rank-deficient matrix, resulting in a massive condition number. This is analogous to a matrix formulation of a linear sytem of equations to solve for the coefficients of a cubic polynomial where 2 rows in the matrix are almost identical, as discussed earlier.
- Should the GM exhibit a marked discontinuity, such as that of the forked monopole (figure 14 in Miller [26]), overlapping FMs and their corresponding mismatch error may require several iterations in the vicinity of the detected discontinuity. Excessive samples in the slowly-varying regions adjacent to the resonant peak cause the problem discussed above. The implemented algorithm screens for excessive sample placement near a discontinuity.

To demonstrate the second problem, consider the original conductance characteristic (GM) of some resonant electromagnetic structure, in figure 7.9(a). Two FMs are constructed with different samples over the same L/λ, as shown in figure 7.9(a). The different sample choices give different FMs: each FM indicates the existence of the marked discontinuity, however,

the exact placement is incorrect. The mismatch error functions are drawn in figure 7.9(b), from which it is clear that the maximum error function occurs at $\approx 0.75L/\lambda$. Note that the exact point-wise error measure of the GM is superimposed on the global, approximate error measures of the FMs. The FMs are thus updated, as indicated in figure 7.10(a), where once again the marked discontinuity as represented by the 2 FMs is shifted over some range. The mismatch error functions are shown in figure 7.10(b). This iterative occurrence can lead to an ill-conditioned transfer function matrix, if followed blindly. Miller [186] suggested building in optional information to assist in the selection of samples; for example, where negative conductance or resistance occurs due to the evaluation of a FM over some band.

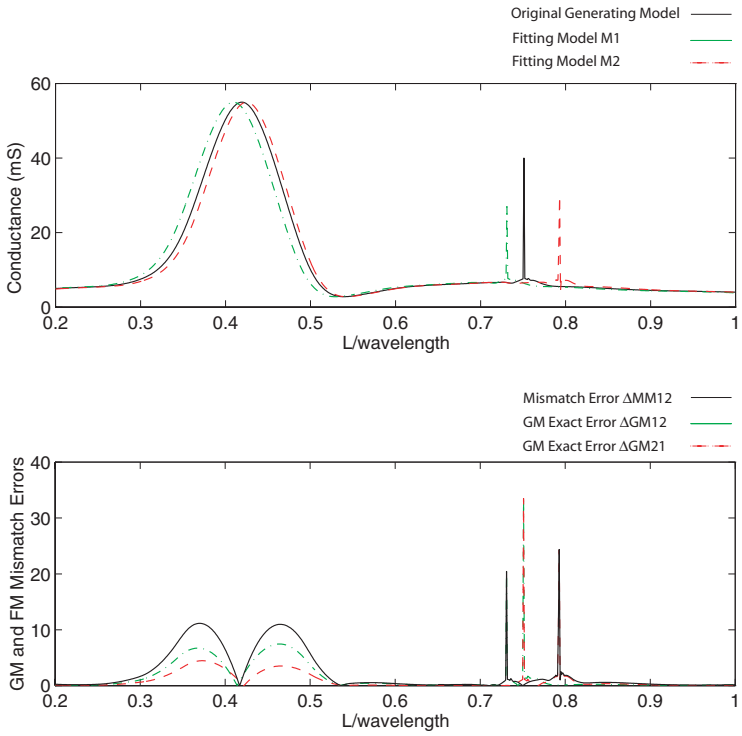

Figure 7.9: Iteration 1: (a) The conductance vs normalized length of an antenna. The GM is given by the solid line and FMs 1 and 2 by the red -. and green -, respectively. (b) The exact GM mismatch error in the solid line and ΔFMs 1 and 2 by the red -. and green -, respectively.

7.4 Conclusions

This chapter provides the core design detail of an instrument which is capable of fitting several accurate, overlapping models to a wide frequency band of interest, irrespective of the degree of resonance of the structure. This design tool, a frequency domain estimation method, whose

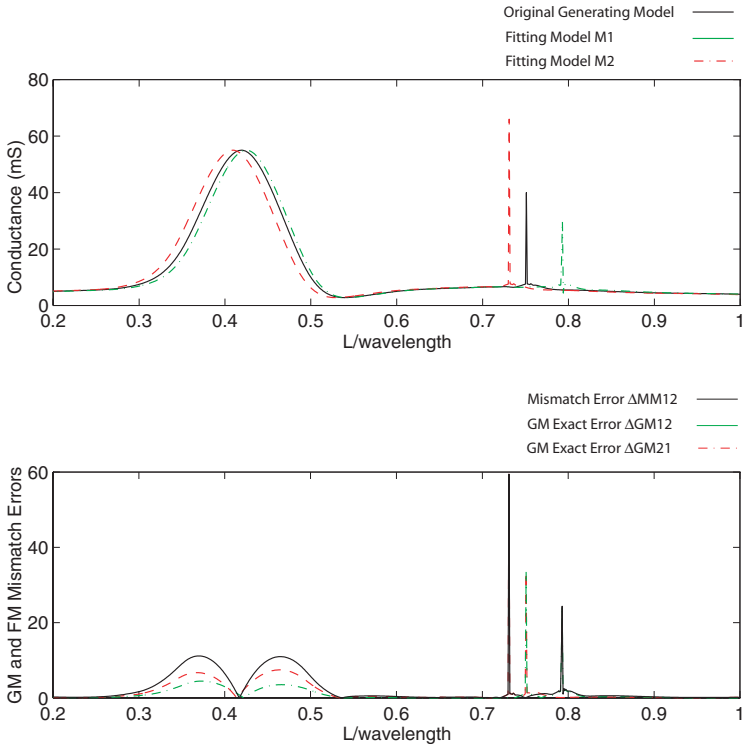

Figure 7.10: Iteration 2: (a) The conductance vs normalized length of an antenna. The GM is given by the solid line and FMs 1 and 2 by the red -. and green -, respectively. (b) The exact GM mismatch error in the solid line and ΔFMs 1 and 2 by the red -. and green -, respectively.

origins lie in the Frequency Domain Prony Method (FDPM), was dubbed a Transfer Function Estimation module. Limitations of the complex frequency domain estimation technique of chapter 2.4.4 were highlighted, with appropriate measures for assessing their influence discussed.

The MoM formulation used in SuperNEC to give a frequency domain discretization of an electric field integral equation, derived from Maxwell's equations, is reviewed in section 7.1. The frequency-dependence of wire-grid models is discussed, and the application of frequency domain estimation models to the SuperNEC Fredholm equation addressed.

Some constraints introduced by sampling of either the time or frequency domain representation were given: it was noted that if a Fourier Transform (or inverse) was required based on a Prony model, that Shannon's sampling theories needed to be considered. The specific case of wideband modelling presented in this document does not elaborate on information theory constraints.

Central to the effectiveness of the TFE concept is the solution of the individual FDPM matrix equation. The accuracy of the nontrivial solution can be substantially reduced by abnormally high matrix condition numbers; the impact of CN on the data and model fits of a resonant, simulated structure was presented in section 7.2.4. The condition number of the transfer function matrix was noted to limit the maximum number of samples in a single fitting model (FM) to 13. The form of the rational function for this approximation was limited to $n = d$, for an odd number of total samples and $n = d + 1$ for an even number, as discussed in section 7.2.3. Perhaps the most puzzling characteristic of the system formulation, it was noted in section 7.2.4 that the CN of the transfer function matrix increases as a function of $\approx 10^{n+d}$, irrespective of the actual number of poles characterizing the system.

Miller's iterative successive-approximation method [24] of section 7.3 defines continuous error measures and an adaptive sampling strategy for model optimization suitable for wideband approximations. The strategy, which is based on overlapping fitting models with a global, relative error measure, was validated on a highly resonant simulated structure (section 7.3.3).

The output provided by the adaptive sampling TFE module is 1 or several FMs defined over the frequency band of interest, which accurately describe the system response for the requisite parameter. The accuracy is determined by the user-specified mismatch error floor.

This chapter concludes with a number of observations of problems inherent to adaptive sampling, with a theoretical illustration given.

Chapter 8

Results - Evaluation of the Frequency Domain Method Implemented in SuperNEC

The previous chapter focused on the nucleus of the TFE design instrument capable of defining an analytical, continuous, broadband description of some EM system response over an arbitrary frequency range. This module was integrated into SuperNEC, the object-oriented electromagnetic code, designed by Nitch [5], using C++. This chapter deals with the details of this integration, the types of responses considered, suitable structures for demonstration of the TFE capabilities and the modelling limitations thereof, and finally, the results obtained when simulations were performed using TFE within SuperNEC. Section 8.1 presents two specific implementations of the TFE design instrument which were integrated into SuperNEC, namely for approximation of the input impedance and current distribution responses. The adaptive sampling strategy is selected using the SuperNEC input cards, with the FMs constructed using iteratively calculated GM samples, as given in section 8.2. The wire segmentation modelling required for SuperNEC has frequency dependence implications, which were discussed in section 7.1.1: the Log Periodic Dipole Array (LPDA) and the HF antenna on an attack helicopter where chosen for validation of the TFE module within SuperNEC and are discussed along with modelling limitations in section 8.3. Section 8.4 presents the results of the simulations by SuperNEC for both the input impedance and current distribution responses.

8.1 Frequency Responses Modeled within SuperNEC

Two specific implementations of TFE were integrated into SuperNEC.

1. A 2-dimensional application, where adaptive sampling TFE is applied to the input impedance problem. Verifications were performed using 2 structures, namely; the HF antenna mounted on an attack helicopter, and the log-periodic dipole array (LPDA).

2. An $(N+1)$-dimensional application is also presented where the current at the midpoint of each of N segments is used as the generating model for TFE.

8.1.1 Input Impedance Response

The 2-dimensional response was discussed in some detail in section 7.1.1, some of which is repeated here. The input impedance is calculated at the source segment, from

$$Z_{input} = \frac{E_{tan} \times \Delta_{input}}{I_{input}} \tag{8.1.1}$$

where Δ_{input} is the length of the source segment, E_{tan} is the tangential electric field on the structure segment and I_{input} the current evaluated at the midpoint of that segment. The transfer function matrix, reproduced from (6.3.14) is given by

$$\begin{bmatrix} s_0^0 Z_0 & \dots & s_0^{d-1} Z_0 & -s_0^1 & \dots & -s_0^n \\ s_1^0 Z_1 & \dots & s_1^{d-1} Z_1 & -s_1^1 & \dots & -s_1^n \\ . & . & . & . & . & . \\ . & . & . & . & . & . \\ . & . & . & . & . & . \\ . & . & . & . & . & . \\ s_{M-1}^0 Z_{M-1} & \dots & s_{M-1}^{d-1} & -s_{M-1}^1 & \dots & -s_{M-1}^n \end{bmatrix} \begin{bmatrix} a_0 \\ a_1 \\ . \\ a_{d-1} \\ b_0 \\ . \\ b_n \end{bmatrix} = \begin{bmatrix} -s_0^N Z_0 \\ -s_1^N Z_1 \\ . \\ . \\ . \\ . \\ -s_{M-1}^N Z_{M-1} \end{bmatrix} \tag{8.1.2}$$

As successive iterations of SuperNEC are executed, the Z_m are calculated, enabling the $M \times M$ transfer function estimation matrix to be populated.

8.1.2 Current Distribution Response on an N Segment Structure

For this $(N+1)$-dimensional case, a transfer function matrix, identical to that of (8.1.2), is constructed for each of the N segments comprising the entire structure. The current at the midpoint of the segment, would replace the Z_m at complex frequency s_m, in (8.1.2). TFE is performed over the range of frequencies s_0 to s_{P-1}, giving a continuous frequency description of the current on *that* segment over *that* range. The current distribution response implementation performs an iterative procedure whereby the maximum mismatch error is used to locate the optimum solution, as measured by an appropriate error floor. This first implementation uses an identical sample selection and update strategy to its 2-dimensional

predecessor where the maximum mismatch frequency is added to each FM on *each* segment over the entire structure. It should be noted that this implementation is purely an initial assessment of the feasibility of further research into the $N+1$-dimensional estimation problem.

8.2 Adaptive Sampling within SuperNEC

Both NEC2 and SuperNEC have an input interface where geometric information and simulation settings are presented in the form of "cards" [1]. A card is defined by an identifier acronym followed by a sequence of integer or floating point variables. Simulations performed over a range of frequencies use the *FR* card, which specifies start (f_1) and end (f_{end}) frequencies. Given the starting frequency, f_1, successive simulation frequencies are calculated by the addition or multiplication by some constant, as specified in the *FR* card.

$$f_n = f_{n-1} + c \tag{8.2.1}$$

$$\text{or} \quad f_n = f_{n-1} \times c \tag{8.2.2}$$

where c is a constant specified by the user in the *FR* card. The samples fed into the TFE matrix from SuperNEC become the GM samples as described in section 7.3.

The frequencies at which simulations are required are adaptively calculated. The first 2 points (f_1 and f_{end} are known) are calculated such that each point is spaced a factor c from the next. 3 models are then constructed with the samples as follows,

$$\begin{aligned} M_1 &= \{f_1, f_2, f_3\} \\ M_2 &= \{f_2, f_3, f_{end}\} \\ M_3 &= \{f_1, f_2, f_3, f_{end}\} \end{aligned}$$

Using the mismatch error function, the frequency of the next required simulation is calculated. The interaction matrix is recalculated, filled, factored and solved at the new frequency; the new information updates the transfer function matrix, its rank increasing by 1. The next frequency point is calculated and the procedure repeats.

[1] Only the input cards facility is discussed here, as it is most familiar to NEC1-4 users. SuperNEC also has a graphical user interface for selecting simulation settings.

8.3 Simulated Structures

8.3.1 Log Periodic Dipole Array

The broadband nature of the LPDA qualifies it as an interesting antenna platform for evaluation of SuperNEC's TFE module. At a particular frequency within the designed frequency range of 47 to 420 Mhz, adjacent dipoles are resonant with minimal cancellation of fields due to the mechanical phase change of consecutive elements [189, pp.71-74]. These dipoles absorb most of the energy from the transmission line and radiate it efficiently. This region of the structure is known as the *active region*. As the frequency increases, the active region moves from the larger dipole elements to the smaller.

The procedure followed in the design of the LPDA is that of Peixero [190], which considers effects of thickness factor and Z_0 of the transmission line. For a given gain requirement of 8 dBi, with a total antenna length limited to 6 m, the design constants, τ, the *scale* factor and σ, the *space* factor are determined. The scale factor, τ, determines the ratio of both consecutive element lengths and spacing,

$$\tau = \frac{L_{n+1}}{L_n} = \frac{d_{n+1}}{d_n} \tag{8.3.1}$$

where L_n denotes the length of the nth dipole and d_n the spacing between dipoles number n and $n+1$. The space factor relates element spacing to element length by

$$\sigma = \frac{d_n}{2L_n} \tag{8.3.2}$$

Truncation coefficients K_1 and K_2 determine the lengths of longest and shortest elements:

$$L_1 \geq K_1\lambda_{max} \tag{8.3.3}$$

$$L_N \leq K_2\lambda_{min} \tag{8.3.4}$$

The number of dipoles comprising the LPDA are obtained from

$$N = \frac{1 + \ln(L_1/L_N)}{\ln(1/\tau)} \tag{8.3.5}$$

The list of constants used in this design are given in table 8.1. The input data files used in SuperNEC define the geometry in a cartesian space of the wire-grid model of the actual structure. The wire-grid model of the LPDA is shown in figure 8.1 in top view and in figure 8.2 in perspective view.

Design Constant	Value
scale factor, τ	0.891
space factor, σ	0.1
truncation coefficient, K_1	0.54
truncation coefficient, K_2	0.34
no. of elements, N	23
characteristic impedance, Z_0	65 Ω
length to diameter ratio, L/D	177.0
total length	5.82 m
segmentation frequency, f_{seg}	200 MHz

Table 8.1: LPDA Design Parameters

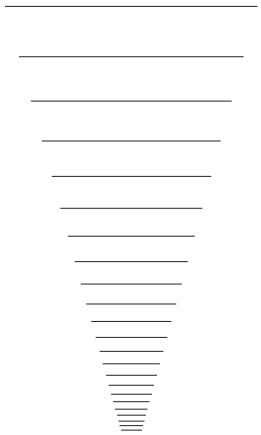

Figure 8.1: Top view of a 200 MHz wire-grid model of an LPDA

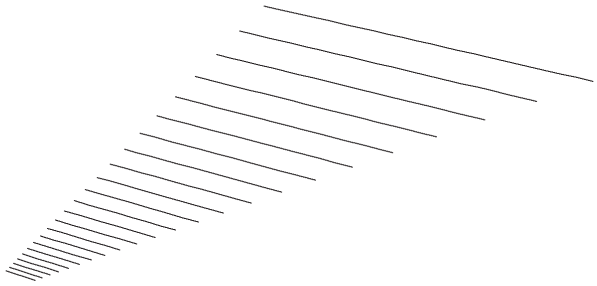

Figure 8.2: Perspective view of a 200 MHz wire-grid model of an LPDA

8.3.2 HF Antenna of an Attack Helicopter

Manual wire grid modelling of an arbitrary structure is clearly laborious; EM simulations (Pty) Ltd market a software package, the *Structure Interpolation and Gridding* (SIG) package [191], which offers a viable solution. Cross-sectional information taken from the engineering drawings of a structure is supplied to SIG, which generates a 3D wire grid model of the entire structure (or specific parts thereof), which is numerically valid at some frequency. SIG has been successfully used in the South African Aerospace industry: more details of its use are given by Givati *et al* [192], where it was utilized for finding radiation patterns of antennas mounted on an attack helicopter. A wire-grid model of the structure at a frequency suitable for extensive TFE testing by SuperNEC was chosen. The model at 25 MHz consisted of 500 segments. Varying segmentation lengths were also used to limit the size of the segmented structure, and hence the representative impedance matrix. Since the segments farthest from the excited elements are subjected to weaker fields, there will be less rapid variation of the induced currents over the lengths of the segments. It therefore becomes feasible to increase segment lengths at large distances (in electrical terms) from the source. Perspective, top and front views of the helicopter wire-grid model designed for 25 MHz are shown in figures 8.3, 8.4 and 8.5, respectively.

Preliminary work has also been done using a much larger wire-grid model of the same structure at a higher frequency, namely 118 MHz. This model, which used the same cross-sectional information as the model described above, was also generated by SIG and is presented in Appendix C.1 for comparative purposes.

8.3.3 Modelling Limitations

1. The size of each model may not exceed 13 in order to prevent ill-conditioning of the transfer function matrix.

2. The frequency range ($f_1 \rightarrow f_{end}$) uses the interaction matrix of a structure with a fixed wire-grid geometry. The posedness of the Fredholm integral equation formulation, with a wire-grid discretization tailored to some frequency, degrades rapidly outside a particular band. Nitch [182] suggests the range

$$f_{model}/5 \leq f \leq f_{model}$$

   to be a valid band of frequencies over which the grid model designed for f_{model} would yield numerically useful results. The segment length at the modelling frequency should be $\lambda_{model}/10$.

3. If the designer does not take cognisance of the limited band of the wire grid model, the

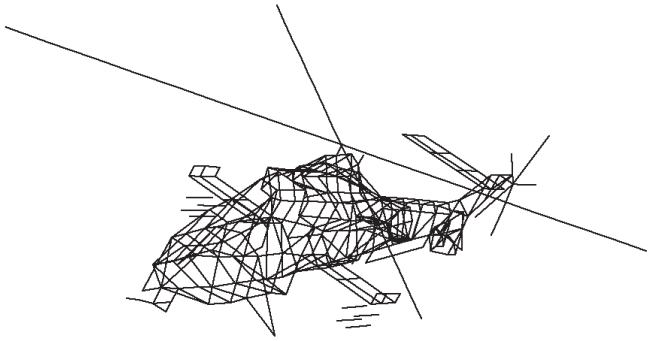

Figure 8.3: Perspective view of an attack helicopter wire-grid model at 25 MHz

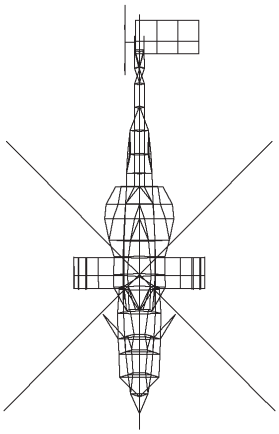

Figure 8.4: Top view of an attack helicopter wire-grid model at 25 MHz

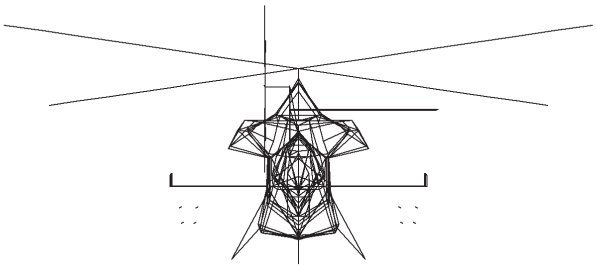

Figure 8.5: Front view of an attack helicopter wire-grid model at 25 MHz

adaptive sampling interaction will still continue, however, the input data received from SuperNEC will be invalid. TFE will optimally approximate invalid data!

8.4 Results

8.4.1 Input Impedance Results

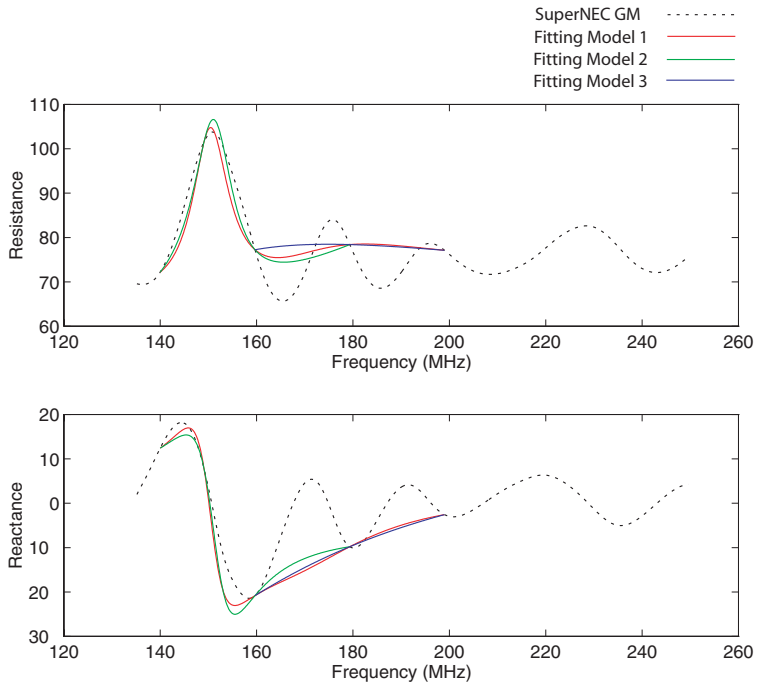

Figure 8.6: A 47 -420 Mhz LPDA, segmented for 200 MHz and simulated over the range 135-250 MHz in SuperNEC. TFE performed over the range 140-200 Mhz: Iteration no. 5.

LPDA

As calculated from the *FR* card of the NEC input file, the start and end frequencies, f_1 and f_{end} are 140 and 200 MHz, respectively. The multiple overlapping model approach of section 8.2 is used. The first simulation performed is that of the starting frequency, 140 MHz: the system impedance matrix is filled, factored and solved, whereupon, the currents distributed over the 201 segments of the LPDA are found. The input impedance of the antenna is calculated using equation (7.1.3). The second iteration occurs at the frequency 200 MHz, again obtained from the *FR* card. Using multiplicative spacing, frequency samples 3 and 4 are calculated to be 159.67 and 179.33 respectively. Following section 7.3, 3 overlapping models are constructed, with a maximum mismatch occurring at $f = 149.1$ MHz. Using this

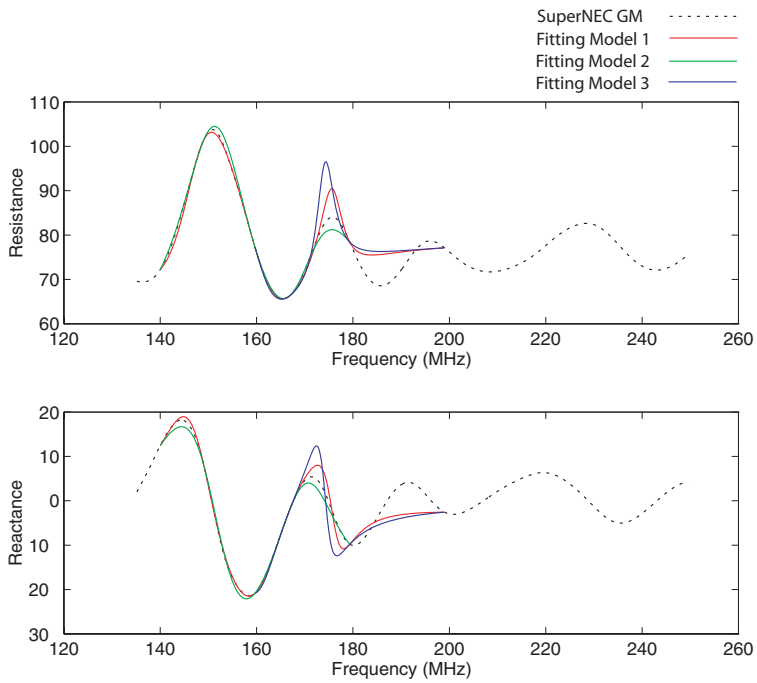

Figure 8.7: A 47 -420 Mhz LPDA, segmented for 200 MHz and simulated over the range 135-250 MHz in SuperNEC. TFE performed over the range 140-200 Mhz: Iteration no. 7.

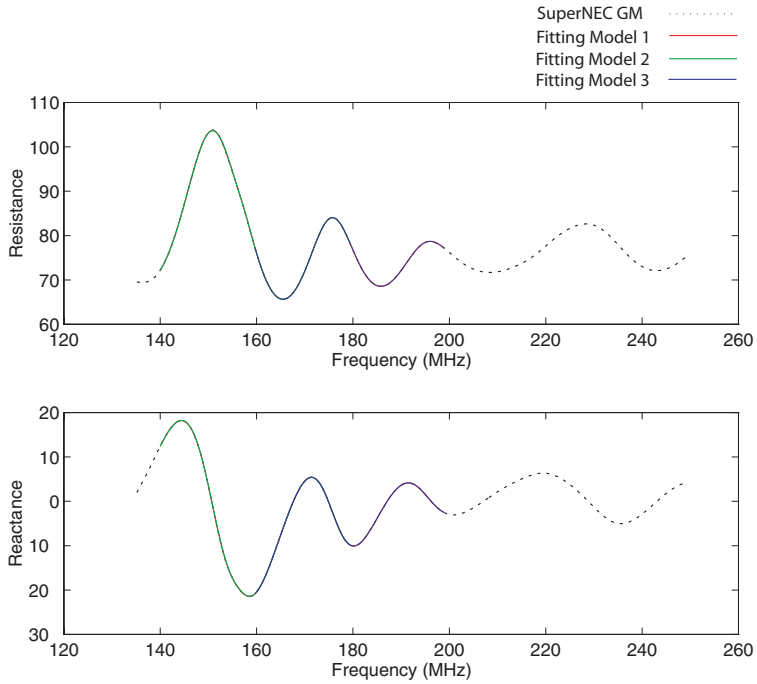

Figure 8.8: A 47 -420 Mhz LPDA, segmented for 200 MHz and simulated over the range 135-250 MHz in SuperNEC. TFE performed over the range 140-200 Mhz: Iteration no. 13.

Iteration No.	Frequency Sample (MHz)
1	140.00
2	200.00
3	159.67
4	179.33
5	149.10
6	166.87
7	165.97
8	174.07
9	188.17
10	193.17
11	143.40
12	177.20
13	155.70

Table 8.2: Iterative sampling placement by TFE within SuperNEC on the LPDA

frequency sample, the results shown in figure 8.6 are achieved, when the TFE models are evaluated at 200 linearly spaced points each. The LPDA characteristic for input impedance was obtained by simulating 670 multiplicatively spaced frequency samples between 135 and 250 MHz.

The accuracy of the models increases with extra samples, as seen in figures 8.7 and 8.8. Figure 8.6 indicates the fit of the TFE models where the error criterion

$$\Delta MM_{ij} \leq 3 \times 10^{-3} \tag{8.4.1}$$

is met for all $i \neq j$.

Table 8.2 details the sample placement for the LPDA adaptive sampling simulation run. The iteration by iteration results are provided in Appendix C.2.

Attack Helicopter

The simulations performed on the HF antenna of the attack helicopter follow the same principles of those of the LPDA. Again, input is provided from the FR card input file, with start and end frequencies, f_1 and f_{end} equal to 10 MHz and 35 MHz, respectively. For each of the first 4 simulation frequencies, the input impedance is calculated by filling, factoring and solving the system impedance matrix. As in section 8.4.1, the third and fourth frequency samples are spaced a constant factor apart, giving $f_3 = 18.36$ MHz and $f_4 = 26.72$ MHz. 3 overlapping models are constructed using the 4 frequency samples (and the input impedance, of course); the mismatch error is evaluated, with the maximum occurring at 21.56 MHz. The mismatch

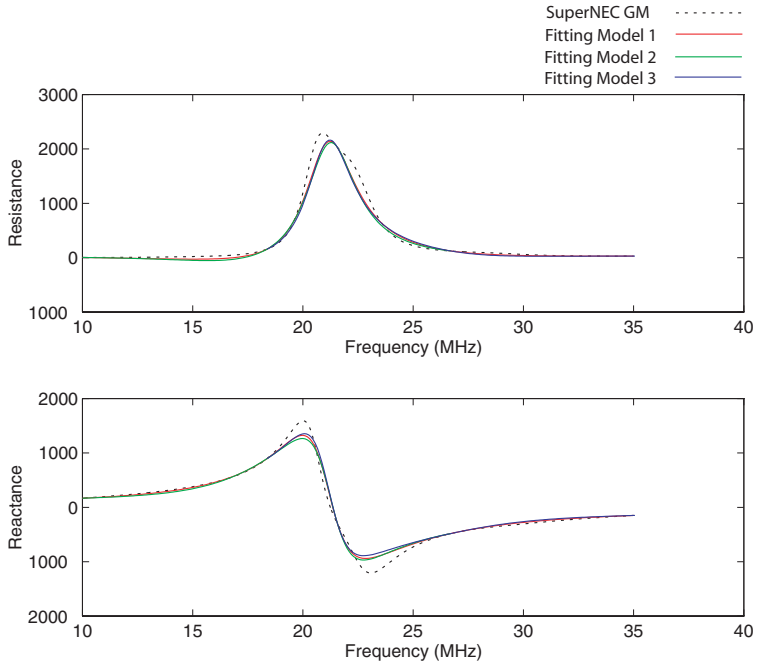

Figure 8.9: An attack helicopter segmented at 25 MHz. TFE applied over the range 10-35 MHz: Iteration no. 5.

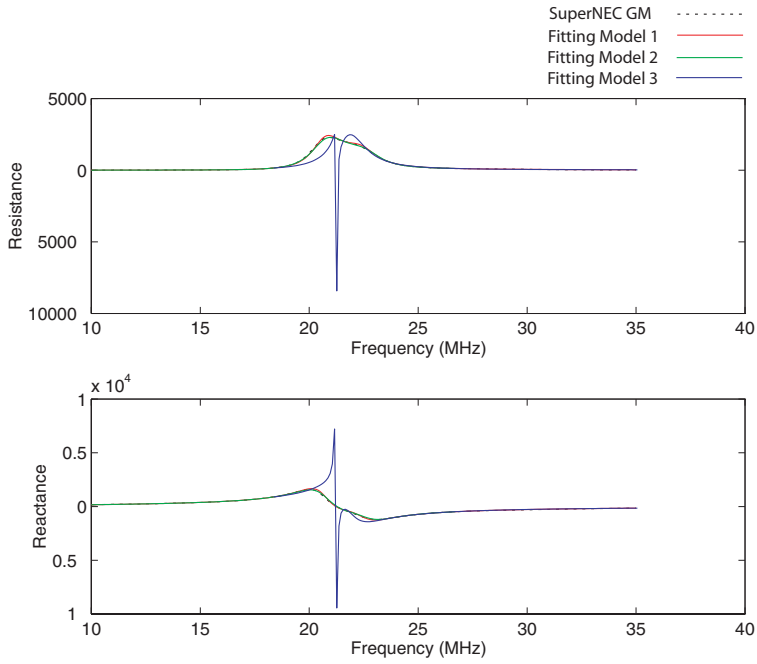

Figure 8.10: An attack helicopter segmented at 25 MHz. TFE applied over the range 10-35 MHz: Iteration no. 7.

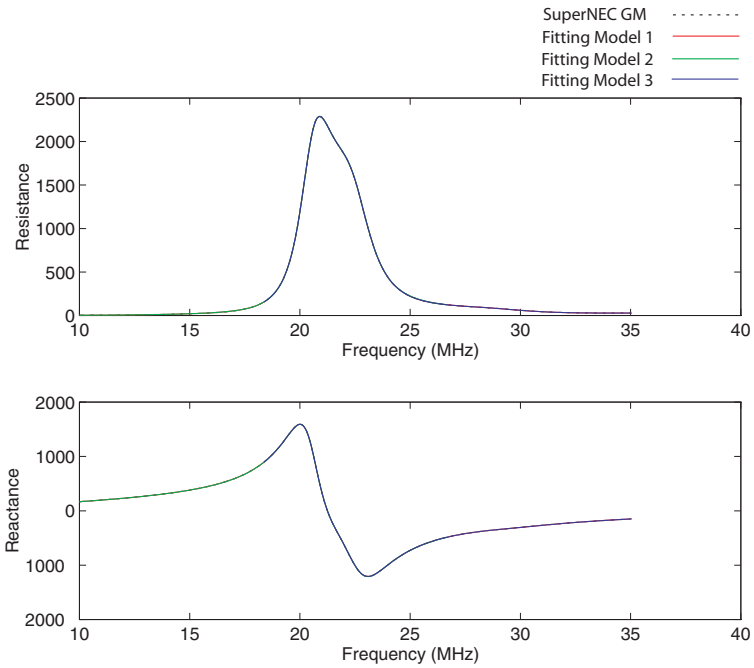

Figure 8.11: An attack helicopter segmented at 25 MHz. TFE applied over the range 10-35 MHz: Iteration no. 13.

Iteration No.	Frequency Sample (MHz)
1	10.00
2	35.00
3	18.36
4	26.72
5	21.56
6	14.30
7	23.80
8	21.26
9	31.86
10	19.86
11	29.86
12	11.50
13	17.80

Table 8.3: Iterative sampling placement by TFE within SuperNEC for the HF antenna on the attack helicopter

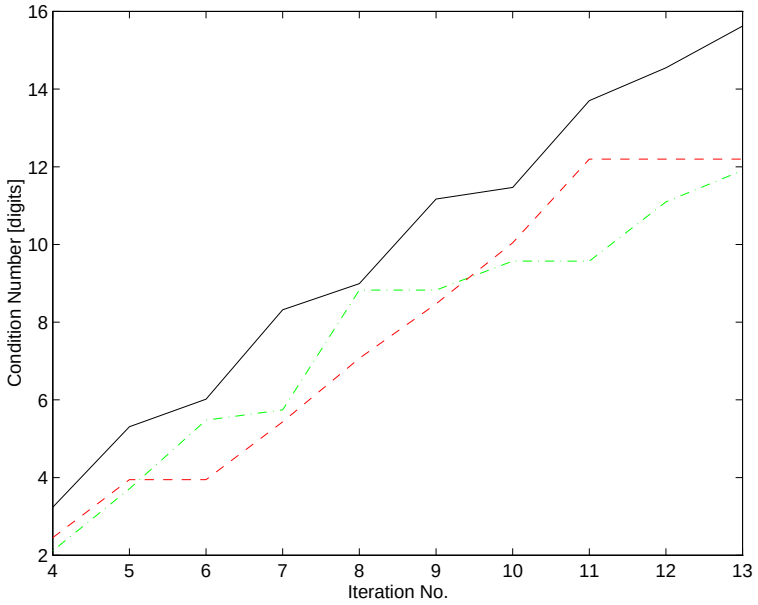

Figure 8.12: The condition number expressed in digits of the helicopter input impedance FMs 1,2 and 3, plotted as a function of iteration number.

error function is also evaluated at 200 linearly spaced points, as in section 8.4.1. The 3 models, evaluated using the same 5 GM samples, are shown in figure 8.9. Note that the reference GM was obtained using 500 multiplicatively spaced samples simulated with SuperNEC. As the number of samples increases, so does the accuracy, with simulations terminated once the mismatch error criterion is met, namely, when

$$\Delta MM_{ij} \leq 3 \times 10^{-3} \tag{8.4.2}$$

is met for all $i \neq j$. As at iterations 7 and 13, the approximation of the input impedance of the HF antenna is shown in figures 8.10 and 8.11, respectively.

The condition number (CN) results of figure 7.2 which represent the increasing CN for increasing numerator and denominator degrees were observed to be $\approx 10^{n+d}$, with n and d defined in (6.3.17). The CN, specified in (7.2.5) and expressed in digits, is given for FMs 1,2 and 3 in figure 8.12. Since FM1 has the most samples its CN will always be larger then that of FMs 2 and 3. The observations of CN variations in figure 7.2 for the simulated resonant system concur with those in figure 8.12. For FM2, the condition number stays the same for iterations $5 \rightarrow 6$ and $11 \rightarrow 13$: this occurs due to the maximum mismatch error being in the overlapping region between FMs 1 and 3 alone. The same argument applies to the constant CN for iterations $8 \rightarrow 9$ and $10 \rightarrow 11$ for FM3.

The resonant peak in figure 8.10 is an artifact of the rational function interpolation model.

A particular set of GM samples creates a number of poles in the complex frequency plane. If the pole location is in the frequency range over which the FMs are being evaluated and there is no zero to provide partial or full cancellation, the result is that the denominator term of (6.3.12) will tend to 0. This tendency which manifests in a spike is clear in figure 8.10. Another common problem inherent to rational function approximation occurs when 2 poles nearly cancel, causing roundoff problems [163].

This addresses Q1 on MBPE in section 2.4.1: **For the approximation shown in figure 2.2, an MBPE implementation by this author [8], using a Prony technique. What caused the spike? Was this due to an ill-conditioned matrix that is an artifact of the Padé method? Or perhaps the MoM discretization of the underlying integral equations being used?**.

8.4.2 Current vs Frequency Results

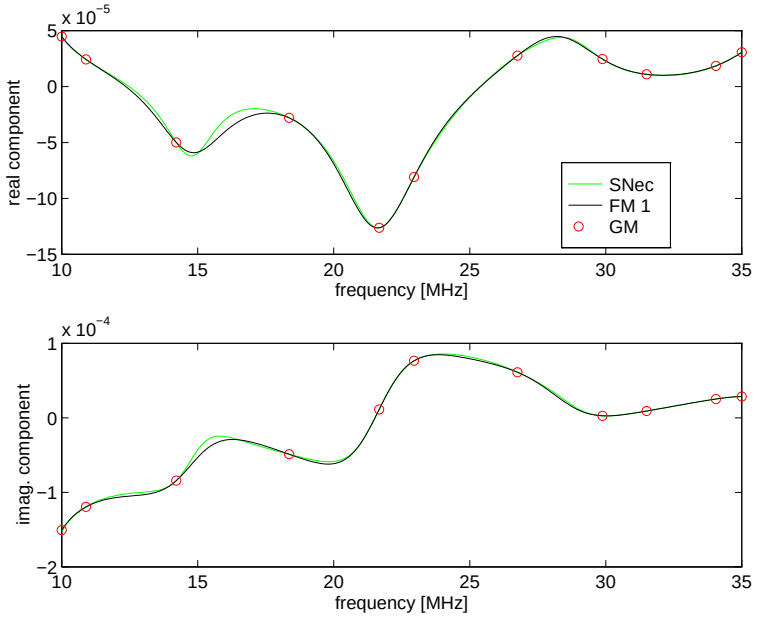

Figure 8.13: Iteration 11: The current at the midpoint of segment 9 as a function of frequency, overlapped with FM1 and the original 11 GM samples.

The $(N+1)$-dimensional application integrated into SuperNEC performs a rational function approximation to the current at the midpoint of each of the N segments in the wire-grid model, as a function of frequency. The frequency range is obviously the same for each of the N segments and is obtained from the FR card, as in section 8.4.1. For each of the N segments, 3 FMs are used with the GM samples being the first 4 multiplicatively spaced samples obtained from SuperNEC in the same fashion as in section 8.4.1. Thus, the initial 4 samples are at

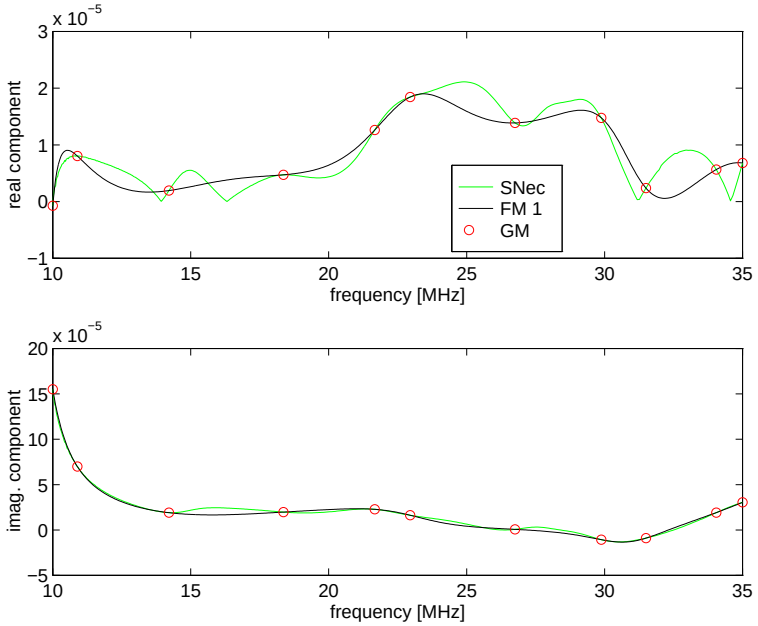

Figure 8.14: Iteration 11: The current at the midpoint of segment 221 as a function of frequency, overlapped with FM1 and the original 11 GM samples.

10.00, 35.00, 18.36 and 26.72 MHz. The mismatch error calculation is performed on a segment by segment basis, with the maximum error frequency and the corresponding segment recorded. The GM at this frequency is requested from SuperNEC and in turn used to construct new FMs. This GM is used in *each* of the overlapping FMs over all N segments. The maximum mismatch errors were found on segments 5, 272, 9, 87, 348, 354, 221, 347 and 176, corresponding to iterations 5 through 13.

This first implementation of a full $(N+1)$-dimensional current estimation tool has one immediate flaw, namely, the sample selection and update strategy which is globally applied over all FMs on the structure. An accurate model of a resonance typically requires about 3 samples per resonance, an observation also made by Miller [185], making a global selection and update procedure ineffective for resonances which have relative frequency shifts between segments.

Figures 8.13 and 8.14 show the approximations of the largest fitting models to the real and imaginary components of the current distribution on segments 9 and 221, respectively, as at iteration 11. The largest fitting model corresponds to FM1 in the standard 3 overlapping model strategy. The current at the midpoints of segments 9 and 221 differ significantly in their degree of resonance, allowing illustration of the effect of relative resonance location on overall model convergence. By comparison with the actual currents, it is clear that the sample placement resulting from the mismatch error at ≈ 33 MHz in figure 8.14 will not significantly improve the FMs of figure 8.13, as there is no resonant behaviour in this area. The global

update of FMs on segment 9 with this new GM sample will only degrade the conditioning of the matrix. This example is representative of the typical resonant variations of the current over a structure, as a function of frequency, thus necessitating an advanced optimization technique.

It is clear that there is significant scope for further work in the sample selection and update methodology such that matrix conditioning is not degraded, thereby providing a more robust estimation model.

8.4.3 Computational Effort

The computational effort and computational advantage of the TFE module implemented in SuperNEC are briefly reviewed in this section. As discussed earlier, several matrix solution techniques exist for the solution of the impedance matrix generated within SuperNEC. The complications of the conjugate gradient and preconditioning options available within SuperNEC are not considered in this section; LU decomposition, a well understood and documented approach is the basis.

Assuming an LU-decomposition of an $M \times M$ system impedance matrix, as in SuperNEC, corresponding to an M segment wire-grid model, the computational effort is

$$A_1 M^2 + A_2 M^3 + A_3 M^2 \tag{8.4.3}$$

where A_1, A_2 and A_3 are implementation-specific constants. These constants are not only a function of processor speed, bus speeds and available RAM, but the implementation of the algorithms as well. In the case of LU-decomposition, it is a function of the forward- and back-substitutions used to solve the matrix. Fill operations involve the MoM calculations used to calculate each interaction element, involving the basis functions and numerical integrals over the thin wire kernel on the segment. Processor-specific enhancements are also used to reduce computational effort required for large wire-grid problems. To evaluate the response of this structure to an excitation at F_{snec} different frequencies in SuperNEC, the computational effort is

$$(A_1 M^2 + A_2 M^3 + A_3 M^2) \times F_{snec} \tag{8.4.4}$$

As shown in figure 8.15, the solve time for wire-grid models numbering thousands of segments can be substantial: in the case of a 1.6 GHz Pentium processor, Poynting Software[193] have benchmarked 8000 segment problems to be solved in approximately 3 hours.

Assuming solution of the transfer function matrix with LU-decomposition, the computational

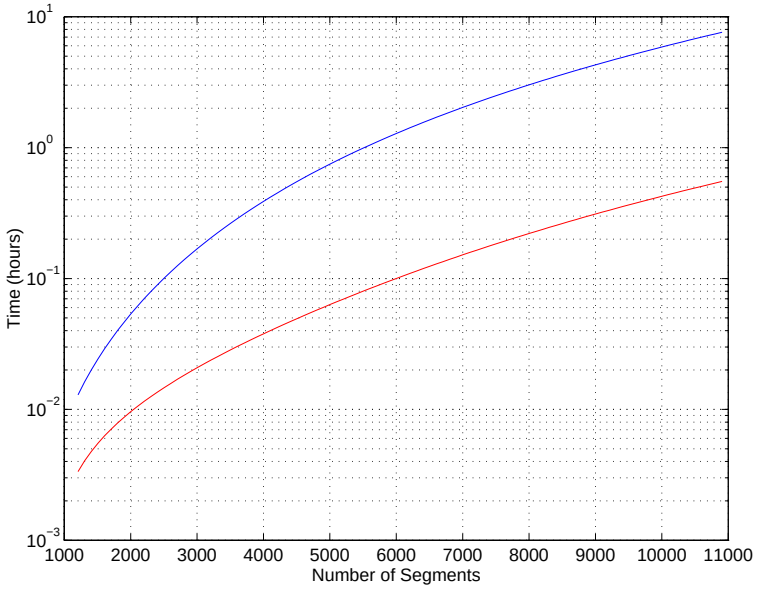

Figure 8.15: Single Frequency Solve Time for SuperNEC on a 1.6 GHz Pentium IV: with standard (blue) and processor-optimized (red) LU decomposition

expense for the fill, factor and solve operations for 1 fitting model is

$$B_1P^2 + B_2P^3 + B_3P^2 \tag{8.4.5}$$

where the matrix is formulated from P GM samples, as in section 6.3 and B_1, B_2 and B_3 are implementation-specific constants. The matrix solvers used to solve the system impedance matrix are also used to solve the transfer function matrix. Therefore, we observe that $B_2 = A_2$ and that $B_3 = A_3$. The fill operations for the transfer function matrix involve simple multiplications, as opposed to the computationally-intensive integrations of the impedance matrix. Though it is typically at least a magnitude of order less, for simplicity sake, assume that $B_1 = A_1$. As part of the adaptive sampling process, to evaluate each rational function at x samples, with y windows spanning the spectrum of interest, an additional overhead is introduced according to

$$C(xy) \tag{8.4.6}$$

where C is an implementation-specific constant.

The computational effort of an adaptive TFE SuperNEC implementation for an M-segment model, involving the solution of the system impedance matrix at F_{snec} frequencies, with y fitting models and $B_i = A_i$ is

$$(A_1M^2 + A_2M^3 + A_3M^2) \times F_{snec} + (B_1P^2 + B_2P^3 + B_3P^2) \times F_{snec} + C(xy) \times F_{snec} \tag{8.4.7}$$

which reduces to

$$[A_1(M^2 + P^2) + A_2(M^3 + P^3) + A_3(M^2 + P^2) + C(xy)] \times F_{snec} \tag{8.4.8}$$

Since $P \leq 13$, the computational effort of the TFE module is insignificant for most impedance matrices, having hundreds or thousands of elements. For very small impedance matrices, the $C(xy)$ term represents a trade-off to be optimized by the designer: more windows and densely spaced mismatch samples accelerate convergence by highlighting anomalies, at the expense of extra computational overhead.

For a single frequency, 500 segment simulation of the Attack Helicopter analyzed in this chapter, the fill, factor and solve times were 10.98, 19.98 and 0.43 seconds [2] , respectively. By substitution in (8.4.3), the implementation specific constants are $A_1 = 4.39 \times 10^{-5}$, $A_2 = 1.6 \times 10^{-7}$ and $A_3 = 1.72 \times 10^{-6}$. In other words, the computational expense in finding the solution to the impedance matrix is:

$$4.39 \times 10^{-5}M^2 + 1.6 \times 10^{-7}M^3 + 1.72 \times 10^{-6}M^2 \tag{8.4.9}$$

For the case of the highest order rational function model, of order 13, and assuming $A_i = B_i$, as discussed earlier, each TFE matrix is solved in some 8 ms; compared with the impedance matrix solve time of some 31 seconds. Clearly, for the large wire-grid models, the ability of the TFE module to effectively describe the wideband response is significant. It must be noted that only solving the impedance matrix at F_{snec} frequencies gives no indication of the response between these frequencies - this is of course one of the motivations for this study starting in the first place!!

8.5 Conclusion

This chapter documents the integration details of the TFE design instrument into SuperNEC and analysis of results for various test cases. The complex frequency domain estimation tool was integrated at 2 different levels, firstly, in the modelling of the 2-dimensional frequency-dependent input impedance and secondly, the modelling of the frequency-dependent current distributed over the N segments of a wire-grid structure. The latter case was noted to be an obvious extension of the 2-dimensional parameter estimation problem, with the same iterative sample selection and update strategy used over all N segments. Section 8.1 briefly addresses these 2 implementations.

The input "cards" frontend used in NEC2, an interface maintained in SuperNEC, provides both structure details and simulation settings: the adaptive sampling strategy, as discussed in

[2] These times are based on a simulation on a Pentium II 266 MHz processor with 64 MB RAM.

section 8.2 uses the FR cards to calculate the frequency range required. The TFE module then tasks SuperNEC to calculate the parameter (current or input impedance) at some frequency. This iterative procedure optimizes the fitting models in their description of the particular response.

The frequency dependence of the structure segmentation for wire-grid models in SuperNEC was explored in section 7.1.1, where emphasis was placed on the ill-posedness of the fredholm integral equation used in the SuperNEC kernel. The actual structures used in the evaluation of the TFE design instrument were the LPDA and attack helicopter HF antenna, as given in section 8.3. Relevant design and modelling details were also given, with a number of limitations noted in section 8.3.3.

The results for both the input impedance and current distributions response modelling were given in section 8.4. For input impedance responses, both the LPDA and the helicopter antenna were described by 3 overlapping fitting models. Given start and end frequencies calculated from the FR input card to SuperNEC, the adaptive sampling TFE module requested frequencies at which SuperNEC was required to perform a simulation, the corresponding results of which enabled the FMs to be refined. Using the global, approximate mismatch errors of chapter 7, iterations were cycled until the error floor of 3×10^{-3} was reached. The corresponding models thus give a continuous wideband description of the input impedance responses of these structures over the specified frequency ranges.

The computational effort associated with the adaptive sampling module was given as a summation of 2 key components, namely, the effort in solving 1 transfer function matrix and the effort in evaluating the mismatch error of several overlapping FMs. The TFE module was shown to give a significant computational advantage to SuperNEC in the modelling of 3-dimensional wire-grid structures, as compared with a standard sampling strategy requiring a low-order interpolation of results.

The current distribution response could also be modeled over *most* of the structure, with certain problems highlighted with respect to resonance locations which are frequency shifted at different segments. Although only a preliminary investigation, the current distribution study showed that a more sophisticated sample selection and update strategy offers significant opportunity for effective $(N + 1)$-dimensional response modelling.

Chapter 9

Conclusions

The conclusions are separated into 3 sections. The first deals with a general overview of the research undertaken, as documented in this dissertation. The novel aspects arising from the work conducted are discussed in section 9.2, followed by a set of recommendations for further study, in section 9.3. The recommendations are broadly classified into theoretical and computational issues and reflect the significant unknowns arising from this research.

9.1 Overview of the Research

Chapter 1 introduced the problem, highlighted its significance and established the overall goal of the work. The summary statement and goal are restated here.

Summary Statement of the Problem: The computational expense required to calculate some electromagnetic response by a complex structure to an excitation over a wide frequency range is prohibitive. Techniques for approximation of such "system responses" have a mathematically weak basis, though have demonstrated utility in providing reduced-order models that can drastically reduce this computational expense.

The Goal of this Theoretical and Computational Work: To develop mathematically justifiable motivating theory, limitations and integration into SuperNEC of a technique for the analytical, continuous, wideband description of the response of an arbitrarily complex conducting body to an electromagnetic excitation. Existing spectral expansions and select parametric models will be critically reviewed as part of the development of this technique, leading to a broad theoretical basis for the solution of our problem. A substantive theory linking spectral expansion methods and integral equation techniques will be explored.

Chapter 2 focussed on heuristic approaches to the problem in general and briefly surveyed

several techniques for reduced-order approximation of a system response or signal. An intuitive development of "expansions" being used in the approximation of a signal or the response of a system was presented. Pulling on a thread of diagonalization and eigenfunction approximations, section 2.2 discussed a guided wave eigen-representation, derived from a source-free consideration of Maxwell's equations. The discrete eigenvalue spectrum was noted to become continuous for a domain end point stretching to infinity, for the guided wave rectangular cavity problem in section 2.3. This chapter presented an extension of these concepts to a general formulation suitable for a description in terms of singularities and natural modes; these would clearly be dependent on the geometry itself.

In section 2.4, we reviewed the existing literature with respect to 4 methodologies or formulations that would be applicable to reduced-order approximations for this electromagnetic problem. In the critical review of section 2.4.1, we explored the contention that Model-Based Parameter Estimation (MBPE) has largely been applied as a mathematical curve-fit, having lost its link to the underlying physics. Relations to EEM, SVD, SEM and a sound mathematical basis are not explored in the literature; they are addressed in this document. Transfer Function Estimation is another abstraction, based on the rational-function approximation used for the spectral domain MBPE. The linear superposition of basis functions, presented in the early sections of the chapter, was evolved into the Eigenmode Expansion Method (EEM) in section 2.4.3. A formal analysis for the exterior scalar scattering problem was presented with questions regarding existence, completeness and orthonormality of bases for the case of nonselfadjoint operators. The Singularity Expansion Method (SEM) was presented in section 2.4.4; it is a formulation defined in terms of natural modes and coupling coefficients which are numerically obtained using the methods in section 6.2.3. The observations of induced currents and scattered fields being described by linear combinations of exponentially damped sinusoidal oscillations, supported by the theoretical representations of canonical problems in terms of natural frequencies, formed the origins of the SEM.

Chapter 3 is largely dedicated to the integral equation theory necessary for the analysis of the radiation and scattering problems for complex structures modeled with perfectly conducting surfaces. Green's methods form the foundation with a logical development from the basic static problem, through the scalar, vector and dyadic inhomogeneous wave equation problems. Section 3.2 reviews derivations of frequency-domain (time harmonic) integral equations in vector and dyadic form specific to the general radiation and scattering problem for a perfectly conducting body; specific reduction of these equations to the magnetic field integral equation (MFIE) and electric field integral equation (EFIE) form used in SuperNEC is given.

In chapter 4, we defined an operator theory framework for EFIE and MFIE equations, study operator properties, the space on which it acts, and its topological and algebraic structure. The focus of the latter part of this thesis is on the EFIE and MFIE, with emphasis on

numerical application of appropriate spectral expansions. This form is later discretized for numerical evaluation. The fundamental theories and formulations that require investigation are the properties of the (integral) operators considered, the spaces in/on which they are applied, and the expansion of points in the function space in terms of its basis elements. The mathematics of function spaces used throughout the document are introduced in section 4.1, starting with Hilbert space. Attention is given to Sobolev spaces in the region and on the boundary of a region, with a motivation for its use tied to power considerations in electromagnetic problems.

In the operator analysis of the EFIE and MFIE, based on a Stratton-Chu representation, we showed in chapter 4 that both the EFIE and MFIE are nonselfadjoint operator equations. The spectral theorems are more complex for this case; we showed that complete sets of basis functions may not be defined, and that the theory of root vectors and Jordan chains needed to be considered. Interior resonance problems and uniqueness of solutions of the MFIE and EFIE formulations were reviewed in section 4.5, in consideration of the well-posedness of the operator equations for the scattering and radiation problems. The behavior of the integral equations under the operation of discretization was also analyzed, as the numerical approximation of the solution of these equations could introduce instabilities. Regularization, reviewed in section 4.6.2, was shown to present a stabilization mechanism by allowing the unknown solution to an unperturbed problem to be approximated by a "regularized solution" of the perturbed problem.

The operator relation between the first and second kind integral operators found in the EFIE and MFIE is key to both the SEM and the Preconditioning of the EFIE. In chapter 5, we considered modification of the first kind ill-posed EFIE by a preconditioning operator to stabilize the equation. The operator relation was shown to enable both the MFIE and EFIE to be written as Hilbert-Schmidt operators and solved using the Fredholm Determinant Theory. These final solutions enable simple series expansions of natural modes at natural frequencies to be written, forming the basis of the SEM. Some of these theoretical origins, presented over 30 years ago are tightly coupled to modern techniques presented today.

For the EFIE and MFIE compact operators, the Fredholm Alternative presents two solution paths. The first, for the resolvent set, where λ is not an eigenvalue, was shown to yield a solution through the SEM. The integral equations were first modified using the preconditioning operator discussed earlier. This enabled the Fredholm Determinant Theory to be applied in calculating the resolvent. The second solution path, with nontrivial solutions to the homogeneous first and second kind equations, was used to analyze the Eigenmode Expansion Method and Singular Function Expansion Method. The EEM, requiring selfadjoint operators to be valid, can be replaced by the SFM, which uses singular function expansions, based on the Method of Schmidt, to calculate an expansion valid for nonselfadjoint operators. However,

using the preconditioning operator again, we showed that the integral equations could be written in a Hermitian form, allowing the EEM to be used. The SFM technique is therefore not required.

In chapter 6, a generic Method of Moment technique in P basis functions was used to reduce the first kind z-directed EFIE to matrix form. For the SuperNEC implementation, using a sine-cosine-constant basis, current and charge boundary conditions were used to reduce the current term to a single unknown, leading to the system impedance matrix. The function spaces necessary to describe the tangential field components on a surface enclosing a region were reviewed: the Sobolev Trace theorem was used to demonstrate that field components in the Sobolev space $H^1(D_+)^3$, for the 3-dimensional case, were projected onto the surface S, in space $H^{1/2}(S)^3$, a fractional order Sobolev space. Well-posedness of the EFIE forms was proven for the exact form of the z-directed Pocklington equation. The reduced, thin-wire kernel, in contrast, is known to be ill-posed. Recasting a well-posed exact form or applying a Tikhonov or MAR method to avoid ill-posedness of the integral equation was shown to be impractical. For these cases, the SuperNEC software core could require some "reconstruction" of the fill implementations. The discretization technique used by default in SuperNEC, based on segmentation criteria, was determined to be sufficient, and recognized to be a "control of dimensionality" regularization method.

The Fredholm Determinant Theory was shown to justify the pole-residue summation form being used for the current term required in the system impedance matrix equation. It clearly follows that a Singularity Expansion Method (SEM) approach for resolvent expansion can be used for a wideband description of the current distribution over a structure. Other spectral expansions derived earlier, including EEM and SFM/SVE were eliminated as viable candidates for integration into SuperNEC, even though their mathematical and theoretical foundations were validated.

Recognize that MBPE can also be viewed as an abstract tool for calculating impulse responses, or transfer functions, depending on the domain of application. The abstract MBPE method is revisited in section 6.3.3. The link to SEM and the underlying physics of the scattering and radiation problem are reviewed. Many of the questions asked in the critical review of MBPE in chapter 2 were answered. We can conclude that the rational function approach derived through the SEM from Maxwell's equations, by way of Stratton-Chu integral equations is valid.

The Fredholm determinant theory is fundamental in arriving at these conclusions, and requires analysis of the integral operators, noting that a Hilbert-Schmidt kernel is required for this theory to be used. Preconditioning is therefore necessary to stabilize the nonselfadjoint integral operators.

The Frequency Domain Prony Method (FDPM) is an abstraction of the SEM where transient data is used to solve for the unknown residues and pole locations of an excited structure. Section 6.3 considers this particular abstraction which uses frequency independent coupling coefficients in the SEM formulation. The FDPM does not require explicit calculation of the natural mode or coupling vectors which are needed for the SEM representation of some electromagnetic field quantity. By incorporating these vectors into a general residue matrix, and limiting the entire function contributions to a constant or simple zero, the frequency domain representation of Prony's method follows. For this investigation, the singularities in the complex frequency domain were constrained to be simple poles. A homogeneous representation of the EFIE formulating equation, in matrix form, gives the general set of simultaneous equations used for the FDPM.

A broadband modelling rationale required several extensions to the basic concept of the FDPM, or MBPE in its spectral domain form, the resulting strategy being referred to as the Transfer Function Estimation (TFE) module. An arbitrarily wide frequency band admitting numerous resonances was one of several problems that could not be addressed by the standard FDPM. Chapter 7 was dedicated to issues central to a wideband estimation strategy, a few of which need to be mentioned again.

The condition number of the transfer matrix typically grows as a function of $\approx 10^{n+d}$ with an increasing number of sample points over the corresponding fitting model. The increasingly ill-conditioned matrix reduces the accuracy of both the data and model fits (c.f. section 7.1.2). Based on observations of these parameters for a simulated resonant system, the maximum number of samples used to construct the rational function was limited to 13; the discretization of the ill-posed EFIE is the cause of the associated high condition number. The TFE module was shown to give a significant computational advantage to SuperNEC in the modelling of 3-dimensional wire-grid structures, as compared with a standard sampling strategy requiring a low-order interpolation of results.

Section 7.3 discussed an adaptive sampling method applied within the TFE module: it utilizes the frequency domain Prony estimator, which imposes no restrictions on equispaced samples. An approximate, global error criterion for multiple models with overlapping frequency bands locates the frequencies at which the mismatch between different fitting models is a maximum. Subsequent frequency samples are thus placed in an intelligent, optimizing fashion. The primary sources of error for adaptive sampling are insufficient sample spacing and oversampling near a discontinuity. The resulting ill-conditioned transfer matrices give meaningless solutions.

Chapter 8 was dedicated to the integration of the TFE module into SuperNEC, the wire-grid structures used for its validation and the results achieved. Two levels of implementations were integrated, namely for modelling the input impedance and current distribution of an

arbitrary radiating or scattering structure. The TFE module iteratively tasks SuperNEC to perform simulation for determining suitable samples for constructing FMs. In the limit as the error floor is reached, the resulting FMs give an accurate wideband description of the input impedance or current distributed over a structure. The preliminary investigation into effective sample search and update strategies have indicated the scope for further research into general $(N+1)$-dimensional response modelling.

The computational effort associated with the adaptive sampling module was given as a summation of 2 key components, namely, the effort in solving 1 transfer function matrix and the effort in evaluating the mismatch error of several overlapping FMs. The TFE module was shown to give a significant computational advantage to SuperNEC in the modelling of 3-dimensional wire-grid structures, as compared with a standard sampling strategy requiring a low-order interpolation of results. The object-oriented SuperNEC, enhanced by the integration of the TFE module, constitutes a powerful design tool for the wideband modelling of electromagnetic responses. The most stable algorithm, namely that of input impedance modelling, provides the design engineer with 1 or several rational function models which specify the input impedance of the structure over the required frequency range to an accuracy corresponding to a chosen error floor. The current distribution can also be obtained although the iterations to reach the error floor may be excessive due to limitations of the present $N+1$-dimensional adaptive sampling algorithm.

9.2 Novel Aspects of the Work

An object-oriented implementation of adaptive Transfer Function Estimation (TFE) has been designed, tested and integrated into a *de facto* electromagnetics code, SuperNEC. TFE can be applied to the input impedance of some radiating or scattering element, yielding an analytical, continuous representation over a spectrum of frequencies. A prototype N segment equivalent is suitable for performing a segment by segment application of TFE to the currents distributed on an entire structure. Given this wideband, analytical approximation of the currents on a wire-grid model, all radiation and scattering parameters can be described over a wide frequency band. The use of SuperNEC as a design tool has been considerably enhanced through the integration of the TFE module. The description of some electromagnetic observable over a spectrum of frequencies is now fully automated with the adaptive, optimizing algorithms in the TFE module. Furthermore, the iterative sample placement enables a meaningful description to be found with a significant decrease in simulation time.

This thesis has several facets interwoven through the 9 chapters; these research focal points represent key contributions to the field. In addressing the problem defined in our Summary Statement, earlier, we performed a theoretical analysis of spectral representation techniques,

providing mathematically sound foundations, linking theories and ultimately selecting a suitable solution for implementation and evaluation in SuperNEC. Peer-reviewed papers, reports and theses documenting these contributions have been published, with others in the review cycle (see Preface). The significance of this work is in the development and evolution of the following theories and implementations:

1. Application of functional analysis techniques to analyze EFIE and MFIE formulations for scattering and radiation from a complex body, approximated by a wire-grid structure, within an operator theory framework.

2. The relation between other prevalent spectral theory techniques, applied specifically to a Fredholm integral equation formulation suitable for the scattering and radiation problem. Linking disparate topics in electromagnetic theory that have a common theoretical basis; the Singular Value Decomposition (SVD), the Singular Value Expansion (SVE), the Singular Function Method (SFM), Singularity Expansion Method (SEM), the Eigenmode Expansion Method (EEM) and Model-Based Parameter Estimation (MBPE).

3. A justifiable mathematical foundation for electric field and magnetic field integral equations applicable to this problem, addressing ill-posedness and non-uniqueness. Assessment of regularization methods and preconditioners to resolve these issues. Linking a key preconditioner, used in the MEFIE and MCFIE and demonstrating the common theoretical basis between these methods and the SEM and TFE.

4. A "spectral expansion" (reduced order representation) method for solution of inhomogeneous vector wave equations applied to the radiation and scattering problem from a perfectly conducting surface. Integration of a rational function model, based on Prony's method, with optimized numerator and denominator orders, based on the underlying theory of the SEM.

5. Implementation of a reduced-order technique, based on a hybrid integral equation-spectral expansion method that provides a significant reduction in the computational expense for solution.

6. Analysis and implementation of a suitable "spectral expansion method" to provide a solution suitable for seamless integration into the objected-oriented framework of *de facto* EM design software, SuperNEC.

9.3 Future Directions

The envisaged scope for further study has 2 distinct components, namely, the theoretical issues and the computational issues.

9.3.1 Theoretical Component

The Method of Analytical Regularization (MAR) was shown in chapter 4 to convert a first-kind linear operator equation into a second kind equation, by applying a "regularizing" operator and inverting part of the equation. The Identity plus Compact form thus lends itself to the application of the Fredholm theory, shown to be at the foundation of many of these methods. Further work is required in this area.

Fractional Order Sobolev space methods were shown to present solutions to the ill-posed nature of the EFIE. While for certain formulations it was shown that a well-posed representation could be given, when cast in the appropriate fractional order Sobolev space, it could not be practically integrated in SuperNEC. Additional work on this topic is required, as there may be other significant benefits when applied in a different setting, sans the SuperNEC constraint.

9.3.2 Computational Component

This effort will be predominantly concerned with optimization issues.

For this study, the selection of numerator and denominator degrees for the rational function in TFE was limited to diagonal form, with possible inclusion of a constant or a zero non-pole component. Further investigation is required for electromagnetic structures to identify optimization methods best suited to the rational function form of TFE. The adaptive sampling approach is recognized as crude: applying the same error criterion over an N segment grid model introduces a global optimization, where a local approximation would suffice.

Utilizing complex-conjugate pairs to yield a different rational function matrix formulation needs to be implemented and tested within SuperNEC. Since the foundations of TFE are found in SEM, there should be a close correlation between the poles predicted by the 2 methods.

Practical implementation of the EEM and SFM would be interesting for assessing useful criteria for limiting the series length of the eigenfunction-type expansion. While inferior to the SEM approach taken in this document, an analytical approach that produces accurate results to some error measure could be valuable.

The use of Rao-Wilson-Glisson (RWG) basis functions integrated into SuperNEC, with Buffa-Christiansen (BC) bases applied on barycentric meshes would be most interesting. The use of a Calderon preconditioner and barycentric refinements with RWG basis functions could be evolved to a wideband solution based on the TFE spectral expansion method presented in this thesis. This would allow fast convergence of iterative solvers in SuperNEC, while still providing adaptive frequency sampling and wideband function approximation over the

frequency band desired.

Appendix A

Derivations, Identities and Formulae

A.1 Deriving Second Vector-Dyadic Green's Theorem

Using the dyadic identity [194, p.111],

$$\nabla \cdot (\mathbf{R} \times \overline{\mathbf{S}}\ ) = (\nabla \times \mathbf{R}) \cdot \overline{\mathbf{S}} - \mathbf{R} \cdot (\nabla \times \overline{\mathbf{S}}\ ) \tag{A.1.1}$$

If dyadic function $\overline{\mathbf{S}}$ is determined by the cross-product of another dyadic function $\overline{\mathbf{Q}}$, then $\overline{\mathbf{S}} = \nabla \times \overline{\mathbf{Q}}$, and with $\mathbf{R} = \mathbf{P}$,

$$\nabla \cdot (\mathbf{P} \times \nabla \times \overline{\mathbf{Q}}) = (\nabla \times \mathbf{P}).\nabla \times \overline{\mathbf{Q}} - \mathbf{P} \cdot (\nabla \times \nabla \times \overline{\mathbf{Q}}) \tag{A.1.2}$$

Integrating over closed normal (use Kellogg's definitions) region V, and using the Divergence theorem,

$$\int_V \left[(\nabla \times \mathbf{P}) \cdot \nabla \times \overline{\mathbf{Q}} - \mathbf{P} \cdot \nabla \times \nabla \times \overline{\mathbf{Q}}\right] dv = \oint_S \hat{\mathbf{n}} \cdot \left(\mathbf{P} \times \nabla \times \overline{\mathbf{Q}}\right) dS \tag{A.1.3}$$

This is the first vector-dyadic Green's theorem. As was the case with the scalar first and second Green's theorems in section 3.1.2, the second vector-dyadic Green's theorem is defined by inter-changing the order of operations. Substituting $\mathbf{R} = \nabla \times \mathbf{P}$ and $\overline{\mathbf{S}} = \overline{\mathbf{Q}}$ in identity A.1.1

$$\nabla \cdot (\nabla \times \mathbf{P} \times \overline{\mathbf{Q}}) = (\nabla \times \nabla \times \mathbf{P}) \cdot \overline{\mathbf{Q}} - (\nabla \times \mathbf{P}) \cdot (\nabla \times \overline{\mathbf{Q}}) \tag{A.1.4}$$

By adding (A.1.2) and (A.1.4), integrating over the normal region V, and using the Divergence theorem (see section 3.1.2),

$$\int_V \left[(\nabla \times \nabla \times \mathbf{P}) \cdot \overline{\mathbf{Q}} - \mathbf{P} \cdot \nabla \times \nabla \times \overline{\mathbf{Q}}\right] dv = \oint_S \hat{\mathbf{n}} \cdot \left[\mathbf{P} \times (\nabla \times \overline{\mathbf{Q}}) + (\nabla \times \mathbf{P} \times \overline{\mathbf{Q}})\right] dS \tag{A.1.5}$$

A.2 Definitions

Lipschitz Continuity Also Lipschitz domain

Lipschitz continuity is a smoothness criterion that is more strict than regular continuity. Given two metric spaces (X, dX) and (Y, dY), where dX denotes the metric on the set X and dY is the metric on set Y (for example, Y might be the set of real numbers R with the metric $dY(x, y) = |x - y|$, and X might be a subset of R), a function is called Lipschitz continuous if there exists a real constant $K \geq 0$ such that, for all $x_1, x_2 \in X$.

$$|f(x) - f(y)| \leq K\,|x - y| \tag{A.2.1}$$

Note that Hölder continuity is a generalization of Lipschitz continuity. The smallest K is the Lipschitz constant.

Hölder Continuity [94, p. 94]

A real, or complex-valued function f is uniformly Hölder continuous, with Hölder exponent α, if and only if for each x, there are constants M and α with $0 < \alpha \leq 1$ such that

$$|f(x) - f(y)| \leq M\,|x - y|^{\alpha} \tag{A.2.2}$$

for all x, y defined on interval I.

The linear space of all functions defined on I that are uniformly Hölder continuous (with exponent α) and bounded are denoted $C^{0,\alpha}(I)$. The integral modulus of continuity is defined by

$$w'(\delta) = \sup_{|h| \leq \delta} \left(\frac{1}{2T} \int_{\infty}^{\infty} |f(x + h) - f(x)| \right) dx \tag{A.2.3}$$

where

$$w'(x) = w(x) \quad |x| < T$$

The function is integral Hölder continuous if $w'(\delta) \leq M\delta^{\alpha}$.

A.3 Vector Identities

$$\boxed{\mathbf{z_0} \times \nabla \times \mathbf{E} = -\frac{\partial}{\partial z}\mathbf{E} + \nabla E_z} \tag{A.3.1}$$

$$\nabla \times \mathbf{E} = \left(\frac{\partial E_z}{\partial y} - \frac{\partial E_y}{\partial z}\right)\mathbf{x_0} + \left(\frac{\partial E_x}{\partial z} - \frac{\partial E_z}{\partial x}\right)\mathbf{y_0} + \left(\frac{\partial E_y}{\partial x} - \frac{\partial E_x}{\partial y}\right)\mathbf{z_0} \tag{A.3.2}$$

Making the following substitutions,

$$p = \frac{\partial E_z}{\partial y} - \frac{\partial E_y}{\partial z}, \qquad q = \frac{\partial E_x}{\partial z} - \frac{\partial E_z}{\partial x}, \quad \text{and} \quad r = \frac{\partial E_y}{\partial x} - \frac{\partial E_x}{\partial y}$$

$$\mathbf{z_0} \times \nabla \times \mathbf{E} = -q\ \mathbf{x_0} + p\ \mathbf{y_0} + 0\ \mathbf{z_0} \tag{A.3.3}$$

$$= \left(\frac{\partial E_z}{\partial x} - \frac{\partial E_x}{\partial z}\right)\mathbf{x_0} + \left(\frac{\partial E_z}{\partial y} - \frac{\partial E_y}{\partial z}\right)\mathbf{y_0} \tag{A.3.4}$$

By definition the gradient of E_z is

$$\nabla E_z = \frac{\partial E_z}{\partial x}\mathbf{x_0} + \frac{\partial E_z}{\partial y}\mathbf{y_0} + \frac{\partial E_z}{\partial z}\mathbf{z_0} \tag{A.3.5}$$

and the partial derivative of the z-component of the total electric vector field is,

$$\frac{\partial}{\partial z}\mathbf{E} = \frac{\partial E_x}{\partial z}\mathbf{x_0} + \frac{\partial E_y}{\partial z}\mathbf{y_0} + \frac{\partial E_z}{\partial z}\mathbf{z_0} \tag{A.3.6}$$

Therefore,

$$\nabla E_z - \frac{\partial}{\partial z}\mathbf{E} = \left(\frac{\partial E_z}{\partial x} - \frac{\partial E_x}{\partial z}\right)\mathbf{x_0} + \left(\frac{\partial E_z}{\partial y} - \frac{\partial E_y}{\partial z}\right)\mathbf{y_0} \tag{A.3.7}$$

Comparing eqns. (A.3.4) and (A.3.7), it is clear that

$$\mathbf{z_0} \times \nabla \times \mathbf{E} = -\frac{\partial}{\partial z}\mathbf{E} + \nabla E_z \tag{A.3.8}$$

A.4 Hilbert-Schmidt Theory and Operators

The Hilbert-Schmidt theorem can be used to find an explicit solution to the non-homogeneous Fredholm equation of the second kind, with symmetric (self-adjoint) kernel [195, pp. 113-115]. It is also noted that the bilinear (series) formula is valid for all the iterated kernels. The representation of the symmetric kernel i.t.o. an absolutely and uniformly convergent series is given. In moving from the finite dimensional to infinite dimensional case, the bilinear series

becomes more complicated in that an integral term needs to be introduced [86, 195].

Hilbert-Schmidt Kernel/Operator [86, p. 112] If $k(x,y)$ satisfies $\int_a^b \int_a^b k^2(x,y)dxdy < \infty$, the kernel $k(x,y)$ is called a Hilbert-Schmidt kernel. The corresponding integral operator,

$$KF = \int_a^b k(x,y)f(y)dy \tag{A.4.1}$$

is a Hilbert-Schmidt operator

Hanson's definition is more general [80, p. 139]. For integral operator $A : \mathbf{L}^2(\Omega) \to \mathbf{L}^2(\Omega)$,

$$(Ax)(\mathbf{t}) = \int_\Omega k(\mathbf{t},\mathbf{s})x(\mathbf{s})d\Omega \tag{A.4.2}$$

with kernel $k(\mathbf{t},\mathbf{s}) \in \mathbf{L}^2(\Omega \times \Omega)$ and the two-norm

$$\|k\|^2 = \int_\Omega \int_\Omega |k(\mathbf{t},\mathbf{s})|^2 \, d\Omega_t d\Omega_s < \infty \tag{A.4.3}$$

where $\Omega \subset \mathbf{R}^n$ is bounded(see below) with

$$\|A\|^2 \leq \int_\Omega \int_\Omega |k(\mathbf{t},\mathbf{s})|^2 \, d\Omega_t d\Omega_s \tag{A.4.4}$$

Hilbert-Schmidt operators are bounded and compact. They can also be approximated by a sequence of degenerate operators. The Hilbert-Schmidt Theorem, as discussed in Gohberg [196, pp.194-196] provides insight into the relation between the HS integral operator and the spectral theory reviewed in section 4.2.3.

Another useful definition is based on definitions of compact and bounded operators and also their relation to degenerate kernels [86, pp. 111-112].

A.5 Series Expansion of a Complex Function

In the complex z-plane, every analytic function $f(z)$ can be represented by a power series, called the Taylor series of $f(z)$. A singularity of an analytic function $f(z)$ is a point $z = z_0$ at which $f(z)$ ceases to be analytic. A zero is a point $z = z_0$ at which $f(z) = 0$. The Taylor series can not be used to expand a function near a point where a singularity occurs [11]. Isolated singularities of $f(z)$ can be represented using the *Laurent series*,

$$f(z) = \sum_{n=0}^{\infty} a_n (z - z_0)^n + \sum_{n=1}^{\infty} \frac{b_n}{(z - z_0)^n} \tag{A.5.1}$$

defined in the immediate neighborhood of z_0, a region of the form $0 < |z - z_0| < R$. The second term in (A.5.1) is called the *principal part*. If the number of terms in the principal part is finite,

$$\sum_{n=1}^{M} \frac{b_n}{(z - z_0)^n} \tag{A.5.2}$$

the singularity is a *pole*, where n is the order of the pole. For an infinite number of terms, an *essential singularity* occurs at $z = z_0$.

A.6 Inverse Laplace Transform and Integral Inversion

The bilateral Laplace Transform is given by

$$x(t) = \frac{1}{2\pi j} \int_{\sigma - j\infty}^{\sigma + j\infty} X(s) e^{st} ds \tag{A.6.1}$$

The Bromwich contour of integration is a straight line in the s-plane, parallel to the $j\omega$ axis, and determined by the value of σ such that $X(\sigma + j\omega)$ converges. For a rational Laplace Transform, the region of convergence is bounded by poles on the one side and extends to infinity on the other [10]. Zepler [197, pp. 184-210] showed that the integral along the circular part of the contour tends to 0 as $R \to \infty$. It follows directly from Jordan's Lemma [11], [197, pp. 184-210], with conditions $Re\{s\} > 0$, $|X(S)| \to \infty$ as $s \to \infty$ for $\pi/2 \leq arg(s) \leq 3\pi/2$.

Cauchy's Integral Theorem states that

$$\oint_C f(z) dz = 0 \tag{A.6.2}$$

where $f(z)$ is an analytic function over the domain enclosed by path C. This contour integral formula is not valid for singularities inside the contour C. In this case, the function has to be represented with a Laurent series, which converges at all points near $z = z_0$, but not z_0 itself. For a simple pole, *Cauchy's Integral formula* [11] gives

$$\oint_C f(z) dz = 2\pi i b_1 \tag{A.6.3}$$

The coefficient b_1 is known as the *residue* of $f(z)$ at $z = z_0$ and is denoted by

$$b_1 = Res\{f(z)\}|_z = z_0 \tag{A.6.4}$$

Once the residues are known, the contour integral can be evaluated using the *Residue Theorem*,

$$\oint_C f(z)dz = 2\pi i \sum_{j=1}^{k} Res\{f(z)\} \tag{A.6.5}$$

where $f(z)$ is an analytic function inside closed path C, except at a finite number of singularities, $z_1 \dots z_k$.

A.7 Solution by Fredholm Determinant Theory

Considering a simple one-dimensional integral for development of the principles of the Fredholm Determinant Theory. For $y(s), x(s) \in L^2(\Omega)$, the integral equation is

$$x(s) = y(s) + \lambda \int_\Omega K(s,t)\, x(t)\, dt \tag{A.7.1}$$

We look to an interpretation of the theory by starting with a discrete version. Equation (A.7.1) can be approximated by n subdivisions across interval Ω such that $\mathbf{x}$ and $\mathbf{y}$ are n-dimensional vectors and kernel $\mathbf{K}$ an $n \times n$ dimension matrix in $\Omega \times \Omega$.

$$\mathbf{x} = \mathbf{y} + \lambda \delta_n \mathbf{K}\mathbf{x} \tag{A.7.2}$$

has a unique solution if

$$d_n(\lambda) = \det(\mathbf{I} - \lambda \delta_n \mathbf{K}) \neq 0 \tag{A.7.3}$$

where δ_n is the width of the subdivision on Ω. Expanding the polynomial terms, it can be shown that

$$\begin{aligned} d(\lambda) = \lim_{n\to\infty} d_n(\lambda) = 1 - \lambda \int_{\Omega_s} K(s,s)\, ds + \frac{\lambda^2}{2!} \int_{\Omega_t}\int_{\Omega_s} \begin{vmatrix} K(s,s) & K(s,t) \\ K(t,s) & K(t,t) \end{vmatrix} ds\, dt \\ - \frac{\lambda^3}{3!} \int_{\Omega_u}\int_{\Omega_t}\int_{\Omega_s} \begin{vmatrix} K(s,s) & K(s,t) & K(s,u) \\ K(t,s) & K(t,t) & K(t,u) \\ K(u,s) & K(u,t) & K(u,u) \end{vmatrix} ds\, dt\, du + \dots \end{aligned} \tag{A.7.4}$$

If $d_n(\lambda) \neq 0$, the unique solution, consistent with Cramer's theorem is

$$\mathbf{x} = \frac{1}{d_n(\lambda)} \text{ adj } (\mathbf{I} - \lambda \delta_n \mathbf{K})\mathbf{y} \tag{A.7.5}$$

We can derive a similar expression for $D_\lambda(s,t)$. Following the discrete (vector) notation, it

suggests a solution for the limit case as [147, pp.67-68]

$$x(s) = y(s) + \lambda \int_{\Omega_t} H_\lambda(s,t)\, y(t)\, dt = y(s) + \frac{\lambda}{\delta(\lambda)} \int_{\Omega_t} \Delta_\lambda(s,t)\, y(t)\, dt \tag{A.7.6}$$

provided $K(s,t)$ is a Hilbert-Schmidt kernel. If $\delta(\lambda) \neq 0$, λ is a regular value of $K(s,t)$ and the resolvent $H_\lambda(s,t)$ is given by:

$$H_\lambda(s,t) = \frac{\Delta_\lambda(s,t)}{\delta(\lambda)} \tag{A.7.7}$$

By the Fredholm Determinant theory and Carleman's method, we can define the modified Fredholm determinant, $\delta(\lambda)$, and the modified first Fredholm minor of $K(s,t)$, denoted $\Delta_\lambda(s,t)$

$$\delta(\lambda) = \sum_{n=0}^{\infty} \delta_n \lambda^n \tag{A.7.8}$$

$$\Delta_\lambda(s,t) = \sum_{n=0}^{\infty} \Delta_n(s,t) \lambda^n \tag{A.7.9}$$

Smithies [147, pp. 65-105] showed that the series were convergent for all complex λ; it should be noted that $\delta(\lambda)$ and $\Delta_\lambda(s,t)$ are integrals. The recursive determinant and minor terms are given by

$$\delta_n = \frac{(-1)^n}{n!} \int_{\Omega_{u_n}} \cdots \int_{\Omega_{u_1}} \begin{vmatrix} 0 & K(u_1,u_2) & \dots & K(u_1,u_n) \\ K(u_2,u_1) & 0 & \dots & K(u_2,u_n) \\ \dots & \dots & \dots & \dots \\ K(u_n,u_1) & K(u_n,u_2) & \dots & 0 \end{vmatrix} du_1\, du_2\, \dots du_n \tag{A.7.10}$$

and

$$\Delta_n(s,t) = \frac{(-1)^n}{n!} \int_{\Omega_{u_n}} \cdots \int_{\Omega_{u_1}} \begin{vmatrix} K(s,t) & K(s,u_1) & \dots & K(s,u_n) \\ K(u_1,t) & 0 & \dots & K(u_1,u_n) \\ \dots & \dots & \dots & \dots \\ K(u_n,t) & K(u_n,u_1) & \dots & 0 \end{vmatrix} du_1\, du_2\, \dots du_n \tag{A.7.11}$$

Another view of the same recurrent minor and determinant is based on the use of the trace of the kernel. Let $\sigma_n = \tau(K^n), n \geq 2$, denote the trace of kernel K^n, where $\tau(K^n) = \int K^n(t,t)\, dt$. For initial iterates $\delta_0 = 1, \Delta_0 = K$, with $n \geq 1$, and K a Hilbert-Schmidt

operator, define [147, pp.94-95]

$$\delta_n = \frac{(-1)^n}{n!} \begin{vmatrix} 0 & n-1 & 0 & \dots & 0 & 0 & 0 \\ \sigma_2 & 0 & n-2 & \dots & 0 & 0 & 0 \\ \sigma_3 & \sigma_2 & 0 & \dots & 0 & 0 & 0 \\ \dots & \dots & \dots & \dots & \dots & \dots & \dots \\ \sigma_{n-1} & \sigma_{n-2} & \sigma_{n-3} & \dots & \sigma_2 & 0 & 1 \\ \sigma_n & \sigma_{n-1} & \sigma_{n-2} & \dots & \sigma_3 & \sigma_2 & 0 \end{vmatrix} \tag{A.7.12}$$

and

$$\Delta_n = \frac{(-1)^n}{n!} \begin{vmatrix} K & n & 0 & 0 & \dots & 0 & 0 & 0 \\ K^2 & 0 & n-1 & 0 & \dots & 0 & 0 & 0 \\ K^3 & \sigma_2 & 0 & n-2 & \dots & 0 & 0 & 0 \\ \dots & \dots & \dots & \dots & \dots & \dots & \dots & \dots \\ K^n & \sigma_{n-1} & \sigma_{n-2} & \sigma_{n-3} & \dots & \sigma_2 & 0 & 1 \\ K^{n+1} & \sigma_n & \sigma_{n-1} & \sigma_{n-2} & \dots & \sigma_3 & \sigma_2 & 0 \end{vmatrix} \tag{A.7.13}$$

The recursive Fredholm determinant theory is key to the solution of the field integral equations in this document and is applied extensively in chapters 4 and 3.

Appendix B

Spectral Derivations and Properties

B.1 Green's Functions and Spectral Representation

This section explores some of the relations between the Green's functions and the spectral representation of the operator L. In essence, this theory bridges the two approaches. The key is that the contour integral of the Green's function in the complex λ plane is related to the delta forcing function. This is known as the spectral representation of the delta function for the operator L, with given boundary conditions.

Since the eigenfunctions span the space, every function in the space can be represented by this basis, including the Green's function. A linear combination of the eigenfunctions, $e_i(\mathbf{r})$, scaled with modal coefficients $g_i(\mathbf{r}';\lambda)$ follows

$$g(\mathbf{r},\mathbf{r}';\lambda) = \sum_i g_i(\mathbf{r}';\lambda)e_i(\mathbf{r}) \quad \text{for } \mathbf{r}_1 < \mathbf{r},\mathbf{r}' < \mathbf{r}_2 \tag{B.1.1}$$

where the modal coefficients are

$$g_i(\mathbf{r}';\lambda) = \int_{\mathbf{r}_1}^{\mathbf{r}_2} w(\xi)e_i^*(\xi)g(\xi,\mathbf{r}';\lambda)d\xi \tag{B.1.2}$$

The modal coefficients are calculated using an inner-product relation, to minimize the norm-squared on the space. $w(\xi)$ is used for normalization.

For a delta forcing function;

$$\begin{aligned} g_i(\mathbf{r}';\lambda) &= \int_{\mathbf{r}_1}^{\mathbf{r}_2} w(\xi)e_i^*(\xi)\delta(\xi-\mathbf{r}')d\xi & \text{(B.1.3)} \\ &= w(\mathbf{r}')e_i^*(\mathbf{r}') & \text{(B.1.4)} \end{aligned}$$

Substituting (B.1.4) in (B.1.1) and (B.1.2), gives

$$\frac{\delta(\mathbf{r}-\mathbf{r}')}{w(\mathbf{r}')} = \sum_i e_i^*(\mathbf{r}')e_i(\mathbf{r}) \tag{B.1.5}$$

This general summation is referred to as the *completeness relation* of the eigenfunction set, $\{e_i\}$. If we consider the modal coefficients as described in (B.5.9), the Green's function is given by

$$g(\mathbf{r},\mathbf{r}';\lambda) = \sum_i \frac{\left\langle \frac{\delta(\mathbf{r}-\mathbf{r}')}{w(\mathbf{r})}, e_i(\mathbf{r}) \right\rangle}{\lambda_i - \lambda} e_i(\mathbf{r}) \tag{B.1.6}$$

$$= -\sum_i \frac{e_i(\mathbf{r})e_i^*(\mathbf{r}')}{\lambda - \lambda_i} \tag{B.1.7}$$

This form of the Green's function is known as the *bilinear series* form [198, pp. 497-499]. It expresses the Green's function as a sum for all i of the orthogonal eigenfunctions evaluated at $\mathbf{r}'$, multiplied by the same orthogonal eigenfunction evaluated at $\mathbf{r}$. If both sides are integrated in the complex λ plane, a contour integral in this complex plane results,

$$\oint_R g(x,x';\lambda)d\lambda = -\sum_i e_i(x)e_i^*(x') \oint \frac{d\lambda}{\lambda - \lambda_i} \tag{B.1.8}$$

The singularities occurring in the complex plane at λ_i are on the real axis for a self-adjoint operator L, since the eigenvalues of the eigenproblem are all real. The singularities are assumed to be simple poles for the purpose of this discussion. The residues are hence unity at all $\lambda = \lambda_i$. By expanding the contour path, $R \to \infty$, and in so doing enclosing all singularities in the λ plane, the integral can be evaluated using Cauchy's Residue Theorem (section A.6). Therefore,

$$\oint_{R_\infty} g(\mathbf{r},\mathbf{r}';\lambda)d\lambda = -2\pi i \sum_i e_i(\mathbf{r})e_i^*(\mathbf{r}') \tag{B.1.9}$$

The Spectral Representation of the delta function is given as the contour integral of the Green's function in the complex λ plane, by

$$\frac{-1}{2\pi i} \oint_{R_\infty} g(\mathbf{r},\mathbf{r}';\lambda)d\lambda = \frac{\delta(\mathbf{r}-\mathbf{r}')}{w(\mathbf{r}')} \tag{B.1.10}$$

B.2 Transverse Field Equations - Rectangular Cavity

Building on Maxwell's equations and boundary conditions alone, the fields within a rectangular cavity bound by perfectly conducting walls can be shown to constitute an eigenproblem (for the source-free case). This section presents the detailed derivations of the transverse field

equations suitable for the analysis of the fields within a rectangular cavity. The initial derivations, in B.2.1, include electric and magnetic currents, though in section B.2.2 the source-free case is considered.

This description enables the overall field to be represented as a superposition of modes of the form $\mathbf{\Psi}_\alpha \exp(j\kappa_\alpha z)$. The general wave vector, $\mathbf{\Psi}$, can be refined to either $\mathbf{E}$ or $\mathbf{H}$, as in section B.2.1. The vector electromagnetic field equations can be transferred into a set of scalar differential equations, through representation of the vector fields as transverse eigenfields, forming an orthonormal set of guided waves, propagating in the z-direction. In an isotropically filled waveguide, it will be shown that the eigenfields can be decomposed into E- and H-modes which have either $E_{z\alpha} = 0$ or $H_{z\alpha} = 0$. This forces the transverse eigenfunctions $\mathbf{E}_{t\alpha}$ and $\mathbf{H}_{t\alpha}$ to be mutually perpendicular.

B.2.1 Transverse Field Equations - With Source Excitations

Maxwell's equations are

$$\nabla \times \mathbf{E}(\mathbf{r}) = -\mathbf{M}(\mathbf{r}) - \mu \frac{\partial \mathbf{H}(\mathbf{r})}{\partial t} \tag{B.2.1}$$

$$\nabla \times \mathbf{H}(\mathbf{r}) = \mathbf{J}(\mathbf{r}) + \epsilon \frac{\partial \mathbf{E}(\mathbf{r})}{\partial t} \tag{B.2.2}$$

It follows that the time-harmonic representations of Maxwell's equations are:

$$\nabla \times \mathbf{E}(\mathbf{r}) = -\mathbf{M}(\mathbf{r}) + j\omega\mu\mathbf{H}(\mathbf{r}) \tag{B.2.3}$$

$$\nabla \times \mathbf{H}(\mathbf{r}) = \mathbf{J}(\mathbf{r}) - j\omega\epsilon\mathbf{E}(\mathbf{r}) \tag{B.2.4}$$

This uses an $\exp(-j\omega t)$ dependence as opposed to the phase lead used by Felsen *et al* [13]. Since the walls of the rectangular cavity are perfectly conducting, there are no tangential components of electric field. For a normal $\mathbf{n}$ existing in the same plane as a cross-section through the cavity, the boundary condition can be stated as

$$\mathbf{n} \times \mathbf{E}(\mathbf{r}) = 0 \quad \text{on} \quad S \tag{B.2.5}$$

where S is a curve denoting the boundary walls of the cavity in cross-section.

For this problem, it is suitable to define a general vector $\mathbf{r} = \boldsymbol{\rho} + z\ \mathbf{z_0}$. Let us consider the guided waves traveling through the waveguide as propagating in the direction of unit vector $\mathbf{z_0}$. A representation of the guided waves in terms of transverse modes traveling in the z-direction ($\mathbf{z_0}$) requires that the fields transverse to $\mathbf{z_0}$ have no dependence on components $\mathbf{E}_z$

and $\mathbf{H}_z$. Taking scalar products of both sides of (B.2.3) with $\mathbf{z_0}$:

$$\begin{aligned} \mathbf{z_0} \cdot (\nabla \times \mathbf{E}(\mathbf{r})) &= -\mathbf{z_0} \cdot \mathbf{M}(\mathbf{r}) + j\omega\mu \mathbf{z_0} \cdot \mathbf{H}(\mathbf{r}) && \text{(B.2.6)} \\ &= -M_z + j\omega\mu H_z && \text{(B.2.7)} \end{aligned}$$

since $\mathbf{z_0}$ is the unit vector in the longitudinal direction. Noting that $\nabla = \nabla_t + \mathbf{z_0}\frac{\partial}{\partial z}$ and using the general identity, $(\mathbf{a} \times \mathbf{b}) \cdot \mathbf{c} = -(\mathbf{b} \times \mathbf{c}) \cdot \mathbf{a}$, for 3 vectors $\mathbf{a}, \mathbf{b}$ and $\mathbf{c}$, gives

$$\nabla_t \cdot (\mathbf{z_0} \times \mathbf{E}(\mathbf{r})) = -j\omega\mu H_z + M_z \tag{B.2.8}$$

A similar analysis of using (B.2.4) gives

$$\nabla_t \cdot (\mathbf{H}(\mathbf{r}) \times \mathbf{z_0}) = J_z - j\omega\epsilon E_z \tag{B.2.9}$$

Taking vector products of both sides of (B.2.3),

$$\mathbf{z_0} \times \nabla \times \mathbf{E}(\mathbf{r}) = -\mathbf{z_0} \times \mathbf{M}(\mathbf{r}) + j\omega\mu \left(\mathbf{z_0} \times \mathbf{H}(\mathbf{r})\right) \tag{B.2.10}$$

Introducing transverse gradient operators and a partial derivative in the longitudinal direction, using the vector identity from (A.3.1),

$$\nabla_t E_z - \frac{\partial}{\partial z}\mathbf{E}_t(\mathbf{r}) = -\mathbf{z_0} \times \mathbf{M}_t(\mathbf{r}) + j\omega\mu \left(\mathbf{z_0} \times \mathbf{H}_t(\mathbf{r})\right) \tag{B.2.11}$$

Similarly, from (B.2.4),

$$\nabla_t H_z - \frac{\partial}{\partial z}\mathbf{H}_t(\mathbf{r}) = \mathbf{z_0} \times \mathbf{J}_t(\mathbf{r}) - j\omega\epsilon \left(\mathbf{z_0} \times \mathbf{E}_t(\mathbf{r})\right) \tag{B.2.12}$$

Solving (B.2.9) for E_z,

$$E_z = -\frac{1}{j\omega\epsilon}\nabla_t \cdot (\mathbf{H}_t(\mathbf{r}) \times \mathbf{z_0}) + \frac{J_z}{j\omega\epsilon} \tag{B.2.13}$$

and substituting into (B.2.11),

$$\begin{aligned} -\frac{\partial}{\partial z}\mathbf{E}_t(\mathbf{r}) &= -\mathbf{z_0} \times \mathbf{M}_t(\mathbf{r}) + j\omega\mu(\mathbf{z_0} \times \mathbf{H}_t(\mathbf{r})) - \frac{\nabla_t}{j\omega\epsilon}\left(-\nabla_t \cdot (\mathbf{H}_t(\mathbf{r}) \times \mathbf{z_0}) + J_z\right) && \text{(B.2.14)} \\ &= -\mathbf{z_0} \times \mathbf{M}_t(\mathbf{r}) - \frac{\nabla_t J_z}{j\omega\epsilon} + \left[\frac{\nabla_t\nabla_t}{j\omega\epsilon} - j\omega\mu\right] \cdot (\mathbf{H}_t(\mathbf{r}) \times \mathbf{z_0}) && \text{(B.2.15)} \end{aligned}$$

Therefore,

$$\boxed{\frac{\partial}{\partial z}\mathbf{E}_t(\mathbf{r}) = \mathbf{z_0} \times \mathbf{M}_t(\mathbf{r}) + \frac{\nabla_t J_z}{j\omega\epsilon} + j\omega\mu\left[\frac{\nabla_t\nabla_t}{\omega^2\epsilon\mu} + \mathbf{1}\right] \cdot (\mathbf{H}_t(\mathbf{r}) \times \mathbf{z_0})} \tag{B.2.16}$$

The identical procedure is used on (B.2.8) and (B.2.12) to give

$$\boxed{\frac{\partial}{\partial z}\mathbf{H}_t(\mathbf{r}) = -\mathbf{z_0} \times \mathbf{J}_t(\mathbf{r}) + \frac{\nabla_t M_z}{j\omega\mu} + j\omega\epsilon\left[\frac{\nabla_t\nabla_t}{\omega^2\mu\epsilon} + \mathbf{1}\right] \cdot (\mathbf{z_0} \times \mathbf{E}_t(\mathbf{r}))} \tag{B.2.17}$$

B.2.2 Transverse Field Equations for the Eigenvalue Problem

The transverse field equations, suitable for representation of the fields in a homogeneously-filled rectangular cross-section cavity, have been derived in section B.2.1. The eigenvalue representation requires the analysis of the source-free case. Recalling (2.2.1) from section 2.2,

$$L\mathbf{\Psi}(\mathbf{r}) = -\mathbf{\Phi}(\mathbf{r}) \tag{B.2.18}$$

as the generalized form of Maxwell's equations for a source-excited, homogeneous, stationary medium, the eigenvalue problem stipulates that $\mathbf{\Phi}(\mathbf{r}) = 0$. Decomposing the operator L into transverse and longitudinal components, the eigenproblem specified in (2.2.8) is

$$K\left(\nabla_t, \frac{\partial}{\partial t}\right)\mathbf{\Psi}(\boldsymbol{\rho}, t) = \kappa_\alpha \Gamma \mathbf{\Psi}(\boldsymbol{\rho}, t) \tag{B.2.19}$$

and noting that the modes characterizing the guided wave are given by a transverse component, propagating uniformly in the z-direction, by

$$\mathbf{\Psi}_\alpha(\mathbf{r}) = \mathbf{\Psi}_\alpha(\boldsymbol{\rho})e^{i\kappa_\alpha z} \tag{B.2.20}$$

the transverse field equations are refined to

$$\kappa_\alpha \mathbf{E}_{t\alpha} = \omega\left[\mu + \frac{1}{\omega^2\epsilon}\nabla_t\nabla_t\right] \cdot (\mathbf{H}_{t\alpha} \times \mathbf{z_0}) \tag{B.2.21}$$

$$\kappa_\alpha \mathbf{H}_{t\alpha} = \omega\left[\epsilon + \frac{1}{\omega^2\mu}\nabla_t\nabla_t\right] \cdot (\mathbf{z_0} \times \mathbf{E}_{t\alpha}) \tag{B.2.22}$$

The subscript, α, indicates that the particular field quantity is a mode. As previously defined, κ_α is the eigenvalue, or mode wavenumber. The longitudinal components are obtained from the transverse eigenmodes; taken from (B.2.8) and (B.2.9),

$$\nabla_t \cdot (\mathbf{z_0} \times \mathbf{E}_{t\alpha}) = -j\omega\mu H_{z\alpha} \tag{B.2.23}$$

$$\nabla_t \cdot (\mathbf{H}_{t\alpha} \times \mathbf{z_0}) = -j\omega\epsilon E_{z\alpha} \tag{B.2.24}$$

The H-mode (TE) calculations

The longitudinal component of the electric field is zero, i.e. $E_{z\alpha} = 0$. Equation (B.2.24) gives

$$\nabla_t \cdot (\mathbf{H}_{t\alpha} \times \mathbf{z_0}) = 0 \tag{B.2.25}$$

Substituting in (B.2.21),

$$\mathbf{E}_{t\alpha} = \frac{\omega\mu}{\kappa_\alpha}(\mathbf{H}_{t\alpha} \times \mathbf{z_0}) \tag{B.2.26}$$

This equation demonstrates the perpendicular relationship between the transverse electric and magnetic field components. Establishing the full effect of the zero longitudinal electric field, (B.2.26) must be substituted into (B.2.22), such that

$$\kappa_\alpha \mathbf{H}_{t\alpha} = \left[\omega\epsilon + \frac{1}{\omega\mu}\nabla_t\nabla_t\right] \cdot (\mathbf{z_0} \times \frac{\omega\mu}{\kappa_\alpha}\mathbf{H}_{t\alpha} \times \mathbf{z_0}) \tag{B.2.27}$$

$$= \left[\omega\epsilon + \frac{1}{\omega\mu}\nabla_t\nabla_t\right] \cdot \left(\frac{\omega\mu}{\kappa_\alpha}\mathbf{H}_{t\alpha}\right) \tag{B.2.28}$$

Therefore,

$$\kappa_\alpha^2 \mathbf{H}_{t\alpha} - \omega^2\epsilon\mu\mathbf{H}_{t\alpha} = \nabla_t\nabla_t \cdot \mathbf{H}_{t\alpha} \tag{B.2.29}$$

If we let $k^2 = \omega^2\epsilon\mu$

$$-(k^2 - \kappa_\alpha^2)\mathbf{H}_{t\alpha} = \nabla_t\nabla_t \cdot \mathbf{H}_{t\alpha} \tag{B.2.30}$$

Setting $\mathbf{h}_\alpha = \mathbf{H}_{t\alpha}$ and normalizing $\mathbf{E}_{t\alpha}$ according to $\mathbf{e}_\alpha = \mathbf{E}_{t\alpha}/Y_\alpha$, then (B.2.26) becomes

$$\mathbf{e}_\alpha = \mathbf{h}_\alpha \times \mathbf{z_0} \tag{B.2.31}$$

where $Y_\alpha = \frac{\omega\mu}{\kappa_\alpha}$. Equation (B.2.29) then becomes

$$\nabla_t\nabla_t \cdot \mathbf{h}_\alpha = -(k^2 - \kappa_\alpha^2)\mathbf{h}_\alpha \tag{B.2.32}$$

Since the divergence of $\mathbf{H}_{t\alpha} \times \mathbf{z_0}$ has already been showed to be zero, it follows that

$$\nabla_t\nabla_t \cdot (\mathbf{H}_{t\alpha} \times \mathbf{z_0}) = 0 \tag{B.2.33}$$

i.e. from (B.2.26),

$$\nabla_t\nabla_t \cdot \left(\frac{\kappa_\alpha}{\omega\mu}\mathbf{E}_{t\alpha}\right) \tag{B.2.34}$$

Therefore,

$$\nabla_t\nabla_t \cdot \mathbf{e}_\alpha = 0 \tag{B.2.35}$$

The E-mode (TM) calculations

For the transverse magnetic mode, the longitudinal component of the magnetic field is zero, $H_{z\alpha} = 0$. Substituting in (B.2.23),

$$\nabla_t \cdot (\mathbf{z_0} \times \mathbf{E}_{t\alpha}) = 0 \tag{B.2.36}$$

In (B.2.22),

$$\kappa_\alpha \mathbf{H}_{t\alpha} = \omega\epsilon(\mathbf{z_0} \times \mathbf{E}_{t\alpha}) \tag{B.2.37}$$

$$\therefore \quad \mathbf{H}_{t\alpha} = \frac{\omega\epsilon}{\kappa_\alpha}(\mathbf{z_0} \times \mathbf{E}_{t\alpha}) \tag{B.2.38}$$

Substituting (B.2.38) into (B.2.21),

$$\kappa_\alpha \mathbf{E}_{t\alpha} = \omega\left[\mu + \frac{1}{\omega^2\epsilon}\right] \cdot \left(\frac{\omega\epsilon}{\kappa_\alpha}(\mathbf{z_0} \times \mathbf{E}_{t\alpha} \times \mathbf{z_0})\right) \tag{B.2.39}$$

$$= \frac{\omega^2\epsilon}{\kappa_\alpha}\left[\mu + \frac{1}{\omega^2\epsilon}\nabla_t\nabla_t\right] \cdot \mathbf{E}_{t\alpha} \tag{B.2.40}$$

Therefore,

$$\nabla_t\nabla_t \cdot \mathbf{E}_{t\alpha} = -(k^2 - \kappa_\alpha^2)\mathbf{E}_{t\alpha} \tag{B.2.41}$$

where $k^2 = \omega^2\mu\epsilon$. If we let $\mathbf{e}_\alpha = \mathbf{E}_{t\alpha}$, then (B.2.41) gives

$$\nabla_t\nabla_t \cdot \mathbf{e}_\alpha = -(k^2 - \kappa_\alpha^2)\mathbf{e}_\alpha \tag{B.2.42}$$

If we substitute

$$Y_\alpha = \frac{\omega\epsilon}{\kappa_\alpha} \quad \text{and} \quad \mathbf{h}_\alpha = \frac{\mathbf{H}_{t\alpha}}{Y_\alpha}$$

then $\mathbf{h}_\alpha = \mathbf{z_0} \times \mathbf{e}_\alpha$. In (B.2.36),

$$\nabla_t \cdot (\mathbf{z_0} \times \mathbf{e}_\alpha) = 0 \tag{B.2.43}$$

$$\therefore \quad \nabla_t\nabla_t \cdot \mathbf{h}_\alpha = 0 \tag{B.2.44}$$

B.2.3 A Complete Field Description

The eigenvalue problem has been specified in terms of eigenvectors, $\mathbf{\Psi}_\alpha$ (c.f. equation (2.2.8)), which represent electric and magnetic fields. A more detailed description in terms of eigenvectors, $\mathbf{e}(\boldsymbol{\rho})$ for the electric field and $\mathbf{h}(\boldsymbol{\rho})$ for the magnetic field, is used in this section. Furthermore, the complete eigenvector set for the homogeneous rectangular cavity comprises

both TM and TE modes. The electric and magnetic fields in the transverse plane, are described by an eigenfunction expansion,

$$\mathbf{E}_t(\boldsymbol{\rho}) = \sum_\alpha V_\alpha^e(z)\mathbf{e}_\alpha^e(\boldsymbol{\rho}) + \sum_\alpha V_\alpha^h(z)\mathbf{e}_\alpha^h(\boldsymbol{\rho}) \tag{B.2.45}$$

$$\mathbf{H}_t(\boldsymbol{\rho}) = \sum_\alpha I_\alpha^e(z)\mathbf{h}_\alpha^e(\boldsymbol{\rho}) + \sum_\alpha I_\alpha^h(z)\mathbf{h}_\alpha^h(\boldsymbol{\rho}) \tag{B.2.46}$$

The superscript, e, denotes that the modal coefficients and eigenfunctions describe the E (TM) modes, while the h refers to the H (TE) modes. It is obvious from this expansion that the TM and TE modes each contain both $\mathbf{e}(\boldsymbol{\rho})$ and $\mathbf{h}(\boldsymbol{\rho})$ mode functions. Similarly,

$$\mathbf{J}_{te}(\boldsymbol{\rho}) = \sum_\alpha i_\alpha^e(z)\mathbf{e}_\alpha^e(\boldsymbol{\rho}) + \sum_\alpha i_\alpha^h(z)\mathbf{e}_\alpha^h(\boldsymbol{\rho}) \tag{B.2.47}$$

$$\mathbf{M}_{te}(\boldsymbol{\rho}) = \sum_\alpha v_\alpha^e(z)\mathbf{h}_\alpha^e(\boldsymbol{\rho}) + \sum_\alpha v_\alpha^h(z)\mathbf{h}_\alpha^h(\boldsymbol{\rho}) \tag{B.2.48}$$

$\mathbf{J}_{te}$ and $\mathbf{M}_{te}$ are referred to as the equivalent transverse electric and magnetic current distributions and are given by

$$\mathbf{J}_{te} = \mathbf{J}_t + \frac{\nabla_t \times \mathbf{M}_z}{j\omega\mu} \tag{B.2.49}$$

$$\mathbf{M}_{te} = \mathbf{M}_t - \frac{\nabla_t \times \mathbf{J}_z}{j\omega\epsilon} \tag{B.2.50}$$

Using the transverse form of Green's Theorem [13], the orthogonality conditions over the cross-sectional domain S are

$$\int\int_S \mathbf{e}_\alpha^e \cdot \mathbf{e}_\beta^{e*} dS = \delta_{\alpha\beta} = \int\int_S \mathbf{e}_\alpha^h \cdot \mathbf{e}_\beta^{h*} dS \tag{B.2.51}$$

$$\text{with} \quad \int\int_S \mathbf{e}_\alpha^e \cdot \mathbf{e}_\alpha^{h*} dS \tag{B.2.52}$$

where the $*$ denotes complex conjugation; normalization to unity is assumed. A similar condition exists for the $\mathbf{h}$ vector mode functions. The mode amplitudes, recognized to have the same form as the Fourier coefficient, are given by

$$V_\alpha(z) = \int\int_S \mathbf{E}_t(\mathbf{r}) \cdot \mathbf{e}_\alpha^*(\boldsymbol{\rho}) dS \qquad I_\alpha(z) = \int\int_S \mathbf{H}_t(\mathbf{r}) \cdot h_\alpha^*(\boldsymbol{\rho}) dS \tag{B.2.53}$$

$$v_\alpha(z) = \int\int_S \mathbf{M}_{te}(\mathbf{r}) \cdot \mathbf{h}_\alpha^*(\boldsymbol{\rho}) dS \qquad i_\alpha(z) = \int\int_S \mathbf{J}_{te}(\mathbf{r}) \cdot \mathbf{e}_\alpha^* dS \tag{B.2.54}$$

where the e and h superscripts have been omitted since the equations apply in both instances.

Solutions of the vector electromagnetic field in the rectangular waveguide are given by the representations in (B.2.45) and (B.2.46). The vector mode functions are evaluated from (B.2.32), (B.2.35), (B.2.42) and (B.2.44) and the modal amplitudes from (B.2.53) and (B.2.54). The "voltage" and "current" coefficients, recognized to be the E- and H-mode modal coefficients, respectively, are found by substituting (B.2.45-B.2.48) into the transverse field equations and simplifying. The first-order transmission line differential equation results [13],

$$-\frac{dV_\alpha}{dz} = j\kappa_\alpha Z_\alpha I_\alpha + v_\alpha \tag{B.2.55}$$

$$-\frac{dI_\alpha}{dz} = j\kappa_\alpha Y_\alpha V_\alpha + i_\alpha \tag{B.2.56}$$

where the modal characteristic impedance, Z_α, characteristic admittance, Y_α and modal propagation constant, κ_α are defined as follows.

For E-modes:

$$Z_\alpha^e = \frac{1}{Y_\alpha^e} = \frac{\kappa_\alpha^e}{\omega\epsilon} \tag{B.2.57}$$

$$\text{where} \quad \kappa_\alpha^e = \sqrt{k^2 - {k_{t\alpha}^e}^2} \tag{B.2.58}$$

For H-Modes:

$$Z_\alpha^h = \frac{1}{Y_\alpha^h} = \frac{\omega\mu}{\kappa_\alpha^h} \tag{B.2.59}$$

$$\text{where} \quad \kappa_\alpha^h = \sqrt{k^2 - {k_{t\alpha}^h}^2} \tag{B.2.60}$$

and $k^2 = \omega^\mu\epsilon$.

B.2.4 Scalarization

Solutions of the vector eigenvalue problems of (B.2.32) and (B.2.42) are facilitated by the introduction of the scalar mode functions, the process being referred to as *scalarization*.

Since any transverse vector can be decomposed into a solenoidal and irrotational component, suitable representations of vector mode sets $\{\mathbf{e}_\alpha^h\}$ and $\{\mathbf{e}_\alpha^e\}$ can be found. Thus, in representing the transverse electric field vector $\mathbf{E}_t$, the irrotational vector set $\{\mathbf{e}_\alpha^e\}$ can be defined in terms of scalar function Φ_α as

$$\mathbf{e}_\alpha^e(\boldsymbol{\rho}) = \frac{\nabla_t \Phi_\alpha(\boldsymbol{\rho})}{k'_{t\alpha}} \tag{B.2.61}$$

The solenoidal mode set, $\mathbf{e}_\alpha^h$ is defined in terms of Ψ_α as

$$\mathbf{e}_\alpha^h = -\frac{\nabla_t \Psi_\alpha(\boldsymbol{\rho})}{k_{t\alpha}} \times \mathbf{z_0} \tag{B.2.62}$$

Similarly,

$$\mathbf{h}_\alpha^e(\boldsymbol{\rho}) = -\mathbf{z_0} \times \frac{\nabla_t \Phi_\alpha(\boldsymbol{\rho})}{k'_{t\alpha}} \tag{B.2.63}$$

$$\text{and} \quad \mathbf{h}_\alpha^h(\boldsymbol{\rho}) = -\frac{\nabla_t \Psi_\alpha(\boldsymbol{\rho})}{k_{t\alpha}} \tag{B.2.64}$$

Using (B.2.32), (B.2.42) and (B.2.61-B.2.64), the scalar mode functions Φ_α and Ψ_α satisfy scalar eigenvalue problems [13]

$$\nabla_t^2 \Phi_\alpha + k_{t\alpha}^2 \Phi_\alpha = 0 \quad \text{in S} \tag{B.2.65}$$

with

$$\Phi_\alpha = 0 \qquad \text{on s if} \qquad k'_{t\alpha} \neq 0 \tag{B.2.66}$$

$$\frac{\partial \Phi_\alpha}{ds} = 0 \qquad \text{on s if} \qquad k'_{t\alpha} = 0 \tag{B.2.67}$$

and

$$\nabla_t^2 \Psi_\alpha + {k'_{t\alpha}}^2 \Psi_\alpha = 0 \quad \text{in S} \tag{B.2.68}$$

B.3 Best Approximation

The eigenfunctions of a self-adjoint operator form an orthogonal basis in $\mathcal{L}_2(a,b)$, such that some function u existing in that same space can be represented as

$$u = \sum_{k=1}^{\infty} \alpha_k u_k \tag{B.3.1}$$

It is necessary, for practical application, to consider a finite approximation to u: consider u_N, a vector in the $\mathcal{L}_2(a,b)$ space given by

$$u_N = \sum_{k=1}^{N} \alpha_k u_k \tag{B.3.2}$$

where u_k is an orthonormal set in $\mathcal{L}_2(a,b)$ for $k = 1, 2, \ldots, N$. The linear manifold given by the sum in eqn. (B.3.2) has different values for different sequences of α_k for $k = 1, 2, \ldots, N$. The best approximation can be determined by the minimum of the norm-squared distance,

as Dudley [16] gives

$$\begin{aligned} ||u - u_N||^2 &= \langle u - u_N, u - u_N \rangle && \text{(B.3.3)} \\ &= \langle u, u \rangle + \langle u_N, u_N \rangle - \langle u_N, u \rangle - \langle u, u_N \rangle && \text{(B.3.4)} \\ &= ||u||^2 + \sum_{k=1}^{N} |\alpha_k|^2 - \sum_{k=1}^{N} \alpha_k \langle \overline{u, u_k} \rangle - \sum_{k=1}^{N} \overline{\alpha_k} \langle u, u_k \rangle && \text{(B.3.5)} \\ &= ||x||^2 + \sum_{k=1}^{N} (\alpha_k - \langle u, u_k \rangle) \overline{(\alpha_k - \langle u, u_k \rangle)} - \sum_{k=1}^{N} |\langle u, u_k \rangle|^2 && \text{(B.3.6)} \end{aligned}$$

Hence the norm-squared is minimized by

$$\alpha_k = \langle u, u_k \rangle \quad \text{for} \quad k = 1, 2, \ldots, N \tag{B.3.7}$$

It can be shown that the error vector is orthogonal to the approximation vector. The error vector is given by

$$\begin{aligned} e_N &= u - u_N && \text{(B.3.8)} \\ &= u - \sum_{k=1}^{N} \langle u, u_k \rangle u_k && \text{(B.3.9)} \end{aligned}$$

Dudley [16] then showed that the inner product of the error vector with any one of the orthonormal vectors, u_k, is zero, since

$$\langle e_N, u_i \rangle = \langle u, u_i \rangle - \sum_{k=1}^{N} \langle u, u_k \rangle \langle u_k \rangle \langle u_i \rangle = 0 \tag{B.3.10}$$

for $i = 1, 2, \ldots, N$. Hence a linear combination of these orthonormal vectors gives

$$\langle e_N, x_N \rangle = 0 \tag{B.3.11}$$

The particular significance of these derivations is that the N-term approximation to the infinite summation of orthonormal vectors satisfies a minimum norm-squared criterion. The general finite eigenfunction expansion of eqn. (B.3.2) is thus formulated such that the weighting of the basis functions is chosen to minimize the error in the truncated expansion. Note that the weighting functions discussed in this Appendix are synonymous with the so-called modal or Fourier coefficients mentioned throughout the document. Similarly, the orthonormal basis functions are the eigenfunctions of some operator L, with associated boundary conditions.

B.4 Properties of Spectral Representations

A number of useful spectral properties for properties are noted below, based on Naylor [89].

- Let T be a compact linear transformation of a Hilbert space H into itself and $\lambda \neq 0$. Then the null space $\mathcal{N}(\lambda I - T)$ is finite dimensional [89, p. 449].
- Let T be a compact linear transformation of a Hilbert space H into itself and $\lambda \neq 0$. Either λ is an eigenvalue of T or λ is in the resolvent set $\rho(T)$. That is, $\lambda \neq 0$ is never in the continuous spectrum $C\sigma(T)$ or the residual spectrum $R\sigma(T)$ [89, p. 449].
- The range of $(\lambda I - T)$ is a closed linear subspace of H for all $\lambda \neq 0$.
- Let T be a compact linear transformation of a Hilbert space H into itself and let $\alpha > 0$. The number of eigenvalues with $|\lambda| \geq \alpha$ is finite [89, p. 452].
- The spectrum of T is countably infinite and $\lambda = 0$ is the only possible point of accumulation. Note that if $\lambda = 0$ is in the resolvent set, H must be finite dimensional. However, $\lambda = 0$ can be in the resolvent set or any part of the spectrum [89, p. 452].

The properties discussed below do not require that operator T necessarily be compact. Since self-adjoint operators are normal, the properties follow for these operators as well.

In the case of an operator on a finite-dimensional Hilbert space; a normal operator in matrix form can be represented in diagonal form. In the case of an operator that is self-adjoint, the entries on the main diagonal are real (properties of self-adjoint operators are reviewed in section 4.4.2).

- If x is an eigenvector of T, associated with eigenvalue λ, then x is an eigenvector of the adjoint of T, T^*, associated with eigenvalue $\overline{\lambda}$. Furthermore, $\mathcal{N}(\lambda I - T) = \mathcal{N}(\overline{\lambda} I - T^*)$, where $\mathcal{N}(\cdot)$ denotes the null-space of the operator.
- Null spaces $\mathcal{N}(\lambda I - T)$ and $\mathcal{N}(\mu I - T)$ are orthogonal whenever $\mu \neq \lambda$.
- The residual spectrum of a normal operator is empty.
- A complex number λ is in the spectrum of normal operator T if and only if there exists a sequence x_n, $\|x_n\| = 1$ for all n, such that $\|(\lambda I - T)x_n\| \to 0$ as $n \to \infty$.
- The spectrum of a self-adjoint operator T is a subset of the real interval $[-\|T\|, +\|T\|]$.

B.5 A Sturm-Liouville Eigenfunction Expansion

Dudley [16] has compiled extensive analyses of electromagnetic problems that have been defined as Sturm-Liouville equations with appropriate boundary conditions. Felsen [13] and Rozzi [17] also show how cavity and guided wave representations can be compiled into a Sturm-Liouville form (see section 2.2). The application of eigenvalues and eigenfunctions to a general linear, second order differential equation of the form

$$a_0(x)\frac{d^2u(x)}{dx^2} + a_1(x)\frac{du}{dx} + a_2(x)u(x) - \lambda u(x) = f(x) \tag{B.5.1}$$

is considered. The Sturm-Liouville equation is obtained through coefficient transformations and is represented in operator form as

$$(L - \lambda)u = f \tag{B.5.2}$$

The Sturm-Liouville functional equation is the operator form of the so-called Sturm-Liouville equation, given by

$$-\frac{1}{w(x)}\frac{d}{dx}\left[p(x)\frac{du}{dx}\right] + q(x)u(x) - \lambda u(x) = f(x) \tag{B.5.3}$$

where in general λ is a complex parameter independent of x. This equation is in fact derived from (B.5.1) with the coefficient transformations

$$q(x) = a_2(x) \tag{B.5.4}$$

$$p(x) = \exp\left[\int^x \frac{a_1(t)}{a_0(t)}dt\right] \tag{B.5.5}$$

$$w(x) = -\frac{p(x)}{a_0(x)} \tag{B.5.6}$$

Clearly, the Sturm-Liouville operator can be identified as

$$L = -\frac{1}{w(x)}\frac{d}{dx}\left[p(x)\frac{d}{dx} + q(x)\right] \tag{B.5.7}$$

The interesting observation about the general Sturm-Liouville functional equation is that it introduces a continuous eigenvalue λ. We therefore bridge the eigenfunction expansion from a discrete spectrum to include a continuous spectrum as well. Analysis of singularities in the complex λ-plane is appropriate for both the general interior and exterior electromagnetic problem. While the general Sturm-Liouville problem is presented in this section, chapter 2

focuses on a detailed exploration of a transverse eigenproblem admitting a discrete and continuous eigenvalue spectrum.

The eigenproblem is a source-free representation, giving

$$Le_i = \lambda_i e_i \quad \text{where L is a self-adjoint operator} \tag{B.5.8}$$

The eigenmodes of a system are the natural resonant fields which occur. They are not a function of the excitation since they are determined from the source-free solution of the field equations. In analogy to the vibrating string example mentioned earlier, the natural modes are the fundamental and subsequent harmonics of oscillation of the spring. Depending on the excitation, a particular combination of these resonant components will exist. These form the basic observation made by Fourier (c.f. section 2.1).

The *Modal* coefficients represent the weightings applied to a particular mode in its representation of a field. By definition, for a self-adjoint operator L, the modal coefficients are determined by the inner product of that eigenmode with the excitation vector, f

$$\langle (L-\lambda)u, e_i \rangle = \langle u, (L-\lambda)e_i \rangle$$

From (B.5.2) and (B.5.8)

$$\begin{aligned} \langle f, e_i \rangle &= \langle u, (\lambda_i - \lambda)e_i \rangle \\ &= (\lambda_i - \lambda)\langle u, e_i \rangle \\ &= \alpha_i(\lambda_i - \lambda) \end{aligned}$$

Therefore, the modal coefficients are related to the eigenmodes (eigenfunctions) and the eigenvalues by

$$\alpha_i = \frac{\langle f, e_i \rangle}{\lambda_i - \lambda} \tag{B.5.9}$$

The solution of the Sturm-Liouville operator equation is hence found by finite summation as,

$$u = \sum_i \frac{\langle f, e_i \rangle}{\lambda_i - \lambda} e_i \tag{B.5.10}$$

This is the eigenfunction representation of the solution u. It contains singularities in the complex λ plane, with the eigenfunctions e_i and the modal coefficient introducing the effect of the input on the excitation of particular modes.

B.6 Time Domain SEM

To obtain the time domain response from the s-plane problem, we use the inverse Laplace Transform with a Bromwich contour of integration [39]

$$\mathbf{i}(t) = \frac{1}{2\pi j}\int_{\sigma_0+j\infty}^{\sigma_0-j\infty} \mathbf{Z}(s)^{-1}\cdot\mathbf{V}(s)e^{st}ds \tag{B.6.1}$$

Using Cramer's theorem, as in (6.2.7),

$$\mathbf{i}(t) = \frac{1}{2\pi j}\int_{\sigma_0+j\infty}^{\sigma_0-j\infty} \frac{\mathbf{A}(s)}{\Delta(s)}\cdot\mathbf{V}(s)e^{st}ds \tag{B.6.2}$$

The representation of the system admittance matrix as a linear combination of poles, weighted by the residues, as in (6.2.9) is

$$\mathbf{i}(t) = \frac{1}{2\pi j}\int_{\sigma_0+j\infty}^{\sigma_0-j\infty} \sum_{\alpha}\frac{\mathbf{R}_\alpha}{s-s_\alpha}\cdot\mathbf{V}(s)e^{st}ds \tag{B.6.3}$$

Since the natural modes and coupling vectors are the same for a symmetric residue matrix,

$$\mathbf{i}(t) = \frac{1}{2\pi j}\int_{\sigma_0+j\infty}^{\sigma_0-j\infty} \sum_{\alpha}\frac{\mathbf{C}_\alpha\cdot\mathbf{C}_\alpha^T}{s-s_\alpha}\cdot\mathbf{V}(s)e^{st}ds \tag{B.6.4}$$

Since multiplication in the complex frequency plane maps to convolution in the time domain, it follows that

$$\mathbf{i}(t) = \frac{1}{2\pi j}\left[\mathcal{L}^{-1}\left\{\sum_{\alpha}\frac{\mathbf{C}_\alpha\cdot\mathbf{C}_\alpha^T}{s-s_\alpha}\right\} * \mathcal{L}^{-1}\left\{\mathbf{V}(s)\right\}\right] \tag{B.6.5}$$

where $*$ denotes the convolution operator and $\mathcal{L}^{-1}\{\cdot\}$ denotes the inverse Laplace Transform of the argument. Denoting

$$\mathbf{v}(t) = \mathcal{L}^{-1}\{\mathbf{V}(s)\} \tag{B.6.6}$$

it follows that the transient response of the structure to the excitation, $\mathbf{v}(t)$, is

$$\mathbf{i}(t) = \left[\sum_{\alpha}\mathbf{C}_\alpha\cdot\mathbf{C}_\alpha^T e^{s_\alpha t}\right] * \mathbf{v}(t) \tag{B.6.7}$$

The impulse response of the system is thus

$$h(t) = \sum_{\alpha}\mathbf{C}_\alpha\cdot\mathbf{C}_\alpha^T e^{s_\alpha t} \tag{B.6.8}$$

These derivations relate directly to the impulse response and transfer functions discussions

in sections 2.1 and 2.1.3.

B.7 Preconditioned SEM Coupling Coefficients

In this Appendix, a generic form of coupling coefficient will be derived that is consistent with the MFIE approach in the literature today. Thereafter, forms specific to the EFIE will be defined, and a new modified coupling coefficient applicable to MEFIE and MMFIE derived.

The starting point for these derivations is the homogeneous equations for the scattering problem, defined in terms of an impedance operator, $\Gamma(\mathbf{r}, \mathbf{r}'; s)$ and natural mode and coupling vectors, $\mathbf{N}_\alpha(\mathbf{r})$ and $\mathbf{C}_\alpha(\mathbf{r})$.

$$\langle \Gamma(\mathbf{r}, \mathbf{r}'; s_\alpha); \mathbf{N}_\alpha(\mathbf{r}') \rangle = 0 \tag{B.7.1}$$

and

$$\langle \mathbf{C}_\alpha(\mathbf{r}); \Gamma(\mathbf{r}, \mathbf{r}'; s_\alpha) \rangle = 0 \tag{B.7.2}$$

where $\Gamma(\mathbf{r}, \mathbf{r}'; s_\alpha)$ is the kernel of the either the EFIE or MFIE, defined in section 5.1.1, evaluated at $s = s_\alpha$. For an excitation $\mathbf{I}(\mathbf{r}, s)$, the inhomogeneous equation is

$$\langle \Gamma(\mathbf{r}, \mathbf{r}'; s); \mathbf{J}(\mathbf{r}', s) \rangle = \mathbf{I}(\mathbf{r}, s) \tag{B.7.3}$$

Expanding this integral equation near $s = s_\alpha$ using the Taylor series formula,

$$\Gamma(\mathbf{r}, \mathbf{r}'; s) = \sum_{m=0}^{\infty} (s - s_\alpha)^m \times \frac{1}{m!} \frac{\partial^m}{\partial s^m} \Gamma(\mathbf{r}, \mathbf{r}'; s) \Big|_{s=s_\alpha} \tag{B.7.4}$$

$$\mathbf{I}(\mathbf{r}, s) = \sum_{m=0}^{\infty} (s - s_\alpha)^m \times \frac{1}{m!} \frac{\partial^m}{\partial s^m} \mathbf{I}(\mathbf{r}, s) \Big|_{s=s_\alpha} \tag{B.7.5}$$

Let

$$\Gamma_{m\alpha}(\mathbf{r}, \mathbf{r}') = \frac{1}{m!} \frac{\partial^m}{\partial s^m} \Gamma(\mathbf{r}, \mathbf{r}'; s) \Big|_{s=s_\alpha} \tag{B.7.6}$$

$$\text{and } \mathbf{I}_{m\alpha}(\mathbf{r}) = \frac{1}{m!} \frac{\partial^m}{\partial s^m} \mathbf{I}(\mathbf{r}, s) \Big|_{s=s_\alpha} \tag{B.7.7}$$

Assuming that there is a singularity at $s = s_\alpha$, corresponding to a natural frequency, a Laurent series expansion is required. The general form, for some $z, z_0 \in \mathbf{C}$ is

$$f(z) = \sum_{n=0}^{\infty} a_n (z - z_0)^n + \sum_{n=1}^{\infty} \frac{b_n}{(z - z_0)^n} \tag{B.7.8}$$

defined in the immediate neighbourhood of z_0, a region of the form $0 < |z - z_0| < R$, where $R \in \mathbf{C}$. Separating the pole in the Mittag-Leffler series expansion at s_α,

$$\mathbf{J}(\mathbf{r}, s) = \frac{\Psi_\alpha(s)\mathbf{N}_\alpha(\mathbf{r})}{(s - s_\alpha)^{m_\alpha}} + \mathbf{J}_\alpha(\mathbf{r}, s) \tag{B.7.9}$$

The second term, $\mathbf{J}_\alpha(\mathbf{r}, s)$, corresponds to the entire function contribution (c.f. eqn (5.1.39)). Using Baum's assumptions of a single pole approximation, $m_\alpha = 1$.

Substituting (B.7.4), (B.7.5) and (B.7.9) into (B.7.3),

$$\left\langle \sum_{m=0}^{\infty} (s - s_\alpha)^m \times \frac{1}{m!} \frac{\partial^m}{\partial s^m} \Gamma(\mathbf{r}, \mathbf{r}'; s) \Big|_{s=s_\alpha} ; \frac{\Psi_\alpha(s)\mathbf{N}_\alpha(\mathbf{r}')}{s - s_\alpha} + \mathbf{J}'(\mathbf{r}, s) \right\rangle \tag{B.7.10}$$
$$= \sum_{m=0}^{\infty} (s - s_\alpha)^m \times \frac{1}{m!} \frac{\partial^m}{\partial s^m} \mathbf{I}(\mathbf{r}, s) \Big|_{s=s_\alpha}$$

Therefore,

$$\left\langle \left[(s - s_\alpha)^0 \Gamma_{0\alpha}(\mathbf{r}, \mathbf{r}') + (s - s_\alpha)\Gamma_{1\alpha}(\mathbf{r}, \mathbf{r}') + \ldots \right] ; \frac{\Psi_\alpha(s)\mathbf{N}_\alpha(\mathbf{r}')}{s - s_\alpha} + \mathbf{J}'(\mathbf{r}, s) \right\rangle \tag{B.7.11}$$
$$= (s - s_\alpha)^0 \mathbf{I}_{0\alpha}(\mathbf{r}) + (s - s_\alpha)\mathbf{I}_{1\alpha}(\mathbf{r}, \mathbf{r}') + \ldots$$

Combining terms corresponding to $(s - s_\alpha)^{-1}$,

$$\left\langle \Gamma_{0\alpha}(\mathbf{r}, \mathbf{r}'); \Psi_\alpha(s)\mathbf{N}_\alpha(\mathbf{r}') \right\rangle = 0 \tag{B.7.12}$$

Combining terms in $(s - s_\alpha)^0$,

$$\langle \Gamma_{1\alpha}(\mathbf{r}, \mathbf{r}'); \Psi_\alpha(s)\mathbf{N}_\alpha(\mathbf{r}') \rangle + \langle \Gamma_{0\alpha}(\mathbf{r}, \mathbf{r}'); \mathbf{J}'(\mathbf{r}', s) \rangle = \mathbf{I}_{0\alpha}(\mathbf{r}) \tag{B.7.13}$$

Left operating by $\mathbf{C}_\alpha(\mathbf{r})$, the second term disappears, since

$$\langle \mathbf{C}_\alpha(\mathbf{r}); \Gamma(\mathbf{r}, \mathbf{r}'; s_\alpha) \rangle = 0 \tag{B.7.14}$$
$$\text{and } \Gamma_{0\alpha}(\mathbf{r}, \mathbf{r}') = \Gamma(\mathbf{r}, \mathbf{r}'; s_\alpha) \tag{B.7.15}$$

Therefore,

$$\Psi_\alpha(s_\alpha) = \frac{\langle \mathbf{C}_\alpha(\mathbf{r}); \mathbf{I}_{0\alpha}(\mathbf{r}) \rangle}{\langle \mathbf{C}_\alpha(\mathbf{r}); \Gamma_{1\alpha}(\mathbf{r}, \mathbf{r}'); \mathbf{N}_\alpha(\mathbf{r}') \rangle} \tag{B.7.16}$$

This defines the coupling coefficient at s_α. Following [199], the coupling coefficient as a function of all s can be calculated using the preceding method, but not performing the Taylor

expansion in (B.7.5). The class 2 coupling coefficient is so defined as

$$\Psi_\alpha(s) = \frac{\langle \mathbf{C}_\alpha(\mathbf{r}); \mathbf{I}(\mathbf{r}, s)\rangle}{\langle \mathbf{C}_\alpha(\mathbf{r}); \Gamma_{1\alpha}(\mathbf{r}, \mathbf{r}'); \mathbf{N}_\alpha(\mathbf{r}')\rangle} \tag{B.7.17}$$

For the MFIE, the natural modes and coupling vectors are $\mathbf{N}^m_\alpha(\mathbf{r})$ and $\mathbf{C}^m_\alpha(\mathbf{r})$ and the class 2 coupling coefficient defined by

$$\Psi^m_\alpha(s) = \frac{\langle \mathbf{C}^m_\alpha(\mathbf{r}); \mathbf{I}(\mathbf{r}, s)\rangle}{\langle \mathbf{C}^m_\alpha(\mathbf{r}); \Gamma^m_{1\alpha}(\mathbf{r}, \mathbf{r}'); \mathbf{N}^m_\alpha(\mathbf{r}')\rangle} \tag{B.7.18}$$

where the denominator term is given by

$$\langle \mathbf{C}^m_\alpha(\mathbf{r}); \Gamma^m_{1\alpha}(\mathbf{r}, \mathbf{r}'); \mathbf{N}^m_\alpha(\mathbf{r}')\rangle = (-4\pi c)^{-1} \int_S \int_S \mathbf{C}^m_\alpha(\mathbf{r}) \left[\mathbf{n}(\mathbf{r}) \times \nabla\{\exp(-s_n R/c)\} \times \mathbf{N}^m_\alpha(\mathbf{r}')\right] \, dS' dS \tag{B.7.19}$$

with $R = |\mathbf{r} - \mathbf{r}'|$ and the numerator

$$\langle \mathbf{C}^m_\alpha(\mathbf{r}); \mathbf{I}(\mathbf{r}, s)\rangle = \int_S \mathbf{C}^m_\alpha(\mathbf{r}) \mathbf{I}(\mathbf{r}, s) \, dS \tag{B.7.20}$$

For the EFIE, the coupling coefficient is

$$\Psi^e_\alpha(s) = \frac{\langle \mathbf{C}^e_\alpha(\mathbf{r}); \mathbf{I}(\mathbf{r}, s)\rangle}{\langle \mathbf{C}^e_\alpha(\mathbf{r}); \Gamma^e_{1\alpha}(\mathbf{r}, \mathbf{r}'); \mathbf{N}^e_\alpha(\mathbf{r}')\rangle} \tag{B.7.21}$$

For $g(\mathbf{r}, \mathbf{r}') = (4\pi R)^{-1} \exp(-sR/c)$, we have $\nabla' g(\mathbf{r}, \mathbf{r}') = g(\mathbf{r}, \mathbf{r}') [s/c + 1/R] \hat{\mathbf{R}}(\mathbf{r}, \mathbf{r}')$ where unit vector $\hat{\mathbf{R}}(\mathbf{r}, \mathbf{r}') = \mathbf{R}(\mathbf{r}, \mathbf{r}')/R$. The denominator term is thus

$$\begin{aligned}\langle \mathbf{C}^e_\alpha(\mathbf{r}); \Gamma^e_{1\alpha}(\mathbf{r}, \mathbf{r}'); \mathbf{N}^e_\alpha(\mathbf{r}')\rangle = s_\alpha \mu \int_S \int_S \Big[& (-4\pi c)^{-1} \exp(-s_\alpha R/c) \, \mathbf{N}^e_\alpha(\mathbf{r}') \\ & + (c^2/s_\alpha^2) g(\mathbf{r}, \mathbf{r}') [s_\alpha/c + 1/R] \, \hat{\mathbf{R}}(\mathbf{r}, \mathbf{r}') \, \nabla'_t \cdot \mathbf{N}^e_\alpha(\mathbf{r}') \Big] \mathbf{C}^e_\alpha(\mathbf{r}) \, dS' dS\end{aligned} \tag{B.7.22}$$

As before, the numerator is

$$\langle \mathbf{C}^e_\alpha(\mathbf{r}); \mathbf{I}(\mathbf{r}, s)\rangle = \int_S \mathbf{C}^e_\alpha(\mathbf{r}) \mathbf{I}(\mathbf{r}, s) \, dS \tag{B.7.23}$$

The common class 2 coupling coefficient representation is

$$\Psi^{e,m}_\alpha(s_\alpha) = \frac{\langle \mathbf{C}^{e,m}_\alpha(\mathbf{r}); \mathbf{I}^{e,m}(\mathbf{r}, s)\rangle}{\langle \mathbf{C}^{e,m}_\alpha(\mathbf{r}); \Gamma^{e,m}_{1_\alpha}(\mathbf{r}, \mathbf{r}'); \mathbf{N}^{e,m}_\alpha(\mathbf{r})\rangle} \tag{B.7.24}$$

Following the same method as earlier, modified coupling coefficients for the MMFIE can be

derived,

$$\langle(-1/4I + K^2); \mathbf{J}\rangle = \langle(-1/2I + K); \mathbf{J}^i\rangle \tag{B.7.25}$$

and the MEFIE

$$\langle(-1/4I + K^2); \mathbf{J}\rangle = \langle T; \mathbf{M}^i\rangle \tag{B.7.26}$$

Let $P(\mathbf{r}, \mathbf{r}'; s) \equiv (-1/4I + K^2)(\mathbf{r}, \mathbf{r}'; s)$ denote the preconditioning operator. Its derivative with respect to s, evaluated at s_α is

$$P_{1\alpha} = \frac{\partial}{\partial s} P(\mathbf{r}, \mathbf{r}'; s)\bigg|_{s=s_\alpha} \tag{B.7.27}$$

The natural modes and coupling vectors are derived from the homogeneous solution of (B.7.25) and (B.7.26) and their adjoints at $s = s_\alpha$. Since the LHS of both of these equations is the same, the natural modes of the MEFIE and MMFIE are equal, denoted $\mathbf{U}_\alpha(\mathbf{s})$. The same applies to the coupling vectors, $\mathbf{V}_\alpha(\mathbf{s})$. Derived in the same manner as earlier in this Appendix, the class 2 modified coupling coefficients for the MMFIE and MEFIE are

$$\Phi^m_\alpha(s) = \frac{\langle \mathbf{U}_\alpha(\mathbf{r}); [-1/2I + K]_\alpha(\mathbf{r}, \mathbf{r}'); \mathbf{J}^i_\alpha(\mathbf{r}, s)\rangle}{\langle \mathbf{U}_\alpha(\mathbf{r}); P_{1\alpha}(\mathbf{r}, \mathbf{r}'); \mathbf{V}_\alpha(\mathbf{r}')\rangle} \tag{B.7.28}$$

$$\Phi^e_\alpha(s) = \frac{\langle \mathbf{U}_\alpha(\mathbf{r}); T_\alpha(\mathbf{r}, \mathbf{r}'); \mathbf{M}^i_\alpha(\mathbf{r}, s)\rangle}{\langle \mathbf{U}_\alpha(\mathbf{r}); P_{1\alpha}(\mathbf{r}, \mathbf{r}'); \mathbf{V}_\alpha(\mathbf{r}')\rangle} \tag{B.7.29}$$

where $[-1/2I + K]_\alpha(\mathbf{r}, \mathbf{r}') \equiv [-1/2I + K](\mathbf{r}, \mathbf{r}'; s)\big|_{s=s_\alpha}$ and $T_\alpha(\mathbf{r}, \mathbf{r}') = T(\mathbf{r}, \mathbf{r}'; s)\big|_{s=s_\alpha}$. For the class 2 coefficients in (5.1.40), the frequency dependence of the $\Psi^{e,m}_\alpha(s)$ comes from $\mathbf{I}^{e,m}(\mathbf{r}, s)$. Discussion of the application of these modified coupling coefficients is presented in section 5.1.4.

B.8 Characteristic Modes

Baum [39] distinguishes between eigenmodes in the EEM (Eigenmode Expansion Method) and the methods of characteristic modes defined by Garbacz [176], Harrington *et al* [200, 201]. The latter frequency domain model representation contains weighted eigenvalues.

In the characteristic mode derivations of Harrington and Mautz [200], [201], the characteristic currents, $\mathbf{I}_n$, are determined from the eigenvalue equation.

$$Z(\mathbf{I}_n) = v_n M(\mathbf{I}_n) \tag{B.8.1}$$

where v_n are the eigenvalues, $\mathbf{I}_n$ the eigenfunctions, M a weight operator and

$$Z(\mathbf{I}) = [L(\mathbf{I})]_{tan}$$

denotes the symmetric operator for the current $\mathbf{I}$ on the surface of some body S. This is obtained from the operator equation [3, pp. 2-15]

$$\left[L(\mathbf{I}) - \mathbf{E}^i\right]_{tan} = 0 \tag{B.8.2}$$

with

$$L \quad = \quad j\omega\mathbf{A}(\mathbf{I}) + \nabla\Phi(\mathbf{I})$$

Using a MoM solution, we may obtain a modal solution for the current $\mathbf{I}$ on S

$$\mathbf{I} = \sum_n \alpha_n \mathbf{I}_n \tag{B.8.3}$$

Performing an inner product with each term in (B.8.2) with I_m;

$$\sum_n \alpha_n < \mathbf{I}_m, Z\mathbf{I}_n > - < \mathbf{I}_m, \mathbf{E}_i >= 0 \quad \text{for} \quad m = 1, 2, \ldots, \tag{B.8.4}$$

Impedance operator Z can be defined in terms of two real hermitian operators, X and R, such that:

$$R = \frac{1}{2}(Z + Z^*) \tag{B.8.5}$$

and

$$X = \frac{1}{2j}(Z - Z^*) \tag{B.8.6}$$

The weight operator M is chosen such that $M = R$ and $Z = R + jX$. It therefore follows that, using orthogonality,

$$\alpha_n(1 + j\lambda_n) =< \mathbf{I}_n, \mathbf{E}^i > \tag{B.8.7}$$

Therefore,

$$\mathbf{I} = \sum_n \frac{< \mathbf{I}_n, \mathbf{E}^i >}{1 + j\lambda_n}\mathbf{I}_n \tag{B.8.8}$$

There is a relationship between the eigenvalue problem and the weighted eigenvalue problem, which is utilized for computational purposes. Here, the weighted eigenvalue problem is typically reduced to a symmetric unweighted problem and the perturbation (weighting) matrix is positive-definite [202, pp. 34-38]. Calculation of modes and analysis of their convergence was given by Harrington and Mautz [201] for several canonical problems: a cone-sphere, disk

and a wire arrow.

Appendix C

Wire Grid Models and Results

C.1 Additional Helicopter Wired-Grid Models

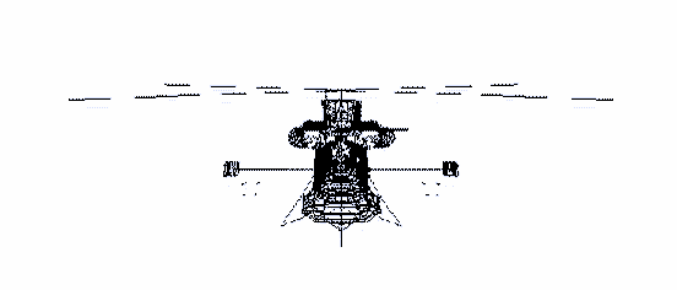

Figure C.1: Front View of an attack helicopter grid model at 118 MHz

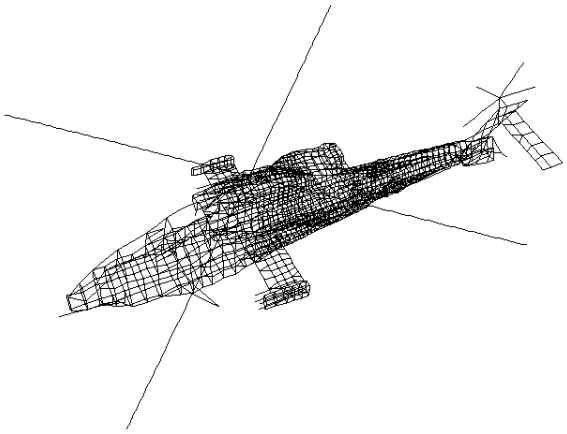

Figure C.2: Perspective View of an attack helicopter grid model at 118 MHz

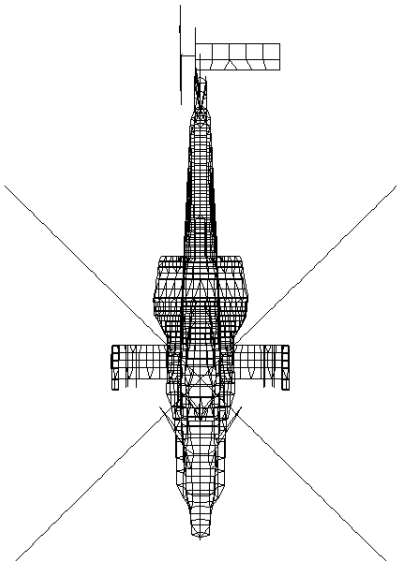

Figure C.3: Top View of an attack helicopter grid model at 118 MHz

C.2 Attack Helicopter Results

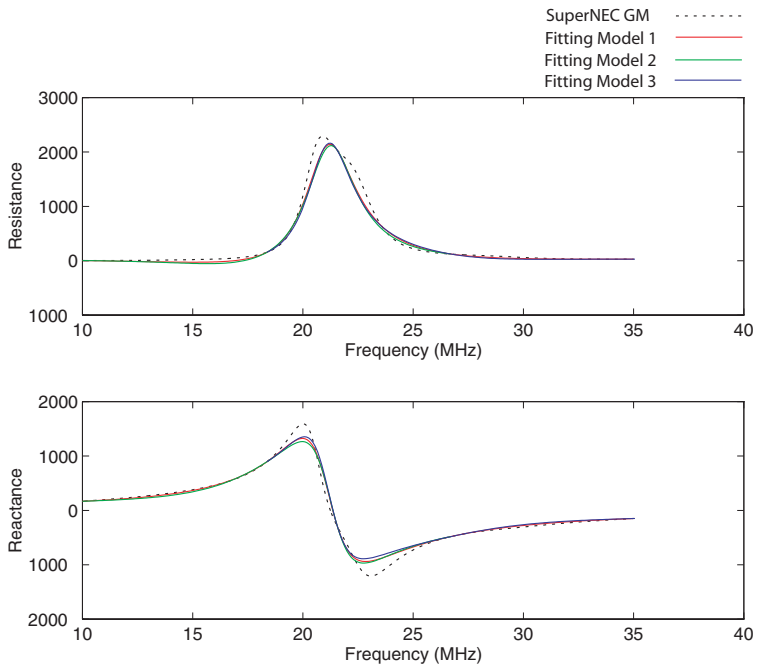

Figure C.4: An attack helicopter segmented at 25 MHz. TFE applied over the range 10-35 MHz: Iteration no. 5.

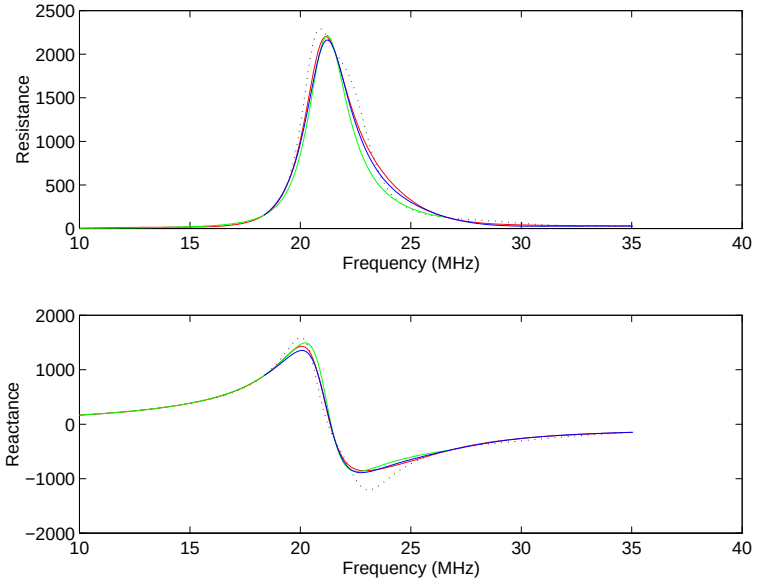

Figure C.5: An attack helicopter segmented at 25 MHz. TFE applied over the range 10-35 MHz: Iteration no. 6.

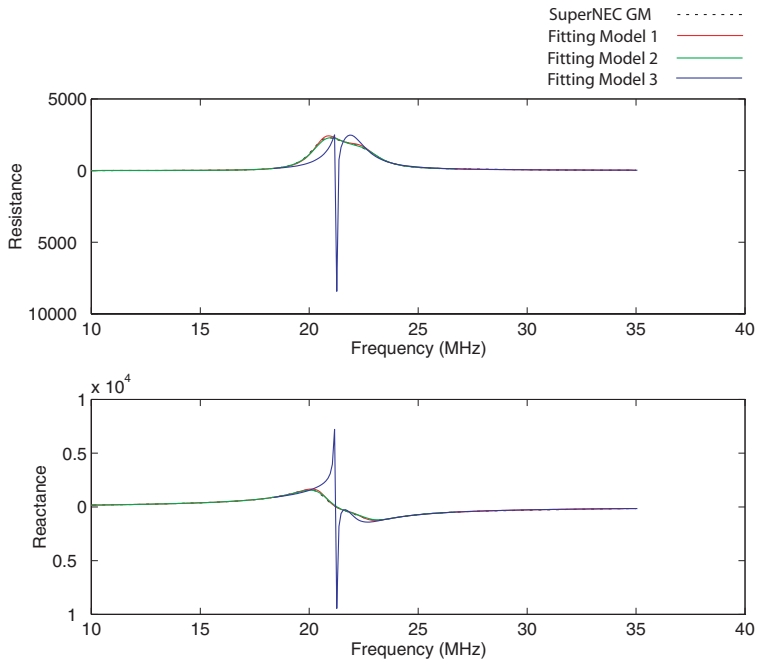

Figure C.6: An attack helicopter segmented at 25 MHz. TFE applied over the range 10-35 MHz: Iteration no. 7.

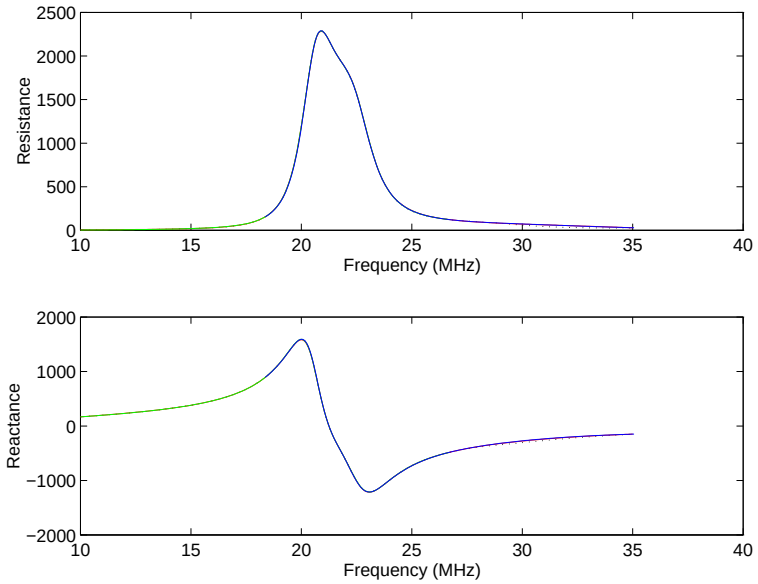

Figure C.7: An attack helicopter segmented at 25 MHz. TFE applied over the range 10-35 MHz: Iteration no. 8.

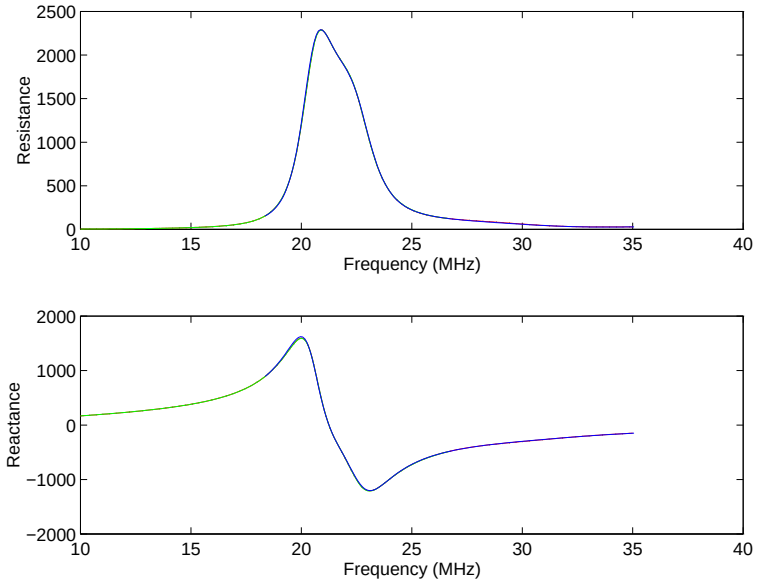

Figure C.8: An attack helicopter segmented at 25 MHz. TFE applied over the range 10-35 MHz: Iteration no. 9.

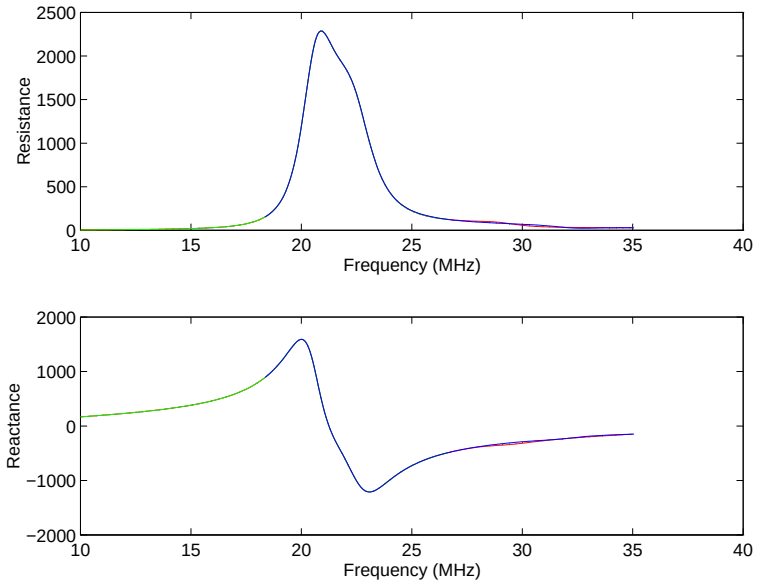

Figure C.9: An attack helicopter segmented at 25 MHz. TFE applied over the range 10-35 MHz: Iteration no. 10.

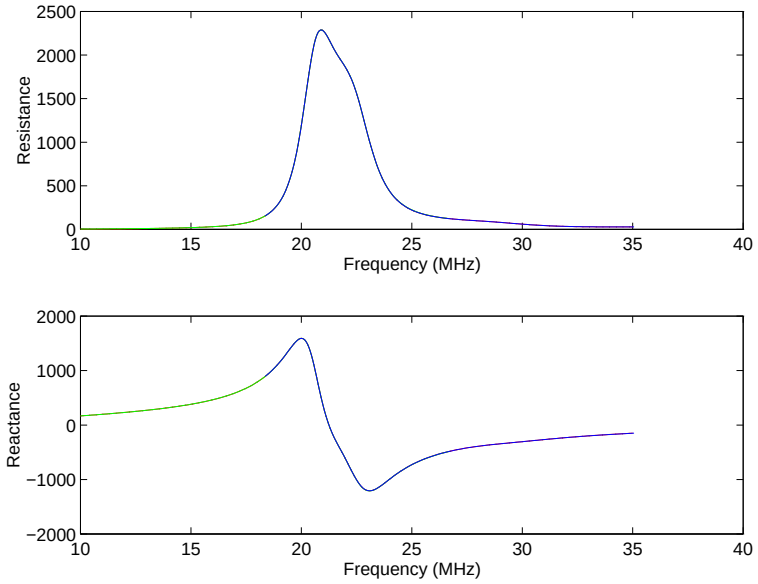

Figure C.10: An attack helicopter segmented at 25 MHz. TFE applied over the range 10-35 MHz: Iteration no. 11.

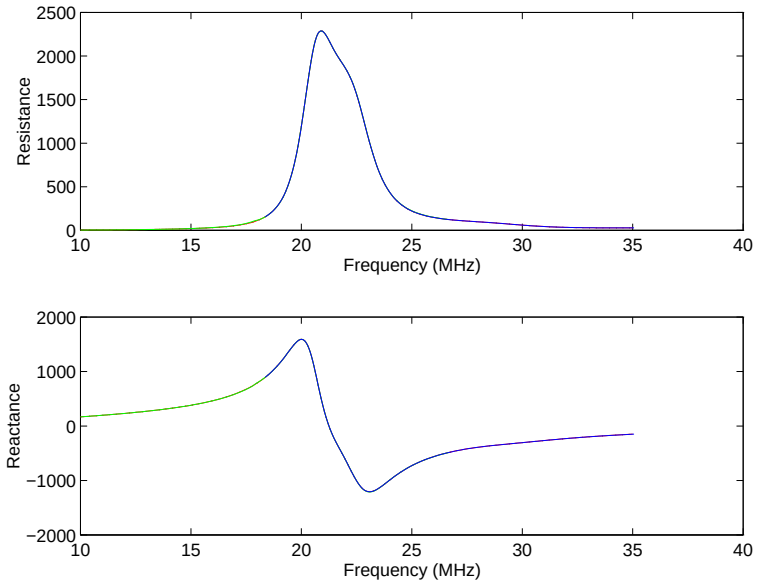

Figure C.11: An attack helicopter segmented at 25 MHz. TFE applied over the range 10-35 MHz: Iteration no. 12.

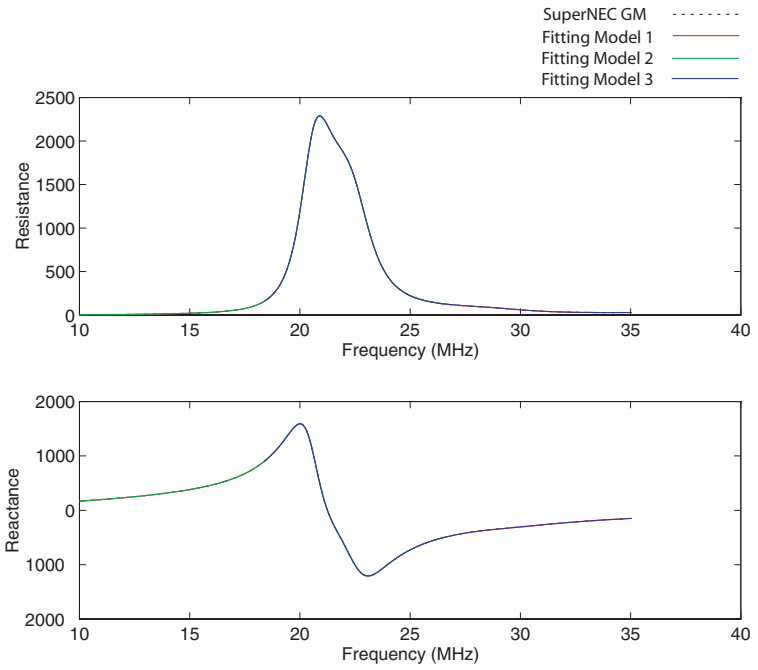

Figure C.12: An attack helicopter segmented at 25 MHz. TFE applied over the range 10-35 MHz: Iteration no. 13.

C.3 LPDA Results

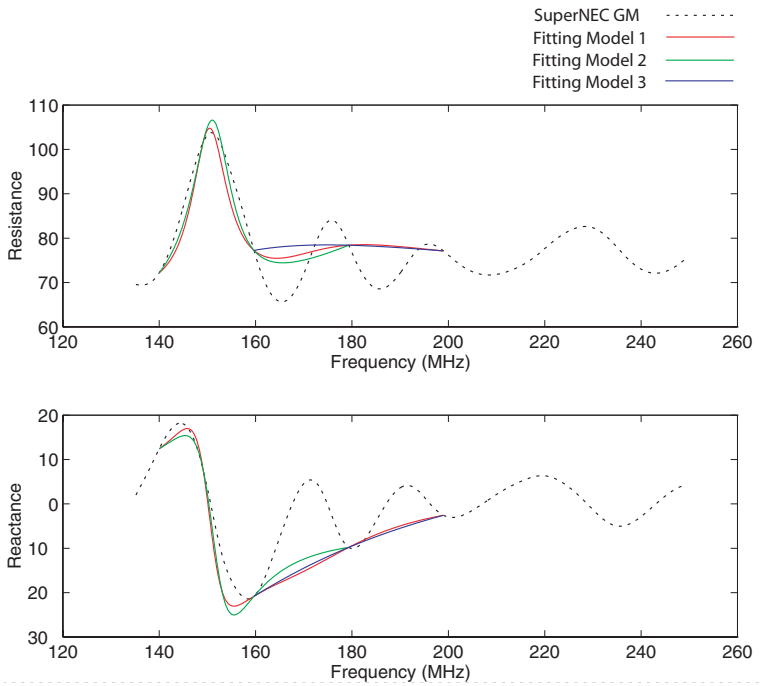

Figure C.13: A 47 -420 Mhz LPDA, segmented for 200 MHz and simulated over the range 135-250 MHz in SuperNEC. TFE performed over the range 140-200 Mhz: Iteration no. 5.

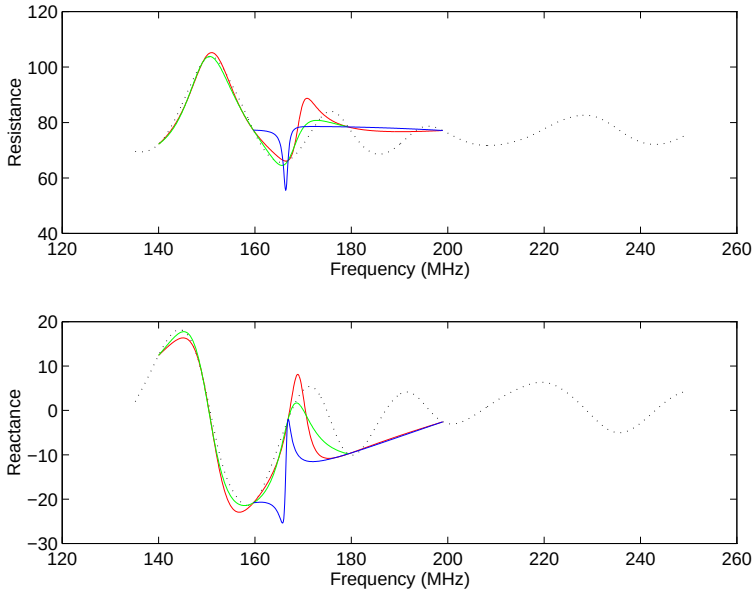

Figure C.14: A 47 -420 Mhz LPDA, segmented for 200 MHz and simulated over the range 135-250 MHz in SuperNEC. TFE performed over the range 140-200 Mhz: Iteration no. 6.

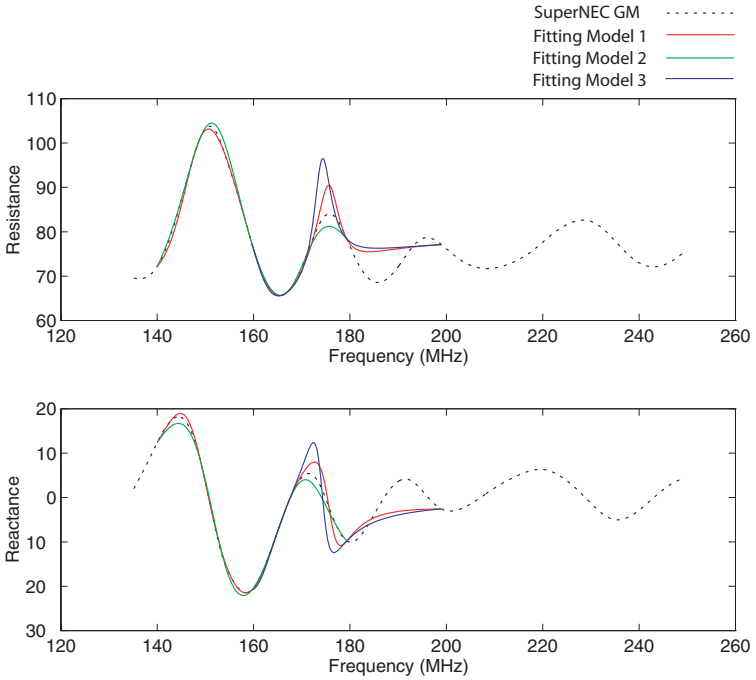

Figure C.15: A 47 -420 Mhz LPDA, segmented for 200 MHz and simulated over the range 135-250 MHz in SuperNEC. TFE performed over the range 140-200 Mhz: Iteration no. 7.

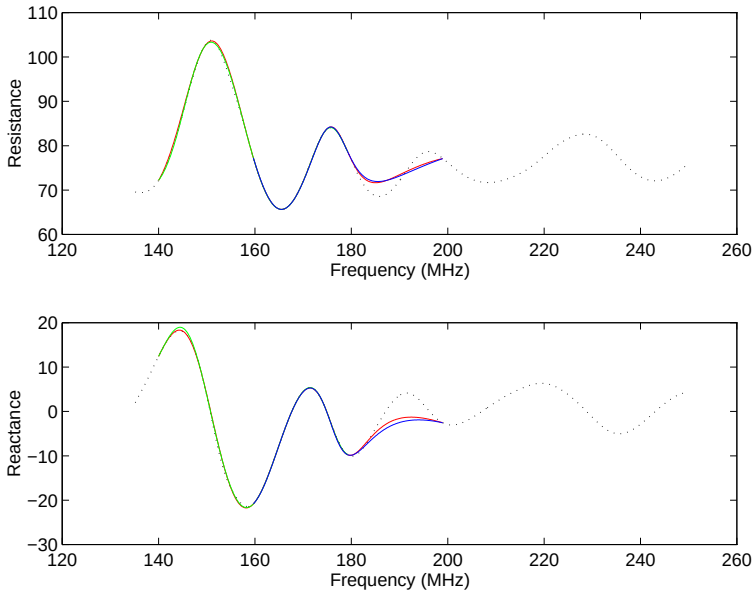

Figure C.16: A 47 -420 Mhz LPDA, segmented for 200 MHz and simulated over the range 135-250 MHz in SuperNEC. TFE performed over the range 140-200 Mhz: Iteration no. 8.

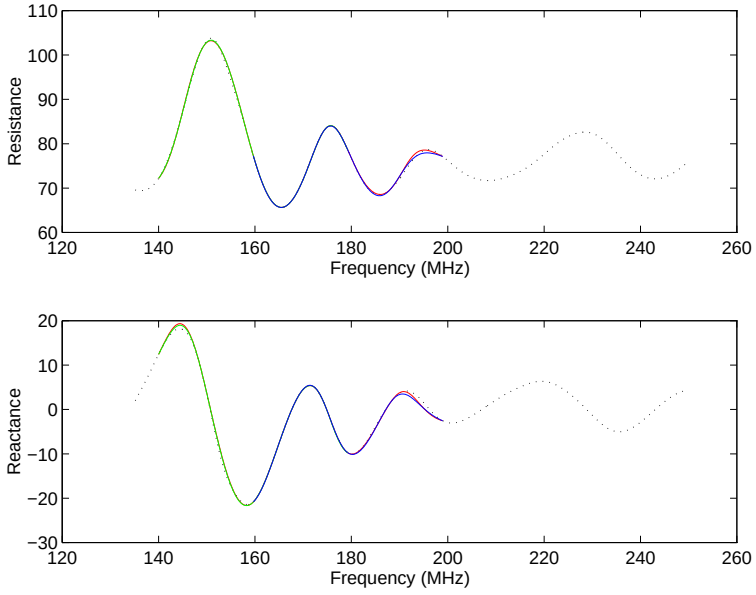

Figure C.17: A 47 -420 Mhz LPDA, segmented for 200 MHz and simulated over the range 135-250 MHz in SuperNEC. TFE performed over the range 140-200 Mhz: Iteration no. 9.

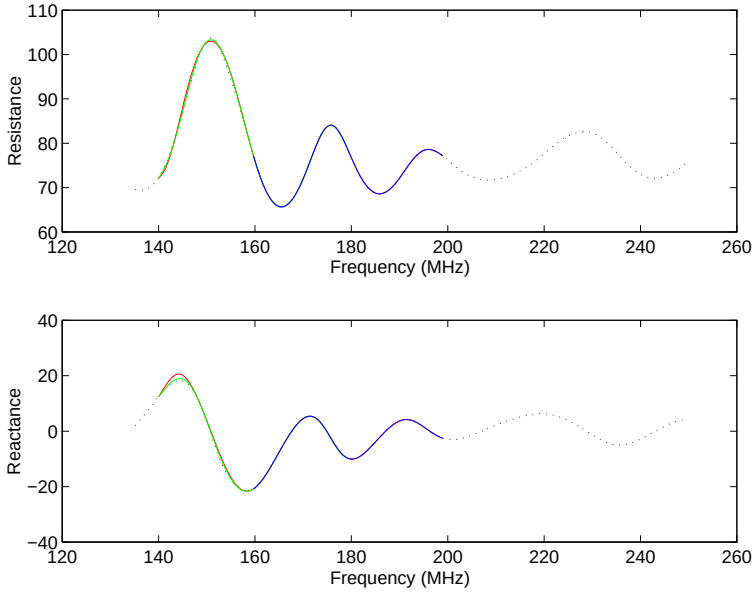

Figure C.18: A 47 -420 Mhz LPDA, segmented for 200 MHz and simulated over the range 135-250 MHz in SuperNEC. TFE performed over the range 140-200 Mhz: Iteration no. 10.

Bibliography

[1] L. Marin, "Natural Mode Representation of Transient Scattering from Rotationally Symmetric Bodies," *IEEE Transactions on Antennas and Propagation*, vol. AP-22, pp. 266–274, March 1974.

[2] K. E. Gustafson, *Introduction to Partial Differential Equations and Hilbert Space Methods*. New York, USA: John Wiley and Sons, 1987.

[3] R. Harrington, *Field Computation by Moment Methods*. New Jersey, USA: IEEE Press, ieee ed., 1993.

[4] G. Burke and A. Poggio, "Numerical Electromagnetics Code (NEC) - Method of Moment," *NOSC Technical Document*, vol. 1, pp. 3–34, January 1981.

[5] D. Nitch and A. Fourie, "A Redesign of NEC2 using the Object-Oriented Paradigm," *IEEE Antennas and Propagation Society International Symposium*, June 1994.

[6] A. Poggio and E. Miller, "Integral Equation Solutions of Three-Dimensional Scattering Problems," in *Computer Techniques for Electromagnetics* (R.Mittra, ed.), pp. 159–164, Oxford: Pergamon, 1973.

[7] E. Miller, "Model-Based Parameter Estimation in Electromagnetics: I – Background and Theoretical Development," *Applied Computational Electromagnetics Society Newsletter*, vol. 10, November 1995.

[8] R. J. Fleming, "Model Based Parameter Estimation applied to SuperNEC," *EM Simulations Inc.*, 1995.

[9] C. Baum, "On the Singularity Expansion Method for the Solution of Electromagnetic Interaction Problems," *Interaction Note 88*, December 1971.

[10] A. Oppenheim, A. Willsky, and I. Young, *Signals and Systems*, pp. 161–170, 573–600. London, United Kingdom: Prentice Hall International, 1983.

[11] E. Kreyszig, *Advanced Engineering Mathematics*, pp. 720–800, 860–882. John Wiley and Sons, 1988.

[12] E. Miller, "A selected survey of computational electromagnetics," *IEEE Transactions on Antennas and Propagation*, vol. 36, pp. 1281–1305, September 1988.

[13] L. Felsen and N. Marcuvitz, *Radiation and Scattering of Waves*, pp. 9–23, 50–93, 180–224, 239–271, 823–832. New Jersey, USA: IEEE Press, ieee ed., 1994.

[14] B. Friedman, *Principles of Applied Mathematics*. New York, USA: John Wiley & Sons, 1956.

[15] P. Dirac, *The Principles of Quantum Mechanics*. Clarendon Press, 1947.

[16] D. Dudley, *Mathematical Foundations for Electromagnetic Theory*, pp. 19–25, 99–135. New Jersey, USA: IEEE Press, ieee ed., 1994.

[17] T. Rozzi, *Open Electromagnetic Waveguides*, pp. 92–103. New Jersey, USA: IEE Press, 1996.

[18] R. Collin, *Field Theory of Guided Waves*. New York, USA: IEEE Press, 2nd ed., 1991.

[19] G. Burke, E. Miller, S. Chakrabati, and K. Demarest, "Using Model-Based Parameter Estimation to Increase the Efficiency of Computing Electromagnetic transfer functions," *IEEE Trans. Magn*, vol. 25, pp. 2807–2809, July 1989.

[20] R. Adve, T. Sarkar, S.M.Rao, E.K.Miller, and D.R.Pflug, "Application of the Cauchy Method for Extrapolating/Interpolating Narrowband System Responses," *IEEE Transactions on Microwave Theory and Techniques*, vol. 45, pp. 837–845, May 1997.

[21] D. R. Pflug, "Model Based Parameter Estimation as a Model Abstraction Technique," in *IEEE Information Technology Conference*, p. 37, 1998.

[22] K. Kottapalli, T. Sarkar, R. Adve, Y. Hua, E. Miller, and G. Burke, "Accurate Computation of Wideband Response of Electromagnetic Systems Utilising Narrowband Information," *Computer Physics Communications*, vol. 68, pp. 125–144, November 1991.

[23] K. Krishnamoorthy, T. Sarkar, X. Yang, E. Miller, and G. Burke, "Use of Frequency-Derivative Information to Reconstruct the Scattered Field of a Conducting Cylinder over a Wide Frequency Band," *Journal of Electromagnetic Waves and Applications*, vol. 5, no. 6, pp. 653–663, 1991.

[24] E. Miller and G. Burke, "Using Model-Based Parameter Estimation to Increase the Physical Interpretability and Numerical Efficiency of Computational Electromagnetics," *Computer Physics Communications*, vol. 68, pp. 43–75, November 1991.

[25] A. Roberts and D. McNamara, "Interpolating Radiation Patterns using Prony's Method," *Proceedings of Symposium on Antennas and Propagation and Microwave Theory and Techniques*, pp. 151–154, 1994.

[26] E. Miller, "Model-Based Parameter Estimation in Electromagnetics: II - Applications to EM Observables," *IEEE Antennas and Propagation Magazine*, vol. 40, no. 3, pp. 43–60, 1998.

[27] K. Virga and Y. Rahmat-Samii, "Wide-band Evaluation of Communications Antennas using Z Matrix Interpolation with the Method of Moments," *IEEE Antennas and Propagation Society International Symposium*, pp. 1262–1265, 1995.

[28] G. Benthien and H. Schenk, *Boundary Element Methods in Acoustics*, ch. Structural-Acoustic Coupling. Computational Mechanics Publications, 1991.

[29] D. Werner and R. Allard, "The Simultaneous Interpolation of Antenna Radiation Patterns in Both the Spatial and Frequency Domains Using Model-Based Parameter Estimation," *IEEE Transactions on Antennas and Propagation*, vol. 48, pp. 383–392, March 2000.

[30] L. Fermelia, G. Rollins, and P. Ramanujam, "The Use of Model-Based Parameter Estimation (MBPE) for the Design of Corrugated Horns," *Program Digest of US URSI Radio Science Meeting, University of Michigan*, p. 388, 1993.

[31] S. Zainud-Deen, S. El-Doda, K. Awadalla, and H. Sharshar, "Model-based Parameter Estimation of Antenna Input Impedance and Radiation Pattern," *Antennas and Propagation International Symposium*, pp. 815–818, July 2006.

[32] J. de Beer and D. Baker, "An Examination of Mechanical Deformation on the Input Impedance of HF LPDA's Using MBPE," *ACES Journal*, vol. 10, pp. 30–37, November 1995.

[33] L. Li and C. Liang, "Generalized System Function Analysis of Exterior and Interior Resonances of Antenna and Scattering Problems," *IEEE Transactions on Antennas and Propagation*, vol. 52, pp. 2064–2072, August 2004.

[34] R. J. Fleming, "A Transfer Function Estimation Method Integrated into SuperNEC for the Approximation of the Wideband Electromagnetic Response of Complex Structures," Master's thesis, University of Witwatersrand, Johannesburg, South Africa, May 2003.

[35] E. Miller, ""smart" Curve Fitting," *IEEE Potentials*, vol. 21, pp. 20–23, February 2002.

[36] A. G. Ramm, "Eigenfunction Expansion of a Discrete Spectrum in Diffraction Problems," *Radio Eng. Electr. Phys.*, vol. 18, pp. 364–369, 1973.

[37] A. G. Ramm, "Theoretical and Practical Aspects of Singularity and Eigenmode Expansion Methods," in *IEEE Transactions on Antennas and Propagation*, vol. AP-28, pp. 897–901, 1980.

[38] A. Ramm, "Mathematical Foundations of the Singularity and Eigenmode Expansion Methods (SEM and EEM)," *Journal of Mathematical Analysis and Applications*, no. 86, pp. 562–591, 1982.

[39] C. Baum, "Emerging Technology for Transient and Broad-Band Analysis and Synthesis of Antennas and Scatterers," *Proceedings of the IEEE*, vol. 64, pp. 1598–1616, November 1976.

[40] L. Marin and R. Latham, "Representation of Transient Scattered Fields in Terms of Free Oscillations of Bodies," *Proceedings of the IEEE*, pp. 640–641, May 1972.

[41] H. Pocklington, "Electrical Oscillations in Wires," *Proceedings of Cambridge Phil. Soc.*, vol. 9, pp. 324–332, 1897.

[42] C. Oseen, " Über die elektromagnetische Schwingungen an dünnen Stäben," *Ark. Mat. Astron. Fys.*, vol. 9, pp. 1–27, 1914.

[43] E. Hallén, " Über die elektrischen Schwingungen in drahtförmigen Leitern ," *Uppsala Univ, Arsskr.*, no. 1, pp. 1–102, 1930.

[44] M. Abraham, " Die elektrischen Schwingungen um einen stabförmigen Leiter, behandelt nach der Maxwell'schen Theorie ," *Ann. Phys. (Leipzig)*, vol. 66, pp. 435–472, 1898.

[45] J. A. Stratton, *Electromagnetic Theory*. New York, USA: McGraw-Hill, 1941.

[46] G. Ross, "A Time Domain Criterion for the Design of Wideband Radiating Elements," *IEEE Transactions on Antennas and Propagation*, vol. AP-16, pp. 355–356, May 1968.

[47] H. Schmitt, C. H. Jr, and C. W. Jr, "Calculated and Experimental Response of Thin Cylindrical Antennas to Pulse Excitation," *IEEE Transactions on Antennas and Propagation*, vol. AP-14, pp. 120–127, March 1966.

[48] F. M. Tesche, "On the Analysis of Scattering and Antenna Problems Using the Singularity Expansion Technique," *IEEE Transactions on Antennas and Propagation*, vol. AP-21, pp. 53–62, January 1973.

[49] K. Umashankar and D. Wilton, "Transient Scattering of an L-shaped Wire Using the Singularity Expansion Method," *IEEE Transactions on Antennas and Propagation*, vol. AP-23, pp. 833–841, November 1975.

[50] K. Umashankar, T. Shumpert, and D. Wilton, "Scattering by a Thin Wire Parallel to a Ground Plane Using the Singularity Expansion Method," *IEEE Transactions on Antennas and Propagation*, vol. AP-23, pp. 178–184, March 1975.

[51] T. Crow, B. Graves, and C. Taylor, "The Singularity Expansion Method as Applied to Perpendicular Crossed Wires," *IEEE Transactions on Antennas and Propagation*, vol. 23, pp. 540–546, July 1975.

[52] K. Cho and J. Cordaro, "Calculation of the SEM parameters from the Transient Response of a Thin Wire," *IEEE Transactions on Antennas and Propagation*, vol. 28, pp. 921–924, November 1980.

[53] P. Barnes, "On the Singularity Expansion Method as applied to EMP Analysis and Simulation of the Cylindrical Dipole Antenna," *Interaction Note 146*, January 1974.

[54] C. Baum, E. Rothwell, K. Chen, and D. Nyquist, "The Singularity Expansion Method and its Application to Target Identification," *Proceedings of the IEEE*, vol. 79, pp. 1481–1492, October 1991.

[55] M. Richards, T. Shumpert, and L. Riggs, "A Modal Radar Cross Section of Thin-Wire Targets via the Singularity Expansion Method," *IEEE Transactions on Antennas and Propagation*, vol. 40, pp. 1256–1260, October 1992.

[56] F. Tesche, "The Far-field Response of a Step-excited Linear Antenna Using SEM," *IEEE Transactions on Antennas and Propagation*, vol. 23, pp. 834–838, November 1975.

[57] M. Richards, "SEM Representation of the Early and Late Time Fields Scattered from Wire Targets," *IEEE Transactions on Antennas and Propagation*, vol. 42, pp. 564–566, April 1994.

[58] S. Licul and W. Davis, "Unified Frequency and Time-Domain Antenna Modeling and Characterization," *IEEE Transactions on Antennas and Propagation*, vol. 53, pp. 2882–2888, September 2005.

[59] C. Dolph and S. Cho, "On the Relationship between the Singularity Expansion Method and the Mathematical Theory of Scattering," *IEEE Transactions on Antennas and Propagation*, vol. AP-28, pp. 888–896, November 1980.

[60] O. D. Kellogg, *Foundations of Potential Theory.* Frederick Ungar Publishing Company.

[61] B. Baker and E. Copson, *Mathematical Theory of Huygen's Principle.* Oxford: Clarendon Press, 2nd ed., 1953.

[62] D. Jones, *Acoustic and Electromagnetic Waves.* Oxford, United Kingdom: Clarendon Press, 1986.

[63] J. van Bladel, *Singular Electromagnetic Fields and Sources*, vol. 28 of *Oxford Engineering Science Series.* Oxford, Great Britain: Oxford University Press, 1991.

[64] C. Grosche, *Path Integrals, Hyperbolic Spaces, and Selberg Trace Formulae*. World Scientific Publishing Co., 1995.

[65] J. Stratton and L. Chu, "Diffraction Theory of Electromagnetic Waves," *Phys. Rev.*, vol. 56, pp. 99–107, July 1939.

[66] N. Morita, N. Kumagai, and J. R. Mautz, *Integral Equation Methods for Electromagnetics*. Norwood, Massachussets, USA: Artech House, 1991.

[67] G. Hsiao and R. Kleinman, "Mathematical Foundations for Error Estimation in Numerical Solutions of Integral Equations in Electromagnetics," *IEEE Transactions on Antennas and Propagation*, vol. 45, pp. 316–328, March 1997.

[68] A. Maue, "Zur Formuliering, eines allgemenen Beugengsproblems durch eine integralgleichung," *Z. Phys.*, vol. 126, no. 7, pp. 601–618, 1949.

[69] W. C. Chew, *Waves and Fields in Inhomogeneous Media*. New York, USA: Van Nostrand Reinhold, 1990.

[70] J. van Bladel, "Some Remarks on Green's Dyadic for Infinite Space," *IRE Trans. Antennas Propagat.*, vol. AP-9, pp. 563–566, November 1961.

[71] Y. Rahmat-Samii, "On the Question of Computation of the Dyadic Green's Functions at the Source Region in Waveguides and Cavities," *IEEE Transactions Microwave Theory Tech*, vol. 23, pp. 762–765, September 1975.

[72] K. Chen, "A Simple Physical Picture of Tensor Green's Function in Source Region," *Proceedings of the IEEE*, pp. 1202–1204, August 1977.

[73] C. Tai, "Comments on "Electric Dyadic Green's Functions in the Source Region," *Proceedings of the IEEE*, vol. 69, pp. 282–285, February 1981.

[74] A. Yaghjian, "Electric Dyadic Green's Functions in the Source Region," *Proceedings of the IEEE*, vol. 68, pp. 248–263, February 1980.

[75] F. Riesz and B. Sz.-Nagy, *Functional Analysis*. second ed., 1955.

[76] T. Jech, *Set Theory: The Third Millennium Edition, Revised and Expanded*. Springer, third ed., 2003.

[77] G. Birkhoff and S. MacLane, *Algebra*. Chelsea, 2nd ed., 1999.

[78] S. Burris and H. Sankappanavar, *A Course in Universal Algebra*. Springer Verlag, 1981.

[79] K. Saxe, *Beginning Functional Analysis*. New York, USA: Springer-Verlag, 2001.

[80] G. W. Hanson and A. B. Yakovlev, *Operator Theory for Electromagnetics : an Introduction.* New York, USA: Springer-Verlag, 2001.

[81] A. Kolmogorov and S. Fomin, *Elements of the Theory of Functions and Functional Analysis : Measure. The Lebesgue Integral. Hilbert Space.*, vol. 2. Albany, New York: Graylock Press, 1961.

[82] G. Folland, *Real Analysis: Modern Techniques and Their Applications.* John Wiley and Sons, 1984.

[83] R. Showalter, "Hilbert Space Methods for Partial Differential Equations," *Electronic Journal of Differential Equations.*

[84] P. Monk, *Finite Element Methods for Maxwell's Equations.* Oxford University Press, 2003.

[85] A. Toselli and O. Widlund, *Domain Decomposition Methods - Algortihms and Theory.* Springer Series in Computational Mathematics, Springer, 2005.

[86] J. Keener, *Principles of Applied Mathematics : Approximation and Transformation.* Cambridge, MA, USA: Westview Press, second ed., 1999.

[87] R. M. Young, *An Introduction to Nonharmonic Fourier Series.* San Diego, USA: Academic Press, 2001.

[88] P. Enflo, "A Counterexample to the Approximation Property in Banach Spaces," *Acta Math*, vol. 130, pp. 309–317, 1973.

[89] A. Naylor and G. Sell, *Linear Operator Theory in Engineering and Science*, vol. 40 of *Applied Mathematical Sciences.* New York, USA: Springer-Verlag, 1982.

[90] W. Arveson, *A Short Course on Spectral Theory.* No. 209 in Graduate Texts in Mathematics, New York, USA: Springer-Verlag, 2002.

[91] I. Gohberg and M. Krein, *Introduction to the Theory of Linear Nonselfadjoint Operators*, vol. 18 of *Translations of Mathematical Monographs.* Rhode Island, USA: American Mathematical Society, 1969.

[92] I. Titeux and Y. Yakubov, *Application of Abstract Differential Equations to Some Mechanical Problems.* Mathematics and its Applications, Dordrecht, The Netherlands: Kulwer Academic Publishers, 2003.

[93] D. Jones, *Methods in Electromagnetic Wave Propagation.* Engineering Science Series, Oxford, United Kingdom: Oxford University Press, 1994.

[94] R. Kress, *Linear Integral Equations*, vol. 82 of *Applied Mathematical Sciences*. Berlin: Springer-Verlag, second ed., 1999.

[95] J. Hadamard, *Lectures on Cauchy's Problem in Linear Partial Differential Equations*. New Haven: Yale University Press, 1923.

[96] C. Green, *Integral Equation Methods*. London, United Kingdom: Thomas Nelson And Sons Limited, 1969.

[97] S. G. Mikhlin, *Integral Equations and their Applications to Certain Problems in Mechanics, Mathematical Physics and Technology*, vol. 4 of *International Series of Monographs on Pure and Applied Mathematics*. New York, USA: Pergamon Press, second ed., 1957.

[98] D. Colton and R. Kress, *Inverse Acoustic and Electromagnetic Scattering Theory*. No. 93 in Applied Mathematical Sciences, Berlin: Springer-Verlag, second ed., 1998.

[99] A. Mohsen, "The Source Simulation Technique for Exterior Problems in Acoustics," *Z. Angew Math. Phys.*, vol. 43, pp. 401–404, 1992.

[100] K. Mitzner, "Numerical Solution of the Exterior Scattering Problem Eigenfrequencies of the Interior Problem," (Boston, MA), p. 75, URSI Radio Science, September 1968.

[101] J. Mautz and R. Harrington, "H-Field, E-Field and Combined-Field Solutions for Conducting Bodies of Revolution," *A.E. Ü* , vol. 32, pp. 157–163, 1978.

[102] A. Yaghjian, "Augmented Electric- and Magnetic-Field Equations," *Radio Science*, vol. 16, pp. 987–1001, 1981.

[103] F. Canning, "Singular Value Decomposition of Integral Equations of Em and Applications to the Cavity Resonance Problem," *IEEE Transactions on Antennas and Propagation*, vol. 37, pp. 1156–1163, September 1989.

[104] F. X. Canning, "Protecting EFIE-Based Scattering Computations from Effects of Interior Resonances," *IEEE Transactions on Antennas and Propagation*, vol. 39, pp. 1545–1552, November 1991.

[105] F. Canning, "Robust Use of Supplementary Conditions for Moment Method Solution near Internal Resonances," *IEEE Transactions on Antennas and Propagation*, vol. 43, pp. 264–269, March 1995.

[106] A. F. Peterson, "The Interior Resonance Problem Associated with Surface Integral Equations of Electromagnetics: Numerical Consequences and a Survey of Results," *Electromagnetics*, vol. 10, pp. 293–312, 1990.

[107] T. Sarkar and S. Rao, "A Simple Technique for Solving E-field Integral Equations for Conducting Bodies at Internal Resonances," *IEEE Transactions on Antennas and Propagation*, vol. AP-30, no. 6, 1982.

[108] D. Colton and R.Kress, *Integral Equation Methods in Scattering Theory.* New York: Wiley, 1984.

[109] R. Kress and A. Mohsen, "On the Simulation Source Technique for Exterior Problems in Acoustics," *Meth. Meth. Appl. Sci.*, vol. 8, pp. 585–597, 1986.

[110] P. Waterman, "Numerical Solution of Electromagnetic Scattering Problems," in *Computer Techniques for Electomagnetics* (R. Mittra, ed.), pp. 97–157, New York, USA: Pergamon, 1973.

[111] A. Tobin, A. Yaghjian, and M. Bell, "Surface Integral Equations for Multi-Wavelength, Arbitrary Shaped, Perfectly Conducting Bodies," in *Digest URSI Radio Sci. Meet.*, (Boulder, CO, USA), p. 7, URSI Radio Science, 1987.

[112] R. Kress, *Linear Integral Equations.* Berlin: Springer, 1989.

[113] G. Fikioris, "A Note on the Method of Analytical Regularization," *IEEE Transactions on Antennas and Progagation Magazine*, vol. 43, pp. 34–40, April 2001.

[114] A. I. Nosich, "The Method of Analytical Regularization in Wave Scattering and Eigenvalue Problems : Foundations and Review of Solutions," *IEEE Antennas and Propagation Magazine*, vol. 41, pp. 34–49, June 1999.

[115] A. Burton and G. Miller, "The Application of Integral Equation Methods to the Numerical Solution of some Exterior Boundary Value Problems," *Proc. Roy. Soc. London A.*, vol. 323, pp. 201–210, 1971.

[116] R. B. Marks, "Application of the Singular Function Expansion to an Integral Equation for Scattering," *IEEE Transactions on Antennas and Propagation*, vol. 34, pp. 725–728, May 1986.

[117] R. B. Marks, "The Singular Function Expansion in Time-Dependent Scattering," *IEEE Transactions on Antennas and Propagation*, vol. 37, pp. 1559–1565, December 1989.

[118] A. Yaghjian, "Banded-matrix Preconditioning for Electric-field Integral Equations," *Proc. IEEE Antennas and Propagation Int. Symp.*, pp. 1806–1809, 1997.

[119] R. J. Adams, "Physical and Analytical Properties of a Stabilized Electric Field Integral Equation," *IEEE Transactions on Antennas and Propagation*, vol. 52, pp. 362–372, February 2004.

[120] R. Adams and G. Brown, "Stabilisation Procedure for Electric Field Integral Equation," *Electronics Letters*, vol. 35, pp. 2015–2016, November 1999.

[121] D. Dudley, "Error Minimization and Convergence in Numerical Methods," *Electromagnetics*, vol. 5, no. 2-3, pp. 89–97, 1985.

[122] G. Hower, R. Olsen, J. Earls, and J. Schneider, "Inaccuracies in Numerical Calculation of Scattering near Natural Frequencies of Penetrable Objects," *IEEE Transactions on Antennas and Propagation*, vol. 41, no. 7, pp. 982–986, 1993.

[123] R. J. Adams, "Combined Field Integral Equation Formulations for Electromagnetic Scattering From Convex Geometries," *IEEE Transactions on Antennas and Propagation*, vol. 52, pp. 1294–1303, May 2004.

[124] R. Adams and N. Champagne, "A Numerical Implementation of a Modified Form of the Electric Field Integral Equation," *IEEE Transactions on Antennas and Propagation*, vol. 52, pp. 2262–2266, September 2004.

[125] G. Roach, "On the Commutative Properties of Boundary Integral Operators," *Proc. American Mathematical Soc.*, vol. 73, pp. 219–227, 1979.

[126] Z. Liu, R. Adams, and L. Carin, "Well-Conditioned MLFMA Formulation for Closed Pec Targets in the Vicinity of a Half Space," *IEEE Transactions on Antennas and Propagation*, vol. 51, pp. 2822–2829, October 2003.

[127] A. de la Bourdonnaye, "Some Formulations Coupling Finite Element and Integral Equation Methods for Helmholtz Equation and Electromagnetism," *Numer. Mathem.*, vol. 69, pp. 257–268, 1995.

[128] F. Andriulli, K. Cools, H. Bagci, F. Olyslager, A. Buffa, S. Christiansen, and E. Michielssen, "A Multiplicative Calderon Preconditioner for the Electric Field Integral Equation," *IEEE Transactions on Antennas and Propagation*, vol. 56, pp. 2398–2412, August 2008.

[129] S. Christiansen and J.-C. Nédélec, "A Preconditioner for the Electric Field Integral Equation based on Calderon Formulas," *SIAM Journal of Numerical Analysis*, vol. 40, pp. 1100–1135, December 2002.

[130] A. Buffa and S. Christiansen, "A Dual Finite Element Complex on the Barycentric Refinement," *Mathematics of Computation*, vol. 76, pp. 1743–1769, 2007.

[131] R. Dreyer and A. Clark, "Preliminary Results for Simply Sparse as a Preconditioner to SIM," *IEEE Antennas and Propagation International Symposium*, vol. 2, no. 6, pp. 238–241, 2002.

[132] H. Contopanagos, B. Dembart, M. Epton, J. Ottusch, V. Rokhlin, J. Visher, and S. Wandzura, "Well-Conditioned Boundary Integral Equations for Three-Dimensional Electromagnetic Scattering," *IEEE Transactions on Antennas and Propagation*, vol. 50, pp. 1824–1830, December 2002.

[133] D. Holliday, L. de Raad, and G. St-Cyr, "Forward-Backward : A New Method for Computing Low-Grazing Angle Scattering," *IEEE Transactions on Antennas and Propagation*, vol. 44, pp. 722–729, May 1996.

[134] D. Kapp and G. Brown, "A New Numerical Method for Rough Surface Scattering Calculations," *IEEE Transactions on Antennas and Propagation*, vol. 44, pp. 711–721, May 1996.

[135] F. X. Canning and R. B. Marks, " Comments and Reply on "Protecting EFIE-Based Scattering Computations from Effects of Interior Resonances " ," *IEEE Transactions on Antennas and Propagation*, vol. 41, pp. 387–389, March 1993.

[136] M. Nashed, "Operator-Theoretic and Computational Approaches to Ill-Posed Problems with Applications to Antenna Theory," *IEEE Transactions on Antennas and Propagation*, vol. 29, no. 2, pp. 220–231, 1981.

[137] P. Hansen, *Regularization Tools : A MATLAB Package for Analysis and Solution of Discrete Ill-Posed Problems*. Danish Center for Research and Education, 1995.

[138] A. Tikhonov, "The Regularization of Incorrectly Posed Problems," *Dok. Akad. Nauk. SSSR*, vol. 153, no. 1, pp. 42–52, 1963.

[139] A. Tikhonov, "The Solution of Incorrectly Posed Problems and the Method of Regularization," *Dok. Akad. Nauk. SSSR*, vol. 151, no. 3, pp. 501–504, 1963.

[140] A. Tikhonov and V. Glasko, "The Approximate Solution of Integral Equations of the First Kind," *USSR Computational Mathematics and Mathematical Physics*, vol. 4, pp. 236–247, 1964.

[141] R. J. Fleming, "A Common Theoretical Basis for the Preconditioned Field Integral Equations and the Singularity Expansion Method," *Progress in Electromagnetics Research M*, vol. 5, pp. 111–136, 2008.

[142] R. J. Fleming, "A Calderon Preconditioner and SEM Equivalence Relation applied to Wideband Frequency-Domain EFIE Solutions," *IEEE Transactions on Antennas and Propagation*, Submitted 2009.

[143] R. J. Fleming, "Singular Function Expansions to Precondition Electric Field Integral Equations," *Progress in Electromagnetics Research*, Submitted 2009.

[144] L. Marin, "Natural Mode Representation of Transient Scattered Fields," *IEEE Transactions on Antennas and Propagation*, vol. AP-21, pp. 809–818, November 1973.

[145] S. G. Mikhlin, *Mathematical Physics, An Advanced Course*, vol. 11 of *Applied Mathematics and Mechanics*. Amsterdam, Holland: North Holland Publishing Company, 1970.

[146] N. Young, *An Introduction to Hilbert Space*. Cambridge, United Kingdom: Cambridge University Press, 1988.

[147] F. Smithies, *Integral Equations*. London, United Kingdom: Cambridge University Press, 1958.

[148] E. Goursat, *A Course in Mathematical Analysis*, vol. II. New York, USA: Ginn and Company, 1917.

[149] M. Golberg, *Solution Methods for Integral Equations Theory and Applications*. Mathematical Concepts and Methods in Science and Engineering, New York, New York: Plenum press, 1979.

[150] S. Steinberg, "Meromorphic Families of Compact Operators," *Arch. Rat. Mech. Anal.*, vol. 31, pp. 372–379, 1968.

[151] L. W. Pearson, "Evidence that Bears on the Left Half Plane Asymptotic Behavior of the SEM Expansion of Surface Currents," *Electromagnetics*, vol. 1, pp. 395–402, 1981.

[152] C. Baum, *Transient Electromagnetic Fields*, ch. The Singularity Expansion Method, pp. 128–177. Sprinker-Verlag, New York, 1976.

[153] M. Morgan, "Singularity Expansion Representations of Fields and Currents in Transient Scattering," *IEEE Transactions on Antennas and Propagation*, vol. AP-32, pp. 466–472, May 1984.

[154] E. Heyman and L. Felsen, "A Wavefront Interpretation of the Singularity Expansion Method," *IEEE Transactions on Antennas and Propagation*, pp. 706–718, July 1985.

[155] J. Brittingham, E. Miller, and J. Willows, "Pole Extraction from Real-Frequency Information," *Proceedings of the IEEE*, vol. 68, pp. 263–273, February 1980.

[156] A. Householder, "On Prony's Method of Fitting Exponential Decay Curves and Multiple-Hit Survival Curves," Technical Report ORNL-455, Oak Ridge National Laboratory, Oak Ridge, TN, February 1950.

[157] M. Rahman and K. Yu, "Total Least Squares Approach for Frequency Estimation using Linear Prediction," *IEEE Transactions Acoustics, Speech and Signal Processing*, vol. ASSP-35, pp. 1440–1454, October 1987.

[158] Y. Hua and T. Sarkar, "On SVD for Estimating Generalized Eigenvalues of Singular Matrix Pencil in Noise," *IEEE Transactions Signal Processing*, vol. 39, pp. 892–900, April 1991.

[159] T. Sarkar and O. Pereira, "Using the Matrix Pencil Method to Estimate the Parameters of a Sum of Complex Exponentials," *IEEE Antennas and Propagation Magazine*, vol. 37, pp. 48–55, February 1995.

[160] Ö. Ergül and L. Gürel, "Efficient solution of the electric-field integral equation using the iterative lsqr algorithm," *IEEE Antennas and Wireless Propagation Letters*, vol. 7, pp. 36–39, 2008.

[161] A. G. Ramm, "Nonselfadjoint Operators in Diffraction and Scattering," *Mathematical Methods in the Applied Sciences*, no. 2, pp. 328–346, 1980.

[162] P. Hansen, "Computation of the Singular Value Expansion," *Computing*, vol. 40, no. 3, pp. 185–199, 1988.

[163] W. Press, B. Flannery, S. Teukolsky, and W. Vetterling, *Numerical Recipes in Pascal: The Art of Scientific Computing*, ch. 3.2, 9.3-9.6. Cambridge University Press, first ed., 1989.

[164] R. King, *The Theory of Linear Antennas*. Cambridge, Massachusetts: Harvard University Press, 1956.

[165] S. Schelkunoff, *Advanced Antenna Theory*, p. 132. New York: Wiley, 1932.

[166] K. Mei, "On the Integral Equations of Thin Wire Scatterers," *IEEE Transactions on Antennas and Propagation*, vol. AP-13, pp. 374–378, May 1965.

[167] D. Jones, "Note on the Integral Equation for a Straight Thin Wire Antenna," *IEE Proc*, vol. 128, pp. 114–116, 1981.

[168] B. Rynne, "The Well-posedness of the Integral Equations for Thin Wire Antennas with Distributional Incidental Fields," *Journal of Mechanics and Applied Mathematics*, vol. 52, no. 4, pp. 489–497, 1999.

[169] V. Hutson and J. Pym, *Applications of Functional Analysis and Operator Theory*. Academic Press, 1980.

[170] B. Rynne, "The Well-Posedness of the Integral Equation for Thin Wire Antennas," *IMA Journal of Applied Mathematics*, vol. 49, pp. 35–44, 1992.

[171] B. Rynne, "On the Well-posedness of Pocklington's Equation for a Straight Wire Antenna and Convergence of Numerical Solutions," *Journal Electromagnetic Waves and Applications*, vol. 1489-1503, no. 14, 2000.

[172] R. Adams, *Sobolev Spaces*. Academic Press, 1975.

[173] B. Rynne, "Convergence of Galerkin Method Solutions of the Integral Equation for Thin Wire Antennas," *Advances in Computational Mathematics*, 1991.

[174] P. J. Davies, B. P. Ryme, and B. Zubik-Kowal, "The Time-Domain Integral Equation for a Straight Thin-Wire Antenna with the Reduced Kernel is Not Well-Posed," *IEEE Transactions on Antennas and Propagation*, vol. 50, pp. 1165–1166, August 2002.

[175] R. Bancroft, *Understanding Electromagnetic Scattering Using the Moment Method: A Practical Approach*. Norwood, MA. USA: Artech House, 1996.

[176] R. J. Garbacz and R. H. Turpin, "A Generalized Expansion for Radiated and Scattered Fields," *IEEE Transactions on Antennas and Propagation*, vol. AP-19, pp. 348–358, May 1971.

[177] A. Householder, "Unitary triangularization of a nonsymmetric matrix," *J. Ass. Comput. Mach.*, vol. 5, pp. 339–342, October 1958.

[178] M. V. Blaricum and R. Mittra, "A Technique for Extracting the Poles and Residues of a System Directly from its Transient Response," *IEEE Transactions on Antennas and Propagation*, vol. AP-23, pp. 777–781, November 1975.

[179] R. Prony, "Essai experimental et analytique, etc.," *Paris J.l'Ecole Poltechnique*, vol. 1, no. 2, pp. 24–76, 1795.

[180] N. Younan and C. Taylor, "On Using the SVD-Prony Method to Extract Poles," *Electromagnetics*, vol. 11, pp. 223–233, 1991.

[181] J. Stoer and R. Bulirsch, *Introduction to Numerical Analysis*, ch. 2.2. New York, USA: Springer-Verlag, 1980.

[182] D. Nitch, "Wire Segment Size as a Function of Frequency," 1997. Private communication.

[183] P. Hansen, "Numerical Tools for Analysis and Solution of Fredholm Integral Equations of the First Kind," *Inverse Problems*, vol. 8, pp. 849–872, 1992.

[184] Trueman and Kubina, "Verifying Wire-Grid Model Integrity with a Program CHECK," *ACES Journal*, vol. 5, no. 2, pp. 17–42, 1990.

[185] E. Miller, "Minimising the Number of Frequency Samples Needed to Represent a Transfer Function using Adaptive Sampling," 12^{th} *Annual Review of Progress in Applied Computational Electromagnetics: Conference Proceedings*, vol. 2, pp. 1132–1139, March 1996.

[186] E. Miller, "Using Model-Based Parameter Estimation to Estimate the Accuracy of Numerical Models," 12^{th} *Annual Review of Progress in Applied Computational Electromagnetics: Conference Proceedings*, vol. 1, pp. 588–595, March 1996.

[187] N. Sachdeva and N. Balakrishnan, "A Comparison of FDTD Techniques for 2-d Scatterers," *12th Annual Review of Progress in Applied Computational Electromagnetics*, March 1996.

[188] G. Burke, "Nec-MoM Update," *ACES Newsletter*, vol. 7, pp. 31–37, July 1992.

[189] A. Fourie, *Antennas in Practice*. Givati, Fourie and Associates cc., 1994.

[190] C. Peixero, "Design of Log Periodic Antennas," *IEE Proceedings*, vol. 135, no. 2, 1988.

[191] *Structure Interpolation and Gridding (SIG) software package*. PO Box 1380, Pinegowrie, 2123, South Africa: EM Simulations (Pty) Ltd.

[192] O. Givati, A. Fourie, and J. Dresel, "Radiation Patterns of Antennas Mounted on an Attack Helicopter," 12^{th} *Annual Review of Progress in Applied Computational Electromagnetics: Conference Proceedings*, vol. 2, pp. 802–817, March 1996.

[193] B. Orchard, "Timing Results for SuperNEC Version 2.4," 2003. Private communication.

[194] C.-T. Tai, *Generalized Vector and Dyadic Analysis*. IEEE Press Series on Electromagnetic Waves, New York, USA: IEEE Press, 1993.

[195] F. Tricomi, *Integral Equations*. New York, USA: Courier Dover Publications, dover ed., 1985.

[196] I. Gohberg, S. Goldberg, and M. Kaashoek, *Basic Classes of Linear Operators*. Basel, Switzerland: Birkhäuser Verlag , 2003.

[197] E. Zepler and K. Nichols, *Transients in Electronic Engineering*. Great Britain: Chapman and Hill, 1st ed., 1971.

[198] G. Arfken, *Mathematical Methods for Physicists*. 3rd: Academic Press, New York, USA ed., 1985.

[199] C. E. Baum, "On the Singularity Expansion Method for the Case of First Order Poles," *Interaction Note 129*, 1972.

[200] R. Harrington and J. Mautz, "Theory of Characteristic Modes for Conducting Bodies," *IEEE Transactions on Antennas and Propagation*, vol. AP-19, pp. 622–628, September 1971.

[201] R. Harrington and J. Mautz, "Computation of Characteristic Modes for Conducting Bodies," *IEEE Transactions on Antennas and Propagation*, vol. AP-19, pp. 629–639, September 1971.

[202] J. H. Wilkinson, *The Algebraic Eigenvalue Problem.* New York, USA: Oxford Press, 1967.